TURBOCHARGER AND DIESEL ENGINE MATCHING USING AERODYNAMIC COMPRESSOR PERFORMANCE CONTROLS

BY

NICKOLAS (P.) KYRTATOS

THESIS SUBMITTED FOR THE DEGREE OF
DOCTOR OF PHILOSOPHY
IN THE FACULTY OF ENGINEERING OF THE
UNIVERSITY OF LONDON

MARCH 1979

DEPARTMENT OF MECHANICAL ENGINEERING
IMPERIAL COLLEGE OF SCIENCE AND TECHNOLOGY
LONDON, SW7 2BX

To my parents

Στούς γονεῖς μου

TURBOCHARGER AND DIESEL ENGINE MATCHING USING AERODYNAMIC COMPRESSOR PERFORMANCE CONTROLS

Nickolas P. Kyrtatos

ABSTRACT

The flow characteristics of reciprocating internal combustion engines differ from those of rotary machines. Consequently, matching turbochargers and engines presents problems such as the limited compressor stable flow range and, in certain cases, the need to control turbocharger boost.

From several turbomachinery flow controls available, attention was given to compressor inlet prewhirl. This can regulate the compressor discharge pressure at constant speed and influence the compressor flow range.

An aerodynamic method is proposed to replace the variable inlet guide vanes normally used in such applications. High pressure fluid jets are ejected obliquely into the inflow, from orifices around the periphery of the inlet pipe, varying the jet flow to obtain variable prewhirl.

Initial experimental investigations were followed by a theoretical analysis of the flow. The flow model developed considers a single unbounded axisymmetric jet ejected at various angles into a cross flow.

A design method is developed using the analysis and experimental results. This enabled prototype aerodynamic prewhirl inducing devices to be designed and tested on turbocharger compressors. The applicability of the method was verified by simulation and experimental investigations on a turbocharged diesel engine.

ACKNOWLEDGEMENTS

The author wishes to acknowledge the contributions of the following people towards the successful completion of the present research work:

Dr. N. Watson (Supervisor)

Dr. A. Goulas

Dr. M. Marzouk

Mr. C. Busby

Mr. D. Grant

Mr. W. Masters

The efforts of Messrs. J. Nash and P.A. Stables of the National Research and Development Corporation with respect to British Patent Appl. No. 37489/78 are appreciated.

Thanks are also due to Mrs. E.M. Noel and Miss R. Dudley for typing the manuscript.

CONTENTS

	Page
ABSTRACT	1
ACKNOWLEDGEMENTS	2
CONTENTS	3
NOTATION	10
CHAPTER 1 - THE TURBOCHARGED DIESEL ENGINE	14
1.1 ON THE DEVELOPMENT OF SUPERCHARGED ENGINES	14
1.2 THE LIGHT DUTY DIESEL ENGINE	20
1.2.1 Introduction	20
1.2.2 Comparison with Gasoline Engines	21
1.2.3 Combustion Chamber Types	23
1.2.4 Performance Improvement of Small Diesels - Turbocharging-Problems	25
CHAPTER 2 - THE CENTRIFUGAL COMPRESSOR	26
2.1 THE CENTRIFUGAL COMPRESSOR - INTRODUCTION	28
2.2 DESCRIPTION - COMPONENTS	28
2.3 THE FLOW PATH - MORPHOLOGY OF FLOW-DESIGN	30
2.3.1 Inducer	30
2.3.2 Impeller	30
2.3.3 Diffuser	32
2.3.3.1 Vaneless diffuser	33
2.4 CENTRIFUGAL COMPRESSOR PERFORMANCE	34
2.5 OFF-DESIGN PERFORMANCE	35
2.5.1 Introduction	35
2.5.2 Surge	38
2.5.2.1 Definition of surge	41
2.5.2.2 Prediction of surge	42
2.5.3 Stall	43

2.5.3.1 Definition of stall 43

2.5.3.2 Fluid dynamic considerations 43

2.5.3.2.1 Diffuser (vaneless) 43

2.5.3.2.2 Impeller-inducer 46

2.5.3.3 Prediction of stall 46

2.5.4 Interrelation of Stall and Surge 47

2.5.5 Off-Design Testing Methods 49

2.5.6 Preventive Methods - Design Techniques 50

CHAPTER 3 - TURBOCHARGER MATCHING AND TURBOMACHINERY FLOW CONTROL 55

3.1 TURBOCHARGER MATCHING 55

3.2 MATCHING PROBLEMS 57

3.2.1 Influence of Engine on Compressor 59

3.3 POSSIBLE SOLUTIONS TO MATCHING PROBLEMS 60

3.4 EXTERNAL/SYSTEM METHODS 60

3.5 TURBO-ASSISTANCE METHODS 61

3.6 TURBOMACHINERY FLOW CONTROL 61

3.6.1 Turbine Controls 61

3.6.1.1 Constant area throttling devices (restrictions) 61

3.6.1.2 Turbine by-pass (wastegate) 61

3.6.1.3 Variable geometry 65

3.6.1.4 Aerodynamic methods 68

3.6.2 Compressor Controls 68

3.6.2.1 Constant area throttling devices (restrictions) 68

3.6.2.2 Discharge blow-off 68

3.6.2.3 Flow recirculation 69

3.6.2.4 Variable geometry 69

3.6.2.4.1 Variable geometry mechanisms 71

3.6.2.4.2 Control and aerodynamic aspects of prewhirl 79

3.6.2.4.3 Interrelation of V.G. methods - system optimisation 86

3.6.2.5 Aerodynamic methods 87

CHAPTER 4 - AN AERODYNAMIC METHOD FOR CONTROL AND RANGE IMPROVEMENT OF ROTARY COMPRESSORS - PART I 90

4.1 INITIAL EXPERIMENTS 90

4.1.1 Introduction 90

4.1.2 The Experiments 90

4.1.3 Flow Visualisation - Observations on Profile Variation 97

4.1.4 Comments on Results 97

4.2 ANALYTICAL APPROACH 99

4.3 THE JET IN CROSS FLOW 100

4.3.1 Introduction 100

4.3.2 Qualitative Description 100

4.3.3 Relevant Literature 107

4.4 MATHEMATICAL MODELLING OF A JET IN CROSS FLOW 113

4.4.1 Introduction 113

4.4.2 General Description of Model 114

4.4.3 Analysis 115

4.4.3.1 Coordinate system 115

4.4.3.2 Coordinate transformation equations 115

4.4.3.3 Conservation of mass 117

4.4.3.4 Conservation of momentum in ξ-direction 120

4.4.3.5 Conservation of momentum in ζ-direction 121

4.4.3.6 Conservation of energy-density function 124

4.4.3.7 Notes on curvilinear coordinates 125

4.4.4 Synthesis 129

4.4.4.1 Derivation of equations defining the jet 129

4.4.4.2 Entrainment coefficients 133

4.4.4.3 Cross flow velocity profile 135

4.5 THEORETICAL RESULTS USING MODEL 135

4.6 REVIEW OF EXPERIMENTAL RESULTS 139

4.7 ALTERNATIVE ARRANGEMENT 143

4.8 DESIGN OF NEW ARRANGEMENT 145

4.9 ADAPTOR AND HARDWARE DESIGN 149

4.10 INVESTIGATIONS USING THE JET-NOZZLE DEVICE 149

4.10.1 Introduction 149

4.10.2 Jet-Arrangement Performance Experiments 151

4.10.2.1 Description of experimental rig 151

4.10.2.2 Qualitative observations 153

4.10.2.3 The experiments 161

4.10.2.4 Results from the experiments 161

4.10.2.5 Comparison of the two jet arrangements 168

4.10.2.6 Interaction of compressor and jet device (predictions) 168

4.10.2.7 Conclusions 179

4.10.3 Compressor Performance Experiments using the Jet Device 180

4.10.3.1 Introduction 180

4.10.3.2 The (3-D) compressor map 181

4.10.3.3 The experiments 183

4.10.3.4 External jet flow supply experiments 183

4.10.3.5 Notes on noise from centrifugal rotors 186

4.10.3.6 Recirculation jet flow supply experiments 188

4.10.3.6.1 Noise level measurement apparatus 189

4.10.3.6.2 Definition of instability initiation point 189

4.10.3.6.3 Results 191

4.11 COMMENTS ON EXPERIMENTS - APPLICATION POTENTIAL OF THE DEVICE 193

CHAPTER 5 - THE ENGINE AND TURBOCHARGER SIMULATION 198

5.1 THE ENGINE SIMULATION - INTRODUCTION 198

5.2 THE COMPUTER CODE 199

5.3 INDIRECT INJECTION DIESEL ENGINE SIMULATION 200

5.3.1 Divided Chamber Model 200

5.3.2 Combustion - Heat Release 201

5.3.2.1 Introduction 201

5.3.2.2 Heat release model 202

5.3.3 Heat Transfer 204

5.3.4 Valve Discharge Coefficients 205

5.3.5 Numerical Stability 205

5.3.6 Program Outline 207

5.4 THE "VARIABLE PERFORMANCE" COMPRESSOR MODEL 208

5.4.1 Introduction 208

5.4.2 Expected Shape of the (3-D) V.P. Compressor Map 209

5.4.3 Presentation of Limiting Surfaces 215

5.4.4 Space Orientation of Working Point 215

5.4.5 The Control Subroutine 216

5.4.6 The VCOMP Subroutine - Interpolation Method 216

5.4.7 The Efficiencies Associated with the V.P. Compressor 219

CHAPTER 6 - AN AERODYNAMIC METHOD FOR CONTROL AND RANGE IMPROVEMENT OF ROTARY COMPRESSORS (PART II) 221

6.1 INTRODUCTION 221

6.2 THE DESIGN PROCEDURE FOR THE JET ARRANGEMENT 221

6.3 DESIGN DEFINING PARAMETERS 223

6.4 SHAPE OF JET EJECTION ORIFICES 223

6.5 MEASUREMENT OF INDUCER INLET ANGLES 226

6.6 PRELIMINARY SIMULATION RESULTS 227

6.7 THE DESIGN 230

6.7.1 Compressor Inlet Velocity Triangles 230

6.7.2 Relation Between Prehwirl Angle and Relative Flow Angle 230

6.7.3 Required Prewhirl Profile 233

6.7.4 Choice of Design Velocity Ratio 237

6.7.5 Equivalent Jet Cross-Section 237

6.7.6 The Two Alternative Designs 239

6.7.7 Adaptor Design 246

6.8 THE VARIABLE PERFORMANCE COMPRESSOR EXPERIMENTS 247

6.8.1 The Experimental Rig 247

6.8.2 The Experiments 257

6.8.3 Observations 259

6.8.4 Results 261

6.8.4.1 Introduction 261

6.8.4.2 Improvement in surge margin 261

6.8.4.3 Drop in pressure ratio 265

6.8.4.4 Recirculation jet flow 265

6.8.4.5 Efficiencies 267

6.8.4.6 Velocity ratios 270

6.8.4.7 Mass ratios 273

6.8.4.8 Compressor power 273

6.8.4.9 Comparison of jet arrangements 273

6.8.5 Comments on the Experiments 279

CHAPTER 7 - THE TURBOCHARGED ENGINE SIMULATION AND EXPERIMENTAL INVESTIGATIONS 281

7.1 INTRODUCTION 281

7.2 THE SIMULATION RUNS 281

7.2.1 Simulation Results 285

7.2.2 Comments 292

7.3 THE EXPERIMENTS 293

7.3.1 Experimental Results 295

7.3.2 Experiments Near Surge 298

7.3.3 Comments 301

CHAPTER 8 - CONCLUDING REMARKS 304

8.1 THE AERODYNAMIC PREWHIRL INDUCING DEVICE 304

8.2 COMPARISON WITH ALTERNATIVE DESIGNS 305

8.3 CONTRIBUTION 311

8.4 PROBLEM AREAS 313

8.5 SUGGESTIONS FOR FUTURE WORK 314

REFERENCES 316

NOTATION

CHAPTER 3

U_1 = inducer velocity at mean radial station

C_{θ_1} = absolute tangential velocity at inducer inlet

U_2 = impeller peripheral velocity

C_{θ_2} = absolute tangential velocity at impeller

r = radial distance from axis

E = work per unit mass of air

CHAPTER 4

R = ratio of jet velocity to cross flow velocity

V_o = cross flow velocity

ρ_o, ρ_s = cross flow density

θ_j = initial jet ejection angle

θ = local jet trajectory angle

ρ = local jet density

v_j = initial jet velocity

u = jet velocity

h = linearising factor

ε_ξ = entrainment coefficient along trajectory

ε_ζ = entrainment coefficient normal to trajectory

r_j = jet radius at ejection

r = local jet radius

D = jet diameter at ejection = $2.r_j$

x,y,z = Cartesian axes

ξ,η,ζ = curvilinear axes

$\dot{m}_x$ = inlet mass flow

N = rotational speed

C_x = axial velocity

c = absolute velocity

U = peripheral velocity

ω = relative velocity

α = absolute flow angle

β = relative flow angle

θ = incidence angle to normal plane

CHAPTER 5

m = shape parameter in VIBE correlation

α = transformation coefficient in VIBE correlation

h = heat transfer coefficient

b = constant in SITKEI correlation

p = pressure

T_g = gas temperature

d_e = equivalent diameter

w = representative velocity

RF = relaxation factor

PR = pressure ratio

PRCR = critical pressure ratio for choked flow

$\dot{m}_E$ = net compressor flow, inlet flow, cross flow or engine flow rate

$\dot{m}_j$ = jet flow or recirculation flow rate

r_p = compressor pressure ratio

R = ratio of jet velocity to cross flow velocity

η_c = compressor efficiency

η_T = overall system efficiency

T_o = total temperature

γ = ratio of specific heats

C_p = specific heat at constant pressure

CHAPTER 6

D = ejection orifice diameter

x = distance of ejection point from compressor face

R = distance of ejection point from compressor centre-line

θ = inclination angle

ϕ = inclination angle

$\dot{m}$ = mass flow rate

N = rotational speed

Ω = rotational frequency

A = cross section area

θ = prewhirl angle, local jet trajectory angle

β = relative flow angle

c = absolute velocity

U,u = peripheral velocity

ω = relative velocity

θ_j = initial jet ejection angle

D, D_j = initial jet diameter

x,y,z = Cartesian coordinates (jet notation Chapter 4)

$\dot{m}_\varepsilon$ = net compressor flow, inlet flow, cross flow or engine flow

$\dot{m}_j$ = jet flow or recirculation flow

r_p = compressor pressure ratio

CHAPTER 7

$\dot{m}_\varepsilon$ = net compressor flow, inlet flow, cross flow or engine flow

$\dot{m}_j$ = jet flow or recirculation flow

r_p = compressor pressure ratio

R = ratio of jet velocity to cross flow velocity

m = mass ratio

CHAPTER 1

THE TURBOCHARGED DIESEL ENGINE

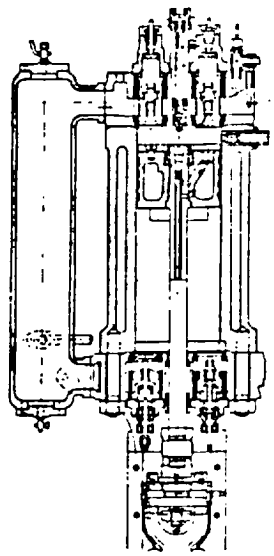
1.1 ON THE DEVELOPMENT OF SUPERCHARGED ENGINES

The advantages to be gained by increasing the mass of the air charge in the cylinder of an internal combustion engine were recognised by Rudolf Diesel himself.

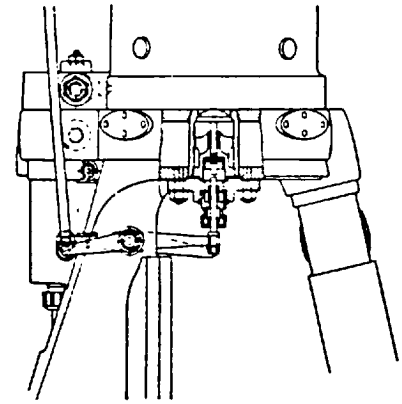
The history of supercharging diesel engines began when, in 1896, he built a research engine where the air inducted by the piston underside was subsequently led into the combustion space (Figure 1.1). This encapsulated for the first time the idea of supercharging, through which the indicator diagram would be widened and the mechanical efficiency increased, and dealt with the principle of the simplest form of mechanical supercharging. In the following decades mechanical supercharging was employed in various forms to increase the specific power of four and two stroke engines.

Superchargers that were mechanically driven either by the engine or by external power sources continued to exist after the development of the exhaust gas driven turbo-supercharger, in some cases in conjunction with it, the series connection of the two machines being one of the first forms of multiple stage supercharging. (Piston underside pumps and externally powered blowers still remain nowadays mainly in a few large 2-sc engines.)

The use of the waste energy in the exhaust gases to provide the motive power for increasing the charge air density, was first foreseen in a patent taken out in 1905

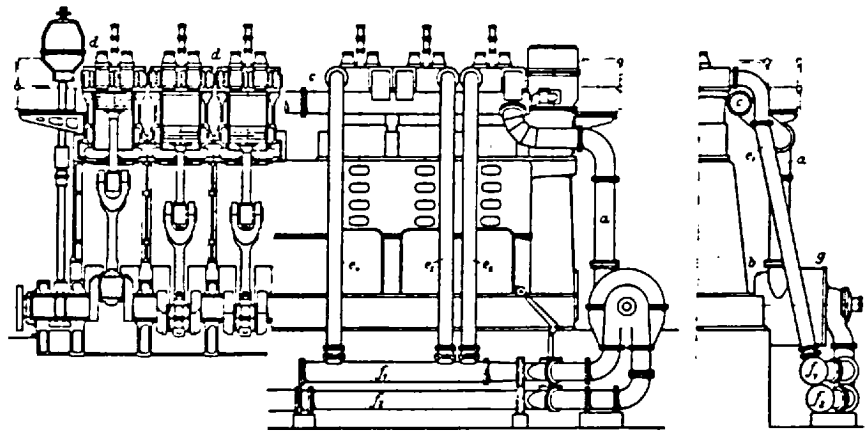


Cylinder of the experimental engine 250/400, with piston underside utilized as charge compressor (1896)



Cam-operated pressure valve of the experimental engine 250/400 (1896)

FIG.1.1 Rudolf Diesel's Research Engine (55)



Six-cylinder four-stroke diesel engine by SLM with Büchi turbocharging (1927)

FIG.1.2 SLM 6-Cylinder Engine (55)

by the Swiss engineer Alfred Buchi, where he proposed expanding the exhaust gases through a turbine to drive a supercharger.

The first experiments he did while employed by Gebrüder Sulzer A.G., in Winterthur between 1911 and 1914 with pressure ratios of up to 3.5. The first practical application of turbocharging was made in 1925, with the successful trials of the twin-screw ferries Preussen and Hansastadt Danzig. Each ship had two two-cylinder four-stroke turbocharged engines built by Vulkanwerft in Stettin under licence of Machinenfabrik-Augsburg (M.A.N.)(4)*. These installations were in the nature of a compromise with respect to Buchi's principles, as no cylinder scavenging effect could be achieved without altering the standard design of the engines, nevertheless a 78 per cent increase in bmep was achieved, thereby raising each engine's output from 1250 kW (1700 bhp) at 240 rev/min to 2953 kW (4015 bhp) at 317 rev/min. The exhaust gases from all cylinders of each engine passed along a common duct to a Vulcan built turboblower. These ships were a mile-stone in diesel engineering history when they entered commercial service in 1927 (2).

However the breakthrough in exhaust gas supercharging came with Buchi's famous Swiss Patent No. 122644 of 30 November 1925 about the so-called pressure wave process and the effectiveness of pressure fluctuations in the exhaust gas manifold. The first pulse-turbocharged engine subsequently ran in 1926 at the Schweizer Locomotiv und Machinenfabrik (SLM), Winterthur, using a Brown Boveri turbo-

---

*Numbers in brackets designate references at end of thesis.

blower. The four-cylinder four stroke unit was equipped with charge air aftercooling and developed 552 kW (750 bhp) at 250 rev/min. Further tests were made on a six-cylinder engine (see Figure 1.2) featuring a turbo-blower with two gas entries, witnessed by Professor Stodola from the E.T.H. Zurich (3). As a result of these successful investigations the Buchi system rapidly gained favour and many firms took licences from the Buchi-Syndicate (comprised of Buchi, SLM and BBC) and by 1927 35 engines were built using this system. From the earliest experiments power increases of 100 per cent over the naturally aspirated engine version were achieved for short time intervals. However because of structural constraints with the contemporary engines, the practical power increases were of the order of 50 per cent, corresponding to a bmep of 8.5 - 9 bar.

The first practical application of exhaust gas turbochargers in four-stroke Otto-engines and two-stroke Diesel-engines came much later (1).

The first ocean-going installation was the British vessel Raby Castle which went to sea in 1928. Her 8-cylinder four-stroke North East Marine Werkspoor engine had its service rating increased by 30 per cent by fitting a BBC turbo-blower. By 1929, 79 turbocharged engines had been built totalling 162 MW (220000 bhp) output.

In the 1930's great interest was taken in the Buchi system for rail traction. In 1933, BBC turbochargers began to be used on Maybach 12 cylinder lightweight engines developing 441 kW at 1400 rev/min for Germal railcars.

The Flying Hamburger prototype subsequently established a world speed record of 215 km/h in June 1939 (5).

Great advances in turbocharging have been made since the second World War. Turbocharging has proved to be the most successful method of reducing cost, space requirements and weight of diesel installations. It also contributed to improvements in specific fuel consumption, reduction in noise, and superior engine performance at altitude when compared with the naturally aspirated engine.

Today the single stage turbocharger with charge cooling, permits bmep values of 21 bar using current standard turbocharger compressors. These are limited to a maximum useful pressure ratio of 3.5 in continuous operation, by aerodynamic and stress consideration, when using present day commercially available aluminium alloys.

Already at pressure ratios above 3 the compressor isentropic efficiency falls, and the useful operating range narrows down, creating matching problems with consequent loss in engine flexibility. In addition, the low reaction single stage axial flow turbine employed very successfully in pulse turbocharging, begins to fall off in efficiency above expansion ratios of 2.5 (6).

It appears that bmep levels will continue to increase. Two stage turbocharging will probably find wider application with slow-speed two-stroke large engines, because the relative cost is lower and also the efficiency increase of the charging system (achieved through two stages with intercooling) will be more pronounced with

these engines.

With medium speed four-stroke engines, increases of bmep can possibly be achieved by single stage turbocharging, with further development of the current turbochargers in aerodynamics and materials. In the longer term two stage turbocharging would probably be employed for four-stroke engines as well, but this would mean a more extensive redesign of the engine (1).

The development trend in bmep of the high speed diesel engine over the last 30 years lags behind the medium speed engine. The reason can be explained by the relative late development of a suitable small turbocharger, its high cost in relation to the engine and difficulties in matching to obtain a satisfactory torque curve.

However, the combined effect of legislation on power to weight ratio, pollutant emission, and the high cost of producing a large range of engines, has led to the increasing use of turbocharging on automotive type diesels. Engine users for transport applications have tended to operate much closer to the development curve than operators of power generation stationary engines.

Before 1970 diesel designers were well ahead of users' demands, but since then users have been keener to take advantage of the higher rating possibilities (7). During the last 20 years progressively smaller diesel engines have been turbocharged. This followed developments in precision casting techniques for the turbine and compressor wheels, and heat resistant materials for the radial flow turbines.

Other developments included raising component efficiencies, dealing with bearing and design problems and with vane vibration (8). The introduction of these simpler, lighter, more compact, lower cost units, led to a considerable expansion of the turbocharger market, meeting the needs of the medium size truck engines. Recently a new generation of very small turbochargers has been introduced to match the flow requirements of passenger car size engines.

After half a century of commerical applications, continued development in turbocharging is seen as the principal means of maintaining the competitiveness of the diesel engine.

1.2 THE LIGHT DUTY DIESEL ENGINE

1.2.1 Introduction

In the era of relatively inexpensive fuel, the gasoline engine, with its low initial cost, from a long history of mass production, and its refined performance, was the obvious choice in the light duty engine class for passenger cars and light commercial vehicles. The recent emphasis on powerplant efficiency stemming from the escalation of fuel costs, and the current and proposed legislation on engine emissions, resulting from the increasing public concern on environmental pollution, has rendered the "low emissions" gasoline engine (i.e. with emission control appendages) less attractive economically. In the light of these developments the economic viability of alternative powerplants has been reconsidered.

The lightweight high speed diesel engine has long been used round the world in applications where fuel economy and durability are of prime importance. A number of factors however, related to consumer acceptability, tend to inhibit the wider use of the diesel engine for passenger cars, where the potentially largest market for lightweight diesels exists.

1.2.2 Comparison with Gasoline Engines

Comparisons of the characteristics of the current lightweight diesels and gasoline engines of similar power is as follows (9 - 16).

Cost: First cost is higher for the diesel and also for its auxiliary components, mainly the fuel injection equipment. Stronger driveline components may be needed, if the engine speed is lower.

Maintenance: Periods between overhauls are approximately twice as long, but the injection equipment maintenance is expensive. The absence of ignition systems reduces maintenance as well as increasing reliability. Engine durability is higher. Oil changes are more frequent and oil with greater dispersant and anti-corrosion properties is needed.

Fuel economy: The prime advantage of the diesel engine is its efficiency with (typically) 30 per cent better fuel economy than the petrol engine.

Power to weight ratio: The diesel is heavier (and bulkier) than the equivalent gasoline engine. The installation weight, with heavy duty starter and battery is also

greater.

Noise: The diesel is generally noisier but similar noise levels can be achieved with proper design, although this might add to the total package cost.

Smoothness: (Vibration and Torque recoil) Since the diesel operates unthrottled, its cyclic torque fluctuation is not very load dependent, unlike the petrol engine and the greatest difference is at low speed idle and light load. Improvement in engine mountings is possible.

Drivability: Hot drivability can be similar but the diesel has superior cold drivability.

Starting: In the lightweight diesel, starting aids are normally used during cold starting which have an inconvenient delay in operation.

Manufacture: Constructional similarities mean that the same production lines can be used but closer control of tolerances is needed for diesel engines.

Exhaust emissions: The diesel has better overall emissions characteristics than the untreated gasoline engine. Because of the preferred torque curve for passenger cars, smoke is problematic at low speeds and high loads. Particulate emissions are much higher, due to the eterogenous combustion. Odour emission is generally higher for the diesel.

Many of the above diesel characteristics can be improved using existing technology, and any such improvement can only strengthen the case for the diesel.

1.2.3 Combustion Chamber Types

Diesel engine combustion chambers may be classified into one of two types - open chamber and divided chamber. In the first, most extensively used in truck and larger engines, fuel is injected directly into the space above the piston. (direct injection, D.I.)

Divided chamber engines employ injection into a flask shaped chamber, into which part of the charge has been compressed, with a restriction between the prechamber and the main chamber. (indirect injection, I.D.I.)

Swirl chamber engines are a special form of prechamber engine in which the entrance to the prechamber is so arranged as to give an intense swirling motion to the air charge in the prechamber. A larger portion of the air charge is compressed into the swirl chamber than would be the case with a prechamber; 50 per cent as against 25 per cent or so, and the restriction between the swirl and main chamber is less pronounced than for the prechamber design.

The advantages of the swirl chamber diesel versus the open-chamber type are as follows (17):-

A. Higher speed (and bmep, with less smoke) is feasible (and therefore higher horsepower).

1. Higher volumetric efficiency.

(a) From larger intake and exhaust valves (more room for the valves since nozzle is at the side).

(b) From lack of induction swirl.

2. Lower ignition delay.

(a) From heated chamber.

3. Higher secondary swirl.

(a) From swirl chamber blowoff.

B. Less machanical stress and noise.

1. Lower rate of pressure rise and lower maximum pressure in main chamber.

C. Less maintenance.

1. Self-cleaning pintle nozzle.

2. Less mechanical stress.

D. Wider range of fuels (can serve as a multi-fuel engine with minimal changes).

E. Smoother and quieter idling.

F. Reduced nitrogen oxides.

The primary disadvantage of the swirl chamber diesel is a greater sfc than the open chamber type.

A. Higher sfc (but may be lower with emission controls).

1. Greater heat loss to coolant.

(a) From the flow of combustion gases through the throat (may lead to heat cracks in cylinder head and sealing problems).

(b) From higher surface-to-volume ratio.

(c) From the higher secondary swirl (may decrease lube-oil life, or piston and ring life).

(d) Retarded combustion.

2. More energy in the exhaust gases (may decrease valve life and encourage cracking and sealing problems in the exhaust manifold.

Indirect injection systems are used on almost all small automotive diesels because despite its higher thermal efficiency the D.I. system is not suitable. Combustion of

the D.I. system is rougher and not efficient at high speeds and difficulties can be encountered in starting D.I. engines with small cylinders.

1.2.4 Performance Improvement of small Diesels - Turbocharging-Problems

A naturally aspirated engine is inferior in terms of torque, drivability and noise, when compared with a naturally aspirated petrol engine of the same capacity. For light duty applications the prime requirement is obtaining good performance over as wide a speed range as possible, good transient response, good part load performance, low smoke emission, low noise and low maximum cylinder pressures, without excessive cost, i.e. the emulation of the equivalent petrol engine without sacrificing the fuel economy advantages of the diesel engine (18).

A meaningful increase in power and torque for the diesel engine can be realised either by increasing the swept volume or by turbocharging. The swept volume can be increased either by increasing the displacement of individual cylinders or by increasing the number of cylinders. For passenger car use the second choice is preferable considering vibration, wear and fuel consumption. However this will result in a further increase in weight and cost (19, 20).

Turbocharging offers a means of substantially improving the specific power of the diesel without penalising fuel economy. The increased air intake density allows increased power. The frictional losses increase only slightly and thus improved brake power is also possible, provided the

boost process is reasonably efficient. For economic reasons the turbocharged engine must be rated at least 30 per cent above the power output of its naturally aspirated version, and at the same time, preserve a workable torque curve shape (21).

The problem of turbocharging the automotive engine is to achieve high b.m.e.p. at low speed. In most automotive applications (except where a torque converter is employed in the transmission train) the turbocharger has to contend with a wide speed and load range. For a small high speed diesel engine the speed range would be at least 4:1. Limits are imposed bot h from the engine (thermal and mechanical) and the turbocharger (aerodynamic and mechanical). At high engine speeds and loads the available energy for the turbine is high, hence the high pressure ratio subsequently developed by the compressor, introduces maximum cylinder pressure as a controlling factor.

The maximum acceptable cylinder pressure will be severely limited in the case of the light duty engine. As the engine speed falls the energy availability is reduced. As a result, and also because the compressor efficiency decreases at low speeds, the boost pressure falls, reaching a condition where output is smoke limited.

A more severe problem, especially with small engines at low speeds, is that the airflow demand is such that the lower limits in aerodynamic performance of the compressor are reached. This may also occur at medium speeds and high loads. At higher engine ratings, choking of the compressor

passages or turbocharger speed limits may be reached at high speeds. Turbocharger response to changes in engine operating conditions may also be a problem in certain installations.

CHAPTER 2

THE CENTRIFUGAL COMPRESSOR

2.1 INTRODUCTION

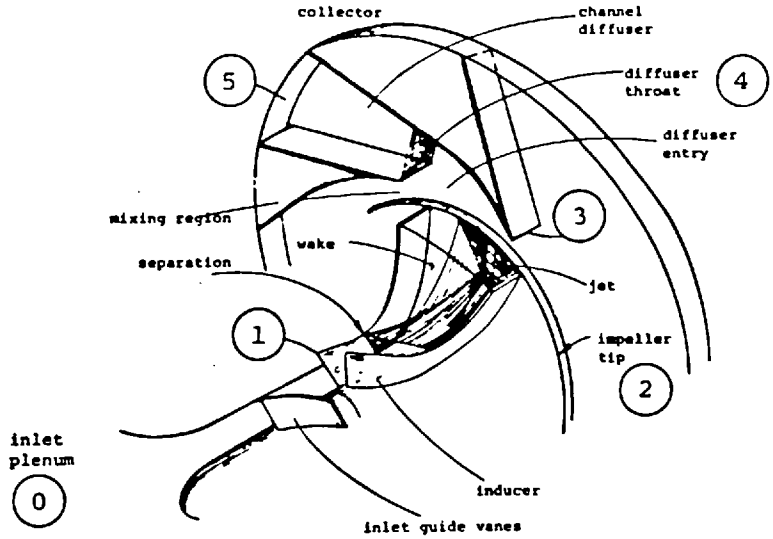
The centrifugal compressor enjoyed some technical attention during the early days of aircraft gas turbine, but was subsequently superseded by the axial compressor.

The advent of small gas turbines and the almost universal use of centrifugal compressors in supercharging reciprocating internal combustion engines has revived the interest in these flow machines, which have advantages such as smaller length, efficient operation over a wide speed range, are not liable to loss of performance due to deposit buildup etc.

2.2 DESCRIPTION - COMPONENTS

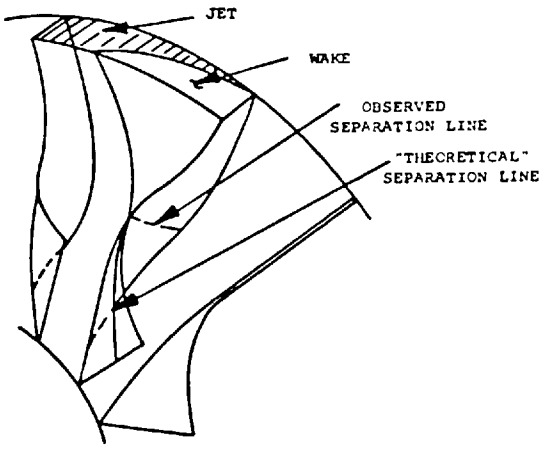
A centrifugal compressor consists essentially of a rotating impeller followed by a diffuser. The various elements of a centrifugal compressor are shown in Figure 2.1 (from ref.22).

Air is drawn from the inlet plenum, through the inlet guide vanes (if applicable), into the eye of the impeller. At the entry to the impeller the flow is turned into the direction of motion of the impeller blades by the inducer. The function of the impeller is to increase the energy level of the fluid by whirling it outwards thereby increasing the angular momentum of the fluid. Both the static pressure and the velocity are increased within the impeller. The purpose of the diffuser is to convert the kinetic energy of the fluid leaving the impeller into pressure energy. The diffuser can be either of the parallel wall (vaneless) type or



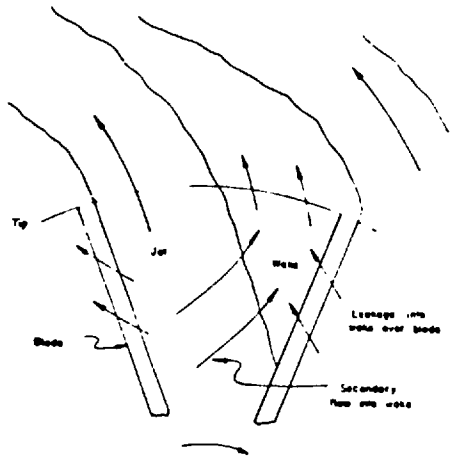
SCHEMATIC OF COMPRESSOR STAGE FLOW REGIONS

FIG.2.1 The Elements of a Centrifugal Compressor (22)



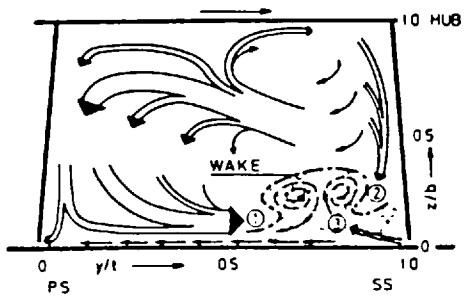
SCHEMATIC OF SEPARATION LINE GEOMETRY

FIG.2.2 The Jet-Wake Pattern in the Impellor Channel



SCHEMATIC OF SEPARATED FLOW MODEL

FIG.2.3 The Jet-Wake Pattern in the Impeller Channel (22)



Basic secondary flow pattern in the radial part of the centrifugal impeller (meas. area IV)

FIG.2.4 The secondary Flow Pattern in the Impeller Channel (23)

incorporate some form of vanes or channels. Outside the diffuser is a scroll or volute to collect the flow and deliver it to the outlet pipe.

The flow in the centrifugal compressor is most complicated, as it occurs in rotating coordinates, has major viscous phenomena, is usually separated and is often unsteady.

2.3 THE FLOW PATH - MORPHOLOGY OF FLOW - DESIGN

2.3.1 Inducer

The inducer of a high performance impeller usually produces the largest portion of internal diffusion within the impeller, so good impeller performance will depend essentially upon good inducer performance.

Many inducers are designed based on axial compressor rotor experience. Although this tends to produce long impellers, many times the inducers perform better than their axial progenitors. It is speculated that the radial impeller following and coupled to the inducer serves to stabilise separation in the inducer (22). Other contemporary designs employ fairly short inducers and there seems to be a tendency towards the mixed flow type, as the flow dynamics within the impeller are better understood.

2.3.2 Impeller

The first function of the impeller is to add necessary work to the flow, i.e. to increase the stagnation enthalpy.

There are three kinds of losses which impair the efficiency with which the work process is accomplished

- disc and shroud friction
- internal flow irreversibilities

- discharge mixing losses.

The last two are more serious and arise from fluid dynamic phenomena not yet thoroughly understood. The second function of the impeller is to diffuse the relative flow entering its inducer, since the inlet kinetic energy is lost irreversibly if there is no relative diffusion within the impeller. The diffusing ability is adversely influenced by the curvature of the impeller passages.

The coriolis force tends to stabilise the boundary layers on the suction, i.e. trailing side of the impeller blades. This stabilisation suppresses turbulence and indeed may laminarise the boundary layer. Consequently, momentum exchange with the through flow is retarded and the boundary layer becomes weak in its ability to tolerate diffusion without separation. The flow separation usually commences in the range of most extreme channel curvature (superposition of the meridional turning to radial and the blade shape).

Measurements by Eckardt (23) showed a reduction of turbulence intensity immediately before separation onset: "After a steady increase of fluctuation intensity in the axial inducer, possibly caused by an accumulation of dumped tip clearance material, the intensity is drastically reduced, corresponding to turbulence stabilisation when the channel curvature and Coriolis forces become increasingly effective. Aft of the designated separation onset there is then a rapid fluctuation intensification in the highly pulsating wake regions" (23).

On the pressure, i.e. the driving side of the blade, the effect is reversed and the boundary layer is destabilised by Coriolis forces. This enhances mixing and momentum exchange with the throughflow. Consequently, the pressure side boundary layers are invigorated.

After separation onset there is a rapid growth of the wake area in the shroud-suction side corner of the flow channel. This effect is presumably in strong interconnection with the strengthening secondary flow intensity. While secondary vortices peel the b.l's off the channel walls, feeding low energetic fluid into the wake, system rotation and curvature effects suppress turbulent mixing at the jet/wake shear layer; so the distorted flow is preserved and enhanced up to the impeller discharge.

Figures 2.2, 2.3 (22) show the jet/wake configuration while Figure 2.4 (23) shows the secondary flow pattern developed inside the impeller channel.

The flow separation impairs the diffusion potential and the highly distorted jet/wake velocity pattern at the impeller discharge causes a further reduction in efficiency due to mixing losses.

2.3.3 Diffuser

A wide variety of diffusers are employed with centrifugal impellers. These may be divided into two classes depending on whether the principal objective is wide range or high stage efficiency (22).

The high efficiency class includes:

- Vaneless plus cascade (1-3 row)
- Thin vane: single or multiple row

- Contoured vane: single or multiple row
- Vane island: curved or straight passages
- Pipe diffuser: circular or non-circular cross-section
- Rotating wall vaneless plus vaned diffuser.

The wide range class includes:

- Dump collector
- Vaneless diffuser: with dump collector or scroll or scroll plus discharge diffuser

Only the wide range class will be considered here.

2.3.3.1 Vaneless diffuser

The vaneless diffuser which, in its simplest form is defined by two parallel walls in the meridional plane, is widely employed in (turbo) superchargers and process compressors because of the broad operating range and acceptable efficiency at low pressure ratio it offers. Such range is often essential in order to match a given design to a wide variety of applications (25). Further the vaneless diffuser is less expensive than a vaned diffuser and tolerant to erosion and fouling. Also in the vaneless diffuser a supersonic flow can diffuse to subsonic flow without the possibility of shocks.

Some of the factors which influence the pressure loss in a vaneless diffuser are: (29)

1. The formation of the boundary layers on the side walls of the diffuser. The momentum loss in these boundary layers is a direct cause for pressure loss (wall friction loss).
2. The unsteady flows at the entrance of the diffuser caused by the compressor blade wakes which extend into the entrance section of the diffuser. The mixing of these flow

regions with different velocities and flow angles is a source of pressure loss.

Backflow can occur from the vaneless diffuser into the impeller, especially when the impeller meridional velocity distribution is badly defective on one wall. However, backflow into the impeller is less frequent with vaneless diffusers than with vaned diffusers, because of the absence of local pressure disturbances caused by vane pressure loading.

3. The unsymmetric flow with respect to a midpoint between the two diffuser walls. In experiments (24) it was found that such unsymmetric flows show in general a large skewedness which may result in a pressure loss.

4. The exit loss of kinetic energy.

The friction loss increases as the direction of swirl comes closer to the circumferential direction or the flow rate decreases, while the exit loss increases with the flow rate. In the case of vaneless diffuser with small exit to inlet radius ratio, the exit loss is large and the friction loss is small and the pressure loss in the diffuser increases with the flow rate. In the case of diffuser with a large exit to inlet radius ratio, the friction loss is significant and the pressure loss increases when the flow rate decreases.

2.4 CENTRIFUGAL COMPRESSOR PERFORMANCE

The performance of a compressor is normally specified by curves of pressure ratio against mass flow for various fixed values of rotational speed. Efficiency contours are usually superimposed. The compressor characteristic

curves are experimentally obtained by progressively throttling the discharge flow while maintaining constant rotational speed. Figures 2.5-2.8 show typical examples of compressor performance maps. The surge line is the locus of the points defining the lower limits of stable operation of the compressor, on each characteristic.

The position of maximum delivery at a particular rotational speed is referred to as the choking limit. The surge free flow range (stable range) is defined as the ratio of maximum or choke flow to the surge flow along a constant speed line. A specific operating point on the compressor map is selected and the aerodynamic design criteria are applied on this point which is called the design point.

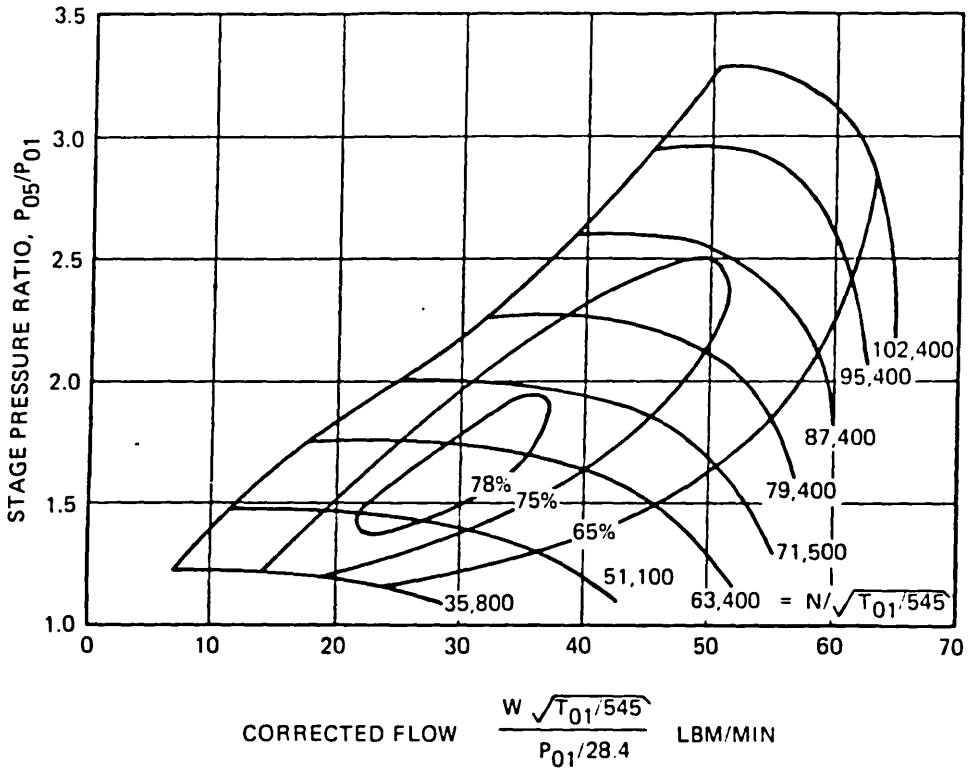
The equilibrium running points are the operating points of a system incorporating the compressor, on the characteristic curves. The locus of these points for a series of speeds is the equilibrium running line or operating line. This indicates whether the machine operates within the stable range and shows the position of the operating points relative to the efficiency contours, Figure 2.9.

2.5 OFF DESIGN PERFORMANCE

2.5.1 Introduction

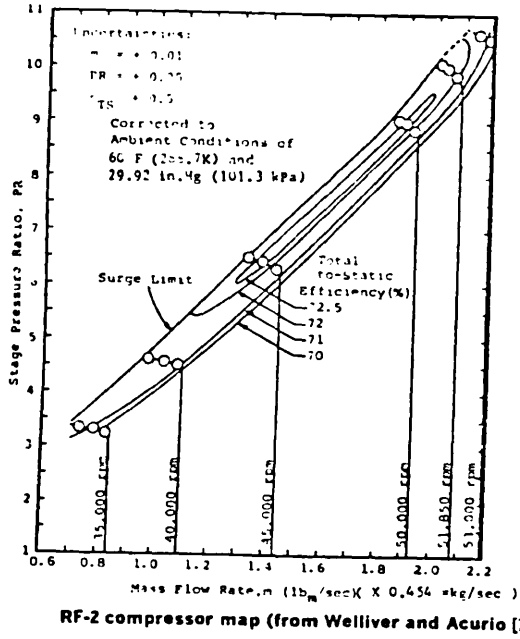
Most centrifugal compressors demonstrate potential instability regions. When the working fluid is compressible, these regions can lead to a breakdown of the flow process.

As the flow through a compressor is throttled from the design point to lower flows the steady flow pattern eventually becomes unstable.



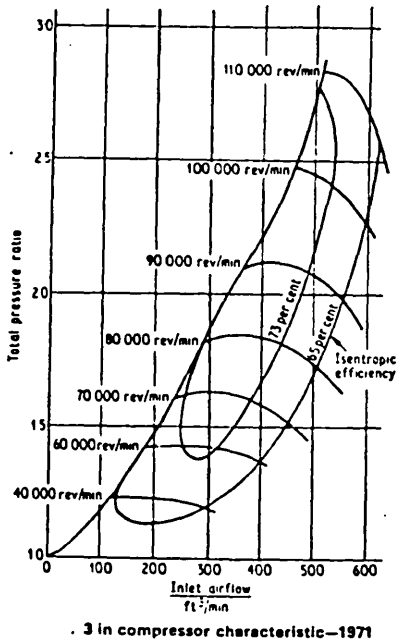
Model TV61 compressor performance map

FIG.2.5 AIRESEARCH TV-61 Compressor Map (25)
(Turbocharger Type)



RF-2 compressor map (from Welliver and Acurio [7])

FIG.2.6 BOEING-AAVLABS RF2
Compressor Map (29)
(High Performance)



. 3 in compressor characteristic—1971

FIG.2.7 HOLSET Compressor
Map (8)
(Turbocharger Type)

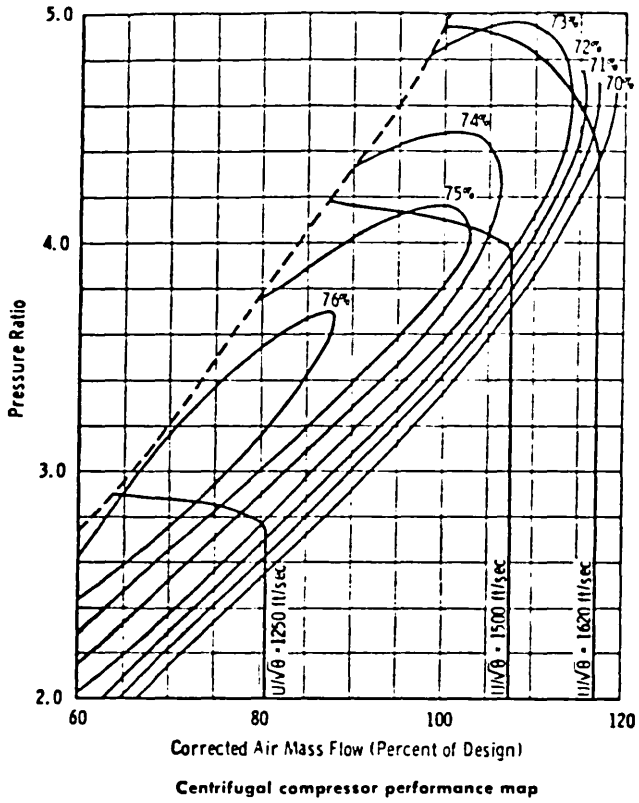


FIG.2.8 Gas Turbine Compressor Map (65)

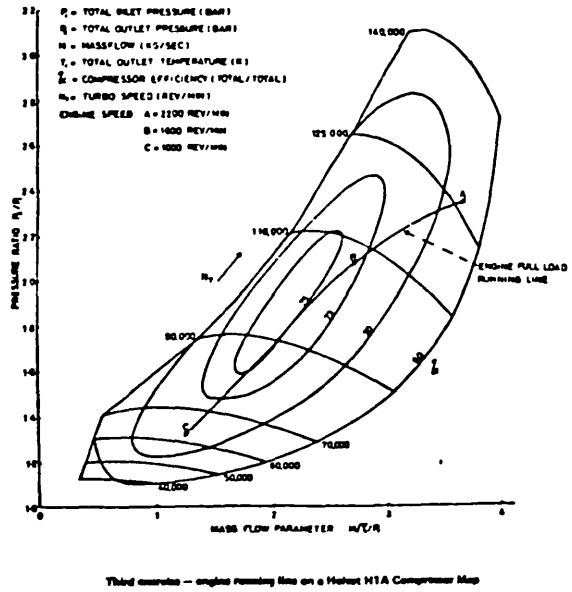


FIG.2.9 The Engine Equilibrium Running Line on a Compressor Map

Unstable operation of a compressor can be broken into two aspects;

- system instability (surge);
- stage instability (stage stall).

2.5.2 Surge

Surge is what is commonly observed on the test stand or in an application when the system demonstrates large flow oscillations. Sometimes these oscillations occur randomly, especially at inception of the instability encountered upon reducing the mass flow through the stage by throttling.

Surge must be regarded as a typical self-excitation of a dynamic system, when a driving source and a responding system can be recognised.

The driving source is normally the stall of the stage but it may be powerfully influenced by feedback from the oscillating system. The system oscillation involves capacitances, inductances and resistances (by electrical analogy), the former two determining frequency and the latter determining damping and thereby amplitude.

The sequence of events taking place during one of these oscillations can be described as:

1. A rapid drop in compressor flow at roughly constant pressure to negative flow.
2. A slow blowdown process where the compressor acts as a very high loss throttling device for the low velocity reverse flow.
3. A rapid change of mass flow at nearly constant pressure to a value associated with unstalled operation at large negative incidence on the compressor blades.

4. A slow repressurisation of the plenum during which the compressor mass flow changes quite gradually and the compressor operating point essentially moves along the steady state characteristic finally reaching an axial velocity at which the blades stall, the compressor is no longer able to deliver the necessary pressure rise, and the cycle starts all over again (28).

There are usually two different kinds of surge (29, 30, 31). Sometimes the operation of a centrifugal compressor becomes rough and unstable before reaching a distinct surge point.

That milder disturbance occurs at a higher flow rate and usually does not preclude operation of the compressor.

Sometimes the transition region between the stable operation and surge is characterised by erratic pulsations of small magnitude (31). Further flow reduction can cause distinctly audible surge, with catastrophic breakdown where the flow reverses entirely through the stage, from discharge collector to inlet.

Large alternating dynamic forces are created within the compressor as a result of the increased pressure and mass flow oscillations.

Violent changes occur, especially in the diffuser throat pressure. These violent pressure variations create the noise traditionally associated with surge; mechanical damage may also result. The reverse flow through the impeller produces a violent torque reversal which may endanger the rotating elements.

The difference between mild and true surge tends to diminish with increasing Mach number, and single stage compressors with transonic inlet conditions often do not exhibit a mild surge condition (33).

Toyama et al (29) describe the events leading to a surge cycle as follows: "When the compressor is started up with wide open throttle, it runs very stably with high tone noise. As the operating point moves towards the surge line, the high tone noise disappears and the noise level becomes a little lower. As the operating point approaches the surge line the noise roughens. With further closing of the valve surge starts. The surge is identified by a "womp" noise emitted for a very short period. All instruments show perturbed signals at this moment, but return to their original values in a few seconds. Note especially that a "steady" condition follows this until the next surge.

When surge first occurs at the "surge point" the interval between surges is long (1-2 mins.) but the more the throttle valve is closed the shorter the interval becomes". A hysteresis effect may be observed, where the discharge throttle must be opened further than the minimum normal stable flow position, to come out of a surge cycle.

Since more than one surge condition is possible in centrifugal compressors it is difficult to strictly identify surge as the operating condition where audible evidence of unsteady flow occurs, exactly because of the ambiguity of this definition. This is reflected by the fact that in compressor performance maps the surge line lies usually where the test operator becomes "alarmed". A surge

condition may not be audible or reflect increased vibration for a given compressor on ambient suction, whereas the same compressor may behave entirely differently with high suction pressure conditions (33).

Compressor surge in gas turbines is more readily identified since a surge condition will normally make the engine inoperable either on turbine overtemperature shutdown, flame out or excessive vibration (33).

2.5.2.1 Definition of Surge

Surge may be defined as a self induced vibration of a system, including a compressor, resulting in large amplitude oscillations of the total flow through the compressor and a periodic variation of pressures and velocities, due to some inherent instability in some part of the operating range of the compressor. For this condition to exist, the slope of the compressor characteristic must be positive, i.e. the pressure ratio to increase with increasing flow, and a time interval must exist between a change in flow condition in the compressor passages and the static pressure adjustment in the external pipes (27,31,32,33,35).

Surge oscillations are possible only when the mechanical energy input from the compressor is greater during oscillatory flow than during a (mean) steady flow, and this can occur only if the characteristic is somewhere positively sloped so that high mass flow and high mechanical energy input per unit mass go together (27).

2.5.2.2. Prediction of Surge

In the design of a centrifugal compressor the accurate prediction of range from design point to the surge line, is second in importance only to the prediction of efficiency. Despite this importance, requisite design tools are inadequate. No widely accepted means are available for the designer. Using correlations ofpast experience may be adequate for replication of previously developed designs but is inadequate for the evolution of new designs (22).

Most of the prediction methods employ the compressor static operating curve (characteristic) and the geometry of the external system. The general character of the surge cycle will be a function of these variables and the pressure time relationship during the surge process may be computed (36,57,58).

Since the frequency and amplitude of the oscillations and effectively the surge point depend on the parameters of the system in which the compressor operates, the same compressor will most probably surge at different points in different installations (31).

The apparent paradox that compressors sometimes demonstrate the same nominal surge line on test stands as they do on engines can be explained since it is shown (57) that the amplitude of oscillations is primarily dependent on the compressor and throttle characteristics and relatively insensitive to discharge volume (26).

The above mentioned linearised analyses are restricted to infinitesimal departures from an equilibrium situation and are fundamentally unable to describe the large amplitude pulsations encountered during a surge cycle.

Other methods use non-linear modelling to examine the time dependent behaviour of a compressor system subsequent to a perturbation from steady operating conditions (27).

Although there is considerable ambiguity for predicting surge, the choke points of impeller and diffuser may be predicted with acceptable accuracy. Consequently a conservative component matching process is to position the design point relative to choke and to initially accept whatever falls to the left side of the design point (if anything) as margin (33).

2.5.3 STALL

2.5.3.1 Definition of Stall

Flow ranges for centrifugal compressors and the broadness of the efficiency islands are dictated by the stalling characteristics of the impeller and the diffuser which are intrisically controlled by the blading contours and operating Mach numbers (33).

Stall in the impeller or the diffuser is the flow condition when these elements cannot stably sustain their operations.

In rotating stall one finds from one to several cells of severely stalled flow rotating around the circumference although the annulus averaged mass flow remains constant in time once the pattern is fully developed (27).

2.5.3.2 Fluid Dynamic Considerations

2.5.3.2.1 Diffuser (vaneless)

The flow in a vaneless diffuser is seldom symmetric with respect to depth at the inlet.

At a small flow rate it has been observed (38) that a reverse flow occurs alternatively on the diffuser walls and further downstream the reverse flow disappears on both walls. By studying stability of inviscid uniform swirl flow in parallel wall vaneless diffusers Jansen (37) showed that inward swirl flow is unstable and rotating stall is induced in it by a small disturbance.

In normal operating conditions, the pressure loss in a vaneless diffuser varies continuously with respect to the flow rate. When rotating stall occurs, the wall friction force, as well as the exit loss of the K.E., varies with time due to the rotation of the non-axisymmetric distribution of the velocity, but the time-averaged values do not change much. Hence the time averaged pressure rise may not change much, since the radial pressure gradient in the diffuser is mostly balanced by the centrifugal force acting on the swirl flow.

As the flow rate is reduced, the zone of inward swirl flow grows, and finally reaches the exit of the diffuser, the fluid in the scroll or discharge plenum is sucked back into the diffuser, and the diffuser stalls. As a consequence the system may surge (35).

In (39) it was attempted to correlate the diffuser inlet flow angle with the stalling behaviour of the compressor. The parameters which influence the critical diffuser inlet flow angle are: (39)

1. The ratio of the width to the inlet radius of the diffuser.
2. The ratio of exit radius to inlet radius.
3. The distortion of the inlet main flow.

4. The inlet Mach number.
5. The Reynolds number.
6. The inlet B.L. thickness.
7. The variation of diffuser width w.r.t. radius.

It is reported that the distortion of the velocity distribution at the diffuser inlet does not significantly influence the critical flow rates for rotating stall (35).

In cases of narrow diffusers with large radius ratio it is expected that as the flow rate is reduced, rotating stall occurs first and the diffuser stalls later.

However, in a diffuser with a small radius ratio or with large width ratio, rotating stall may never occur, providing the distortion of the diffuser inlet flow is not severe (35).

If the boundary layers fill up the diffuser passage, there is a complicated momentum exchange between them, which prevents the flow from reversing. Hence narrow width diffusers are less susceptible to reverse flow (39)(but have higher friction losses).

Parallel wall diffusers, typically exhibit an unstable or positive slope pressure recovery flow characteristic since their frictional losses increase with decreasing flow.

Generally compressors with vaneless diffusers can exhibit a "mushy" stall characteristic with an ill-defined surge line precipitated by marginal impeller and vaneless diffuser stabilities. In contrast compressors with vaned diffusers usually have a clearly defined surge line since the vaned diffuser stall tends to predominate (33).

2.5.3.2.2. Impeller-inducer

The stalling limit of a centrifugal impeller is sometimes experimentally decided by testing the impeller with a vaneless diffuser, assuming that since the vaneless diffuser is normally suitable for wide range of flow rates, it is not the cause of surge (35).

Rotating stall in the inducer leads to unstable operation and low efficiencies in the stage. The flow disturbances originating in the inducer may be responsible for poor aerodynamic conditions leaving the impeller which can lead to incipient stall in the diffuser.

The presence of inducer rotating stall in the tested compressor is indicated in (30,40).

In (ref.41) a reversed flow was observed at lower flow rates within the inlet duct, the inducer and the impeller channels, as well as along the shroud casing. The generation of the reversed flow was attributed primarily to a separated flow at the inducer inlet leading edge at lower flow rates. A three-dimensional eddy appeared within the inducer channel at lower flow rates. The eddy became stronger towards the shroud suction side, governing the flow pattern within the compressor channels at lower flow rates.

2.5.3.3 Prediction of stall

Improved analytical 3-D flow modelling of the processes within the compressor will provide the ultimate prediction tool for off-design performance predictions.

In the meantime several simplified models or correlations have been proposed.

(a) Impeller

The impeller performance parameters involved in the correlations proposed include:

Inducer RMS relative inlet angle.

Impeller Mach numbers.

Impeller tip absolute flow angle.

Impeller relative velocity ratio.

Impeller diffusion factor (33,34).

(b) Diffuser (Vaneless)

An analysis to calculate the flow behaviour of a vaneless diffuser assuming axisymmetric flow w.r.t. the diffuser walls is presented in (24). However the assumed situation seldom exists.

Ref.38 proposes a method to evaluate the velocity distribution assuming the flow is not symmetric using momentum integral equations.

2.5.4 Interrelation of Stall and Surge

The dynamic behaviour of the stage must be considered in defining the true surge behaviour of a system.

The frequency of surge oscillations (i.e. the system resonant frequency) is typically one order of magnitude less than the frequency of the passage of rotating stall cells (26,27). In fact during a surge cycle the compressor may pass in and out of rotating stall as the mass flow changes with time. Because of the frequency difference there is no fundamental connection between stall propagation and surge, except that the falling pressure characteristic which is necessary for surge excitation may originate in the stall propagation regime, but there is little possibility of the stall propagation acting as a driving force for surge (26).

Diffuser or inducer stall can occur in the unstable branch of the compressor characteristic or even in the stable branch. When this stall is oscillatory it will cause instability and could be interpreted to initiate surge if it occurs in the unstable branch. This however may only be coincidental (29, Balje, disc.).

Concerning the total pressure rise versus flow-rate characteristic curve, an impeller with radial blades has a weak negative gradient. If the impeller is combined with a large radius-ratio vaneless diffuser the characteristic curve of the compressor as a whole may have a positive gradient and the compressor may run into surge in spite of the fact that neither the impeller nor the diffuser stalls.

In the case of a low pressure ratio compressor however, the compressor often runs stably at an operating condition where the characteristic curve has a weak positive gradient. In the case of an impeller with backward leaning blades, the characteristic curve of the impeller has a large negative gradient in spite of the opposing trend of pressure loss in the diffuser.

If there are some kinds of stabilising factors in a system, the system probably does not run into surge unless either the impeller or the diffuser stalls and the pressure ratio of the compressor decreases discontinuously with the flow rate. If this is the case, the surge limit of a compressor system may be used to determine the stalling limit of either the impeller or the diffuser (35).

Generally, oscillatory flow phenomena will precede surge when the negative dynamic resistance is caused by

progressive stall. An oscillatory flow is frequently observed when the total compressor system is completely stable. The overall dynamic resistance is positive even though local "circuit elements" may have a negative dynamic resistance.

A growth of stall intensity as the flow decreases is needed to develop the necessary negative dynamic resistance (29, Bullock disc.). In multistage compressors it is possible for an isolated stage to operate in stall without the overall compressor surging (33).

Many centrifugal compressor designers tend to agree that increasing flow degradation in the diffuser triggers massive flow reversal through the stage and that the diffuser inlet flow is most sensitive and critical for surge. However there might be other contributing causes such as the flow in the inducer initiating or helping initiate surge (29). In particular surging at the low speed operation of a well designed compressor is usually triggered by stalling of the flow near the inlet; surging at high speeds results from stalling of the flow near the outlet (29 Bullock disc.).

2.5.5 Off-Design Testing Methods

Impeller stall is normally determined audibly and may or may not trigger system surge dependent upon complete system stability. At low speeds and ambient suction, impeller stall may not be audible (34) but instability in the discharge pressure and fluctuations in the inlet temperature can provide imminent stall indications. The use of sensitive microphones in the inlet and pressure transducers along the impeller shroud help to define more clearly

impeller stall (34).

Impeller testing with vaneless diffuser configurations may or may not, at ambient suction conditions, exhibit an audible surge or sudden reduction in head; thus more positive instrumentation techniques are required to determine instability (33). An observer equipped with steady state discharge instrumentation would not detect the details of the process but observe time averages only. As a result of recording time-averaged pressure readings a gradually stalling compressor may appear as a suddenly stalling one. Unobtrusive instrumentation is essential since the slightest disturbance will affect the behaviour of the unstable flow situation.

2.5.6 Preventive Methods - Design Techniques

In order to obtain the desired flexibility, the range of the compressor, indicated by the ratio of maximum flow to minimum flow must be as large as possible. The range of centrifugal compressors rapidly decreases as the impeller tip speed is increased.

An extension of the surge free range of operation of centrifugal compressors is therefore an important part of compressor research (31). If rotating stall is encountered it may not be possible to return to an unstalled condition merely by opening the throttle because of hysteresis effects. In this situation the only way to come out of stall may be to decrease rotational speed considerably resulting in a sizeable loss of pressure ratio. Also because of the extremely low efficiencies associated with the presence of rotating stall, and the large stresses resulting from the

unsteady flow field, operation for any substantial length of time in this mode, may have adverse effects on blade life (27). Also the low flow rates obtained may result in serious consequences in other parts of the system (large temperatures in combustion chamber, and turbine, incomplete combustion etc.) (27).

On the other hand if surge occurs, the transient consequences such as inlet overpressures can also be severe. However, the circumstances may be more favourable for returning to unstalled operation by opening either the throttle or internal bleeds, since the compressor can be operating in an unstalled condition over part of each surge cycle (27).

The most effective means of delaying the occurrence of surging or reducing the magnitude of the surging pulsations is to maintain a negative slope or reduce the positive slope of the characteristic curve (31). The ideal means of accomplishing this end is to locate and eliminate the cause of flow breakdown, which produces the positive slope of the characteristic curve. Unfortunately attempts to correct the flow breakdown at low flows often adversely affect the upper range of operation to such an extent that the overall performance is less satisfactory (31).

The volume of the system has a definite effect on the surge point. In general the greater the volume of any part of the system, the slower will be the response of the related pressures to changes in the mass flow rate.

In as much as the volume of the compressor unit is

small compared with that of the entire system the surge free range probably could be extended by increasing the effective capacity of the compressor unit or decreasing that of the auxiliary piping. All such investigations should be made on the actual installations with which the compressor is to be used. These modifications would either make the response of the compressor unit to small variations in mass flow slower, or speed up the response of the external system. If the compressor and its associated inlet and discharge volumes can be decoupled, the mechanism of surge could be inhibited by blocking the interaction (22). These means of changing the surge point would be applicable only when the positive slope is small compared with the slope of the throttle characteristic curve. If the slope changes abruptly little would be gained (31).

Many compressors have in fact a gradually stalling mode, with steep positive slopes not appearing till the flow is greatly reduced and hence extension of the surge free region without excessive penalties becomes a possibility (36). One effective method of increasing the compressor operating range is to provide sufficient impeller stability, so that the downstream diffuser can operate well into its positive incidence zone. Impeller stability is improved by improving the stability of the inducer or by the use of tip backsweep, since increasing backsweep provides a more negatively sloped static pressure versus flow characteristic (33). For a backward leaning impeller the discharge stagnation pressure increases with reducing mass flow rate, i.e. the

stage discharge velocity increases and finally reaches tip speed at zero mass flow. The increased kinetic energy available stabilises the diffuser (22).

Adjustments of impeller stall limits are made by changing the passage area ratio by modifications to either the inlet or exit blade heights. By step-closing the vaneless diffuser immediately above the impeller tip, the impeller is "tricked into believing" it has a smaller exit blade height. This results in a slight reduction in efficiency and work factor but produces the desired stall displacement quite effectively (34). High impeller blade number to reduce aerodynamic loading also increases stability (44).

An attempt was made (31) to influence the position of the surge point by introducing a fluctuating flow at the compressor inlet. This forced periodicity of flow was found to have negligible effect (31). A well known resort to prevent recirculation and to improve efficiencies in pumps at low flows is the use of inlet suction rings or flow dividers (33).

By reducing the diffuser width downstream for wide diffusers, it may be possible to reduce the critical inlet flow angle, but such modification of diffuser width with respect to radius is not effective for narrow diffusers (39). In vaned diffusers tapering spanwise the diffuser leading edge results in a gradual unloading of the blade leading edge at high incidences and prevents abrupt stall (36). Other methods include:

- Quick acting check valves between the compressor outlet and the discharge volume in an effort (unsuccessful) to isolate the feedback loop (36).
- Acoustic suppressors in the form of chambers connected to the compressor discharge generally via restrictions, acting as a series capacitor-resistor in parallel with an oscillating circuit to reduce the amplitude of oscillations (59).

One method of delaying the change in slope of the characteristic curve is the use of variable-angle pre-rotation vanes upstream of the compressor. As throttling at the inlet is increased, the incoming air is given a rotation in the direction of impeller travel and the greater the amount of prerotation the less will be the pressure rise of the compressor.

For any given setting of the vanes, the amount of the absolute prerotation will be proportional to the volume flow and, consequently, any slight decrease in volume flow will tend to increase the pressure rise of the impeller and thus delay the critical value of positive slope (31).

In process compressors surge is usually prevented by automatically opening a blow-off or recirculation valve to maintain flow through the compressor at a rate above the allowable calculated value - even though a lower flow rate is needed by the load system.

CHAPTER 3

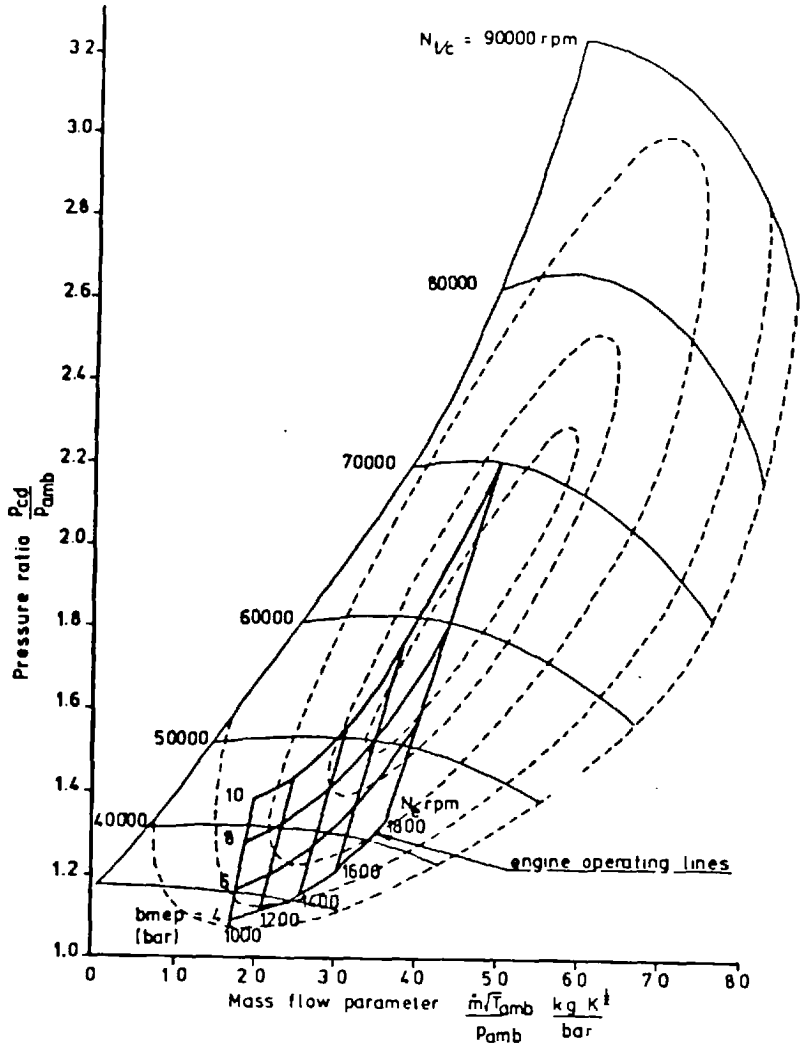
TURBOCHARGER MATCHING AND TURBOMACHINERY FLOW CONTROL

3.1 TURBOCHARGER MATCHING

The object of matching turbochargers to engines is to obtain the best overall engine performance. As it has been described, the stable airflow range of the compressor is limited. Also, since the maximum efficiency of aerodynamic blading normally occurs with a slight degree of separation, the stable operating limit often lies adjacent to the maximum efficiency point (42). If the "free-floating" turbocharger system is used, the turbocharger speed, airflow and boost pressure, adjust themselves to variations in engine speed, fuelling and altitude.

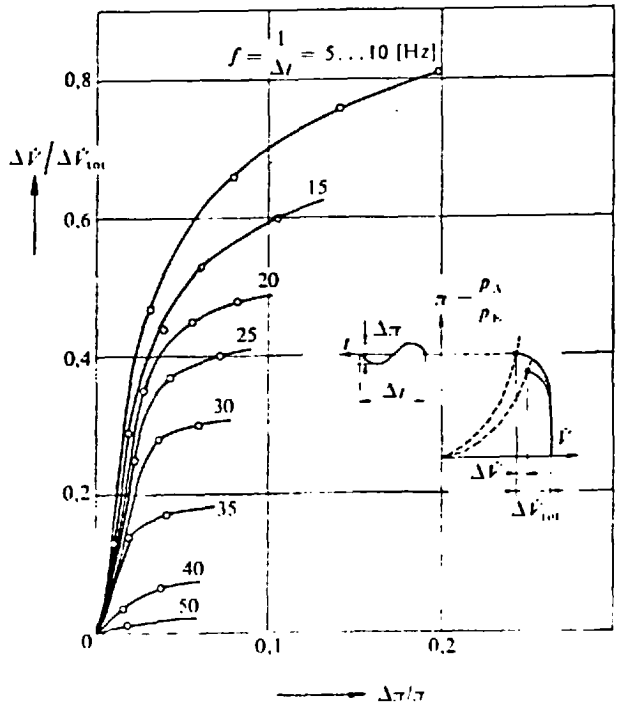
The assembly of turbine and compressor of suitable proportions can be built up to produce a number of different boost pressure curves on a given engine, by varying the rotor speed with respect to mass flow, i.e. changing the turbine swallowing capacity, and by employing compressor rotors having their peak efficiencies in differing airflow ranges (43).

In automotive engine applications there are wide speed and load variations hence large airflow variations (see Figure 3.1). This increases the complexity of turbocharger matching. The torque-speed characteristic is predominantly important in such engines and a torque curve without back up is unacceptable to a conventional vehicle transmission system. To get the required torque curve the turbine can be appropriately sized to give optimum low speed boost



- Compressor characteristics showing engine steady-state operating conditions

FIG.3.1 The Automotive Engine Operating Area on a Compressor Map



– Measured displacement of the compressor surge limit with pulsating back-pressure. The non-dimensional volume flow displacement of the surge limit is taken as ordinate, the related pressure amplitude as abscissa. The readings were taken on an experimental VTR 250 compressor with an impeller 280 mm in diameter and a vaned diffuser.

p_A = Pressure at compressor outlet
p_E = Pressure at compressor inlet
f = Frequency of pressure pulsations

FIG.3.2 Influence of Engine on Compressor Stability Characteristics (46)

(and also good transient response).

For a low speed match, a small turbine effective area would be necessary to raise the availability of energy where the flow is low. Assuming that the range of airflow demand of the engine can be accommodated within the stable airflow range of a certain compressor, the turbocharger match may be selected so that at high speeds the engine operating line runs into the low efficiency choke region of the compressor and the boost is thereby controlled. However, the high exhaust manifold pressure level, resulting from the small turbine area, will increase the pumping work of the engine. There is also the possibility of the turbocharger's overspeeding. Hence a compromise must be made, selecting a larger turbine, which will result in lower levels of boost at low speeds.

The matching requirements are certainly dependent on features such as careful control of the fuelling curve, optimisation of fuel injection equipment and turbocharger efficiency. By using various matching techniques and component optimisations the flexibility of the simple, hence desirable, free floating system has been enhanced.

3.2 MATCHING PROBLEMS

In the foregoing it was assumed that the surge free flow range of the compressor was adequate. There are however cases where the matching problem becomes more critical. The main ones are:

- Very highly turbocharged engines required to work over a speed range (e.g. traction engines).

With increasing engine ratings higher boost pressures are required. As the design pressure ratio in a centrifugal compressor is increased, the surge free range is reduced. Hence to obtain maximum torque at the desired speed and desired power at rated speed, the stable limits of the compressor may be reached at lower speeds and possibly turbocharger overspeeding may be encountered at the rated conditions.

Conversely to ensure an adequate surge margin at low speeds, the boost has to be limited to low pressure levels. At the rated speed and high compressor pressure ratios however, the operating line would end up far removed from the surge line and into the low efficiency region. Also the desirability of matching engine operation close to the point of peak efficiency, which in turn is near the surge line, can lead to insufficient flow margin during transient operation.

- High speed automotive diesel engines, especially passenger car engines.

The very small turbochargers capable of matching the airflow requirements of these wide speed range (typically 4:1) engines have generally relatively low efficiency (small rotors, casting imperfections, large clearances etc.). The limited exhaust energy availability at low engine speeds, coupled with the low compressor efficiency at this operating condition will result in low boost. If a smaller turbine is used, the excessive boost at high engine speeds will be unacceptable frommechanical loading

considerations for this type of engine. If a larger compressor with improved efficiency at low-medium speeds is used, it will probably not have adequate stable flow range at low flows. On the other hand using fuel delivery to control boost over such a wide speed range leads to an impossible fuel injection equipment problem (18).

3.2.1 Influence of Engine on Compressor

Due to the breathing characteristics of the engine, the air flow rate into the engine cylinder is not steady. The amplitude and frequency of the pressure fluctuations in the compressor delivery line might influence the performance of the compressor. If the compressor speed is constant, the instantaneous flow rate will fluctuate along a constant speed line.

Depending on the design of the intake system and the engine timing, it is possible for the instantaneous flow rate through the compressor to be less than the flow rate at surge for part of the time (45). It seems unlikely however that flow reversals will occur, unless a natural frequency of the system is excited (71).

The lower the frequency and/or the greater the amplitude of pulsation the lower the compressor efficiency and the shorter the flow range with the surge line shifted to a point of higher mass flow depending also on the flatness of the compressor characteristic (45, 46) (see Figure 3.2). On 6-cylinder engines, the instantaneous demand varies by less than 10 per cent from the mean demand, and adequate damping is normally provided by the inlet manifold volume.

4-cylinder engines, usually with crossed crankshafts, have a wide fluctuation in instantaneous demand over the two revolutions of the cycle (varying between zero and 2.2 times the mean value). A large reservoir volume is thus required between the compressor outlet and the engine intake ports if heavy fluctuation between surge and choke is to be avoided. V-8 engines where the demand varies by $\pm$20 per cent through the cycle are normally satisfactory if the two manifolds are of reasonable volume and interconnected (8).

3.3 POSSIBLE SOLUTIONS TO MATCHING PROBLEMS

Several methods have been proposed to overcome matching problems. In all cases any benefit has to be weighted against the cost and possible increased complexity. These methods can be broadly classified into three categories: 1) External/system methods, 2) Turbo-assistance methods, 3) Turbomachinery flow control.

3.4 EXTERNAL/SYSTEM METHODS

These influence the outlay or components of the turbocharging system but are not directly applied to the turbocharger. Some of these are:

- Multiple stage turbocharger system
- Register system (47)
- Combination blower-turbocharger
- Inlet resonance chambers (48)
- Pulse converters
- Intercooling/aftercooling

3.5 TURBO-ASSISTANCE METHODS

The turbo-assistance methods provide the desired response and torque characteristics by using an external energy supply directly on the turbocharger rotor:

- Pelton wheel mounted on the turbocharger shaft driven by high pressure oil jet (49, 50, 8, 44).
- Air injection on to the compressor impeller (50, 51, 52).
- Hyperbar parallel high supercharging system. This provides a separate combustor before the turbine, thus effectively making the turbocharger independent of the engine (53).

3.6 TURBOMACHINERY FLOW CONTROL

The available control schemes will be classified into turbine (hot end) controls and compressor (cold end) controls.

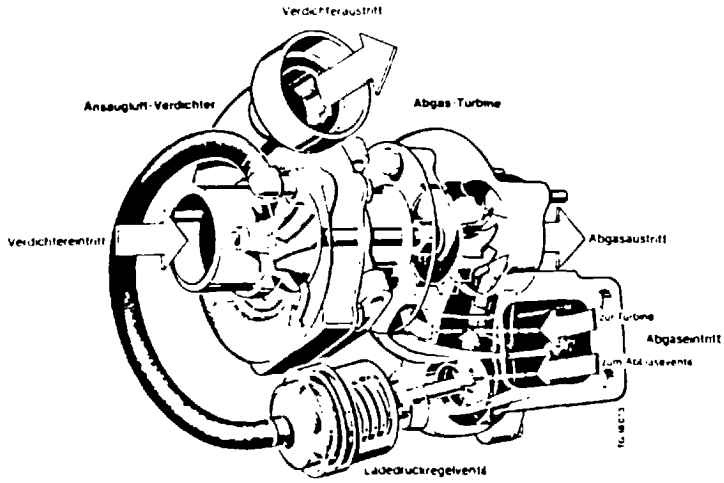
3.6.1 Turbine Controls

3.6.1.1 Constant area throttling devices (restrictions)

The pressure drop across an orifice is proportional to the square of the through flow. Usually placed downstream of the turbine, the restriction reduces the available turbine energy by reducing the turbine expansion ratio and becomes increasingly effective as the engine speed and mass flow are increased. The boost pressure is thus controlled. However the engine pumping work, hence sfc, are increased (43).

3.6.1.2 Turbine by-pass (wastegate)

This is normally a valve mounted on the exhaust system upstream of the turbine and can open to allow some of the exhaust gas to by-pass the turbine (see Figures 3.3, 3.4, 3.5) (54, 55).



Abgasturbolader mit Ladedruckregelventil (Garrett)

FIG.3.3 Turbocharger with Waste-Gate (54)

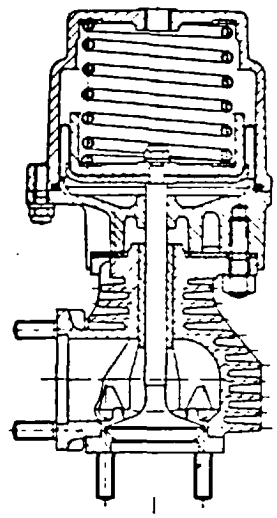
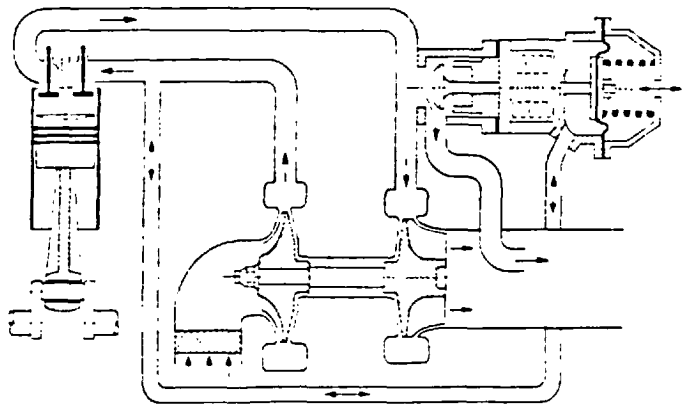


FIG.3.4 Waste-Gate (54)



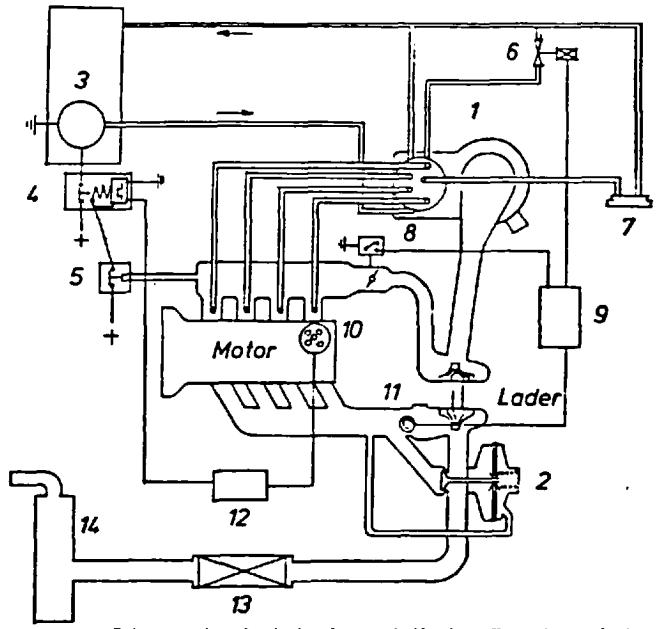
Control scheme of a boost-pressure controlled exhaust waste gate

FIG.3.5 Boost Controlled Waste-Gate. Schematic Arrangement (55)

Early applications of the waste-gate system were directed towards limiting turbocharger speeds at altitude conditions (8). Traditional designs of waste-gate have controlled the operating valve by the turbine inlet pressure (see Figure 3.6) (54) but this control strategy throws away a vital part of the energy which could be available under transient conditions. For light duty operation it is definitely preferable to allow the waste-gate to be controlled by the boost pressure and in this way an additional turbine inlet pressure of as much as 0.3 bar can be utilised under the transient conditions required for light duty operation (18). However an improved torque characteristic may be obtained using the exhaust manifold pressure for waste-gate control (see Figure 3.7) (116). The adoption of an exhaust waste-gate will permit a low speed match to be made, avoiding excessive boost and high exhaust manifold pressures at high speeds.

For a passenger car engine the turbocharger built can be chosen such as to give useful boost at as low an engine speed as possible. The waste-gate operating point would then be set so that the boost at full speed does not exceed the desired figures (18). Thus an acceptable torque curve can be obtained. The additional advantage of the waste-gate is the relief of engine back pressure at high speeds.

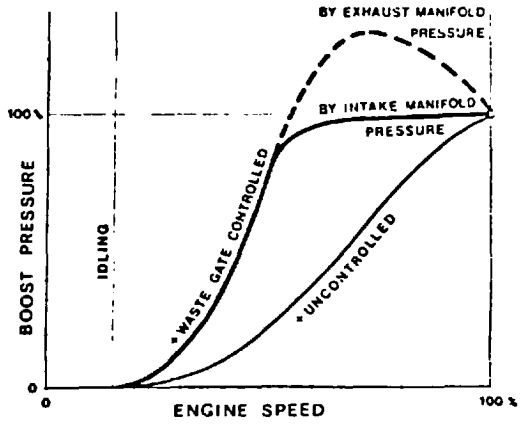
It is estimated (18) that the wastegated turbocharger can achieve excellent performance when applied to a passenger car diesel engine. The weight and space penalties are



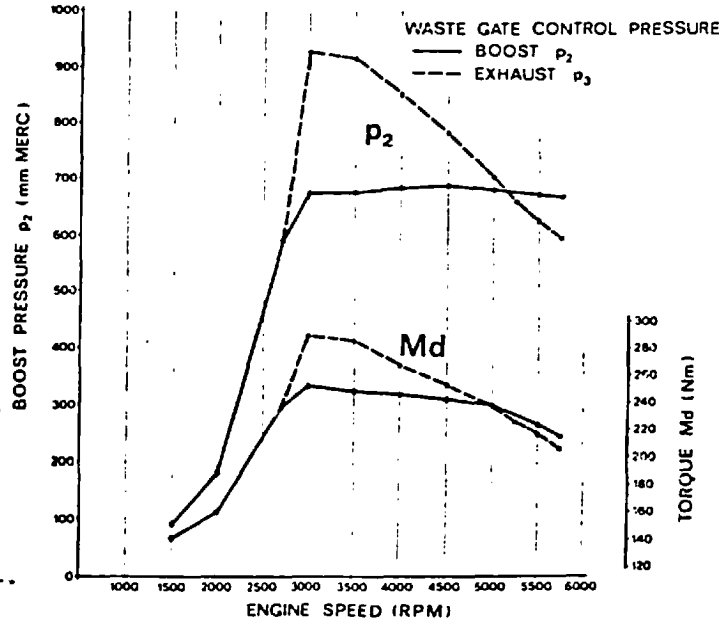
Schema der Ladedruck- und Kraftstoffregelung beim Saab-Turbo-Motor

1 Gemisch-Regelung
2 Ladedruck-Regelventil
3 Benzinpumpe
4 Benzinpumpen-Relais
5 Überdruckschalter
6 Impulsventil
7 Warmlaufregler
8 Drosselklappenschalter
9 Steuergerät für Lambda-Sonde
10 Zündverteiler
12 Steuergerät für Drehzahlbegrenzung
13 Abgaskatalysator
14 Auspufftopf

FIG.3.6 Turbine Inlet Pressure Controlled Wate-Gate (SAAB) (54)



- Boost pressure control characteristic



Boost pressure and torque 4-cyl 2-L engine

FIG.3.7 Performance Comparison for Two Waste-Gate Control Systems (116)

much less than would be incurred if the equivalent 30-50 per cent increase in engine swept volume were incorporated in order to give a naturally aspirated engine with the same performance, but it is estimated that the cost penalty is about equivalent.

The main disadvantage of the waste-gate however is the potential unreliability. The unit has to operate under severe flow and thermal conditions imposed on the valve and control mechanisms, and the possibility of failure during operation will result in unacceptable engine performance.

3.6.1.3 Variable geometry

Variable geometry represents the ultimate control solution since, at least theoretically, it can provide optimum machine performance for every operating point, being therefore equivalent to a continuous series of different machines, one for each operating condition. Practically this cannot be realised, since only parts of the machine can be variable, and these only within a certain range.

Generally rotating parts cannot vary their geometry during operation, in view of the high rotational speeds involved, and so by their very nature have a specific design point.

The use of variable geometry is often an improvisation of an existing design. If, however, variable geometry is stipulated as a design requirement, it is necessary to specifically design the machine blading to provide optimum performance over the anticipated operating range. This may require some compromises with maximum performance, in favour of improved overall performance.

The question of variable geometry for turbomachines will be treated more extensively under "compressor controls". For the turbine side, developing a variable geometry mechanism that can work efficiently and reliably, being continuously exposed to a hot and corrosive environment presents a formidable engineering problem. Although a practical solution would be clearly desirable it has not been successfully implemented to date. The difficulties increase with the continuing trend towards higher maximum cycle temperatures. The options available for variable geometry turbine components are:

- Variable turbine nozzle rings

Changing the angle of the nozzle vanes, changes the effective area of the turbine and gives different pressure ratio-mass flow characteristics (see Figure 3.8) (56). The results obtained with such components have not been very satisfactory. Large clearances in the vane assembly are required to avoid seizing at high temperatures from relative thermal expansion and fouling. The resulting leakage losses reduce the turbine efficiency. This is more pronounced in the partly closed vane position and it reduces the possible increase in turbine power.

Radial turbines where the deflection of the nozzle vanes is smaller than in axial turbines suffer less in this respect. Another possibility to the same effect is closing sectors of vanes, but partial admission also reduces the turbine efficiency.

- Variable geometry vaneless housings

The effective area of the turbine can also change by

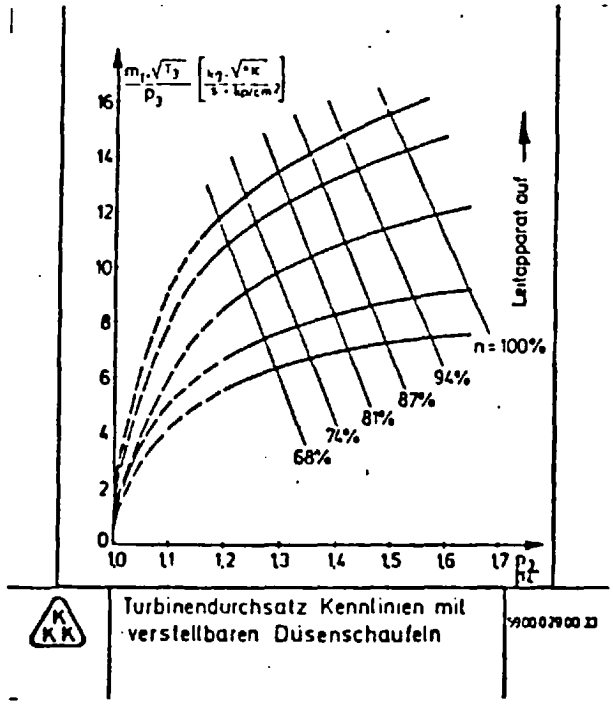


FIG.3.8 Effect of Variable Geometry on Turbine Characteristic Curve (56)

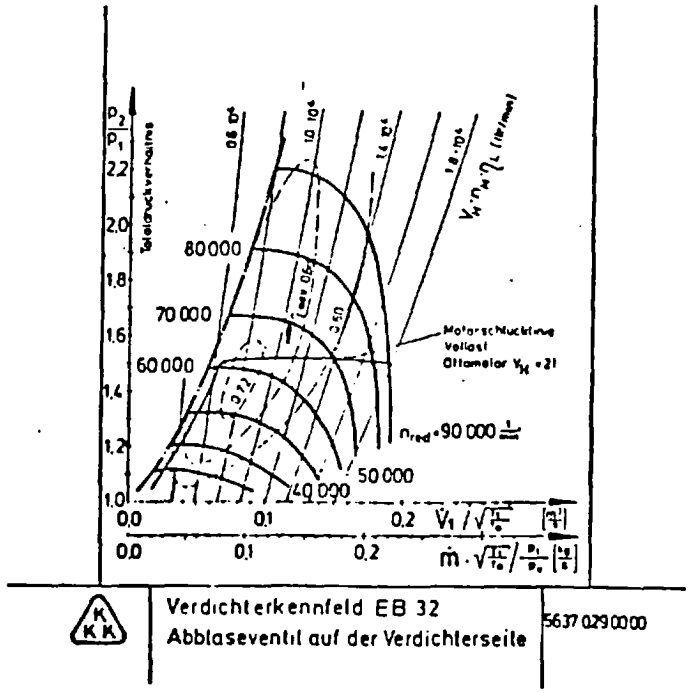


FIG.3.9 Engine Operating Line on Compressor Map with Compressor Blow-Off Valve (BMW 2002-turbo) (56)

changing the flow passages in the turbine housing but this method has also enjoyed little success.

3.6.1.4 Aerodynamic methods

Air injection upstream of the turbine to increase the turbine inlet temperature and mass flow and thus provide power augmentation has been used in petrol engines (54).

3.6.2 Compressor Controls

3.6.2.1 Constant area throttling devices (restrictions)

These orifices can be placed upstream or downstream of the compressor to reduce the overall pressure ratio. Suction throttling is generally more efficient than discharge throttling. For the same overall pressure ratio, suction throttling increases the volume of gas flowing to the compressor. Hence at constant rotational speed and assuming constant compressor efficiency, the pressure ratio developed by the compressor will decrease and the power required will decrease (61, Jackson disc.).

3.6.2.2 Discharge blow-off

A pressure relief valve can be used downstream of the compressor, to waste some of the discharge flow, when the pressure exceeds a preset limit, thus controlling the discharge pressure. Blow-off valves are inefficient arrangements since the dumped fluid has been compressed beforehand. Since the flow through the compressor is larger than the flow through the rest of the system this method can also be used to maintain the operating point within the stable operating range of the compressor. At high speeds the discharge temperature may be high since the compressor will work in an area of low efficiency (43, 8, 56, 54) (see Figure 3.9).

3.6.2.3 Flow recirculation

If it is impractical to dump the blown-off flow to the atmosphere (e.g. in process compressors), the flow is recirculated back into the inlet plenum. Since the inlet temperature is increased by the hot recirculated discharge fluid mixing with the inlet flow, the overall compression efficiency is reduced.

3.6.2.4 Variable geometry

Substantial increases in the compressor flow range can be obtained by variable compressor geometry. Also high efficiency can be maintained throughout the operating range (56, 42). Larger compressor flow range may be beneficial in the following cases (42).

1. Combination airbleed-shaftpower gas-turbines

These are commonly used as aircraft auxiliary power units (APU), operating at constant speed. Large flow range is required between the pure bleed and pure shaftpower operating modes. Since such large range cannot be attained with fixed geometry components, it is normal to operate at lower compressor efficiency under bleed conditions, and to limit pure shaftpower output to provide a tolerable operating surge margin. Significant performance increases can be obtained in such gas turbine applications, by using variable geometry either in the compressor or turbine components.

2. Multi-stage compressors

The arrangement of two radial compressors or an axial and a radial or two axial compressors are common features

of several gas turbine powerplants. With high stage pressure ratios, some performance compromise may be necessary to provide a surge free acceleration under all environmental operating conditions. The low and high speed surge characteristics are essentially determined by the first and second stage surge lines respectively. Incorporating variable geometry could improve the overall surge characteristic of multi-stage compressors, thereby avoiding the necessity to compromise engine performance.

Variable geometry is also used in process compressors for good efficiencies over a wide and stable range of part loads and to ease the startup process, by unloading the impeller.

3. Gas turbine driven radial compressors

Both single and two shaft gas turbines are in use driving radial compressors either directly or through intermediate gear trains. The two-shaft arrangement simplifies the engine starting problem because it is not necessary to unload the driven compressor during the start cycle. Unloading methods selected for single-shaft arrangements may comprise:

- inlet throttling
- variable inlet guide vanes
- flow recirculation
- variable diffuser

Inlet flow regulation is prevalent where the compressor is required to operate against a fixed downstream restriction, or over a relatively small flow range. If a large flow

range is desired, then a variable diffuser system can serve to both regulate the driven compressor surge line (for either a single or two shaft gas turbine) and to act as an unloading device for a single shaft gas turbine during startup.

4. Ultra high pressure ratio centrifugal compressors

Such high (≈10:1) ratios cause conflicting demands between the impeller and the diffuser if both are to operate in their respective regimes of minimum loss over the complete compressor operating range. The reconciliation of these demands can be achieved by variable geometry either in the impeller or the diffuser. At pressure ratios other than design, the minimum loss regimes of the impeller and diffuser depart, the departure increasing with change in pressure ratio from the design value. Thus the higher the design pressure ratio the higher the departure at part load conditions.

The relative displacement of the minimum loss regimes results in reduced overall efficiency and, moreover, irregular surge lines. A fixed geometry turbine operating line lies almost parallel with the diffuser minimum loss regime. Selection of optimum impeller and diffuser matching at the design pressure ratio can, therefore, result in stalled impeller operation at part load.

5. Variable head or capacity blowers pumps or fans operating at constant speed

6. Internal combustion engine turbocharger compressors

3.6.2.4.1 Variable geometry mechanisms

The following variable geometry methods have been

employed on centrifugal turbomachinery (44, 42).

1. Variable pitch impeller blades

This method of variable geometry is fairly common in large low speed hydraulic turbomachinery (c.p. propellers, Kaplan turbines). However at higher rotational speeds, the resulting structural limitations make this form of flow regulation impractical.

2. Variable diffuser

If the impeller could achieve its function without stalling and choking restrictions, a variable diffuser downstream of the impeller could provide almost constant pressure ratio with flow variation from zero to design flow. In practice flow limits occur with variable diffuser systems due to overheating at low flow stemming from internal flow recirculation, and efficiency reduction at high flow prior to impeller choking.

There are three possibilities for variable diffuser:

- Restagger of vanes, for vaned diffusers
- Varying the width between front and rear shrouds, suited mainly for vaneless diffusers
- Rotating diffuser

For efficiency reasons most gas turbine radial compressors are of the vaned type, flow regulation being obtained by vane restagger. Most investigators agree that the amount of diffusion of the flow between the diffuser leading edge and the throat of the vane section is most critical for stability (29, 44). When the adverse pressure gradient reaches a limiting value for that particular diffuser configuration the diffuser stalls.

Reduction of the throat area with vane restagger reduces the diffusion between the tip and the throat and stabilises the diffuser (see Figure 3.10) (44). (From another point of view the blades are realigned with the flow.) Also at high flows the diffusion throat area may be opened beyond the design position to increase the swallowing capacity of the compressor till the inducer chokes (see Figure 3.11) (42). However, in order to control leakage losses, which drastically reduce efficiency, very tight clearances are required between the adjustable vanes and the side walls, which cannot be sustained practically under the temperature and fouling conditions experienced during operation (22).

Similar effects can be obtained with a vaneless diffuser by changing the width between the diffuser walls.

In the free-rotating diffuser arrangement, the diffuser walls (vaneless or vaneless-vaned diffuser) are allowed to rotate independently of the rotor at a fraction of the rotor speed (see Figure 3.12) (22). The shear forces between the high velocity flow and the walls are thus reduced. Rotation of the sidewalls prevents separation, tends to smooth the distorted flow profiles from the impeller and provides stability for the vaned portion because of the lower velocities entering the vaned region (60, 44, 22).

3. Variable inlet guide vanes

In this arrangement flow regulation vanes are placed in the compressor inlet section to give the incoming air a whirl component. A positive vane angle can be defined as

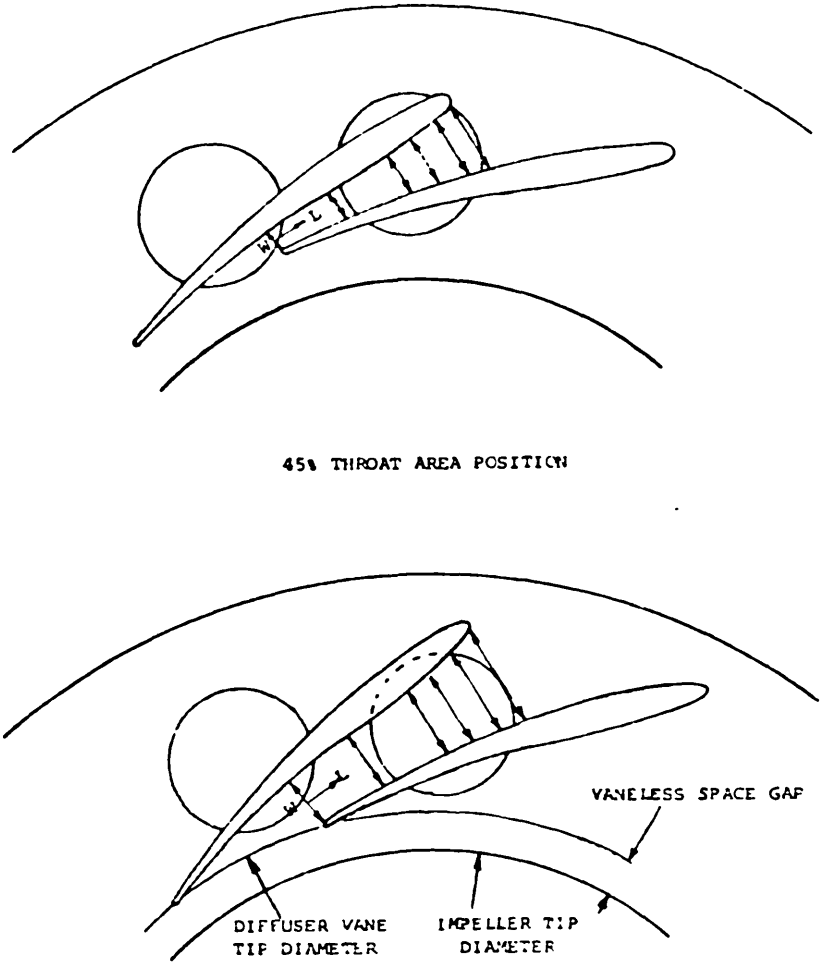
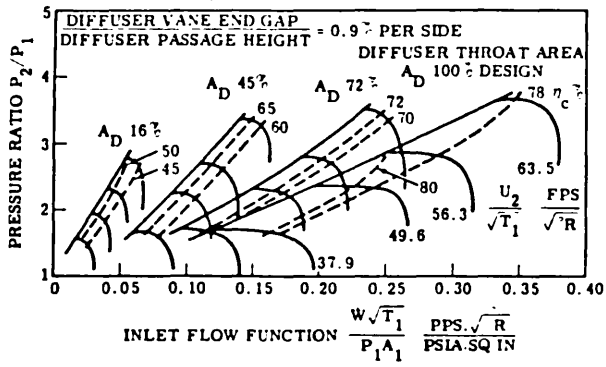
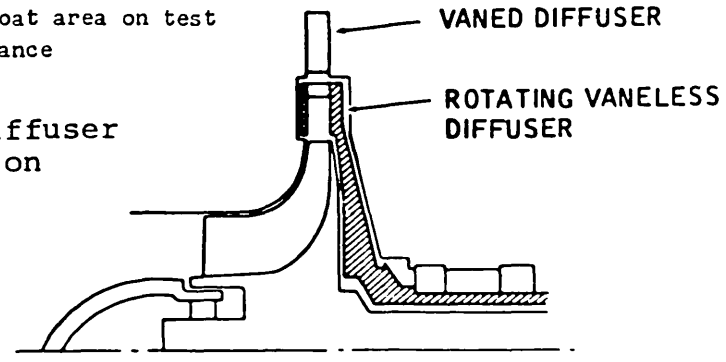


FIG.3.10 Variable Geometry Vaned Diffuser (44)



Effect of diffuser throat area on test compressor performance

FIG.3.11 Effect of Diffuser Throat Area on Compressor Performance (42)



ROTATING WALL DIFFUSER

FIG.3.12 Rotating Diffuser (22)

the one which produces prewhirl in the direction of rotation of the impeller (positive prewhirl), and a negative vane angle as the one which produces prewhirl in the opposite direction (negative prewhirl) (see Figure 3.13) (44).

From the Euler pump equation, assuming one-dimensional flow theory, the theoretical amount of work imparted to unit mass of fluid as it passes through the impeller is given by

$$E = U_2 . C_{\theta_2} - U_1 C_{\theta_1} \qquad (3.1)$$

where

E = work per unit mass of air

U_2 = impeller peripheral velocity

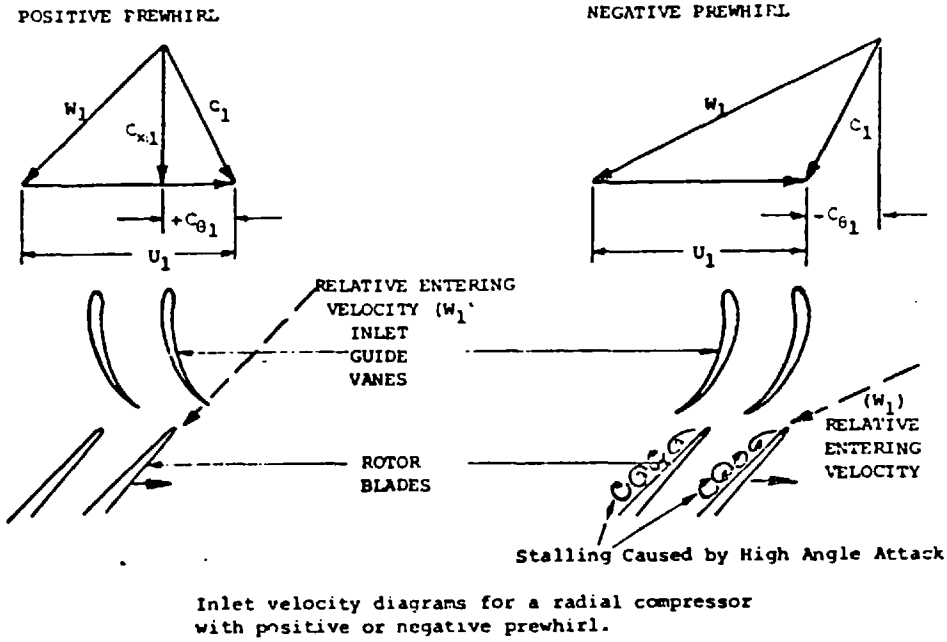
U_1 = inducer velocity at mean radial station

C_{θ_2} = absolute tangential velocity at impeller exit

C_{θ_1} = absolute tangential velocity at inducer inlet

It can be seen from this equation that positive prewhirl reduces the theoretical work of the stage, and negative prewhirl increases it.

The change in the work input capacity is reflected as a change in the pressure ratio developed by the compressor at constant speed. If the prerotation vane angle is variable then the amount of prewhirl can be controlled. Thus the relative velocity vector approaching the rotor blade can be controlled to eliminate the tendency of the rotor blades to stall (positive incidence) as the flow rate through the compressor is reduced, effectively reducing the contribution of the inducer to compressor stall.



Inlet velocity diagrams for a radial compressor with positive or negative prewhirl.

FIG.3.13 Positive and Negative Prewhirl

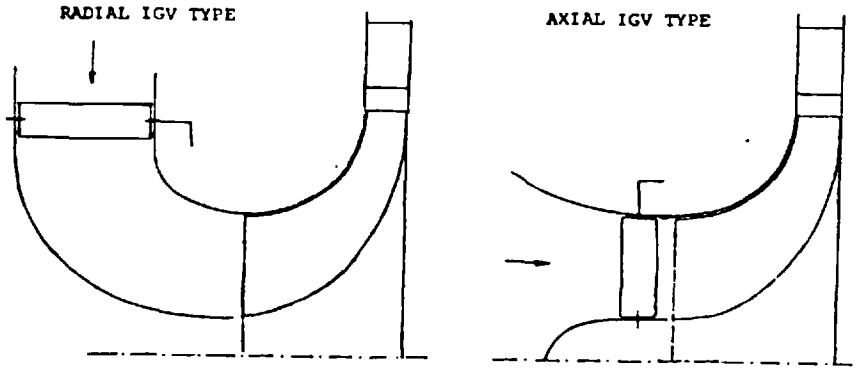


FIG.3.14 Radial and Axial Inlet Guide Vanes

Two general types of inlet guide vanes have been used: radial or axial vanes (see Figure 3.14 (44), Figures 3.15, 3.16). Historically the radial form dates back to the original Whittle gas turbines and produces a free-vortex flow distribution at the inducer leading edge (rC_{θ_1} = constant and axial velocity is constant spanwise). Usually from cost considerations, simple uncambered vanes are used.

A study was conducted (63) to assess the effect of possible prewhirl types on compressor performance, particularly any effects on the magnitude of the impeller incidence loss. Three types of prewhirl were investigated in detail; free vortex, (rC_{θ_1} = constant), forced vortex (C_{θ_1}/r = constant) and constant whirl angle with radius. A radial equilibrium analysis indicated the advantage of forced vortex prewhirl. The free vortex prewhirl yielded the most undesirable inducer characteristics. These preliminary studies were conducted with the assumption that the impeller inducer was composed of radial blade fibres. By adopting an inducer with non-radial fibres it should be possible to accept free vortex prewhirl without incidence loss (63).

Tests of both radial type and axial vanes designed to produce a constant flow angle from hub to tip (62), indicated that for the same guide vane angle the pressure ratio produced by the compressor was almost identical.

One problem common to both types of inlet guide vane design is that of the losses at high stagger angles. Uncambered vanes approach their stall limit at an incidence

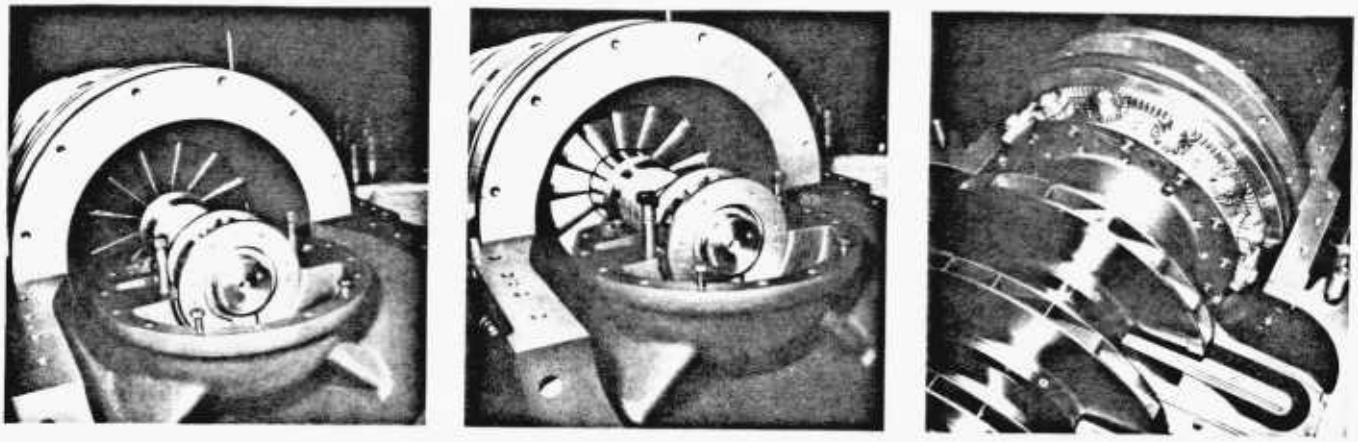


FIG.3.15 Axial Variable Inlet Guide Vanes

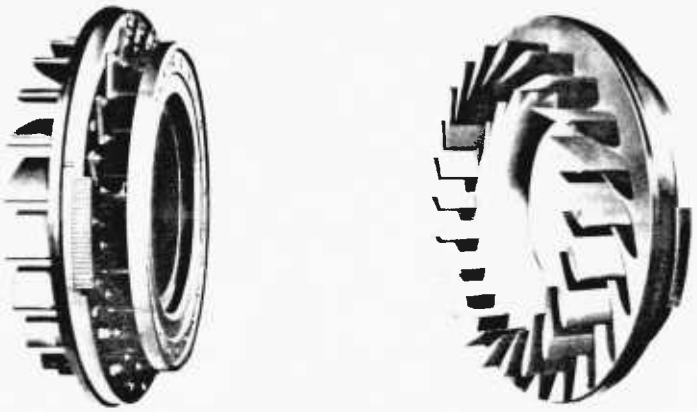


FIG.3.16 Radial Variable Inlet Guide Vanes



FIG.3.16a Axial Variable Inlet Guide Vanes

angle of $\approx 30^{o}$ (42). A relatively large reduction in overall compressor efficiency at prewhirl angles greater than 40° arises from inlet guide vane stalling losses and test results with grossly stalled I.G.V. at 65° indicated an appreciable reduction in efficiency (42, 64) (see Figure 3.17). The flow deflections that can thus provided are limited.

Possible solutions include the variable geometry aerofoil (flapped or slotted/flapped) (see Figure 3.18 (44), Figure 3.19 (64)). Although these are superior aerodynamically they are more complicated and costly to manufacture especially in small sizes. Twisted vanes may provide a better prewhirl distribution but are more costly to manufacture, have higher friction losses when idle (at zero incidence), and can only be used for one mode of prewhirl. The vane activating mechanism is also relatively complicated.

3.6.2.4.2 Control and aerodynamic aspects of prewhirl

The control of the prerotation vanes derives from two mechanisms; the first is due to the loss in total pressure (throttling) caused by the I.G.V. and the second is due to the unloading of the impeller front end because of the imparted prerotation. This latter mechanism is efficient. Throttling may still be the major working mechanism even though it is assumed that the imparted inlet angular momentum and the unloading of the impeller form the basis of the observed behaviour (36). The pressure reduction of the guide vanes is accomplished in three phases (61):

1. Reduction due to gas deflection in the direction of the impeller rotation, expressed by the subtractive term in Euler's equation (3.1) for the theoretical work imparted

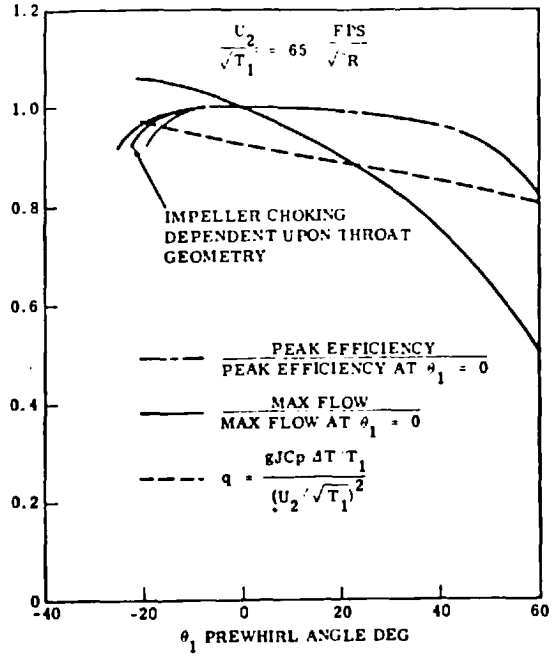


FIG.3.17 Typical effects of IGV's on radial compressor performance (42)

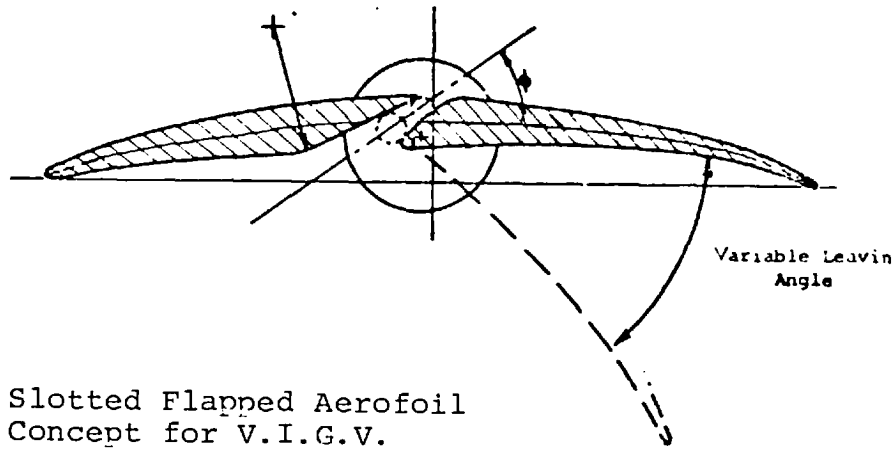


FIG.3.18 Slotted Flapped Aerofoil Concept for V.I.G.V.

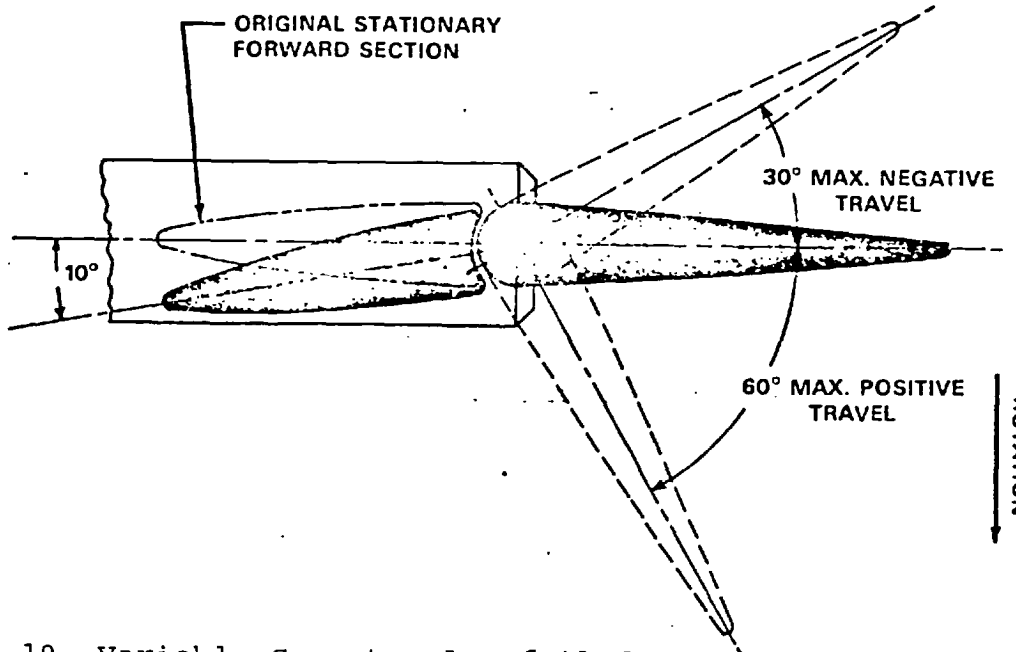


FIG.3.19 Variable Geometry Aerofoil for V.I.G.V. (64)

by the impeller.

2. Inlet pipe throttling effects - Reduction due to pre-rotation alone can take place only at a small angle of deflection. Since the free area between the two adjacent guide vanes is reduced directly as the cosine of the deflection, for a fixed rate of flow, throttling effects appear. The flow is accelerated through the vanes and then suddenly decelerated incurring loss of pressure and efficiency.

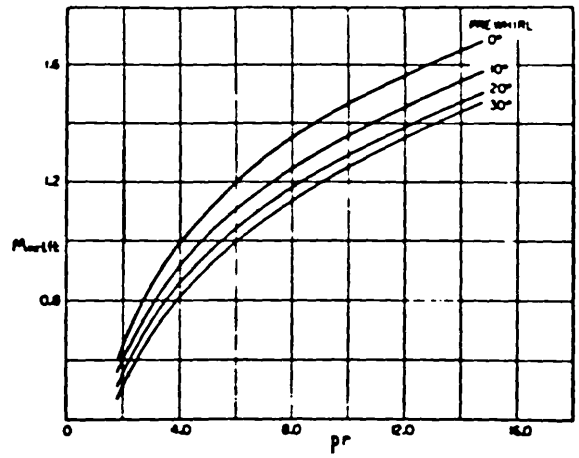
3. In practice pure throttling at the inlet cannot be realised. It is accompanied by the shifting of the operating point on the volumetric impeller exit characteristic curve to a lower pressure. This shifting occurs as a result of gas density reduction by throttling, i.e. pressure reduction beyond the throttle. This is accompanied by an efficiency reduction but not in the same ratio as the pressure reduction. In this manner some power saving is realised by comparison with pure throttling. The actual power saving will be lower because: impeller efficiency is impaired by the presence of guide vanes at the impeller approach and throttling is unavoidable when the flow is deflected with vanes.

Suction throttling can also increase the surge margin by moving the operating point to the right on the compressor map. The system stability is also increased since the negatively sloped throttle characteristic is added to the compressor characteristic. (A simpler method of variable suction throttling is by a throttle valve upstream of the compressor but placing the device too close to the impeller eye will bring a drop in efficiency from the distorted flow

downstream of the valve and possibly an increase in noise level. A throttle some distance from the runner eye increases the length of the unit and can lead to pressure fluctuations (62,Netch,disc.).

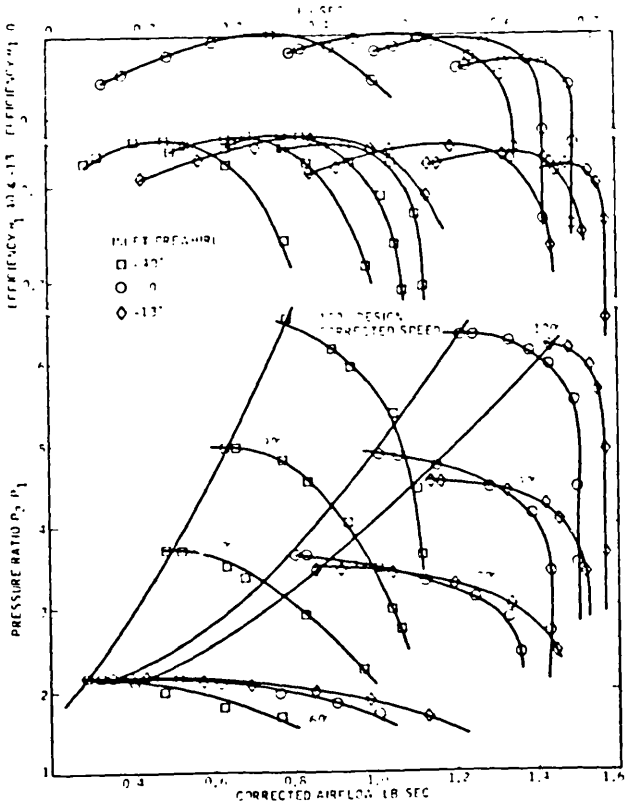
Inlet guide vanes may be employed to control the relative Mach number at the inducer tip, at the expense of a reduction in pressure ratio (22, 42). Figure 3.20 (22) illustrates how inlet guide vane swirl influences the inlet relative Mach number. This measure may be needed because for a given tip geometry increasing the (jet) exit relative Mach number of a centrifugal impeller, will increase discharge mixing losses and will lower the efficiency. If the impeller Mach number ratio (diffusion ratio) is constant, the (jet) exit relative Mach number will change in step with the inlet (tip) Mach number. The latter can be limited with positive preswirl. Hence the (jet) exit relative Mach number will be reduced,reducing the discharge mixing losses and the efficiency drop. However this always tends to raise the absolute Mach number at the impeller discharge, with possible severe impact on the diffuser performance (22).

If surge and choke are dictated by the diffuser, regulation of I.G.V. will merely reduce the pressure level into the diffuser; thus both surge and choke flows will essentially follow a similar variation to that produced by speed changes. At very low speeds and speeds greater than design, the impeller influences the surge and choke flows; therefore, significant changes in the surge and choke flows are possible at the extreme speed ranges with I.G.V. regulation. A radial compressor with a vaneless diffuser



VARIATION OF SHROUD RELATIVE MACH NUMBER WITH PREWHIRL AND PRESSURE RATIO FOR SPECIFIC SPEED (W_a) = 100

FIG.3.20 Variation of Shroud Relative Mach Number with Prewhirl and PressureRatio (22)



VIGV impeller test performance

FIG.3.21 VIGV Compressor Test Performance (33)

may show significant changes in the surge characteristic with I.G.V. regulation provided the vaneless diffuser is not operating close to its stalling limit (42, 63) (see Figure 3.21 (33)) (see Figure 3.22, 3.23 (67)).

The pressure ratio and mass flow can be varied at constant compressor speed by changing the inlet vane angle. Hence for each I.G.V. setting there is a different overall compressor characteristic (66, 36). Therefore varying preswirl angle at a constant compressor speed is equivalent to varying compressor speed without whirl (62, 65) (see Figure 3.24, 3.25 (62)). In a gas turbine this can be used to increase the compressor delivery pressure and mass flow with the increase of ambient temperature, to keep the turbine temperature within reasonable limits (65, 42).

To meet variable head-capacity requirements single and multi-stage blowers and process compressors are frequently equipped with guide vanes at the impeller approach (61). Prewhirl can be used in a two shaft gas turbine to vary the output power without changing the gas producer speed (62). In the past the use of V.I.G.V. on the automotive gas turbine has been primarily for the purpose of minimising acceleration time. A high idle speed may be obtained by simulating the pressure ratio characteristic of a lower speed with positive preswirl (64).

Conversely positive preswirl can be used to lower the mass flow and pressure ratio at a low idle speed for better fuel economy (64). A variable geometry compressor cycle may be designed around part load conditions, with the inlet guide vanes set at a finite positive angle. To

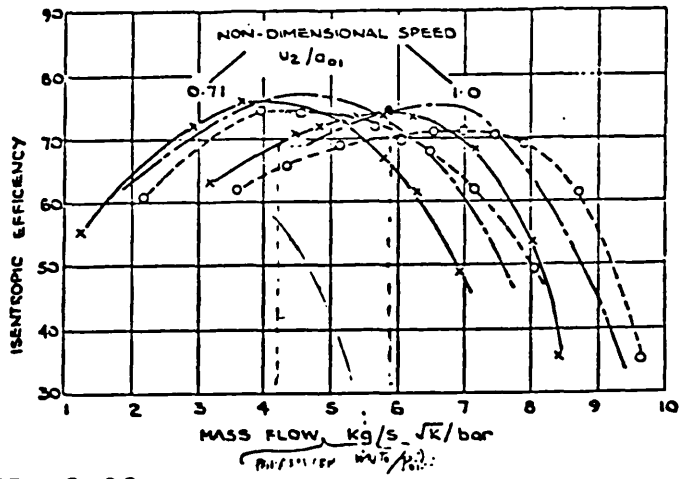


FIG. 3.23 Efficiency performance with flat plate guide vanes (6 7)

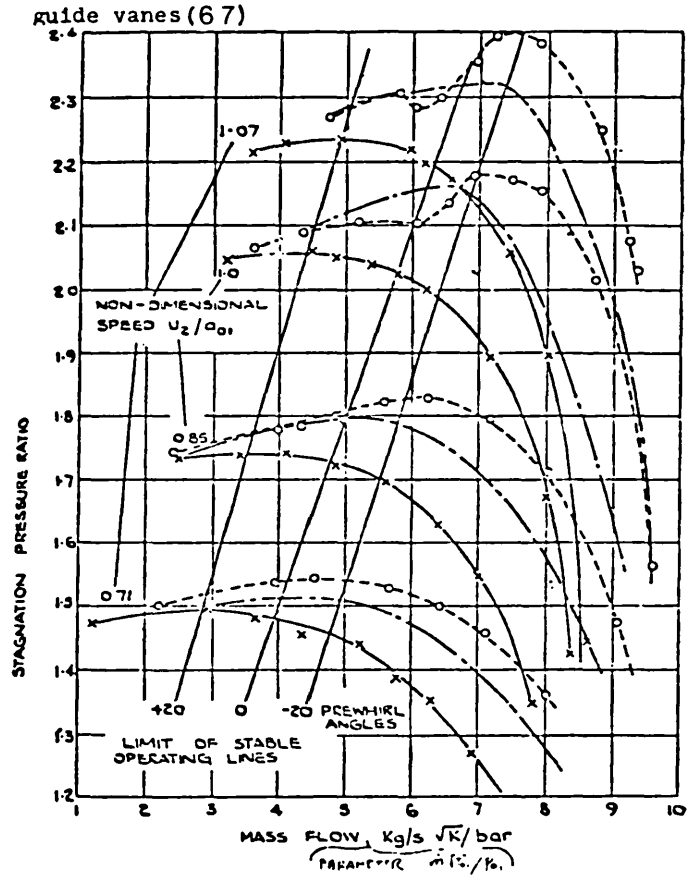


FIG. 3.22 Performance map with flat plate guide vanes (6 7)

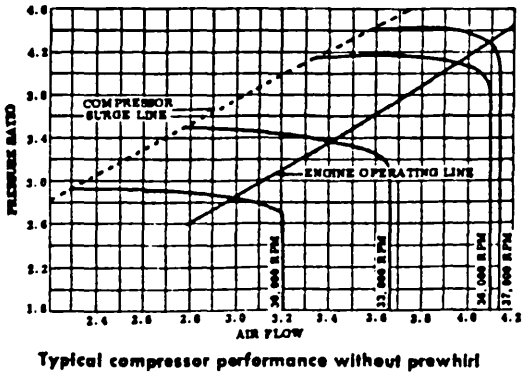


FIG. 3.24 (62)

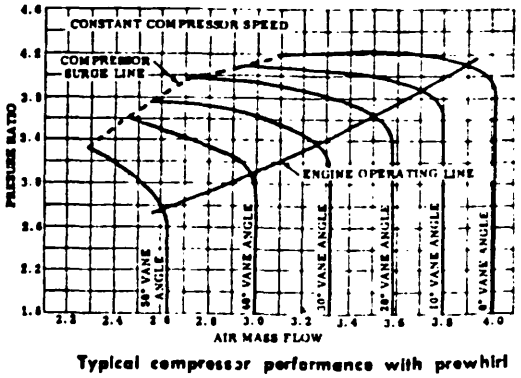


FIG. 3.25 (62)

obtain maximum power, the guide vanes would be opened to the axial position and the rotational speed of the compressor would be increased. This would result in an increase in airflow giving a corresponding increase in power, but it would be expected that compressor efficiency would drop, thus giving increased s.f.c. (66).

Negative preswirl may be employed near maximum gas turbine speed to augment engine power or to simulate the pressure ratio characteristic of maximum speed at a lower speed thus reducing the engine speed range (64). Although negative prewhirl increases the work capacity of the compressor, the pressure ratio developed may drop because of a drop in compressor efficiency. Throttling cannot be avoided and the increased relative Mach number results in impeller choking (42, 62, 61).

It was found (64) that the negative preswirl angle could not be increased beyond 20° primarily due to high guide vane loss. It was suggested that because of the proximity of the rotor to the V.I.G.V. when giving negative prewhirl, the rotor flow field could be inducing the flow to detach from the suction surface.

In turbochargers prewhirl may be used to increase the surge free flow range and control the compressor delivery pressure thus controlling the engine boost pressure.

3.6.2.4.3 Interrelation of variable geometry methods - system optimisation

The full benefit of inducer prewhirl may only be achieved if the initial compressor design was specially performed with a view to accommodate prewhirl (63). When

the use of prewhirl is a further development of an existing design, optimisation of the diffuser may be required (67). Regulation of flow in single stage radial compressors is most effectively achieved by a combination of V.I.G.V. and variable diffusers, providing minimum efficiency penalty with flow reduction. The scheduling of inlet prewhirl with diffuser vane position should be optimised during both initial design and component testing (42).

However such a system of variable geometry may be too complicated and costly. On the other hand the application of prewhirl to a compressor with an optimum diffuser design may be aerodynamically better than the application of a variable diffuser in order to extend the operating range (67). For such an arrangement with V.I.G.V., the additional cost, aerodynamic performance, complexity of the activating mechamism, together with inlet blockage and wake losses at the compressor design point, will have to be considered (6, 67).

Several turbomachinery manufacturers have built fully variable geometry compressors incorporating V.I.G.V. and/or variable diffusers. Some examples are shown in Figures 3.26 (44) and 3.27 (68, 69). However none of these has gained wide commercial acceptance, because of the aforementioned shortcomings.

3.6.3.5 Aerodynamic methods

Complex variable geometry mechanisms can be dispensed with, if flow control is accomplished by aerodynamic methods. These can be classified into:

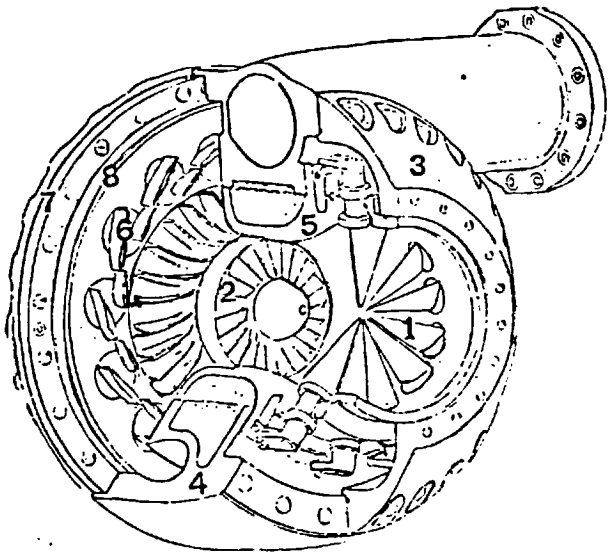


FIG.3.26 WORTHINGTON Variable Geometry Compressor (44)

The more advanced T35GB turbocharger with variable-angle inlet guide vanes and exhaust bypass-valve

1 Compressor inlet
2 Compressor housing
3 Compressor shroud
4 Inlet guide vanes
5 Guide vane control mechanism
6 Rotor assembly with partition
7 Turbine housing
8 Turbine shroud
9 Turbine outlet
10 Bypass valve

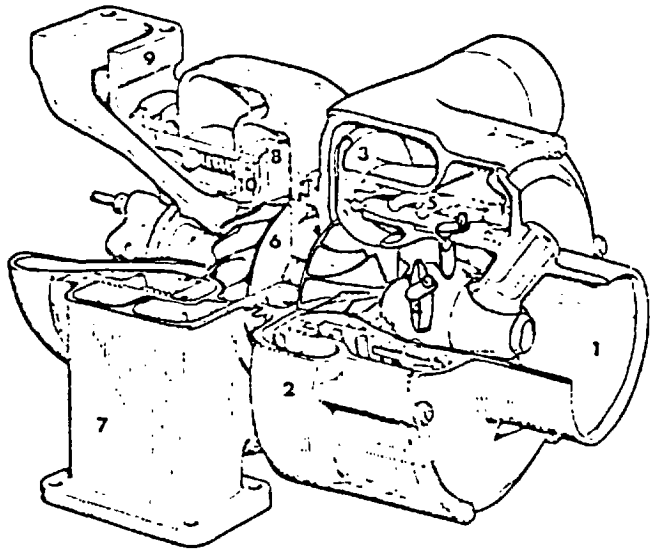


FIG.3.27 FLYGMOTOR Turbocharger with VIGV and Waste-Gate (69)

1. Boundary layer controls (70)

By stabilising the boundary layer, flow separation may be prevented. Boundary layer suction involves removing the low energy fluid through openings in the aerodynamic surface. Boundary layer energisation involves injecting high energy fluid in the direction of flow, in a way that invigorates the slow moving layer. The above methods may be applied to the impeller or diffuser of a centrifugal compressor.

2. Main flow controls

These involve changing the direction of flow of the main stream by injecting a quantity of high energy fluid at some oblique angle to it. Thus the flow angle into the inducer or the diffuser may be changed.

The high momentum content of the fluid leaving the rotor would mean, that to achieve any appreciable flow deflection, the injected fluid must have appropriately high momentum. It may therefore be easier to deflect the low momentum flow at the compressor inlet, i.e. to induce prewhirl to the inflow. With this latter arrangement high pressure fluid from the compressor discharge may be recirculated and injected to provide prewhirl. Thus in addition to the control function of prewhirl, there will be an apparent increase in the compressor flow range by the recirculation.

The method of aerodynamically imparting prewhirl to the inflow of a compressor rotor, by injecting high velocity fluid at some oblique angle to it, varying the quantity of injected fluid to get varying amounts of prewhirl, formed the kernel of the present research work.

CHAPTER 4

AN AERODYNAMIC METHOD FOR CONTROL AND RANGE IMPROVEMENT OF ROTARY COMPRESSORS - PART I

4.1 INITIAL EXPERIMENTS

4.1.1 Introduction

It was thought that the most effective way to evaluate the potential of aerodynamically inducing prewhirl was by direct experiment. The questions that arose in relation to this method can be grouped into two categories:

- The fluid dynamic aspects of flow mixing and resulting flow deflection.
- The problems of applying this method as an efficient flow control system (in particular on a turbocharger).

The lack of background information compelled simultaneous testing of both categories to be adopted.

Although this may be questionable methodologically, it was thought to be more efficient timewise, in view of the uncertainty of the final outcome. It was therefore decided to experiment with such an aerodynamic arrangement on a turbocharger compressor.

4.1.2 The Experiments

The experimental setup is schematically shown in Figure 4.1, and also in Figure 4.2. The turbocharger turbine was driven by hot compressed air supplied from an external source. The flow was controlled with manual valves. Compressor back pressure was provided by a manual valve on the discharge pipe. A calibrated inlet bellmouth was used for compressor flow measurements. Turbocharger speed was measured by the optical method (115).

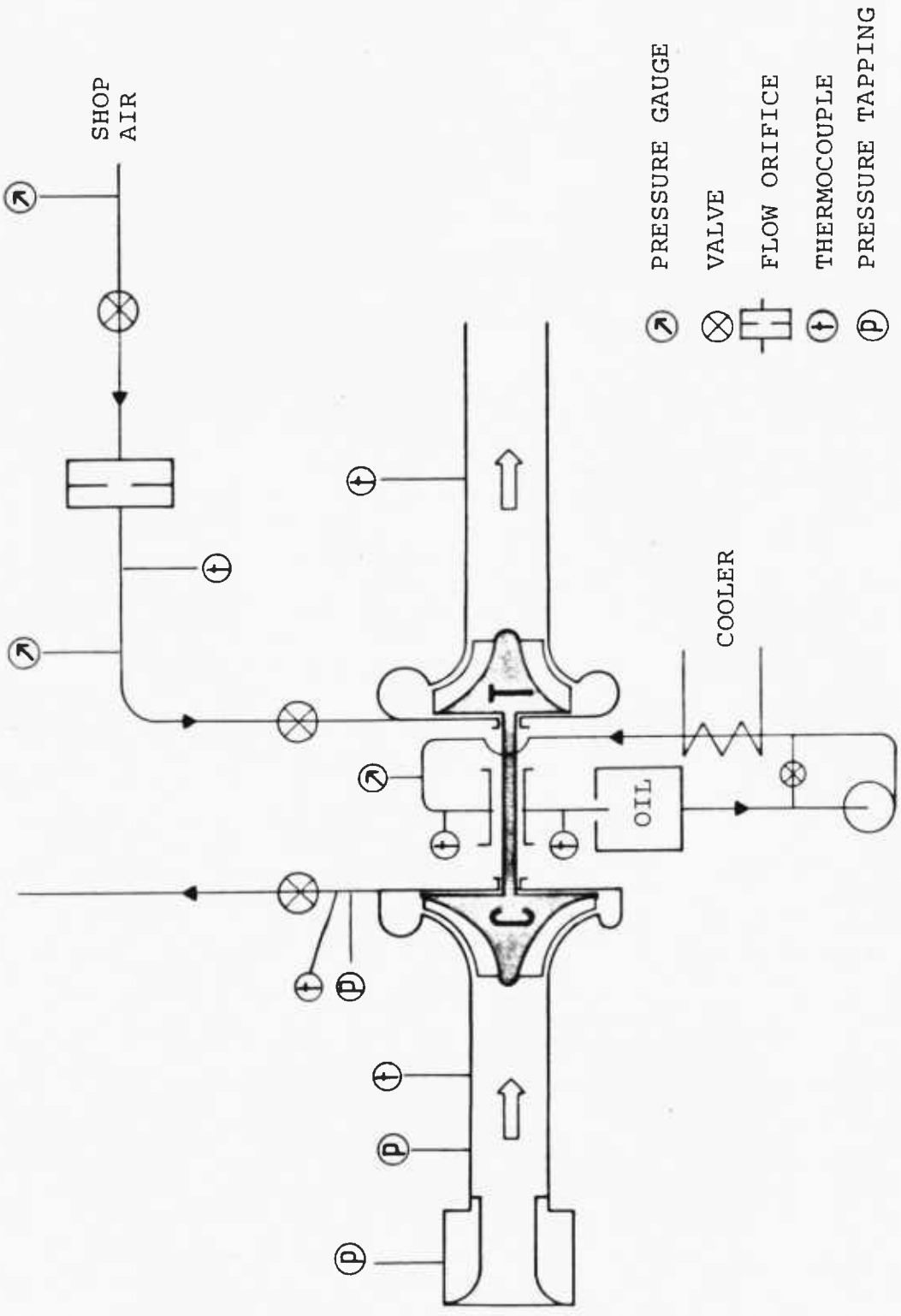


FIG.4.1 TO4B-Y3 Compressor Experimental Set-Up

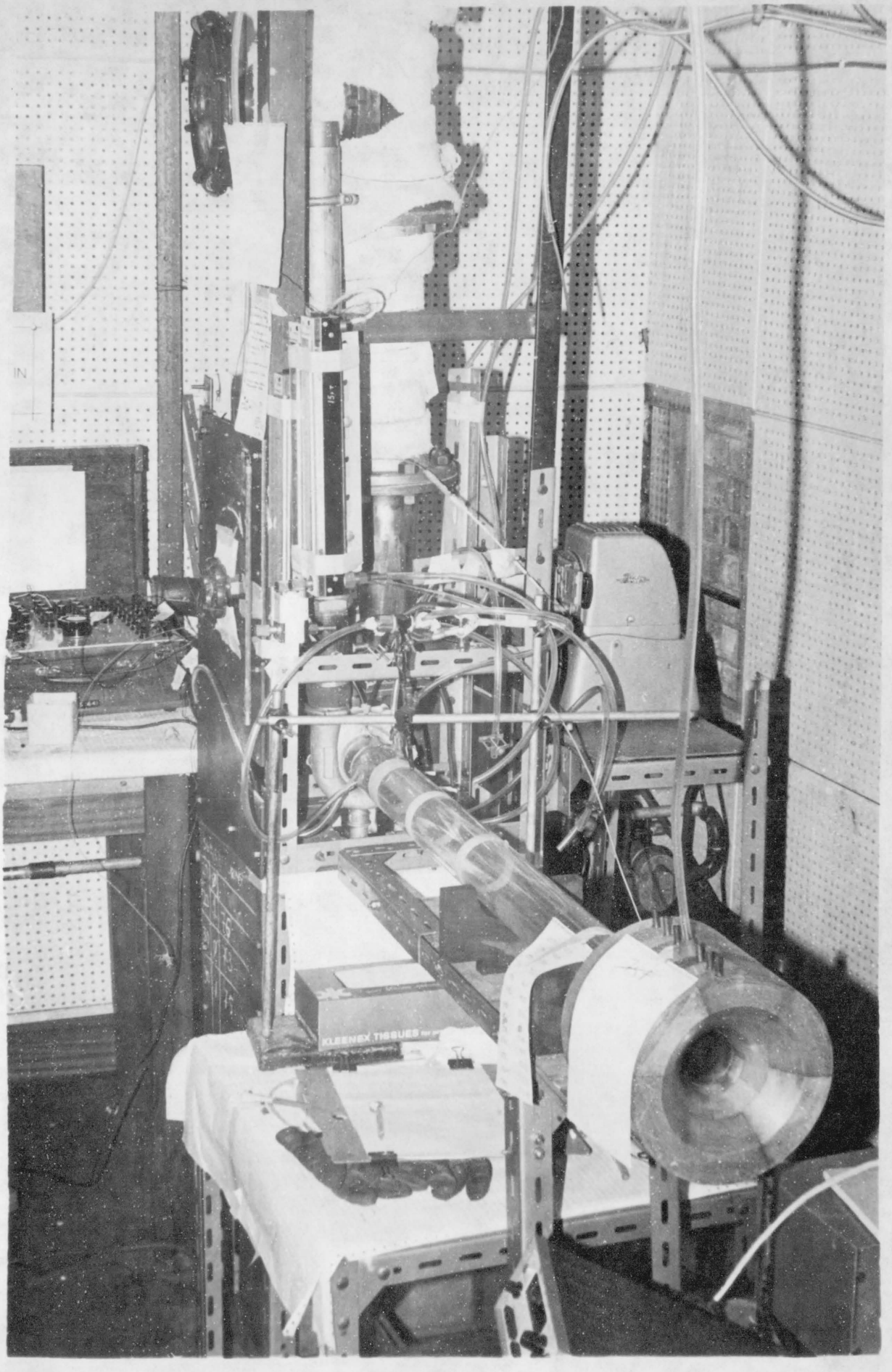


Fig. 4.2 Overall View of TO4B-Y3 Compressor Experimental Rig

The experiments were performed on an AIRESEARCH TO4B series turbocharger with a Y-3 trim compressor.

As there was no obvious arrangement for the air injection, a trial and error process was employed. It was decided to use discreet high pressure air jets to impart the swirl to the inlet flow. Other variables were the size, shape, number, and orientation of the jets and their distance from the impeller eye.

It was decided to use three jets, compromising between complexity of the arrangement and uniform flow profile round the circumference. The ejection axis lay on a plane normal to the inlet pipe axis and its angle to a tangent at the point of ejection was 15° (see Figure 4.4). Steel hypodermic tubing of 1.5 mm^2 cross section was initially used for the injectors.

The jets were fed with compressor discharge air bled from a point upstream of the back pressure valve. An air scoop was used to take advantage of the ram effect. The main recirculation pipe branched into three secondary pipes feeding the jets. The normal procedure of compressor performance mapping was followed. The test speeds were taken from the manufacturers' compressor performance map corrected to ambient conditions.

A steep increase in the noise emanating from the compressor was taken as incipient instability. This was quite arbitrary, but hard surge was avoided to prevent damage to the unit. Because of rig constraints, the maximum possible compressor speed was 75000 rpm.

The recirculating flow was measured with rotameters and regulated with a manually operated valve. Flow visualisation was possible with a battery of woollen tufts supported on steel needles which could traverse in the radial direction of the perspex inlet pipe. These also provided additional indication of compressor instability and reverse flow, when placed close to the impeller inlet. The plane of injection was originally placed 50 cm away from the impeller eye. It was thought that a certain distance would be needed for the flow to settle in a uniform swirling mode since discrete jets were used. It was soon realised that the swirl generated by the jets was small and the prewhirl profile faded away a small distance downstream of the ejection point. The position of the injection plane was twice updated, moving closer to the impeller eye (at 30 cm and 20 cm). No appreciable change in the compressor performance was observed.

The size of the main recirculation pipe and the three secondary pipes was increased. The cross section of the injectors was increased to 4 mm^2. The angle of the axis of the injectors to the tangent at the point of ejection was increased to 20°. The injection plane was placed 9 cm away from the impeller eye.

These changes had some impact on the compressor performance but no definite conclusions could be drawn. The injection plane was placed 6 cm away from the impeller eye. The injector cross section was increased to 16 mm^2. The arrangement is shown in Figure 4.2, 4.3, 4.3A. During the course of these tests a malfunction of the lubrication

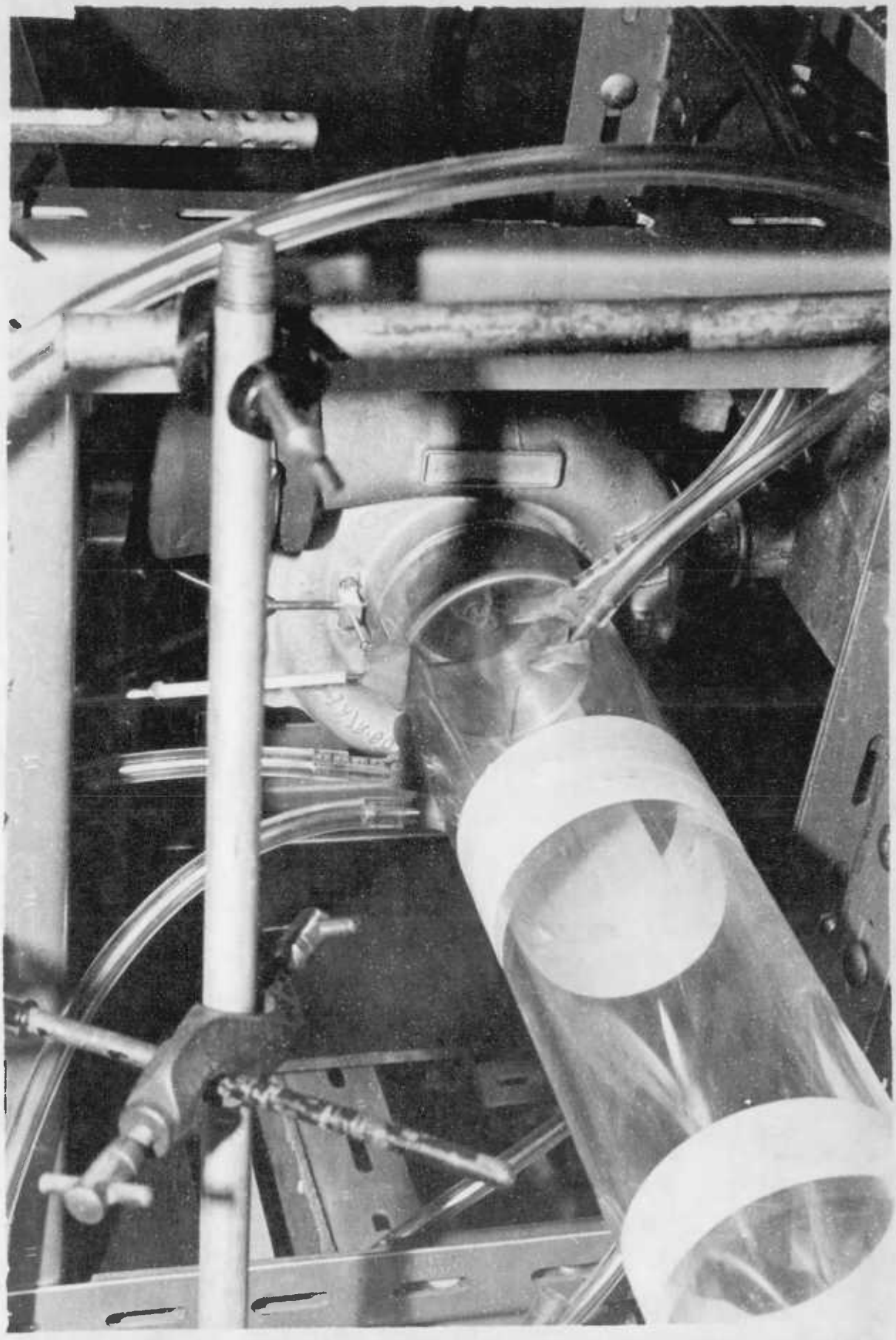


Fig. 4.3 Close-up of Jet Ejectors from Initial Experiments TO4B/Y3 Experimental Rig

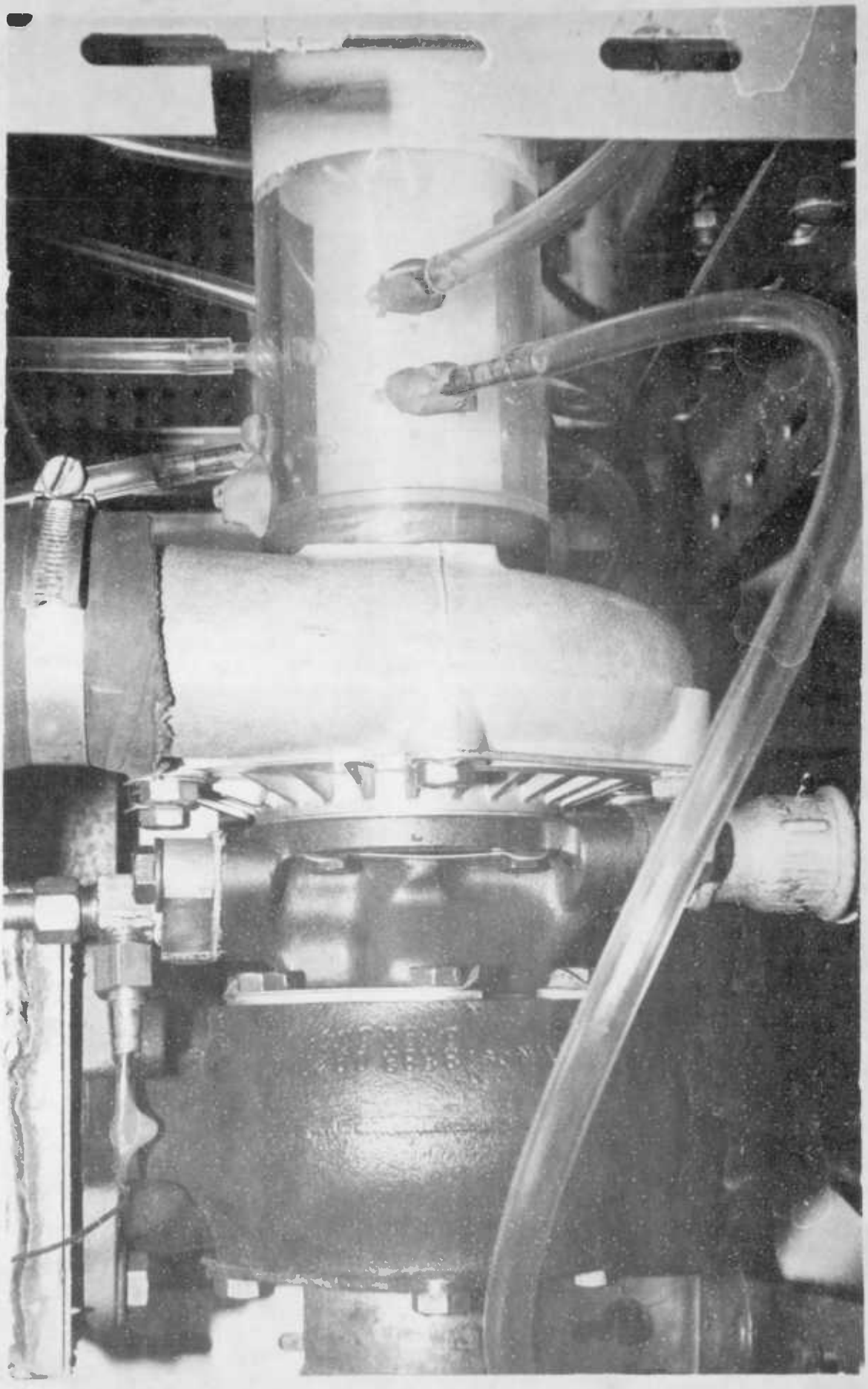


Fig. 4.3a Side View of TO4B/Y3 Turbocharger with Jet Ejectors in Front of Impeller from Initial Experiments

system resulted in excessive vibration of the turbocharger. Damage to the bearings was suspected and the tests were discontinued for the turbocharger to be overhauled. However data for 35000 and 45500 rpm with and without air injection, had already been obtained.

4.1.3 Flow Visualisation - Observations on Profile Variation

These observations were made during the tests with the injection plane placed 9 cm away from the impeller eye. At 3 cm downstream from the injection plane and near the incipient instability flow rate, 40° - 60° of deflection from the axial direction was observed 2 mm away from the inlet pipe wall. Moving further away from the wall in the radial direction towards the axis the deflection quickly diminished, but the flow was very turbulent 5 - 10 mm from the wall.

At 5 cm downstream from the injectiom plane, 35 - 45° of deflection was observed 3 mm away from the wall. Moving radially towards the axis the deflection was quickly diminished but the profile was smoother. At 6.5 cm downstream 25 - 30° of deflection was observed 3 mm away from the wall. The profile was still smoother.

The type of swirl approached a forced vortex variation but most of the flow deflection was near the wall, with little deflection further radially inwards, indicating that the design was not optimum.

4.1.4 Comments on Results

The data obtained from the last and most optimised arrangement in these series of tests is shown in Figure 4.5 in the typical compressor map fashion. Speeds and efficiencies are shown.

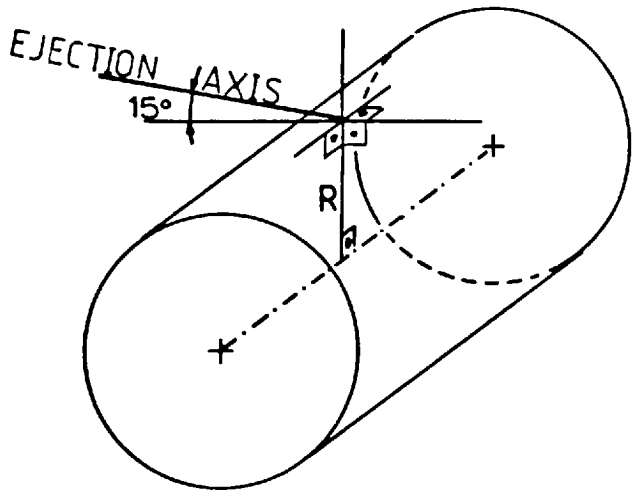


FIG.4.4 Ejection Axis Orientation

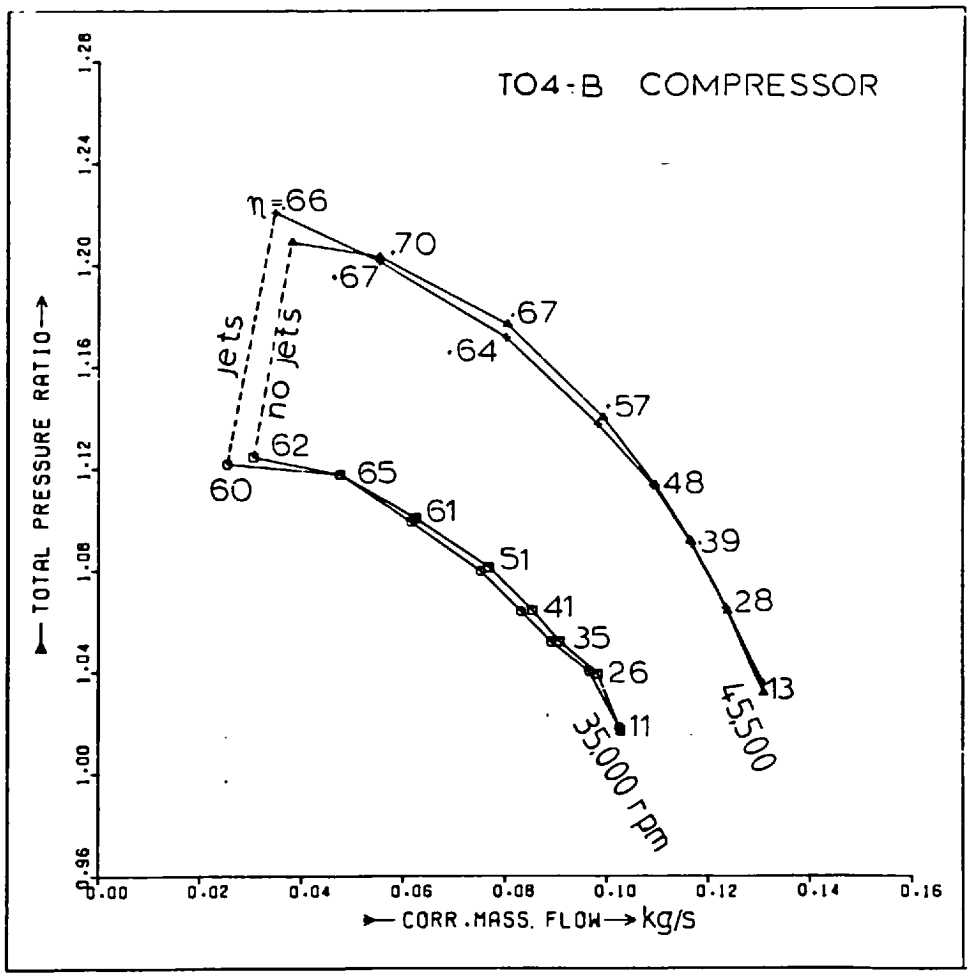


FIG.4.5 TO4B-Y3 Compressor Performance (from initial jet experiments)

Flow deflections of up to 45° were measured 3 cm downstream of the injection plane, 3 mm from the compressor wall, with the compressor mass flow at the stability limit. However the profile was soon destroyed further away from the wall and strong turbulence prevailed. This indicated that only a thin layer near the pipe wall was affected. Some improvement in the stable flow range (determined audibly) is evident in Figure 4.5, but the arrangement of the jets was certainly non-optimum.

These tests verified that some deflection of the compressor inlet air was possible by high pressure fluid injection, but a more fundamental approach was essential to explain the phenomena observed and enable the design of an effective arrangement.

4.2 ANALYTICAL APPROACH

The need for a theoretical model emerged, to be able to predict the flow field, resulting from the interaction of two streams of fluid under a particular configuration, that is, the deflection of a main flow by oblique ejection of high energy fluid into it. If the influencing parameters in such a flow situation could be singled out, then a "target" flow field could be obtained by varying these parameters. The fluid injection arrangement design could then be optimised, by using the flow model. It may then be possible to attain a flow field equivalent to that obtained through inlet guide vanes, and hence use such an arrangement to control the compressor performance and flow range.

The flow situation can be viewed in two ways:

1. The effect of injection on the main flow

The main flow is deflected under the impulse of high pressure fluid injected obliquely to the main flow with some of the kinetic energy of the fluid injection being lost through friction and mixing.

2. The effect of the main flow on the injection

The high pressure fluid injection can be considered as a jet expanding into a cross flow and deflected by it. In the process it entrains fluid from the surroundings and gives directional momentum to it, at the same time losing some of its initial momentum.

It was decided to adopt the latter formulation.

4.3 THE JET IN A CROSS FLOW

4.3.1 Introduction

The flow situation where a jet issues at some angle to the moving ambient fluid exists in a number of practical cases such as:

- VTOL aircraft during lift-off and transition flight
- fuel injection into certain types of combustion chambers
- thrust control of rocket trajectories
- sewage discharge into flowing streams
- discharge from chimney stack into a wind
- flares from safety systems in petroleum plants
- secondary air injection in combustion chambers
- impingement cooling of turbine blades
- film cooling of turbine blades

4.3.2 Qualitative Description

The turbulent jet ejected in a cross wind is an example of a free turbulent shear flow (see Figure 4.6).

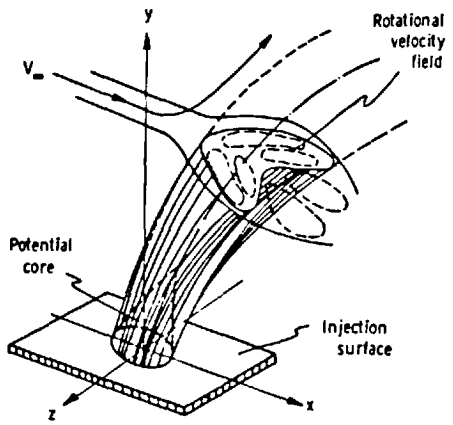


Diagram of the interaction resulting from jet injection into a cross flow (after Abramovich

FIG.4.6 A Jet in a Cross Flow (91)

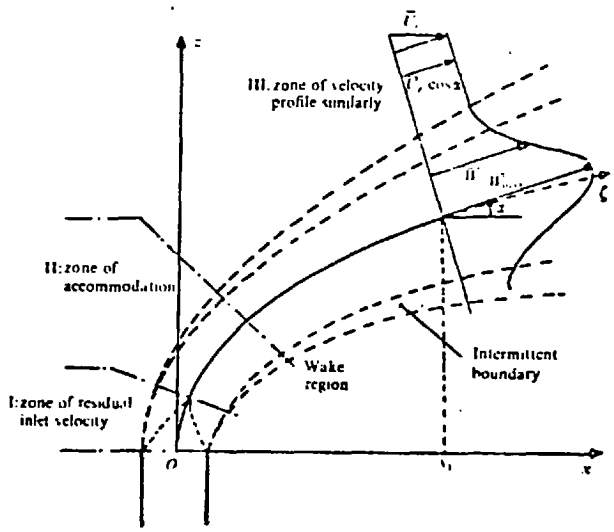


FIG.4.7 Configuration of the Flow in the Plane of Symmetry (76)

From experiments it can be seen that there is a distinct edge to the jet. If cross sections perpendicular to the maximum velocity vector are taken, the direction of flow within the region bounded by the jet edge, is parallel to the maximum velocity vector.

Relative to the maximum velocity stream line the lateral distribution of maximum mean velocity is similar to a Gaussian distribution (see Figure 4.7). The flow field developed is a result of the miximg of two potential streams. At the source the jet has an almost uniform velocity profile and a low turbulence intensity (compared with the expanded jet). Upon entering the cross flow the edges of the jet are subjected to intense shear stress, resulting from the velocity gradient between the jet and the cross stream. In the free jet where the external flow velocity is zero, a uniform entrainment of the surrounding fluid occurs. The entrained fluid is accelerated as the jet spreads and the jet fluid is correspondingly decelerated. In the presence of the cross flow this is complicated by the potential flow surrounding the jet. The flow is decelerated at the upstream surface of the jet and creates a positive pressure region. The sides are subjected to a lateral shearing stress directed toward the rear. Jordinson (72) has compared this flow to that around a porous cylinder with suction.

Separation occurs at the rear and gives rise to a negative pressure region or wake. This initial stage of the flow is termed the zone of establishment and is similar to the free jet in that there is a constant maximum velocity.

This region of residual inlet velocity, which includes the potential core, extends for about five diameters for a free jet, but is approximately half as long in the deflected jet.

Once the potential core has been consumed the continued lateral diffusion of jet momentum effects a decrease in the maximum velocity along the centre stream-line. This region, which is highly turbulent throughout the entire jet cross section, is termed the zone of established flow, and possesses characteristics similar to the free jet. The external flow is affected very little by the presence of the jet and the static pressure and mean velocity can be considered constant.

At low ratios of jet to cross wind velocity, the potential core is deflected by the pressure field. The point at which the axial velocity begins to decay is shifted downstream. For velocity ratios greater than about four (jet velocity to cross flow velocity), the potential core is conical, with the point approximately above the centre of the jet orifice.

Hence the effect of the pressure forces and the lateral shear is primarily to change the shape of the cross-section from a circle (usually) at the outlet, to a kidney (or horse-shoe) shape. The sides of the jets possess less momentum than the centre because of the lateral mixing process and therefore are readily deflected. This effect is so severe that separation of the cross flow from the edges of the jet occurs just behind the mid-section. A similar phenomenon exists on a circular cylinder but with

the jet the return flow in the centre of the wake is carried by the entrained fluid into the jet and so moves rapidly along the jet direction. The result is a pair of counter-rotating vortices attached to the jet which increase in strength throughout the zone of established flow (see Figures 4.8, 4.9, 4.10, 4.11). These vortices move against the deflecting flow and thus provide a mechanism by which the jet resists deflection. Since the jet trajectory is stationary in space, the strength of the vortices must be such that their intrinsic velocity relative to the surrounding gas equals the component of the cross flow at right angles to the jet trajectory. The vortices lose strength as more gas is entrained, and the jet trajectory curves approach asymptotically the direction of the cross flow. Behind the vortices the cross flow streamlines become roughly parallel again and no discernable wake similar to that behind a circular cylinder can be seen, but a large scale turbulence persists.

With simple jets, entrainment occurs only by the spreading of the turbulent front. In the present case, this is augmented by the action of the vortices which cause an internal ciruclation and hence large scale mixing within the jet. In addition, some external fluid with small momentum is carried into the centre of the wake by the lateral shearing action. The total mass flux across the outside jet boundary is, therefore, significantly greater than in the free jet.

The strong mixing processes disperse the axial

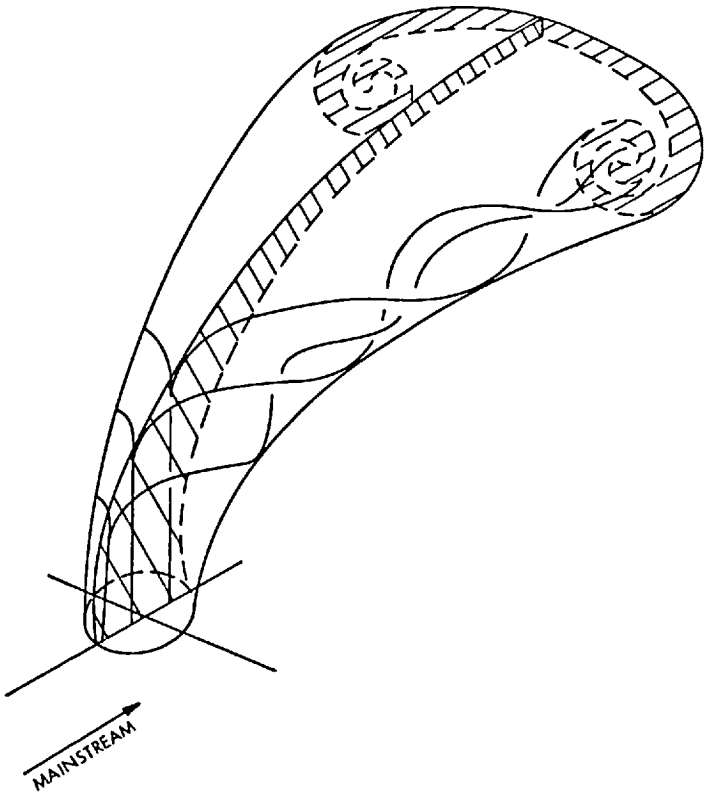


FIG.4.8 Formation of trailing vortices showing distortion of jet fluid.

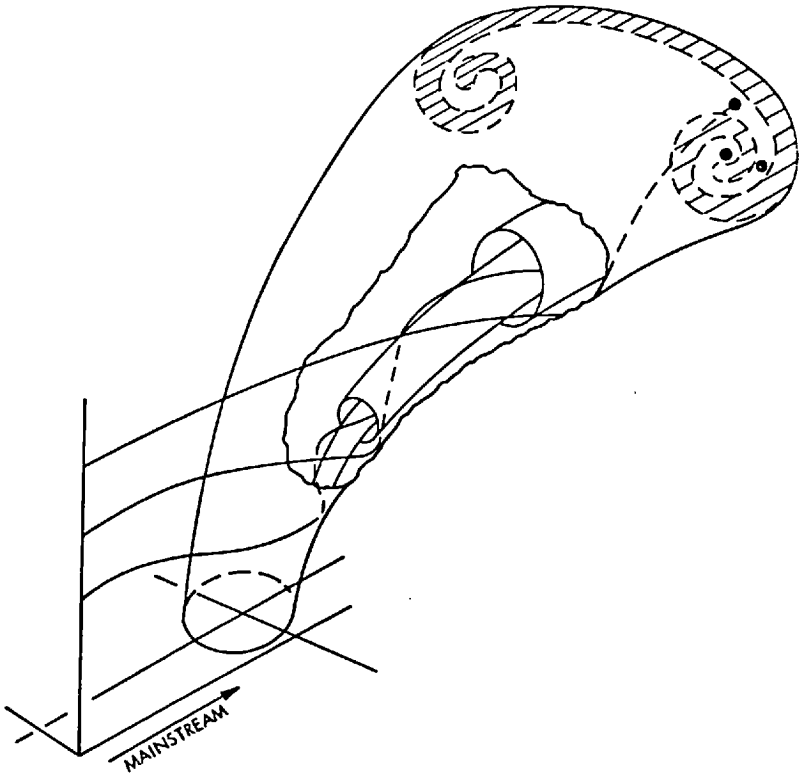


FIG.4.9 Formation of trailing vortices showing entrainment of mainstream fluid into trailing vortices.

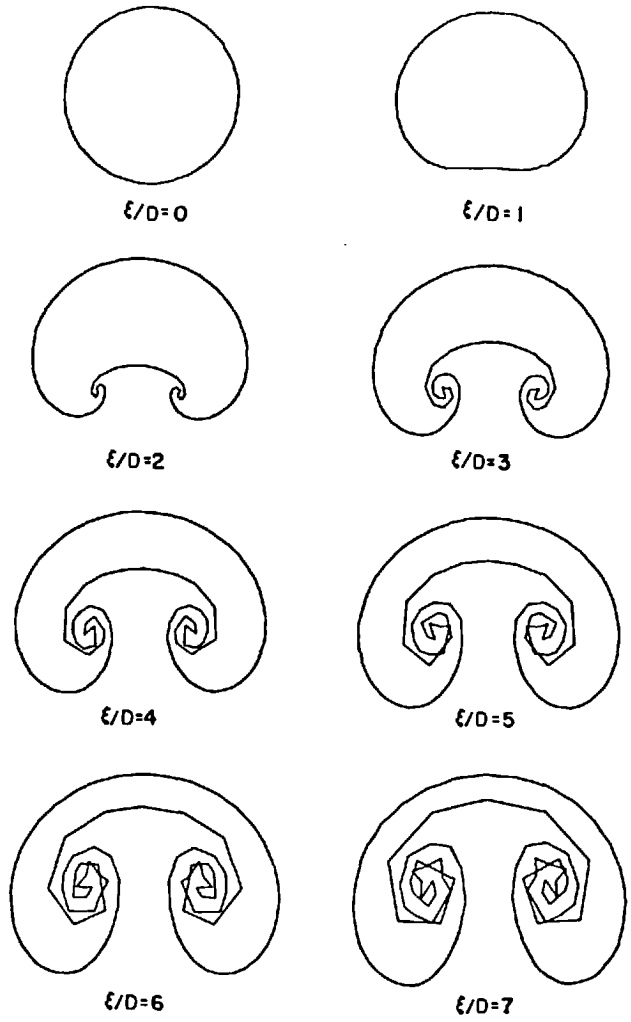


FIG. 4.10 Wake cross sections showing rollup into a pair of vortices. $V_\infty/V_j = 0.25$.

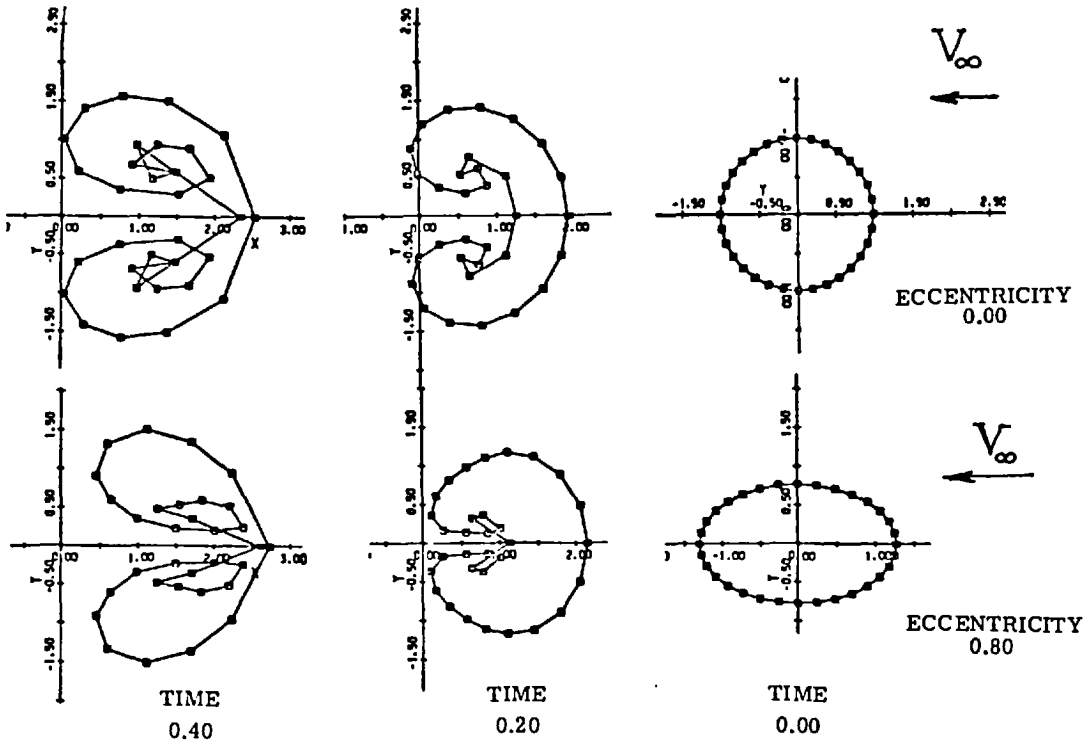


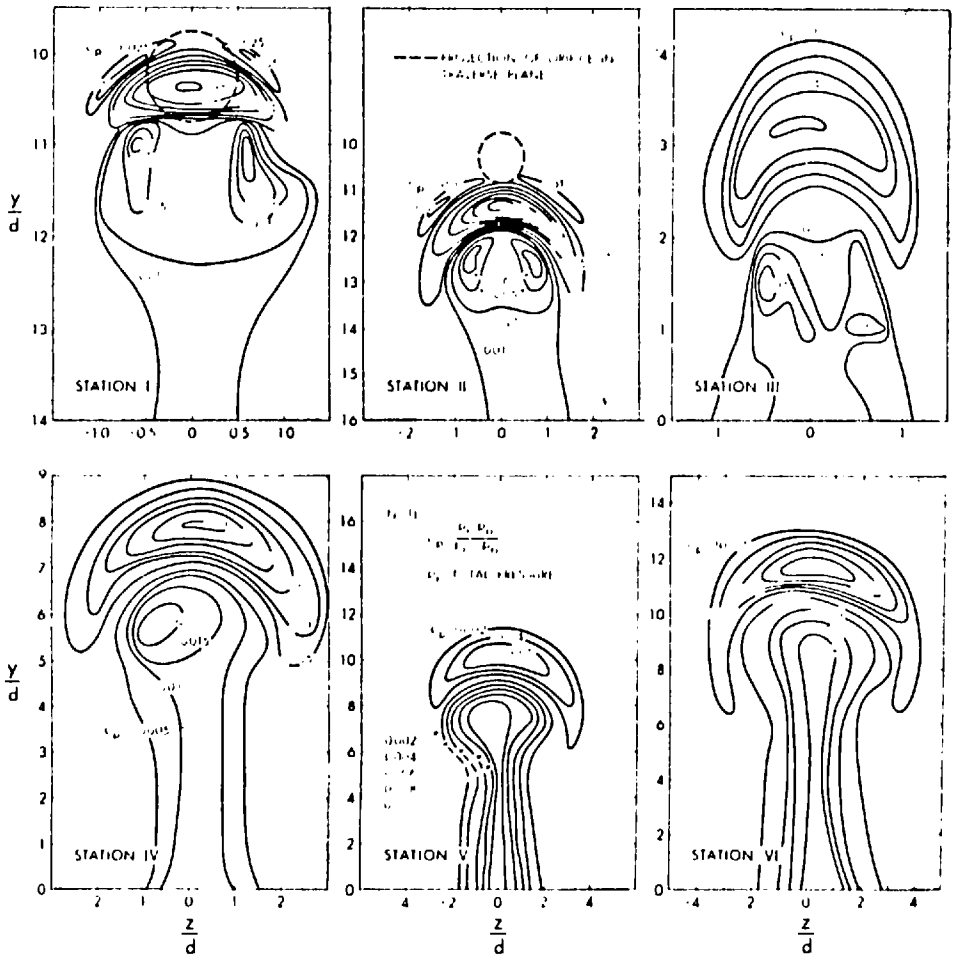
FIG. 4.11 Rolling-up of two jet cross sections, one with circular, the other with elliptic exit nozzle. (81)

momentum over a steadily increasing area and thus the jet is continuously deflected downstream. The cross sectional shape normal to the centre stream-line appears to remain approximately the same (zone of velocity profile similarity) (75).

4.3.3 Relevant Literature

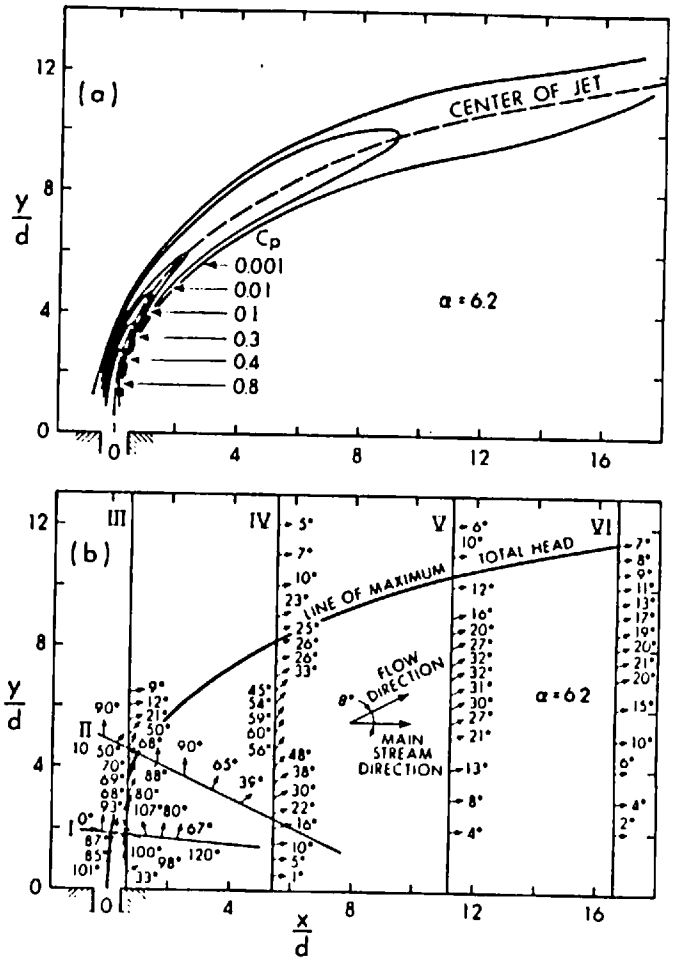
Data are presented (72) obtained with a jet mounted flush to a plane wall ejecting normal to an air stream, for several values of the ratio of jet exit velocity to cross flow velocity. The path of the jet and the shape of the jet cross section were determined from total head measurements. The cross section was found to be of a horse-shoe shape away from the orifice. It was also found that the jet draws up with it air from the floor boundary layer. A boundary layer splitter plate was used reducing the thickness of the b.l. to 2.5 mm at the orifice. Measurements for velocity ratios of 4, 6, 8 are presented (see Figures 4.12, 4.13, 4.14).

An investigation (73) to determine the path and general shape of the wake of a single jet exiting at large angles to the free stream through a range of velocity ratios is presented. The jet exit deflection angles ranged from 30° to 180° from the free stream. Photographs taken of the wake, which was a mixture of compressed air and water vapour, showed that the jet paths were essentially the same when the jet was exiting upward or downward as well as when the jet was located adjacent to a large surface or located away from adjacent surfaces. It was concluded that



Total pressure contours for circular jets in cross-flow. (Reproduced from Jordinson, R., 1956. Flow in a jet directed normal to the wind. Aero. Research Council, England. Copyright belongs to Controller, HMSO.)

FIG.4.12(72)



Constant pressure contours and flow directions for circular jets in cross-flow. (Reproduced from Jordinson, R., 1956. Flow in a jet directed normal to the wind. Aero. Research Council, England. Copyright belongs to Controller, HMSO.)

FIGS.4.13 and 4.14(72)

the primary variables determining the jet path were the deflection angle of the jet at the exit and the effective velocity ratio (square root of the ratio of dynamic pressures for the jet and cross stream). The results were compared with results for the jet path from other investigators and the best empirical fit to these data was determined.

The penetration of air jets issuing from circular, square and elliptical orifices directed perpendicular to an air stream was examined (74). All orifices were of equal cross sectional area. The elliptical orifices examined had axis ratios of 2:1 and 4:1. At low velocity ratios best results were achieved with the square and 4:1 elliptical orifices. At high velocity ratios best penetration was achieved with the square orifices.

A qualitative analysis (75) of the jet shape and behaviour when ejected normal to a cross flow is presented, together with experimental results for a range of velocity ratios. A semi-analytical solution with experimental determination of several variables is given and the results compared with the experimental data. The experimental evidence indicated that the jet flow displays similarity to a free jet if a natural system of axes is chosen.

A Laser-Doppler (77) technique was used to explore the flow field of a nitrogen jet injected into a cross flow of air at a momentum flux ratio of 16. Several traverses were made at right angles to the jet centre line which was obtained from schlieren photographs. Velocities were measured in the direction of the traverse and at right

angles to it. It was found that the excess of the centre line velocity over the parallel cross stream component decreases faster than for a jet without cross flow. Also the jet width increases linearly with distance from an effective origin about one jet diameter upstream of the injection point, with the distance measured along the trajectory. It was further found that the velocity profiles exhibit the same similarity on expansion as free jets.

Experiments on confined turbulent jets in a cross flow are presented (78). A single jet and several arrangements of multiple jets were examined. The main conclusions were:-

The trajectories and structure of a single jet in a cross flow are only mildly affected by an opposite wall, unless the velocity ratio is sufficiently strong so that the jet directly impinges on the wall.

The trajectories and structure of a single row of jets depends strongly on the velocity ratio and the spacing ratio (distance between jets over orifice diameter). For close spacing the behaviour approaches that of a two-dimensional jet (i.e. exiting from a slot).
In this case the upper wall position is quite critical since the two-dimensional jet will present a barrier to the flow and consequently will be bent relatively more quickly forming a recirculation eddy behind it.
In closed spaced jets the side vortices will tend to entangle and drive each other downwards,

but if the spacing is too close, the vortices will be weak so the upward momentum will be preserved further due to less entrainment.

Trajectories are therefore most suppressed for some intermediate value of spacing ratio, depending upon the velocity ratio (see Figures 4.15, 4.16). When the wall is sufficiently near, the jet on impinging on the upper wall spreads sidewise and momentum and temperature are carried away with the fluid in a vortex motion, the jet splitting into two parts.

Experimental jet trajectory data (79) are presented for both confined and unconfined channels in which there is a difinite non-uniform cross flow velocity profile. A one-dimensional analysis is also presented using conservation laws, entrainment function models and an experimental correlation for the length of the potential core, to predict the trajectories and wall impingement points.

A mathematical analysis for the round turbulent jet interacting with the mainstream flow in a wide range of interaction angles and high interaction rates is presented (80). Conservation equations for mass and momentum are derived and the extra unknown quantities (apart from the velocity and the inclination of the trajectory) eliminated by assuming that the jet cross section remains self similar and that entrainment velocity consists of entrainment due to ordinary mixing and due to a counter-rotating vortex pair. With empirical coefficients the model is successful in predicting the trajectory immediately downstream of

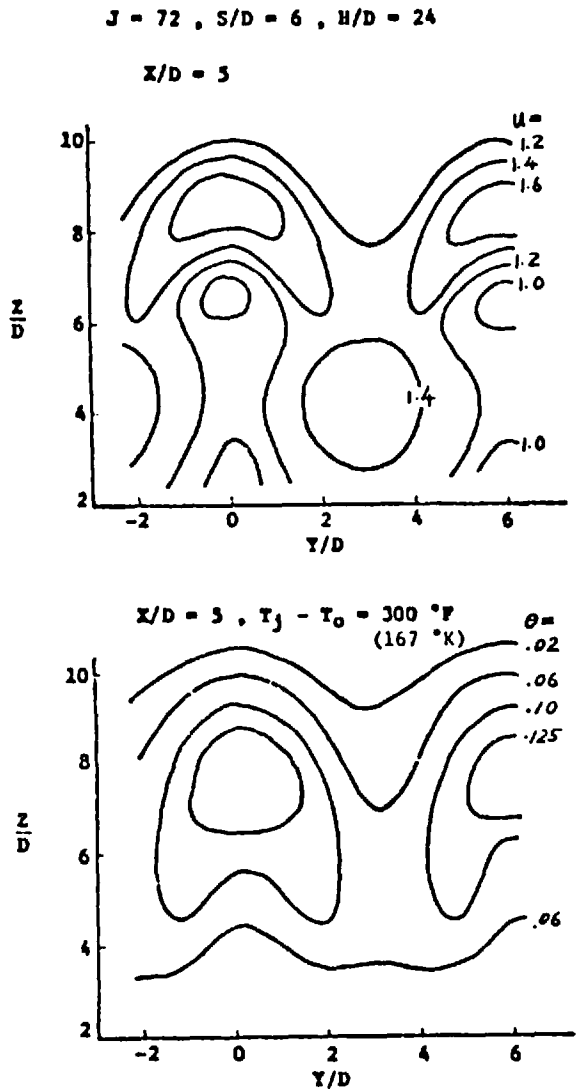


FIG.4.15 Contours of Constant Speed and Temperature for Single Row of Jets(78)

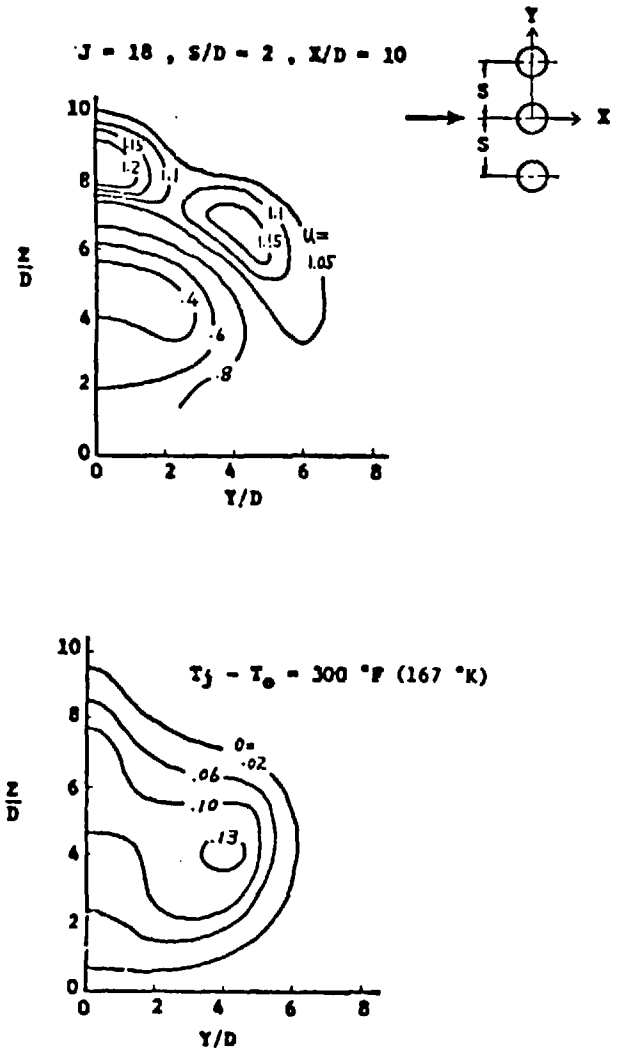


FIG. 4.16 Contours of Constant Speed and Temperature for Multiple Jets (78)

the potential core.

Similar analyses are presented (82, 83, 84). At the extreme end of the analytical spectrum are full numerical solutions.

The three-dimensional imcompressible Navier-Stokes equations are solved (85), written in terms of velocity, vorticity and temperature and assuming a constant turbulent viscosity for an unheated buoyant jet in a cross flow.

A solution procedure is presented (86), employing an elliptic finite difference scheme with three velocity components and pressure as the main dependent variables, for a round turbulent jet deflected by a main stream normal to the jet axis.

4.4 MATHEMATICAL MODELLING OF A JET IN A CROSS FLOW

4.4.1 Introduction

Excluding pure numerical solutions, there are essentially two general methods of handling the problem of predicting trajectories of jets deflected by cross flows. The flow may be modelled mainly by considering the turbulent structure and incorporating various entrainment functions into the conservation statements, to explain the increase in mass flow and the consequent deflection of the path, by acquisition of horizontal momentum flux from the main stream.

Alternatively it is possible to enclose the jet-flow by a semi-porous, flexible boundary and introduce pseudo-drag coefficients to account for the forces which cause the bending of the trajectory. The former is attractive in some respects because it is possible to include directly

the contribution of the attached vortex pair in the wake of the flow; one of the most intriguing features of the motion. Nevertheless, the exact form of entrainment functions is open to considerable speculation and many schemes have been derived (84, Keffer disc.).

4.4.2 General Description of Model

The first approach was adopted in the present work.

The entrainment of ambient fluid is attributed to two mechanisms:

The first is the growth of a turbulent field arising from the presence of a velocity difference between the jet and the ambient fluid, similar to ordinary jets. The second mechanism, peculiar to the deflected jet is due to the presence of the counterrotating vortex pair. It is assumed that these processes are sufficient to describe the dynamics of the jet.

Although large differences in pressure exist in the vicinity of the potential core, in the earliest stages of flow development, they soon diminish further along the trajectory, and little entrainment can be attributed to them. Therefore, if this region is ignored, the assumption of constant pressure may be made. The present model does not account for the potential core.

The analysis describes the mean velocity field and accounts for varied initial angle of injection to the cross flow. A natural system of axes and curvilinear coordinates is used. The cross sectional shape of the jet is represented by an equivalent circle of equal area (see also section 6.7.5). The flow in any jet cross section is assumed co-

axial with the centreline direction. Conservation equations are solved for the jet trajectory and growth. The solution gives the jet trajectory, gradient, growth, mean velocity and mean density at any jet cross section.

4.4.3 Analysis

4.4.3.1 Coordinate system

A system of curvilinear coordinates natural to the deflected jet is adopted (see Figure 4.17). The ξ-axis is the jet maximum velocity streamline. The η-axis is defined by the locus of maximum velocity along lines of constant y in the plane perpendicular to the central stream line. The ζ-axis is perpendicular to the ξ- and η-axes. x, y, z are the longitudinal lateral and vertical Cartesian coordinates relative to the cross flow with origin at the jet source. Referring to Figures 4.18, 4.19

V_o ≡ cross flow velocity

ρ_o ≡ cross flow density

θ_j ≡ initial jet ejection angle

θ ≡ angle between a tangent of the ξ-axis through the ξ-η-ζ origin and a plane parallel to the x-y plane.

v_j ≡ initial jet velocity

u ≡ jet velocity

4.4.3.2 Coordinate transformation equations

If a circular jet cross section is assumed then the transformation equations are:-

$$z = \int_0^{\xi} \sin\theta d\xi \qquad (4.1)$$

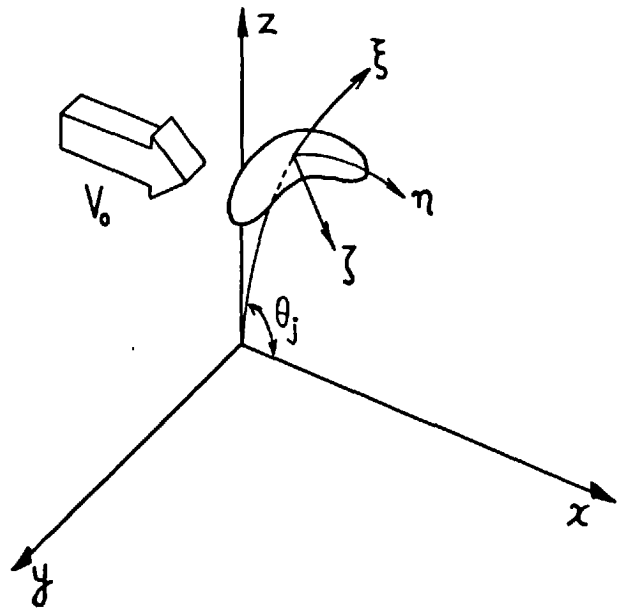


FIG.4.17 Coordinate System

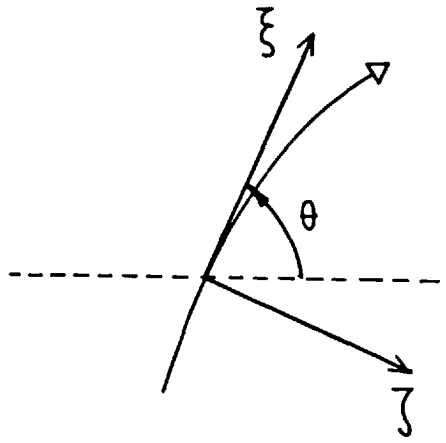


FIG.4.18 Coordinate System

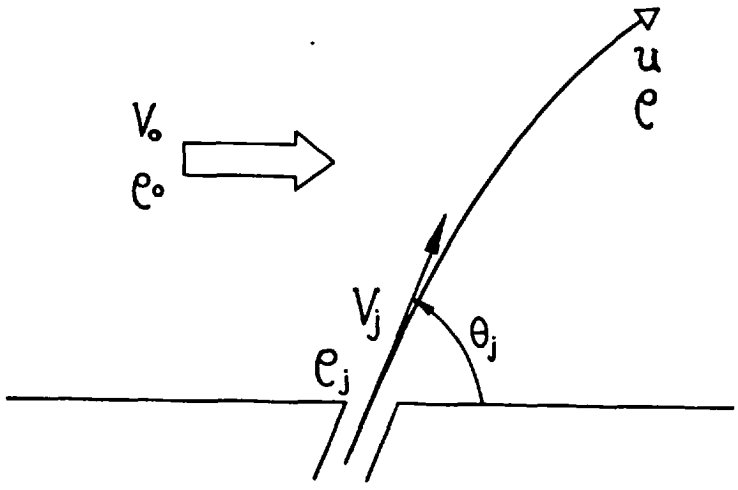


FIG.4.19 Notation

$$x = \int_0^{\xi} \cos\theta d\xi \tag{4.2}$$

4.4.3.3 Conservation of mass

The change of mass flux across and normal to the jet defined cross-section is equal to the flow of mass into the jet across the outer edge per unit increment in ξ (see Figure 4.20)

$$\frac{1}{h_1} \frac{d}{d\xi} \int_A \rho u dA = \oint_C \rho_o v_i dC \tag{4.3}$$

where

u is the jet velocity in the ξ-direction

h_1 is the linearising factor in the ξ-direction (see section 4.4.3.7).

ρ_o is the density of the surrounding fluid, assumed constant.

ρ is the jet density, assumed constant over the defined cross section.

Experimental results indicate (72, 73, 75, 76, 77) that beyond the potential core, the cross-sectional shape appears to be constant along the trajectory. Therefore, to simplify the analysis it is assumed as a first approximation, that the cross-section can be represented by an equivalent circle of radius r, of equal area.

Two major mechanisms contribute to the flow of mass into the jet (entrainment):

a) The velocity difference between jet and surrounding fluid and the subsequent growth of turbulent field from the resulting shear. It is assumed that this depends primarily on the local, parallel to the trajectory, component

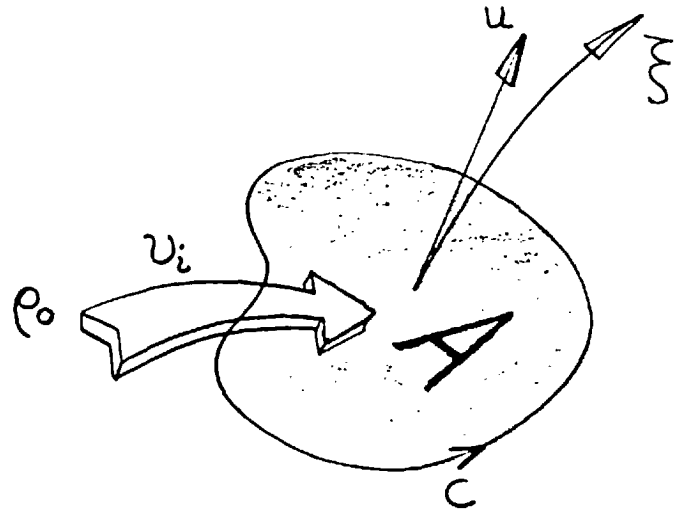


FIG.4.20 Control Volume Notation

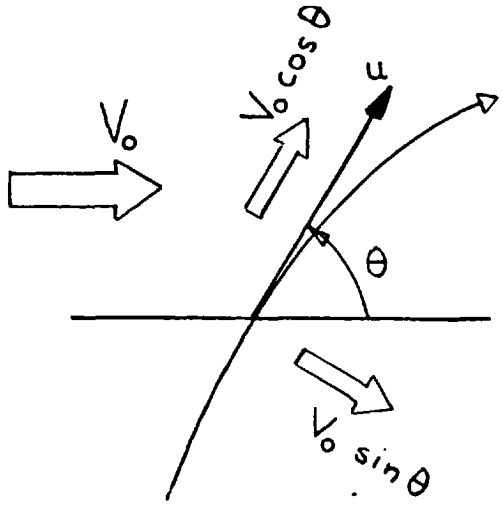


FIG.4.21 Control Volume Notation

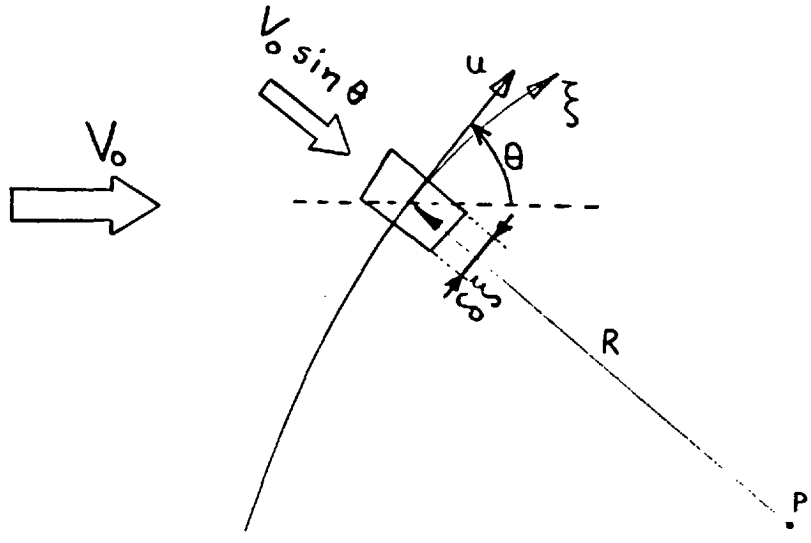


FIG.4.22 Control Volume Notation

of the cross-flow.

b) The vortex formation at the rear of the jet. It is assumed that this depends on the local normal component of the cross-flow.

If $\underset{\sim}{v}_i$ is the velocity vector of the entrained fluid at any point along the circumference of the jet we can have

$$\underset{\sim}{v}_i = \underset{\sim}{v}_\xi + \underset{\sim}{v}_\zeta \tag{4.4}$$

where

v_ξ is the component parallel to the ξ-axis

v_ζ is the component parallel to the ζ-axis

Two entrainment coefficients can be defined, as the ratio of the entrainment velocity to the local velocity difference in the appropriate direction

$$\varepsilon_\xi = \frac{\underset{\sim}{v}_\xi}{u - V_o\cos\theta} \tag{4.5}$$

$$\varepsilon_\zeta = \frac{\underset{\sim}{v}_\zeta}{V_o\sin\theta} \tag{4.6}$$

where

$\varepsilon_\xi \equiv$ entrainment coefficient along trajectory

$\varepsilon_\zeta \equiv$ entrainment coefficient normal to trajectory (see also section 4.4.4.2)

θ = local trajectory angle to horizontal

u = jet velocity

V_o = cross flow velocity

Therefore the RHS of Equation (4.3) using Equation (4.4)

$$\oint_C \rho_o \underset{\sim}{v}_i dC = \oint_C \rho_o \underset{\sim}{v}_\xi dC + \oint_C \rho_o \underset{\sim}{v}_\zeta dC \tag{4.7}$$

and using Equations (4.5), (4.6) in Equation (4.7)

$$\oint \rho_o \underset{\sim}{v}_i dC = \oint \rho_o \varepsilon_\xi (u - V_o \cos\theta) dC + \oint \rho_o \varepsilon_\zeta (V_o \sin\theta) dC \tag{4.8}$$

and assuming the cross section is a circle of radius r

$$\begin{aligned} \oint \rho \underset{\sim}{v}_i dC &= 2\pi r \rho_o \varepsilon_\xi (u - V_o \cos\theta) + 2\pi r \rho_o \varepsilon_\zeta (V_o \sin\theta) \\ &= 2\pi r \rho_o (\varepsilon_\xi \{u - V_o \cos\theta\} + \varepsilon_\zeta \{V_o \sin\theta\}) \end{aligned} \tag{4.9}$$

Hence using Equation (4.9) and (4.3) with $h_1 = 1$ and a circular cross section

$$\frac{d}{d\xi}(\pi r^2 u \rho) = 2\pi r \rho_o (\varepsilon_\xi \{u - V_o \cos\theta\} + \varepsilon_\zeta \{V_o \sin\theta\}) \tag{4.10}$$

4.4.3.4 Conservation of momentum in ξ-direction

The change of momentum flux in the ξ-direction will be equal to the momentum possessed by the entrained mass in this direction, if a non-buoyant jet is assumed (see Figure 4.21).

$$\frac{1}{h_1} \frac{d}{d\xi} \int_A \rho u dA.u = \oint_C \rho_o \underset{\sim}{v}_i dC.V_o \cos\theta \tag{4.11}$$

With the jet cross section assumption and with $h_1 = 1$ then

$$\frac{1}{h_1}\frac{d}{d\xi}\int_A \rho u dA.u = \frac{d}{d\xi}(\pi r^2 u^2 \rho) \tag{4.12}$$

From the mass conservation equations

$$\oint_C \rho_o \gamma_i dC = \frac{d}{d\xi}\int_A \rho u dA = \frac{d}{d\xi}(\pi r^2 u \rho) \tag{4.13}$$

Using Equations 4.12 and 4.13 in Equation 4.11

$$\frac{d}{d\xi}(\pi r^2 u^2 \rho) = V_o \cos\theta \frac{d}{d\xi}(\pi r^2 u \rho) \tag{4.14}$$

4.4.3.5 Conservation of momentum in ζ-direction

In the absence of buoyancy forces the rate of change of momentum in the ζ-direction will be balanced by the centrifugal force in that direction.

Referring to Figure 4.22

$$\text{Rate of change of momentum} = \frac{d}{dt}\left[\frac{dm}{d\xi}\delta\xi V_o \sin\theta\right] \tag{4.15}$$

where m ≡ jet unit mass

Manipulating Equation 4.15

$$\text{R.C.M.} = V_o \sin\theta \frac{d}{dt}\left[\frac{dm\delta\xi}{d\xi}\right] = V_o \sin\theta \frac{d}{dt}\left(\frac{dm}{d\xi}\right)\delta\xi =$$

$$= V_o \sin\theta \frac{d}{d\xi}\frac{dm}{dt}\delta\xi \tag{4.16}$$

But

$$\frac{dm}{dt} = \rho u A = \rho u \pi r^2 \tag{4.17}$$

for a circular jet section. Hence

$$R.C.M. = V_o \sin\theta \frac{d}{d\xi} (\pi r^2 u \rho) \delta\xi \tag{4.18}$$

Alternatively, referring to Figure 4.23: Change of momentum in ξ-direction is equal to the mass entrained times the component of the cross flow velocity in this direction.

$$\left[\oint \rho \underset{\sim}{V}_i dC\right] \delta\xi . V_o \sin\theta = \frac{d}{d\xi} (\pi r^2 u \rho) . \delta\xi . V_o \sin\theta \tag{4.18a}$$

from continuity and circular jet cross section.
The centrifugal force on the jet element

$$Force = \frac{\delta m . u^2}{R} \tag{4.19}$$

where

$$\delta m = \rho . \delta V \tag{4.20}$$

$\rho \equiv$ local jet density

$\delta V \equiv$ elemental volume

$R \equiv$ instantaneous radius of rotation of the elemental volume

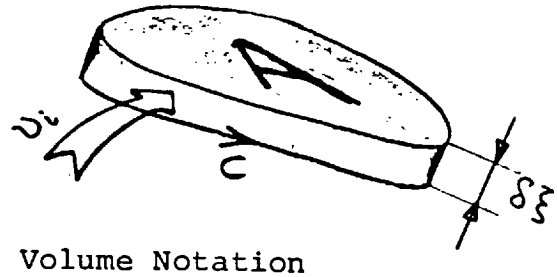


FIG.4.23 Control Volume Notation

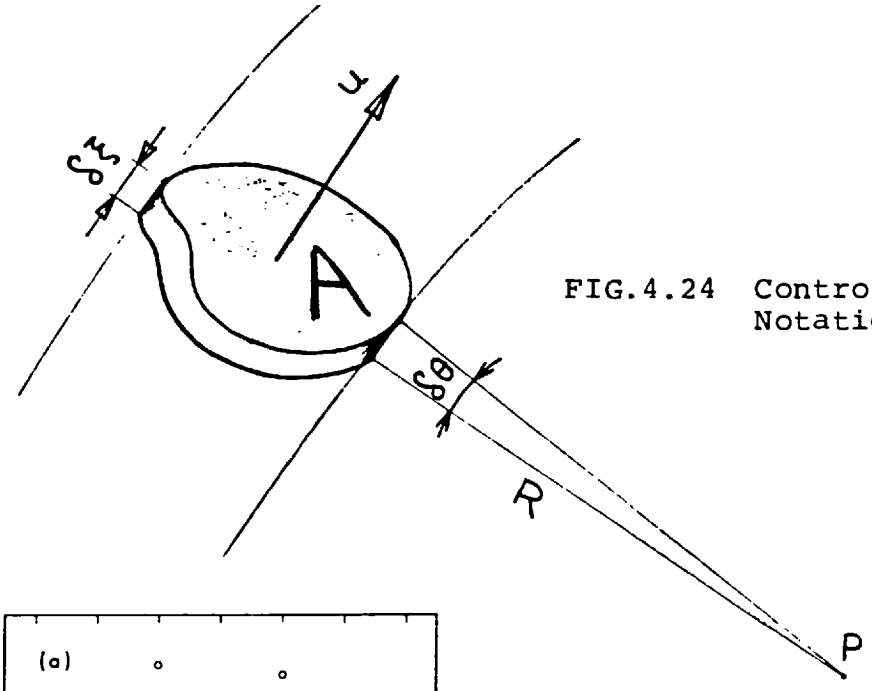


FIG.4.24 Control Volume Notation

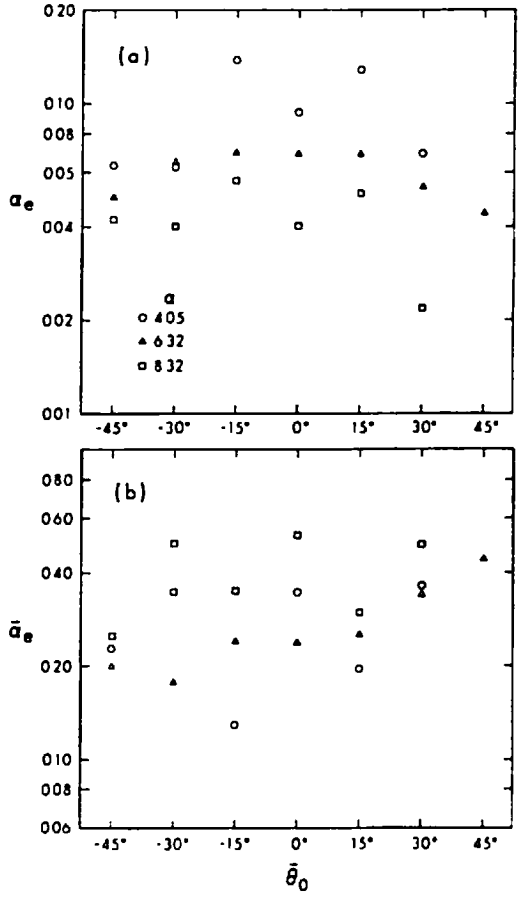


FIG.4.25 Entrainment Coefficients for Circular Jets in a Cross Flow for Various Ejection Angles and Velocity Ratios (80)

But

$$\delta V = A.\delta\xi = A.R.\delta\theta \quad \text{(see Figure 4.24)} \tag{4.21}$$

Hence

$$\delta m = \rho AR\delta\theta \tag{4.22}$$

$$\text{Force} = \frac{\delta m.u^2}{R} = \rho.A.\delta\theta.u^2 = \rho\pi r^2u^2\delta\theta \tag{4.23}$$

assuming circular jet cross section.

The rate of change of momentum will be equal and opposite to the centrifugal force. Hence combining Equations (4.23) and (4.18)

$$V_o\sin\theta \frac{d}{d\xi}(\pi r^2\rho u)\delta\xi = -\pi r^2\rho u^2\delta\theta$$

or in the limit,

$$V_o\sin\theta \frac{d}{d\xi}(\pi r^2\rho u) = -\pi r^2\rho u^2\frac{d\theta}{d\xi} \tag{4.24}$$

4.4.3.6 Conservation of energy - density function

The conservation of energy equation can be applied to a jet element. However the problem is considerably simplified if, instead, a density variation along the jet trajectory is postulated. In this analysis an exponential decay of the difference in density between the jet and the

cross flow was assumed.

The function used was of the form:

$$\rho = \rho_s - (\rho_s - \rho_j)e^{-\lambda z} \qquad (4.25)$$

where

ρ = local jet density

ρ_j = initial jet density

ρ_s = cross flow density

λ = constant

z = vertical height from source

Based on experimental results (91) it is assumed that the jet density becomes equal to the cross flow density after 15 diameters along the trajectory. Hence the value of λ was fixed accordingly.

4.4.3.7 Notes on curvilinear coordinates

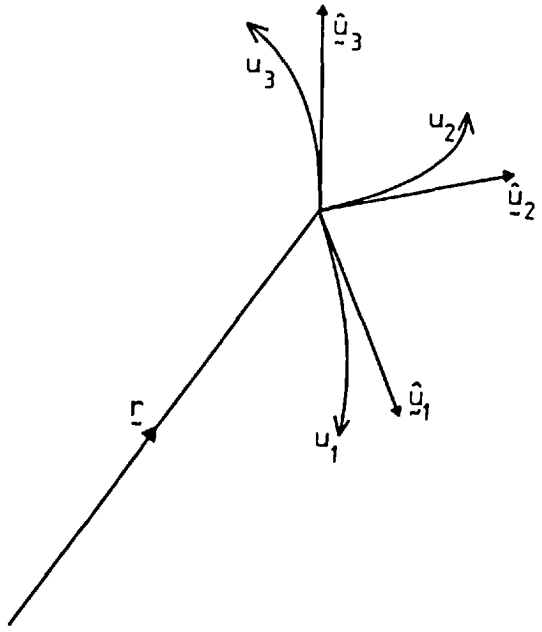
This overview of curvilinear coordinates, explains the concept of the linearising factor h_j and justifies the assumption that it equals unity in the present investigation.

Referring to Figure Curv. 1, $\hat{\underset{\sim}{u}}_1$, $\hat{\underset{\sim}{u}}_2$, $\hat{\underset{\sim}{u}}_3$ are unit vectors tangential to the three axes u_1, u_2, u_3. On spherical coordinates, $\hat{\underset{\sim}{u}}_1$, $\hat{\underset{\sim}{u}}_2$, $\hat{\underset{\sim}{u}}_3$ are mutually perpendicular.

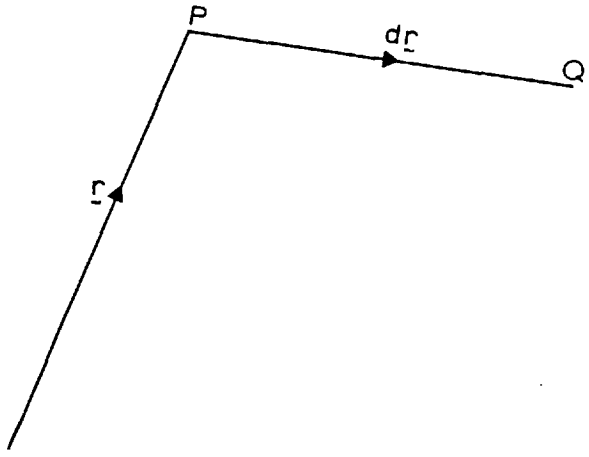
Now,

$$\frac{\partial \underset{\sim}{r}}{\partial u_1} = \left(\text{Lim}\frac{\delta \underset{\sim}{r}}{\delta u_1}\right) \text{ with } u_2,\ u_3 \text{ fixed}$$

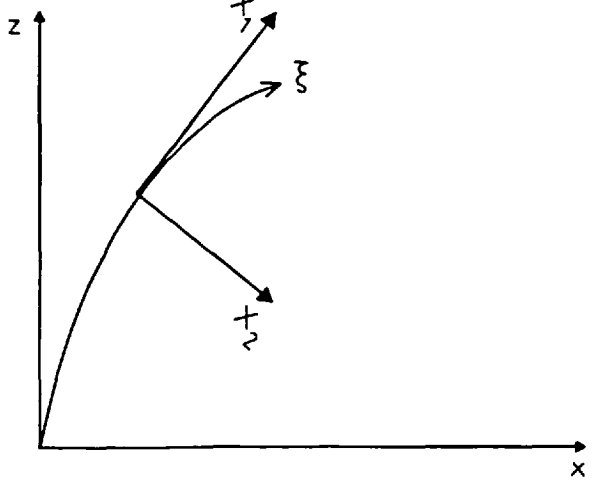
$\equiv$ vector along u_1 axis in the direction $\hat{\underset{\sim}{u}}_1$



F.CURV.1 Curvilinear Coordinates - (3D)



F.CURV.2 Length Element



F.CURV.3 Curvilinear Coordinates - (2D)

$$\frac{\partial \underset{\sim}{r}}{\partial u_1} = \left|\frac{\partial \underset{\sim}{r}}{\partial u_1}\right| \hat{\underset{\sim}{u}}_1$$

i.e. $\hat{\underset{\sim}{u}}_1 = \frac{1}{h_1} \frac{\partial \underset{\sim}{r}}{\partial u_1}$ where $h_1 = \left|\frac{\partial \underset{\sim}{r}}{\partial u_1}\right|$ and is called the scalar factor.

Similarly,

$$h_2 = \left|\frac{\partial \underset{\sim}{r}}{\partial u_2}\right|$$

$$h_3 = \left|\frac{\partial \underset{\sim}{r}}{\partial u_3}\right|$$

The basic assumption is that a length element dS remains unchanged (see Figure Curv. 2).

$$(dS)^2 = d\underset{\sim}{r} . d\underset{\sim}{r}$$

$$(dS)^2 = \left(\frac{\partial \underset{\sim}{r}}{\partial u_i} du_i\right) \cdot \left(\frac{\partial \underset{\sim}{r}}{\partial u_j} du_j\right)$$

$$(dS)^2 = \frac{\partial x_k}{\partial u_i} \frac{\partial x_k}{\partial u_j} du_i du_j \text{ in suffix form}$$

Expanding

$$(dx_1)^2 + (dx_2)^2 + (dx_3)^2 = \left[\left(\frac{\partial x_1}{\partial u_1}\right)^2 + \left(\frac{\partial x_2}{\partial u_1}\right)^2 + \left(\frac{\partial x_3}{\partial u_1}\right)^2\right] (du_1)^2 +$$

$$+ \left[\left(\frac{\partial x_1}{\partial u_2}\right)^2 + \left(\frac{\partial x_2}{\partial u_2}\right)^2 + \left(\frac{\partial x_3}{\partial u_2}\right)^2\right] (du_2)^2 +$$

$$+ \left[\left(\frac{\partial x_1}{\partial u_3}\right)^2 + \left(\frac{\partial x_2}{\partial u_3}\right)^2 + \left(\frac{\partial x_3}{\partial u_3}\right)^2\right] (du_3)^2 +$$

$$+ 2\left[\frac{\partial x_k}{\partial u_1}\frac{\partial x_k}{\partial u_2}\right](du_1 du_2 + ... + ...)$$

If the coordinates are orthogonal then the cross products are equal to zero by definition i.e.

$$\frac{\partial x_k}{\partial u_j}\frac{\partial x_k}{\partial u_i} = 0 \;\forall\; i \neq j$$

But the three brackets are of the form

$$\left[\left(\frac{\partial x_1}{\partial u_1}\right)^2 + \left(\frac{\partial x_2}{\partial u_1}\right)^2 + \left(\frac{\partial x_3}{\partial u_1}\right)^2\right] = \left(\frac{\partial r}{\partial u_i}\right)^2 = h_i^2 \;\forall\; i = 1$$

Hence

$$(dS)^2 = (h_1 du_1)^2 + (h_2 du_2)^2 + (h_3 du_3)^2$$
$$\equiv \{(dx_1)^2 + (dx_2)^2 + (dx_3)^2\}$$

But x_1, x_2, x_3 in Cartesian coordinates are lengths.
Hence $h_i du_i$ should be length.
If (du_i) is an angle, (h_i) is a length
If (du_i) is a length, (h_i) is an angle
Hence h_i is a conversion factor or scale factor relating lengths on the $\hat{u}_i$ to angles on the curved axis.

$$h_i = h_i(u_1, u_2, u_3)$$

Now in two-dimensions (see Figure Curv. 3)

$$h_1^2 = \left(\frac{\partial X_1}{\partial \xi}\right)^2 + \left(\frac{\partial X_2}{\partial \xi}\right)^2$$

If $\frac{\partial^2 \xi}{\partial z^2}$ is small then

$$\frac{\partial X_1}{\partial \xi} = \left(\underset{\delta\xi \to 0}{\text{Lim}} \frac{\delta X_1}{\delta \xi}\right) = 1$$

$$\frac{\partial X_2}{\partial \xi} = \left(\underset{\delta\xi \to 0}{\text{Lim}} \frac{\delta X_2}{\delta \xi}\right) = 0$$

Hence $h_1^2 \simeq 1$.

The linearising factor was calculated (75) for a jet in a cross flow at the point of maximum trajectory curvature and found approximately 0.98.

4.4.4 Synthesis

4.4.4.1 Derivation of equations defining the jet

Dividing the equation of conservation of ξ-momentum (Equation 4.14) by the equation of conservation of ζ-momentum (Equation 4.24)

$$\frac{\frac{d}{d\xi}(r^2u^2\rho)}{r^2u^2\rho\frac{d\theta}{d\xi}} = \frac{V_o\cos\theta\frac{d}{d\xi}(r^2u\rho)}{-V_o\sin\theta\frac{d}{d\xi}(r^2u\rho)} \qquad (4.26)$$

$$\therefore \quad \frac{\frac{d}{d\xi}(r^2u^2\rho)}{r^2u^2\rho} = \frac{d\theta}{d\xi}\left(\frac{\cos\theta}{-\sin\theta}\right) \qquad (4.27)$$

$$\therefore \frac{\frac{d}{d\xi}(r^2u^2\rho)\, d\xi}{r^2u^2\rho} = -\cot\theta d\theta \tag{4.28}$$

$$\therefore \int_{\xi=0}^{\xi=\xi} \frac{\frac{d}{d\psi}(r^2u^2\rho)\, d\psi}{r^2u^2\rho} = -\int_{\theta=\theta_j}^{\theta} \cot a.da \tag{4.29}$$

where j denotes initial (ejection) value.

Denoting $L = r^2u^2\rho$ (4.30) then,

$$\ln(L)\Big|_{\xi=0}^{\xi} = -\ln(\sin a)\Big|_{\theta=\theta_j}^{\theta} \tag{4.31}$$

$$\therefore \ln\left(\frac{L}{(L)_{\xi=0}}\right) = \ln\left(\frac{\sin\theta_j}{\sin\theta}\right) \tag{4.32}$$

$$\therefore L = (L)_{\xi=0}\, \frac{\sin\theta_j}{\sin\theta} \tag{4.33}$$

$$\therefore r^2u^2\rho = r_j^2u_j^2\rho_j\, \frac{\sin\theta_j}{\sin\theta} \tag{4.34}$$

$$\therefore u = \left[\frac{r_j^2u_j^2\rho_j\sin\theta_j}{r^2\rho\sin\theta}\right]^{0.5} \tag{4.35}$$

For a non buoyant jet it is assumed that the radius variation is given by:

$$r = 2.\varepsilon_\xi z + r_j \tag{4.36}$$

where

$\varepsilon_\xi \equiv$ entrainment coefficient in ξ-direction

$z \equiv$ vertical distance from origin

$r_j \equiv$ radius at ejection

Equation (4.36) corresponds to a conical shape for a jet ejected vertically into quiescent fluid (88). The above equation was used for the radius variation of the jet in the cross flow near the source.

For away from the source where the vortex pair dominates the entrainment process, the jet radius variation (assuming circular jet cross section) may be written:

$$r = \varepsilon_\zeta . z + r_p \qquad (4.37)$$

where

$\varepsilon_\zeta \equiv$ entrainment coefficient in ζ-direction

$z \equiv$ vertical distance from origin

$r_p \equiv$ previous jet radius

It is assumed that Equation (4.36) can be used for the region where both mechanisms of entrainment are important.

Using the mass conservation equation (Equation 4.10) and the equation of conservation of ζ-momentum (Equation 4.24)

$$\frac{d\theta}{d\xi} = \frac{-V_o \sin\theta \left[2r\rho_o \left(\varepsilon_\xi (u - V_o \cos\theta) + \varepsilon_\zeta (V_o \sin\theta) \right) \right]}{r^2 u^2 \rho} \qquad (4.38)$$

The coordinate transformation equation (Equation 4.1) can be written as:

$$\frac{dz}{d\xi} = \sin\theta \tag{4.39}$$

Using Equations (4.38) and (4.39), and non-dimensionalising the length z by division with the jet source diameter D, where $D = 2r_j$, to conform with the convention used in relevant experimental result presentation:

$$\frac{d\theta}{d(z/D)} = \frac{D}{\sin\theta}\left[\frac{-V_o \sin\theta . 2r\rho_o\left[\varepsilon_\xi (u - V_o\cos\theta) + \varepsilon_\zeta (V_o \sin\theta)\right]}{r^2 u^2 \rho}\right] \tag{4.40}$$

Substituting Equations (4.25), (4.34), (4.35); (4.36) or (4.37) in (4.40) an equation of the following form can be obtained:

$$\frac{d\theta}{d(z/D)} = F(\theta, z) \tag{4.41}$$

This equation can be solved numerically. The solution will be of the form

$$\theta = \phi(z/D) \tag{4.42}$$

Also, using the coordinate transformation equations (4.1) and (4.2)

$$\frac{dz}{d\xi} = \sin\theta \tag{4.43}$$

$$\frac{dx}{d\xi} = \cos\theta \tag{4.44}$$

Using Equations (4.43) and (4.44)

$$\frac{dz}{dx} = \tan\theta \tag{4.45}$$

$$\therefore \; d(z/D) = \tan\theta d(x/D) \tag{4.46}$$

$$\therefore \; z/D = \int \tan\theta d(x/D) \tag{4.47}$$

$$\therefore \; x/D = \int \cot\theta d(z/D) \tag{4.48}$$

Using Equations (4.42) and (4.48)

$$(x/D) = \int \cot\left[\phi(z/D)\right] d(z/D) \tag{4.49}$$

This equation can be solved numerically.

The solution of Equation (4.41) will give the inclination of the jet trajectory at any point. The solution of Equation (4.49) will give the jet trajectory. Equation (4.35) can then be used to obtain the mean jet velocity over a cross section. Equation (4.36) or (4.37) will give the jet growth. Equation (4.25) will give the local density.

4.4.4.2 Entrainment coefficients

For the present work it was assumed that the two entrainment coefficients are independent of position along the trajectory. It was further assumed, in the subsequent use of the model as a design tool, that the coefficients

are independent of velocity ratio as well as initial ejection angle, in order to minimise the number of variables.

Although the entrainment coefficients are assumed universal constants (83), there is considerable scatter in the published relevant data. If the parameter ε_ξ is assumed to be equal to the entrainment coefficient for circular jets in stagnant ambient fluid, then relevant data can be used.

The results lead to a value of $\varepsilon_\xi = 0.08$ for a top hat profile (89). A value of 0.116 is used elsewhere (90). Analysis of various published data (82) gave a value $\varepsilon_\xi = 0.11$ with an estimated uncertainty of ±20 per cent, for a top hat profile.

The values of the entrainment coefficients may be determined by comparing theoretical and experimental trajectories adjusting ε_ξ and ε_ζ to obtain the best agreement. Decreasing the ε_ξ coefficient has the effect that the ξ-momentum is less readily dissipated hence the jet penetrates further away from the source. Decreasing the ε_ζ coefficient has the effect that the jet is curved less rapidly since the entrainment resulting from the vortex action is decreased.

This procedure was used (83) for a buoyant plume and values of $\varepsilon_\xi = 0.12$ and $\varepsilon_\zeta = 0.60$ were obtained. The values of the coefficients obtained by this procedure (80) are shown in Figure (4.25). Although there is considerable scatter $\varepsilon_\xi (\equiv a_e)$ can be taken roughly equal to 0.06. The coefficient $\bar{a}_e$ however is based on a different definition than ε_ζ, therefore the results cannot be used.

4.4.3 Cross flow velocity profile

To account for the presence of a boundary layer the cross flow velocity profile is expressed as a function of the vertical height

$$V_o = V_{oF}(1 - \exp(-k.\frac{z}{D}))$$

where

V_o ≡ local cross flow velocity

V_{oF} ≡ final cross flow velocity

z ≡ vertical height above origin

D ≡ jet source diameter

k ≡ constant, used to adjust the boundary layer thickness assuming 97 per cent of the final velocity at the edge of the boundary layer.

4.5 THEORETICAL RESULTS USING MODEL

Equation (4.41) was solved numerically using a fourth order Runge-Kutta method. Using the results, Equation (4.49) was solved by Simpson's rule for the trajectory of the jet. Figures (4.26), (4.27), (4.28) show typical results for predicted trajectories of jets in cross flow with velocity ratios of 4, 6, 8 and various initial jet ejection angles.

The final values of entrainment coefficients were determined by comparing the theoretical trajectories obtained with a range of values of entrainment coefficients, with published experimental and analytical data, and selecting the ones which gave the best fit. 90° initial ejection angle jets were used, and the values of the coefficients thus obtained were assumed to apply universally to all

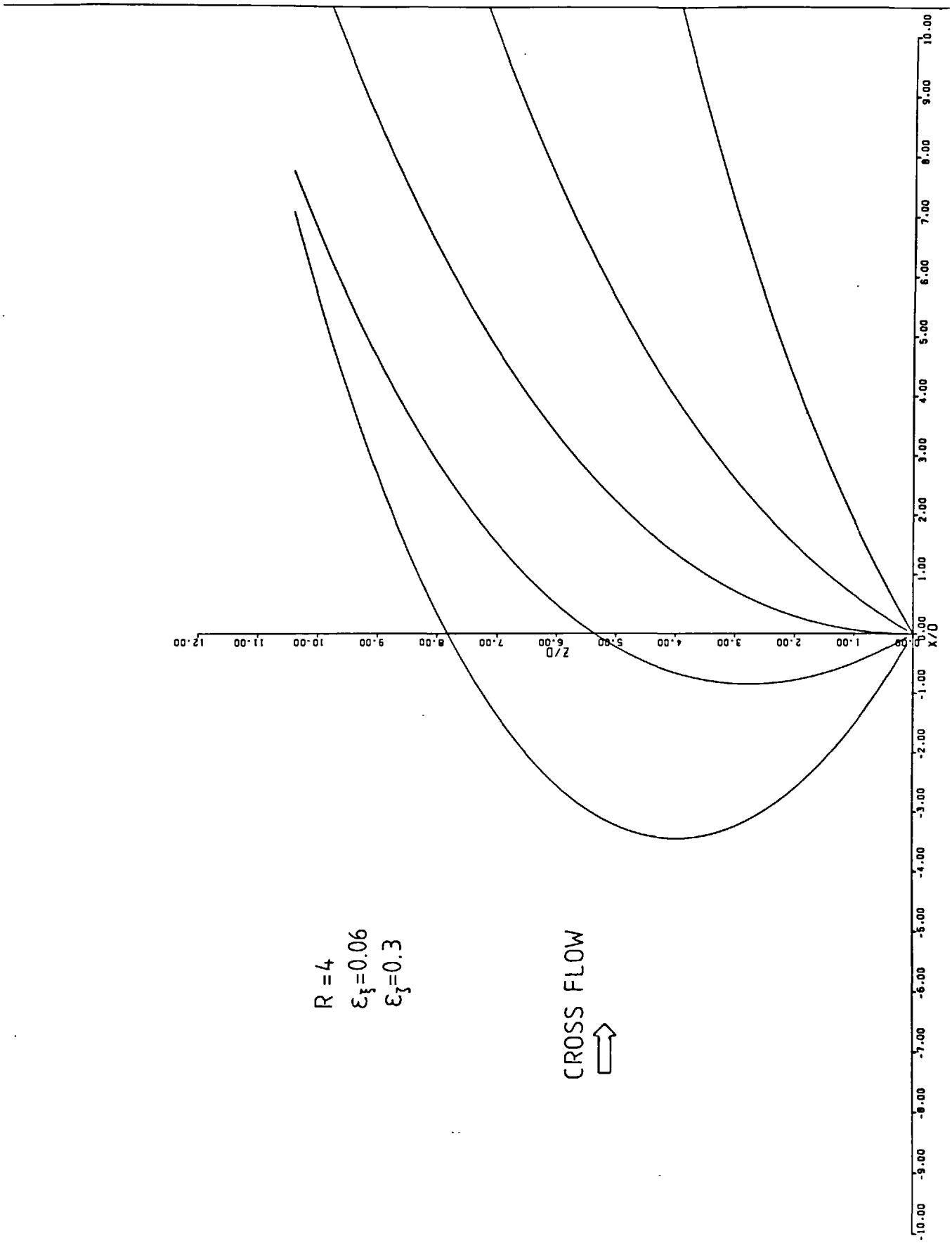


FIG.4.26 Predicted Trajectories for Jets in a Cross Flow at Various Ejection Angles (θ_j = 30°,60°,90°,120° 150°)

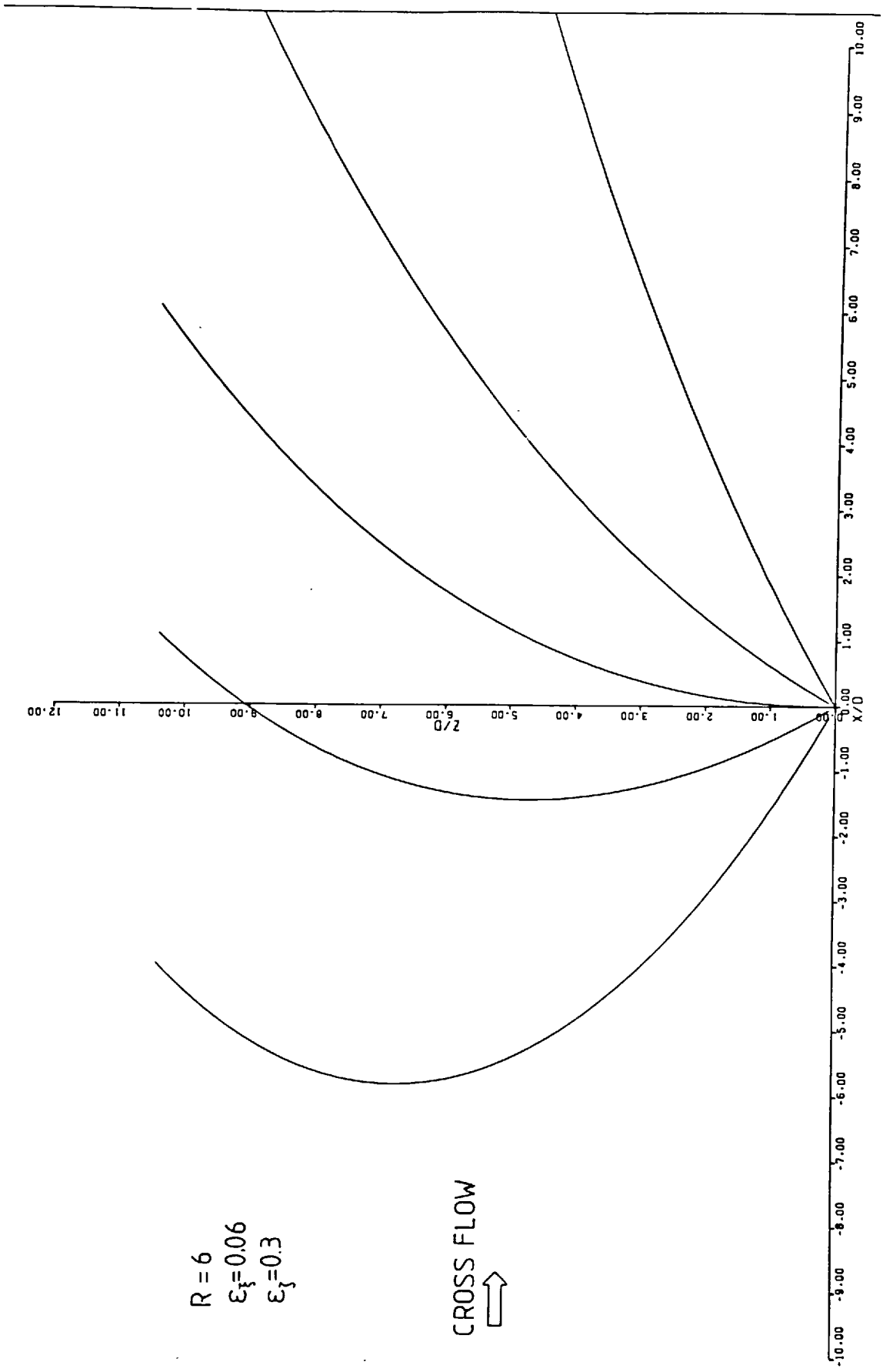


FIG.4.27 Predicted Trajectories for Jets in a Cross Flow at Various Ejection Angles (θ_j = 30°,60°,90°, 120°,150°)

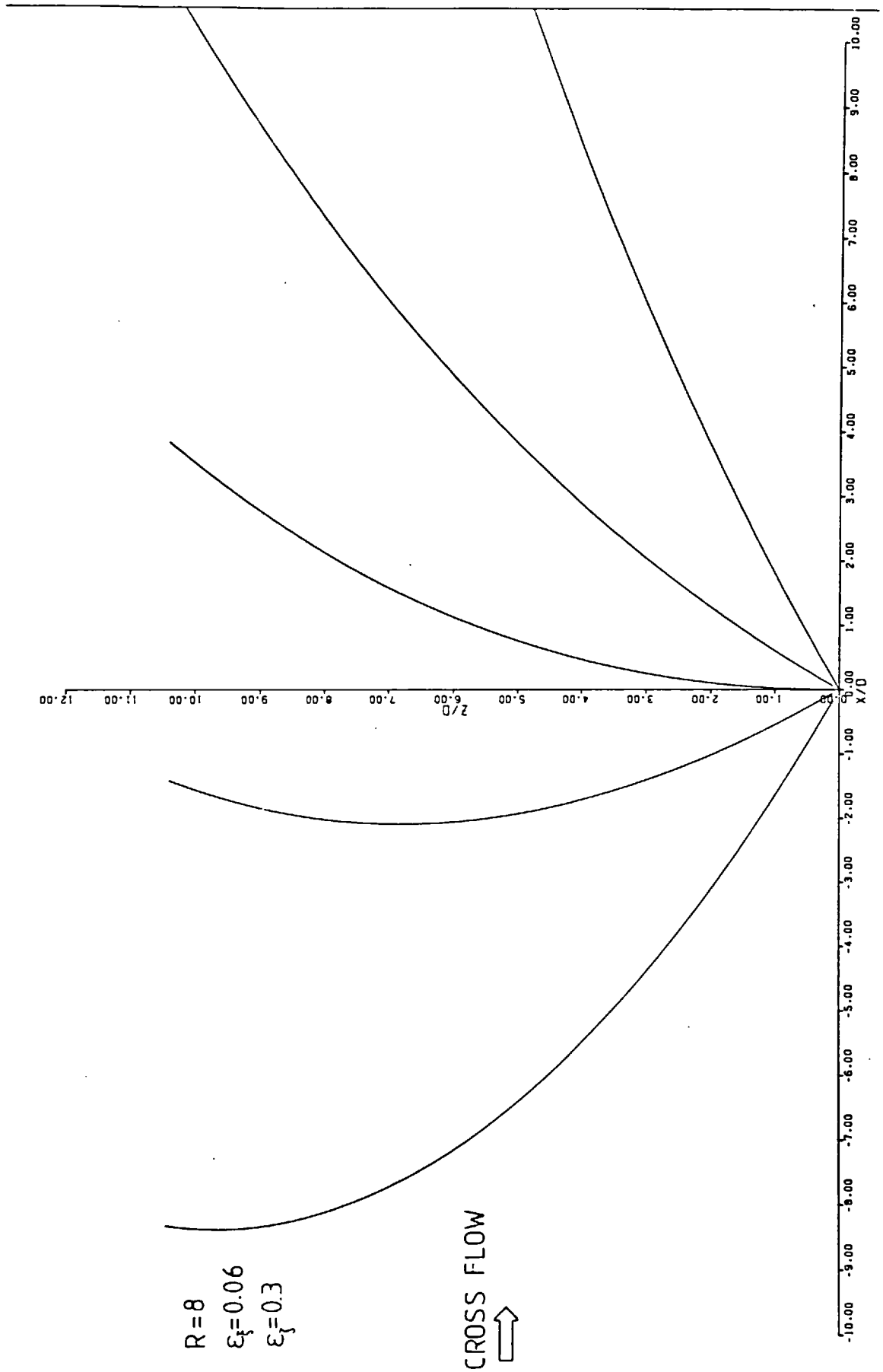


FIG.4.28 Predicted Trajectories for Jets in a Cross Flow at Various Ejection Angles (θ_j = 30°,60°,90°, 120°,150°)

configurations.

Figures (4.29 - 4.35) show theoretical trajectories using the present model superimposed on data from different investigators (73) for 90° ejection angle to determine the coefficients and then for various ejection angles using these coefficients.

4.6 REVIEW OF EXPERIMENTAL RESULTS

With the theoretical background of the jet in a cross flow analysis a reappraisal of the experimental observations and results from the jet-prewhirl configuration was done. It was obvious that the geometry of the arrangement was far from optimum. In the "best" arrangement tested, the jet to cross flow velocity ratios obtained near surge were approximately 4.5.

It can be seen from the 90° ejection angle trajectory for velocity ratio 4 (see Figure 4.26) that any appreciable deflection (gradient of the trajectory) is obtained less than five diameters from the source. In the "best" experimental arrangement the jets were 15 diameters away from the face of the impeller. If the jets were allowed to expand freely, the trajectory gradient would be effectively zero at that distance.

However, in the jet arrangement there are further complications:

- There is more than one jet
- The flow is confined
- The jets eject with one side near an inward curving wall

In the arrangement used the angle of ejection with respect to the tangent to the inlet pipe wall was too small.

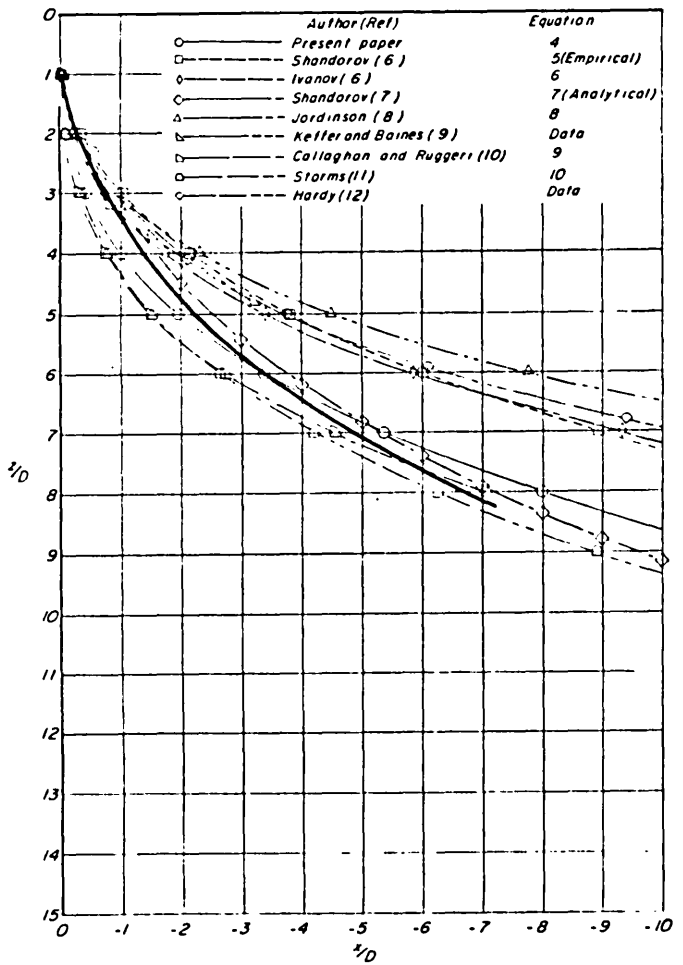


FIG.4.29 Comparison of Predicted Trajectory of a Jet in a Cross Flow with Data from (73) (R = 4)

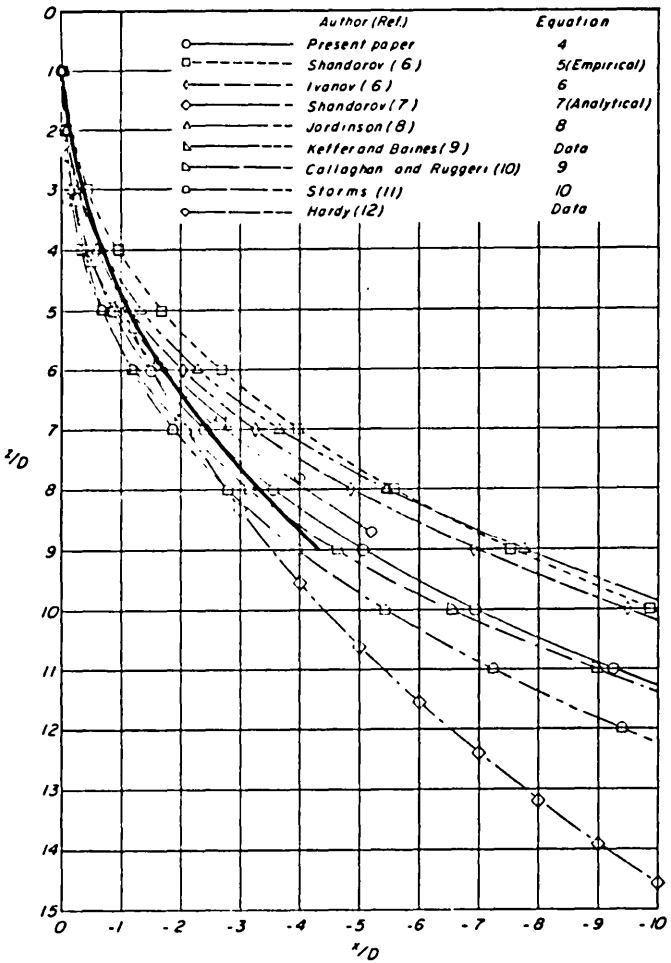


FIG.4.30 Comparison of Predicted Trajectory of a Jet in a Cross Flow with Data from (73) (R = 6)

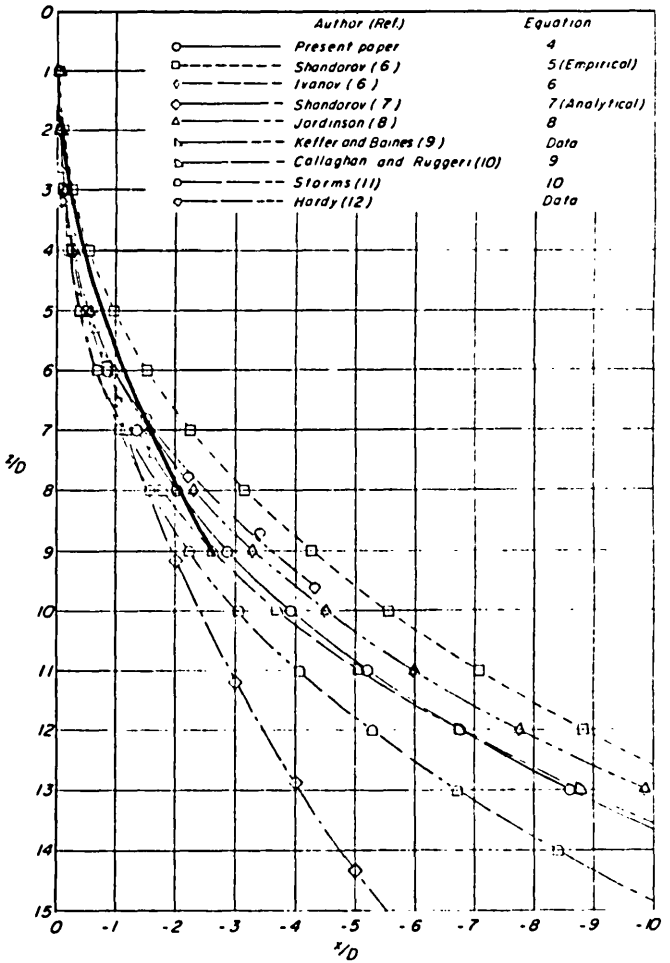


FIG.4.31 Comparison of Predicted Trajectory of a Jet in a Cross Flow with Data from (73) (R = 8)

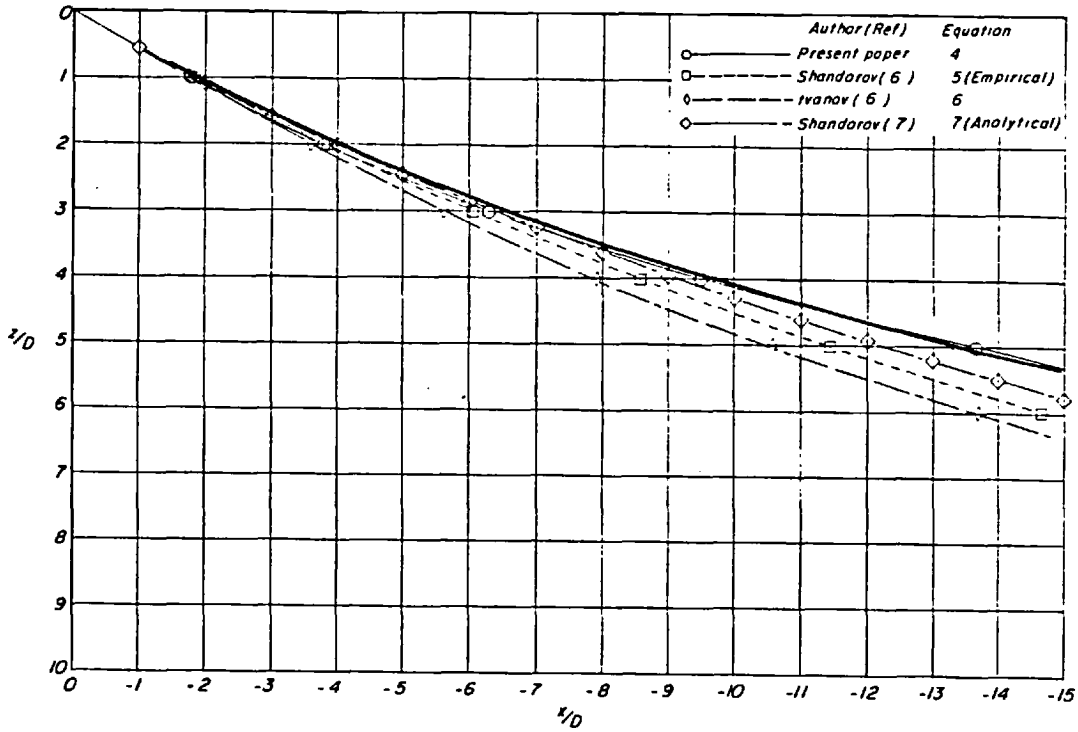


FIG.4.32 Comparison of Predicted Trajectory of a $_{o}$Jet in a Cross Flow with Data in Ref.73 ($\theta_j = 30^{o}$, R = 5)

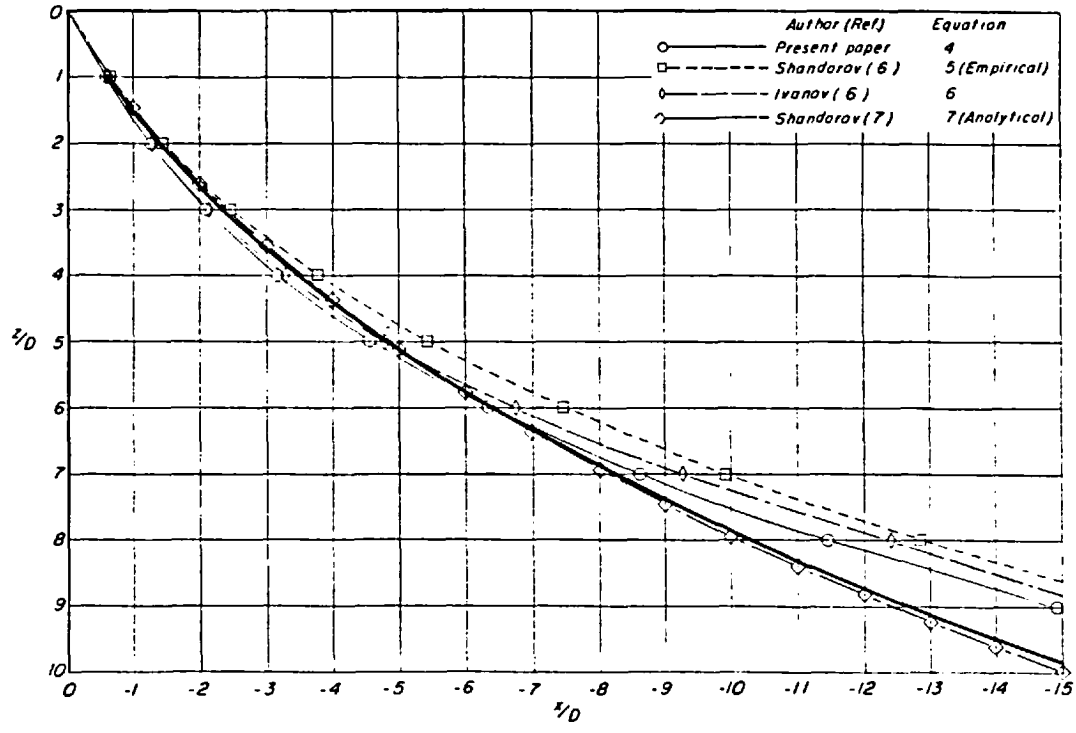


FIG.4.33 Comparison of Predicted Trajectory of a $_{o}$Jet in a Cross Flow with Data in Ref.73 ($\theta_j = 60^{o}$, R = 5)

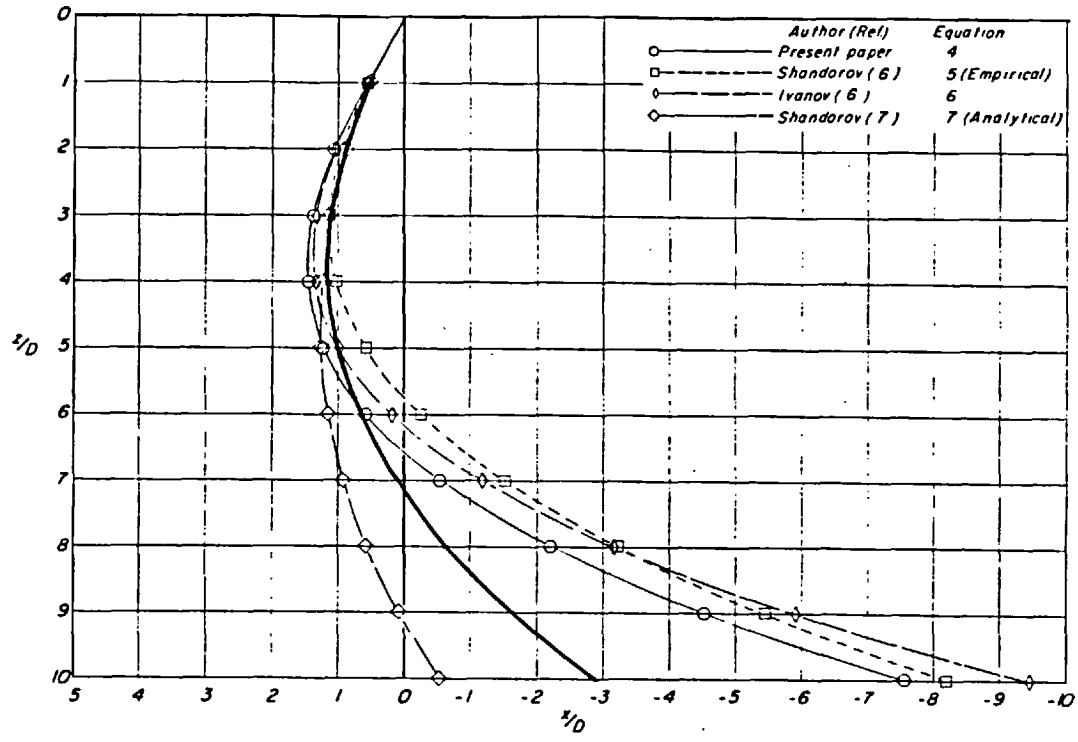


FIG.4.34 Comparison of Predicted Trajectory of a Jet in a Cross Flow with Data in Ref.73 ($\theta_j = 120^o$, R = 5)

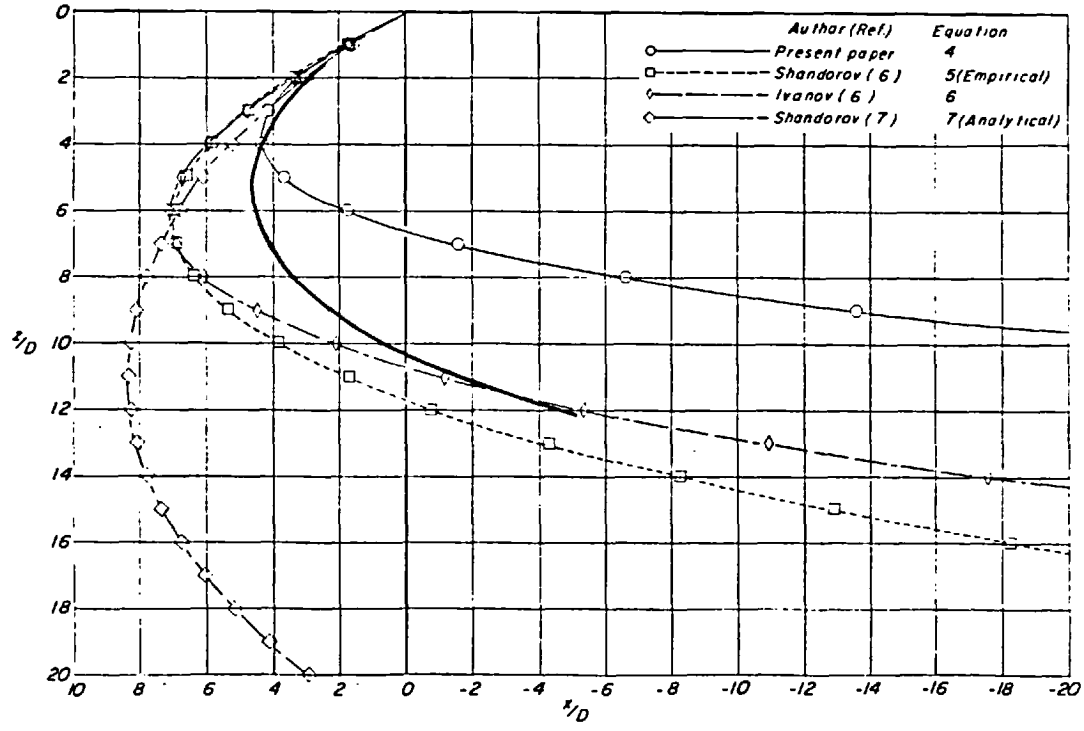


FIG.4.35 Comparison of Predicted Trajectory of a Jet in a Cross Flow with Data in Ref.73 ($\theta_j = 150^o$, R = 5)

The jet was squashed against the wall, before having the opportunity to spread freely and entrain stream fluid.

Because of its momentum, it spread across the wall, forming a thin high speed layer which moved helically downstream. That was observed in the flow visualisation. This thin layer was not curved rapidly by the cross flow since it moved near the wall boundary layer, but because of the larger shear due to the velocity difference it spread further across the wall, its momentum dissipated in the process. The jet near the ejection point formed a barrier which the main flow had to jump and hence the observed large turbulence downstream (see Figure 4.36).

Even if the positioning of the jets was correct, the number of jets would be inadequate. On expansion, the jets would only fill a fraction of the compressor inlet annulus. Hence the flow field presented to the inducer would be composed of alternating patches of high and low pressure and different flow directions. This may create compressor stability problems.

4.7 ALTERNATIVE ARRANGEMENT

It was thought that a radial turbine type vaneless scroll could provide a jet exiting through a slot all around the inlet pipe upstream of the impeller which could present a more uniform flow field to the inducer.

A volute was subsequently designed to give a certain exit whirl angle, based on the method described (92). Nevertheless, after evaluation of this design, it was concluded that such a "turbine type" arrangement would be inferior to the "individual jet" arrangement.

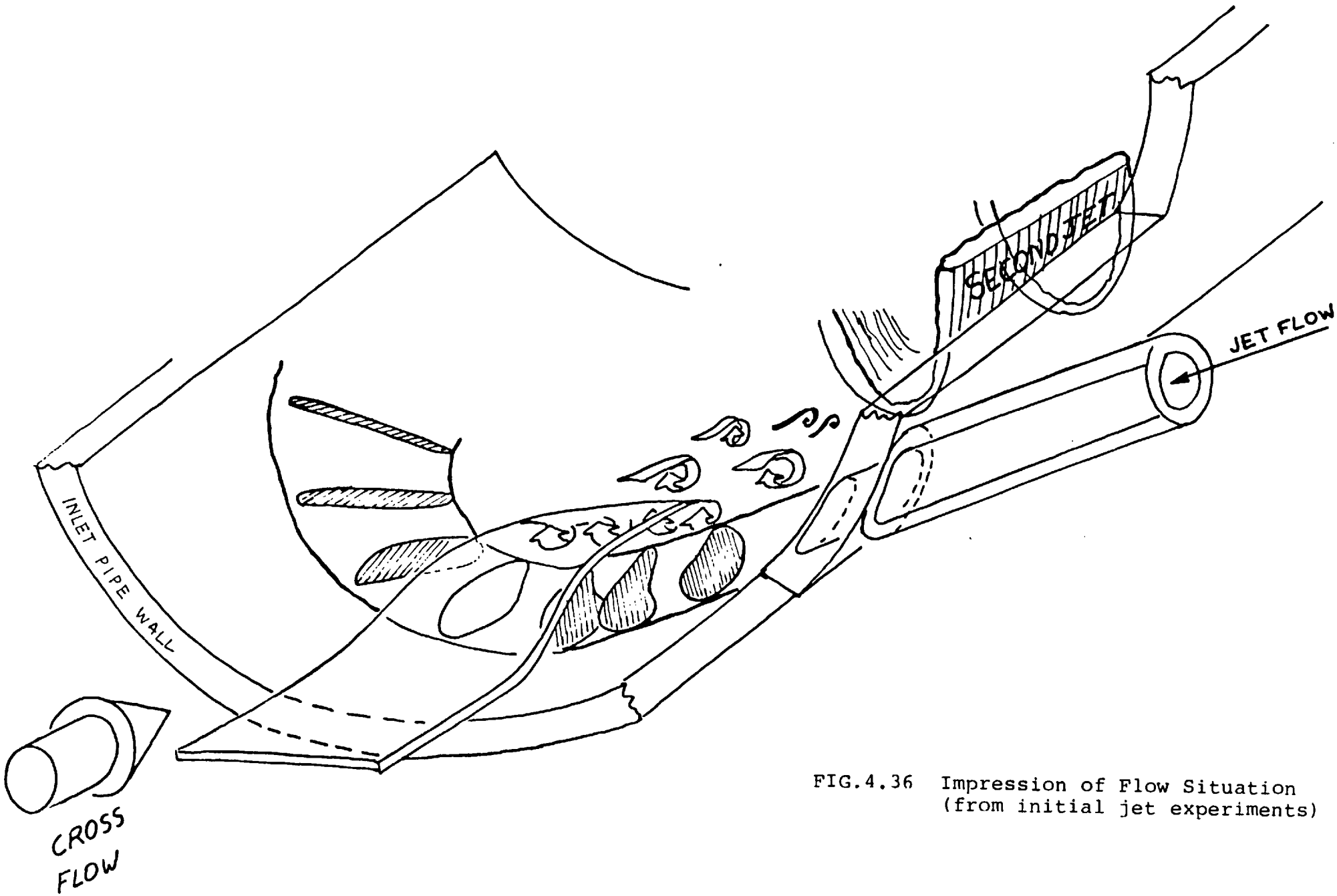


FIG.4.36 Impression of Flow Situation
(from initial jet experiments)

The wall frictional losses on ejection would be higher. For the same mass flow rate, the length of the two parallel walls forming the slot, would be much larger than the cumulative peripheral wall length of the individual jet circular orifices. The width of the slot would be very small in comparison. Hence the jet penetration would be limited.

The main argument against this arrangement, however, is that the jet obtained through ejection from a slot would be "two-dimensional". It would present an uninterrupted barrier to the cross flow and would tend to form a re-circulation eddy behind it (see Section 4.3.3), (77), (78), (see Figure 4.37).

In addition, the lack of the secondary entrainment mechanism, due to the counterrotating vortices of the single jet, will limit the jet expansion and the jet will affect only part of the inducer (see Figure 4.38).

4.8 DESIGN OF NEW ARRANGEMENT

Based on the analysis determining the trajectory of a jet in a cross flow, as well as relevant experimental data from other investigators, the prewhirl producing jet arrangement was redesigned.

It was assumed that a velocity ratio R = 4 (jet velocity to cross flow velocity) would be available. A provisional source diameter of D = 4 mm was chosen (assuming circular source cross section). Then the jet trajectory for R = 4 and 90° ejection angle, as well as the growth of the jet cross section, was determined. No other initial

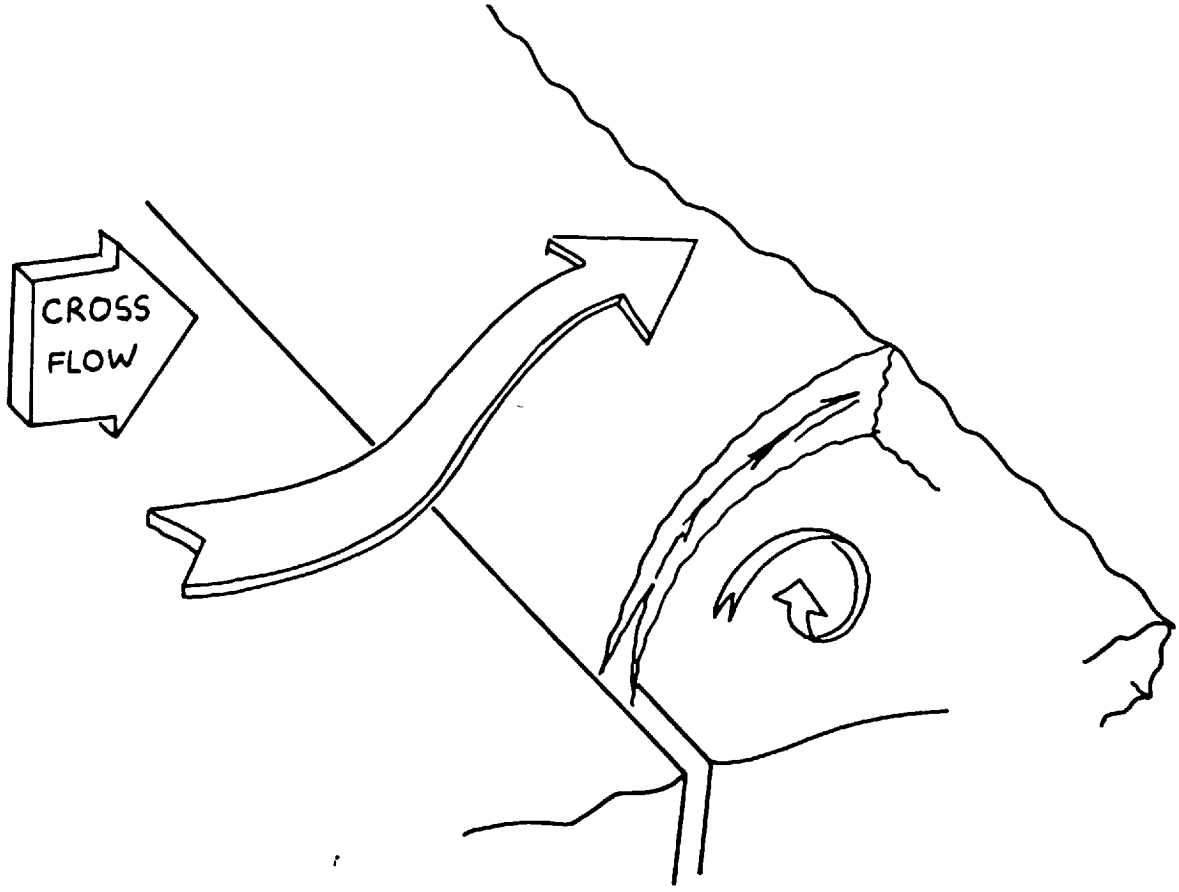


FIG.4.37 (2D) Jet in a Cross Flow (slot ejection)

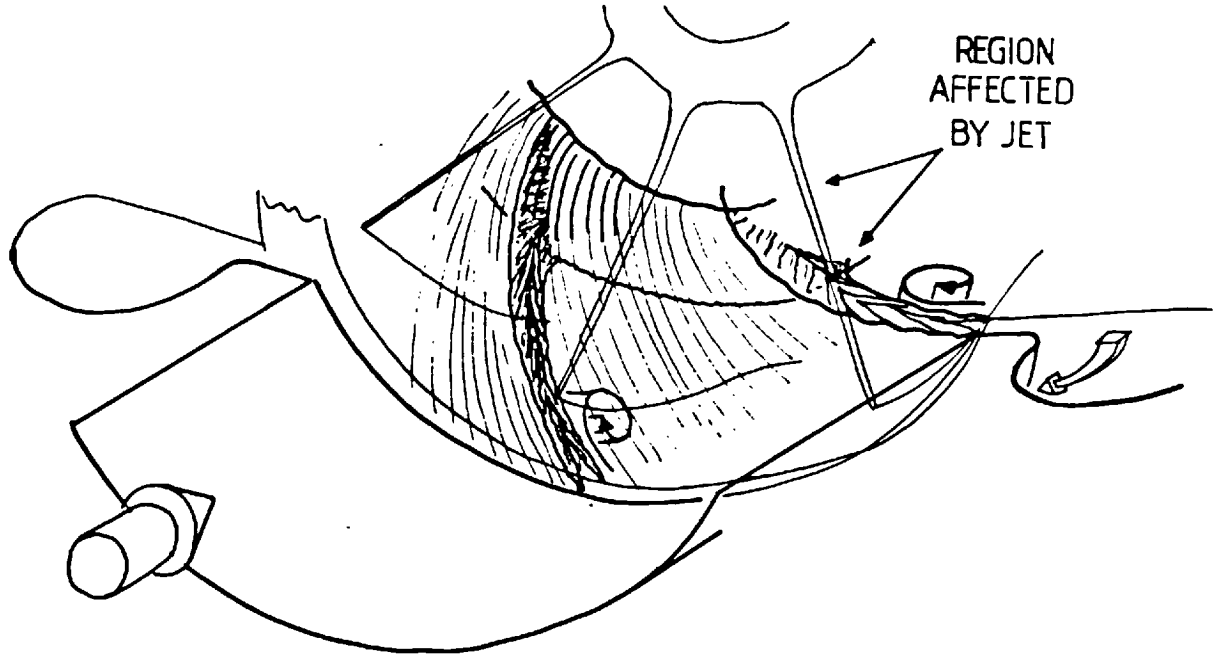


FIG.4.38 Slot Ejection Effect on Compressor Face

initial ejection angle was examined at that stage.

It was postulated that deflection (trajectory gradient) of 40° would be required. For R = 4 this deflection is obtained when $x/D \simeq 2$.

Although a larger deflection angle can be obtained at a smaller x/D, the entrainment hence the jet growth, would be less, therefore more jets would be required. It was not known at the time if the compressor was capable of providing that mass flow recirculation, in all operating conditions.

Then the cross sectional area of the expanded jet for R = 4 and x/D = 2 was obtained (circular jet cross section). Knowing the annulus area of the compressor face, the number of jets required to fill this area was determined to be 6 or 7.

Using experimental data (72), (73) and (76) the actual shape and cross section for R = 4, x/D = 2, were found (similar to Figure 4.12). Then using the empirical procedure schematically depicted in Figure 4.39, the angle of the ejection axis to the tangent to the inlet pipe was determined.

The final design was as follows:-

Diameter of source = 4 mm

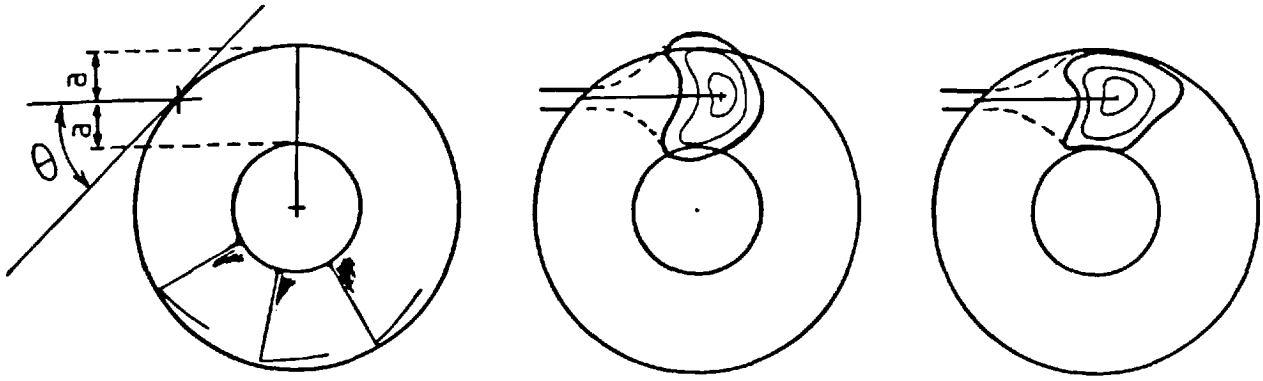
Ejection angles:

- To axial plane = 90°
- To tangential plane = 47°

Distance of ejection plane from inducer blade plane = 8 mm

Number of jets = 6 or 7, equally dispersed round the circumference of the inlet pipe

Although the 7 jet arrangement involved a larger jet to jet interaction (overlap) on expansion, it was thought



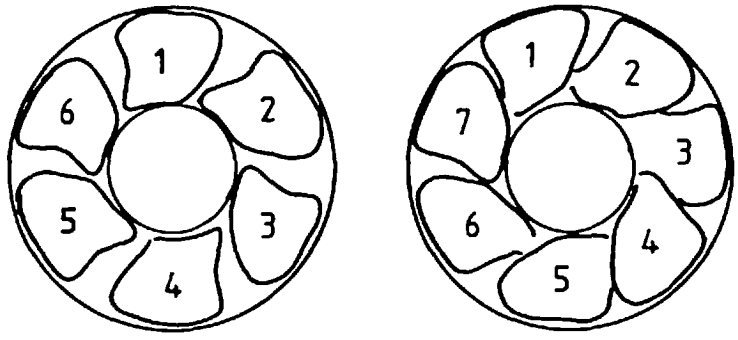


FIG.4.39 Empirical Method for Determination of Jet Orientation and Number of Jets

preferable, since it was less liable to create resonance problems with the even number of compressor blades, and the overlap might provide a more uniform prewhirl profile.

4.9 ADAPTOR AND HARDWARE DESIGN

In designing the hardware for the jet prewhirl device it was thought suitable to adopt the "turbine" type scroll concept, where all the flow feeding the jets would be collected, before ejection, to minimise pipe friction losses. Further, to facilitate interchangeability, the jet orifices for each design were drilled in separate "nozzle rings".

With the new design, the jets had to be placed near the impeller face. The compressor cover had to be suitably machined to accommodate an adaptor which carried the nozzle ring. The arrangement is shown in Figure 4.40.

The cross sectional area of the scroll and the feeder pipe at the scroll inlet, were arrived at taking into account the total jet orifice flow area. The inlet adaptor and the interchangeable nozzle rings were machined out of perspex, and polished to become transparent.

4.10 INVESTIGATIONS USING THE JET-NOZZLE DEVICE

4.10.1 Introduction

With the new design there were three basic questions to be answered:-

1. Whether (variable) prewhirl was beneficial in certain operating regions of the compressor to be tested and to what extent it could be used to control the compressor performance.

It was not known how, and to what extent, prewhirl, imparted through any sort of arrangement, would influence

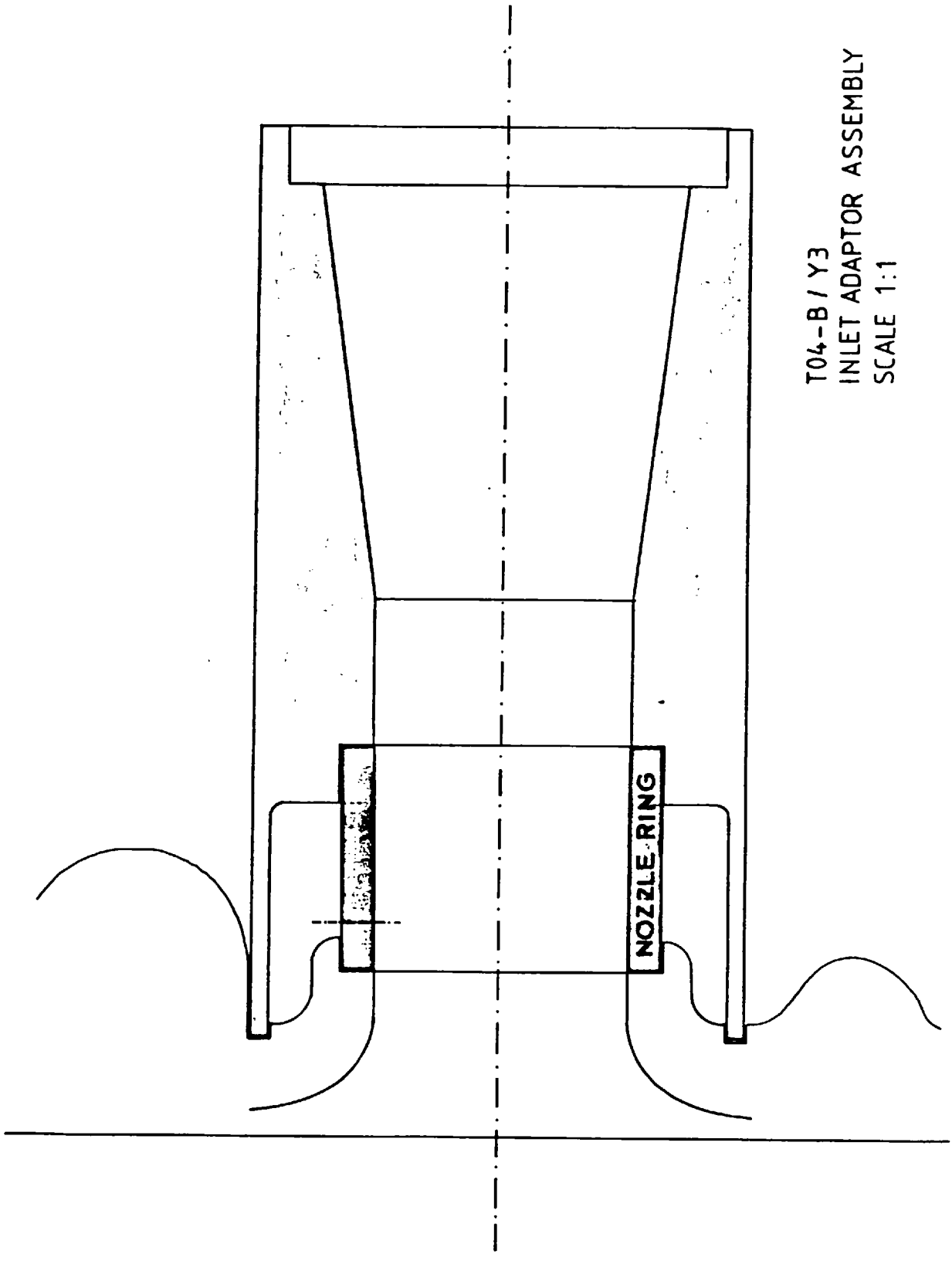


FIG.4.40 Adaptor and Nozzle Ring Assembly for Compressor TO4B-Y3

the stable flow range and the performance of the compressor to be tested.

2. Whether the single, unbounded, round, jet-in-a-cross-flow theoretical model developed, could be used to design a jet arrangement which was capable of producing a prewhirl profile as required by 1. above.

The oblique jet arrangement is exceedingly complicated compared with the basic model, with jet interference, confined flow, differential entrainment and possible wall attachment.

3. In the case of recirculated flow, whether the compressor was capable of providing the necessary flow required by 2. above, at the appropriate operating regions referred to in 1.

Simultaneous testing of the compressor with the jet prewhirl arrangement would involve at least two of the questions above and consequently, any trends in the results obtained, could not be attributed with confidence to a particular cause.

It was therefore decided to decouple these three questions as follows:-

a) Test the multiple jet arrangement performance separately.

b) Test the compressor with the jet arrangement, with

1) external flow supply

2) flow recirculation

4.10.2 Jet Arrangement Performance Experiments

4.10.2.1 Description of experimental rig

The experimental rig constructed to examine the performance of the multiple jet configuration is schematically

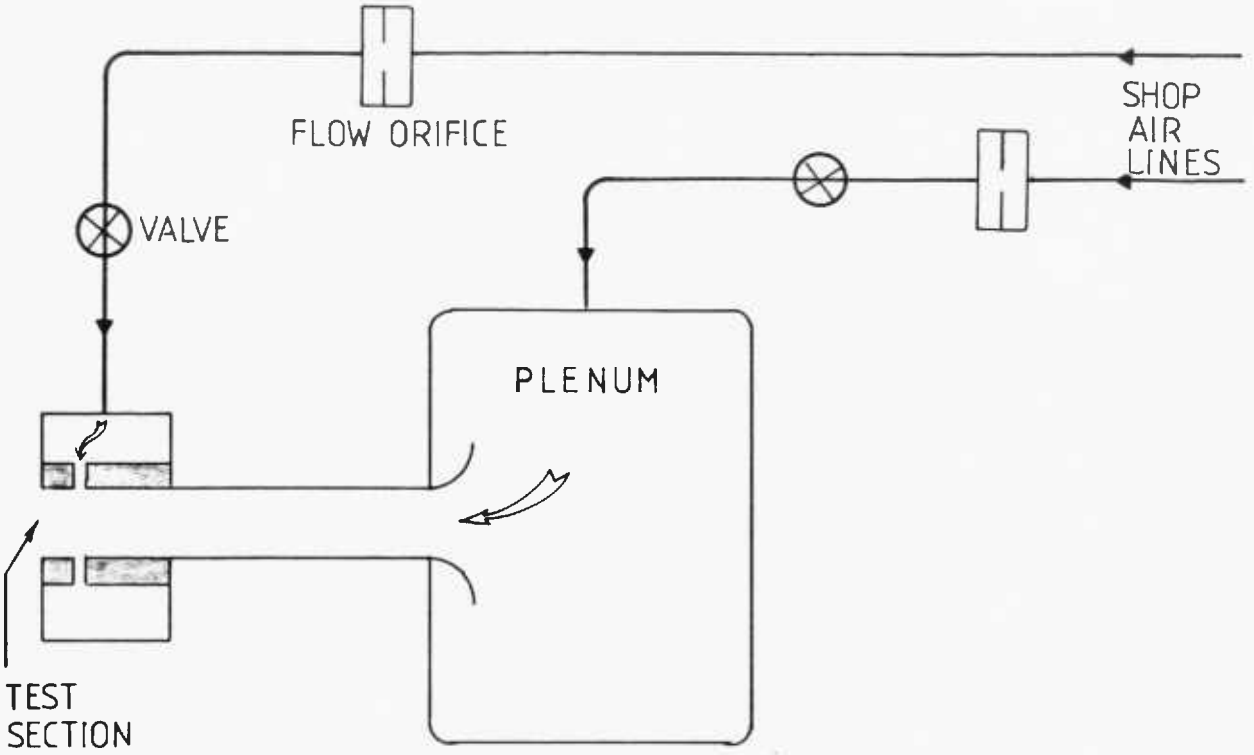


Fig. 4.41 Steady-state Jet Performance Test Rig

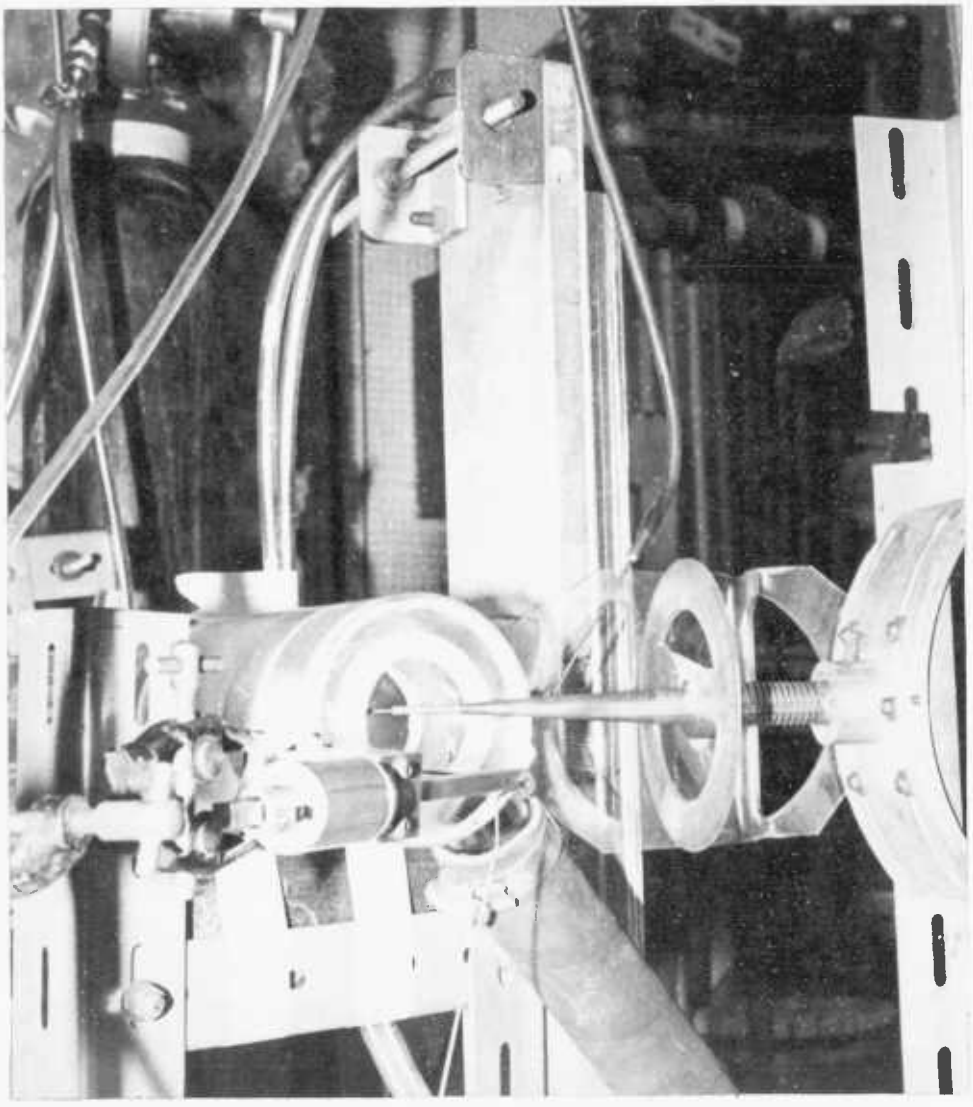


Fig. 4.42 Front View of Jet Test Rig

presented in Figure 4.41. Compressed shop air was used to simulate the cross flow and the jet flow. For the cross flow the air passed through a measuring orifice and a flow regulation valve, into a settling tank, through a flared inlet, to the test section. The air for the jets passed through a flow measuring orifice and a regulation valve to the scroll-nozzle ring assembly. A pitot tube mounted on a traversing base was used to measure the jet dynamic head. The flow angles were measured with a 25° wedge shaped yawmeter on a traversing base. The arrangement is shown in Figures 4.42, 4.43, 4.44.

4.10.2.2 Qualitative observations

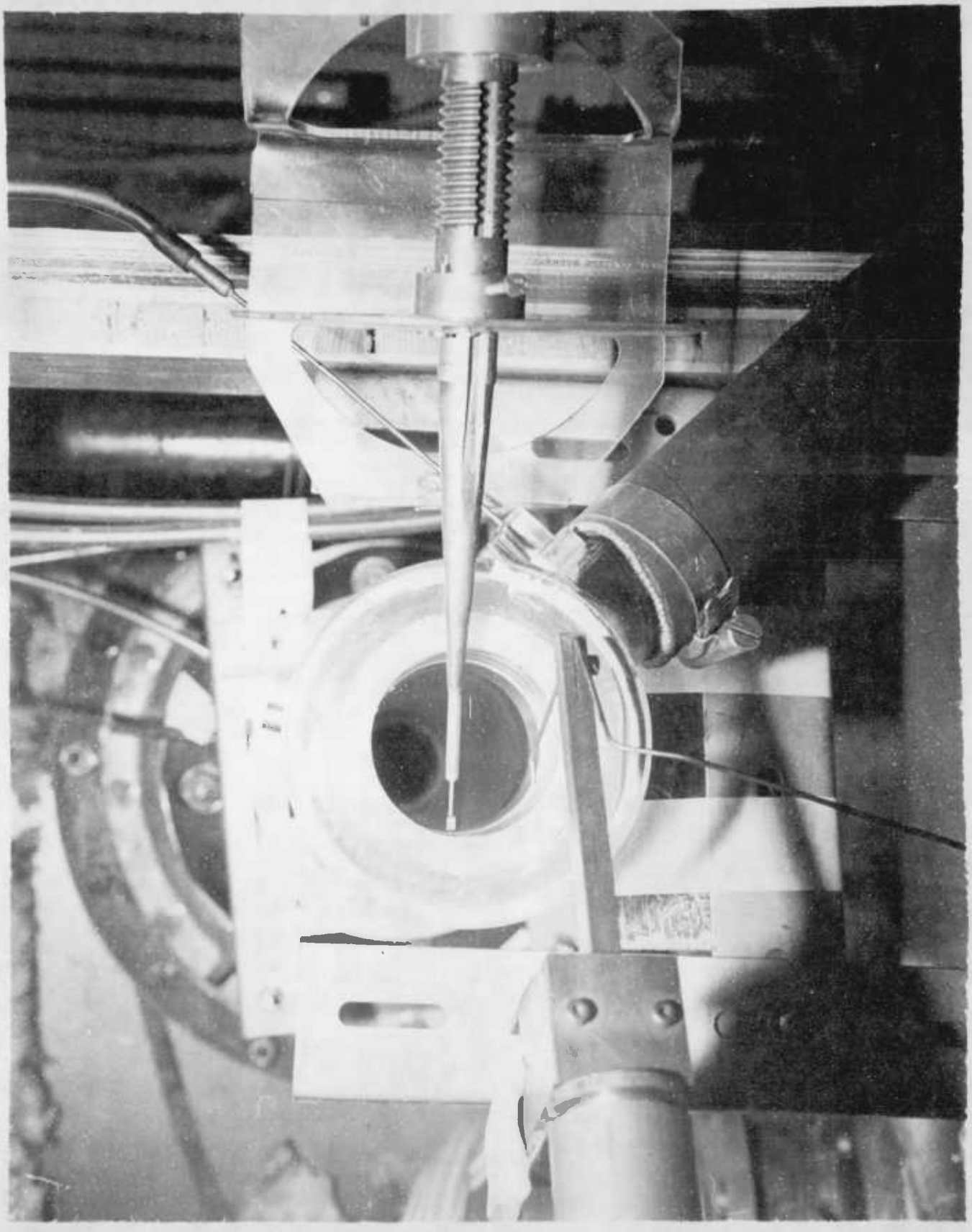
Qualitative observations of the flow field were made using the 7-jet nozzle ring. The test section was taken to coincide with the position of the impeller face when the device is fitted to the compressor.

Discrete patches of flow were found by pitot tube traversing, corresponding to the discrete jets. The flow angle across these patches was not uniform. The cumulative flow profile resembled a forced vortex profile and the flow was generally turbulent. The deflection of the boundary layer at the test section was measured using oil tracks and was found to range between 60° and 70° to the axial direction.

From the predictions, assuming a trajectory gradient of 40° and taking into account the curvature of the wall at the point of contact, deflections not more than 50° were expected near the wall.

This discrepancy may be explained as follows. If just two jets are considered for simplicity, referring to Figure 4.45,

Fig. 4.43 Front View Close-up of Jet Test Rig



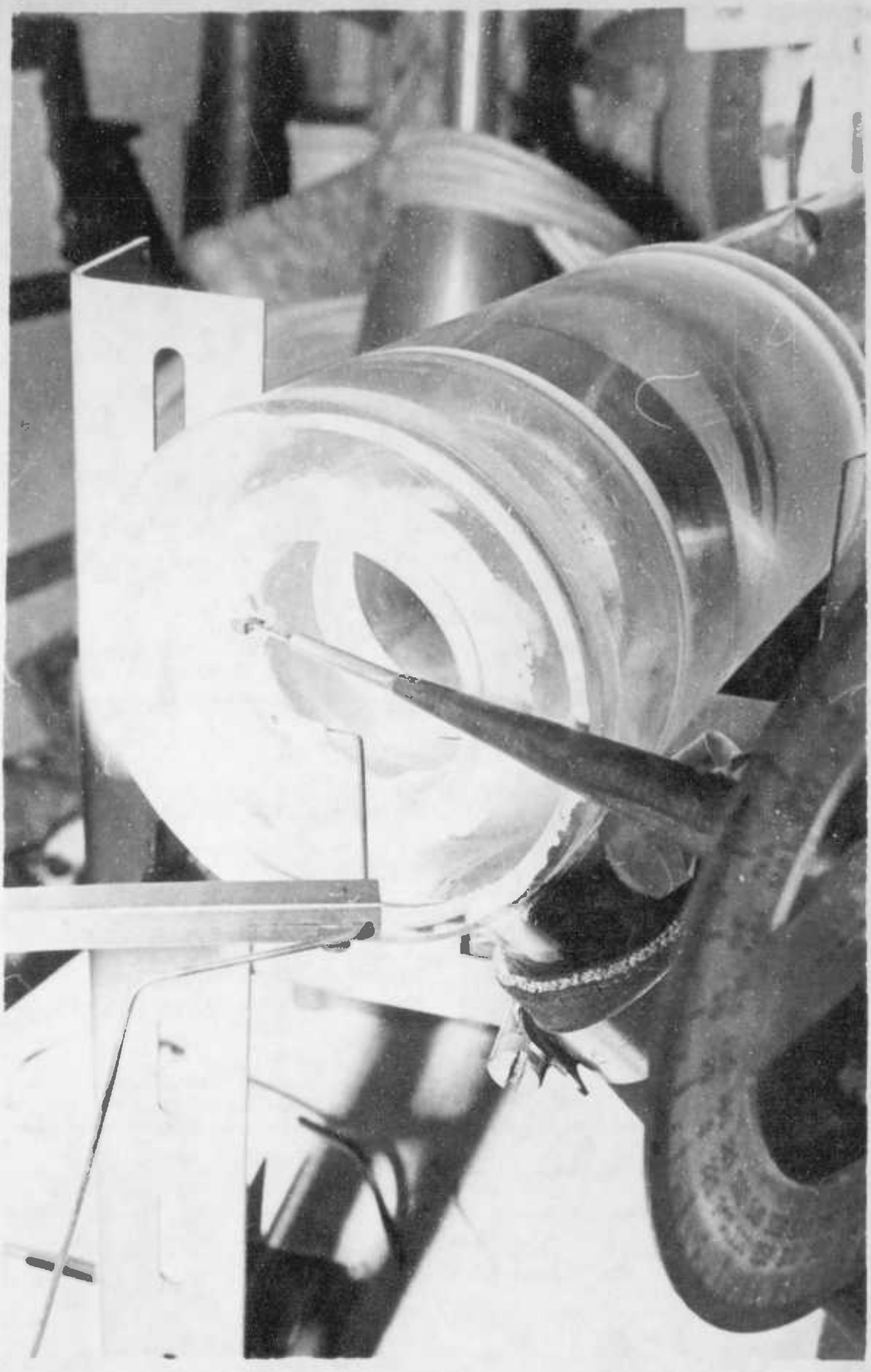


Fig. 4.44 Close-up of Test Section Showing Traversing Yawmeter and Pitot Tube

it can be seen that the second jet, if the velocity ratio is appropriate, will tuck underneath the first jet and a portion of it (shown cross hatched) will be screened and protected from the cross flow. Thus the momentum of the second jet will be preserved and the jet will tend to expand further in the z-direction, so that its cross section at the inducer plane will be larger (shown in dotted line). In doing so, this second jet will fill part of the low pressure region (wake) below the first jet, but may also push the first jet towards the wall.

As the first jet moves towards the wall it suffers differential entrainment, since one side approaches the slow moving boundary layer near the wall while the other side receives the full strength of the cross flow. The resulting pressure field may force the nearside of the jet to attach to the wall. Although the velocity of the attached flow may decrease, its direction will not change much (i.e. the helix angle will not increase, or $\partial^2\theta/\partial\xi^2 \simeq 0$). This may explain the large flow angles observed in the boundary layer.

With higher velocity ratios prevailing, the jets will tend to attach or even hit the wall. With the system fitted on the compressor, this may be further provoked by the centrifugal field resulting from the impeller dominated flow.

Because of the discrete patches of the flow field in front of the impeller, any sector of the inducer blade will receive flows whose angles of approach differ as the blade rotates. The two extreme positions are shown in Figure 4.46.

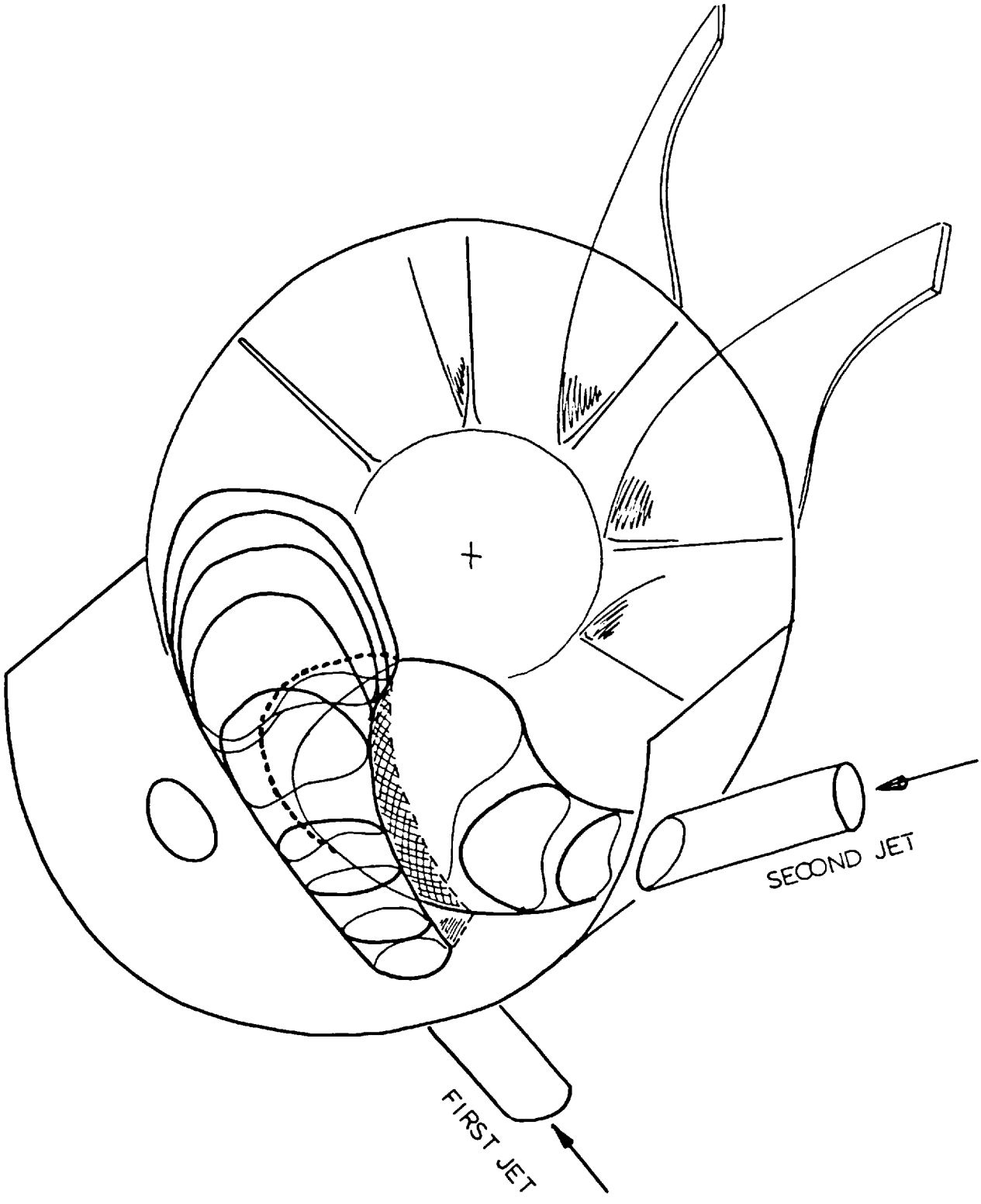


FIG.4.45 Impression of Flow Situation (Jets near Compressor Face)

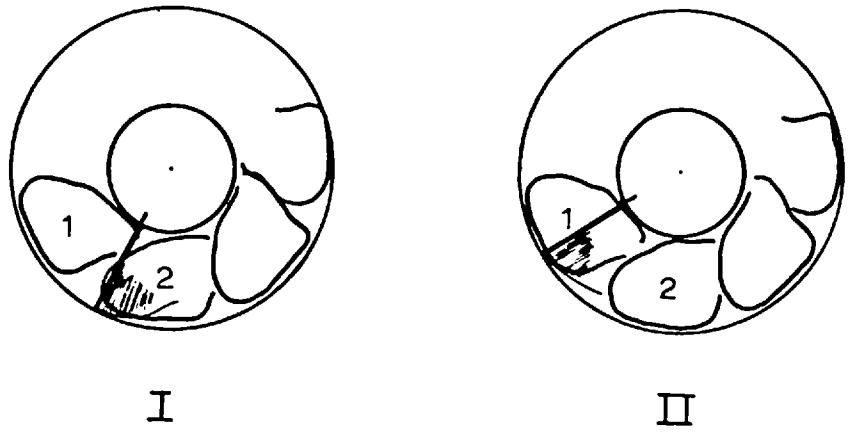


FIG.4.46 Inducer Blade Position Relative to the Jets

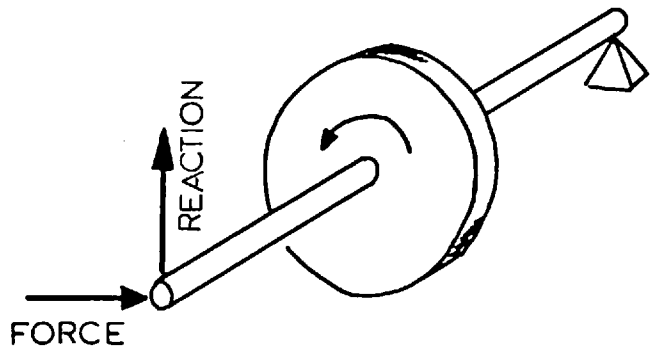


FIG.4.48 Forces in a Gyroscope

I) The blade touches the underside of the first jet with its root lying in the most turbulent part, influenced by the offside vortex. Part of the blade lies inside the (extended) upper part of the second jet.
II) The blade lies completely inside one jet cross section. The radial distribution of flow angle is much smoother.

It would seem that the benefit of inducer stabilisation, if any, but aligning the inlet flow vectors accordingly, will not be fully realised if there are flow angle differences or discontinuities round the circumference.

However, pulsating inlet flow was found to have little influence on compressor stability (31) (Section 2.5.6). Jet interaction and subsequent mixing may smooth the peripheral flow angle differences. The increased turbulence at inlet may not necessarily be detrimental to the compressor performance.

Turbulence stabilisation was found to have a dominating effect on separation (23), because momentum transfer is inhibited (see also Section 2.3.2).

It is interesting, in this context, to consider the effect of the two counterrotating vortices of the deflected jet on the impeller (inducer) channel boundary layer. Consider the impeller passage and the jet (see Figure 4.47). It can be assumed that the mass of fluid in a vortex will behave according to the gyroscopic laws of motion . The reaction of a gyroscope to a force tending to tilt the spin axis is a vector perpendicular to both the force and the spin

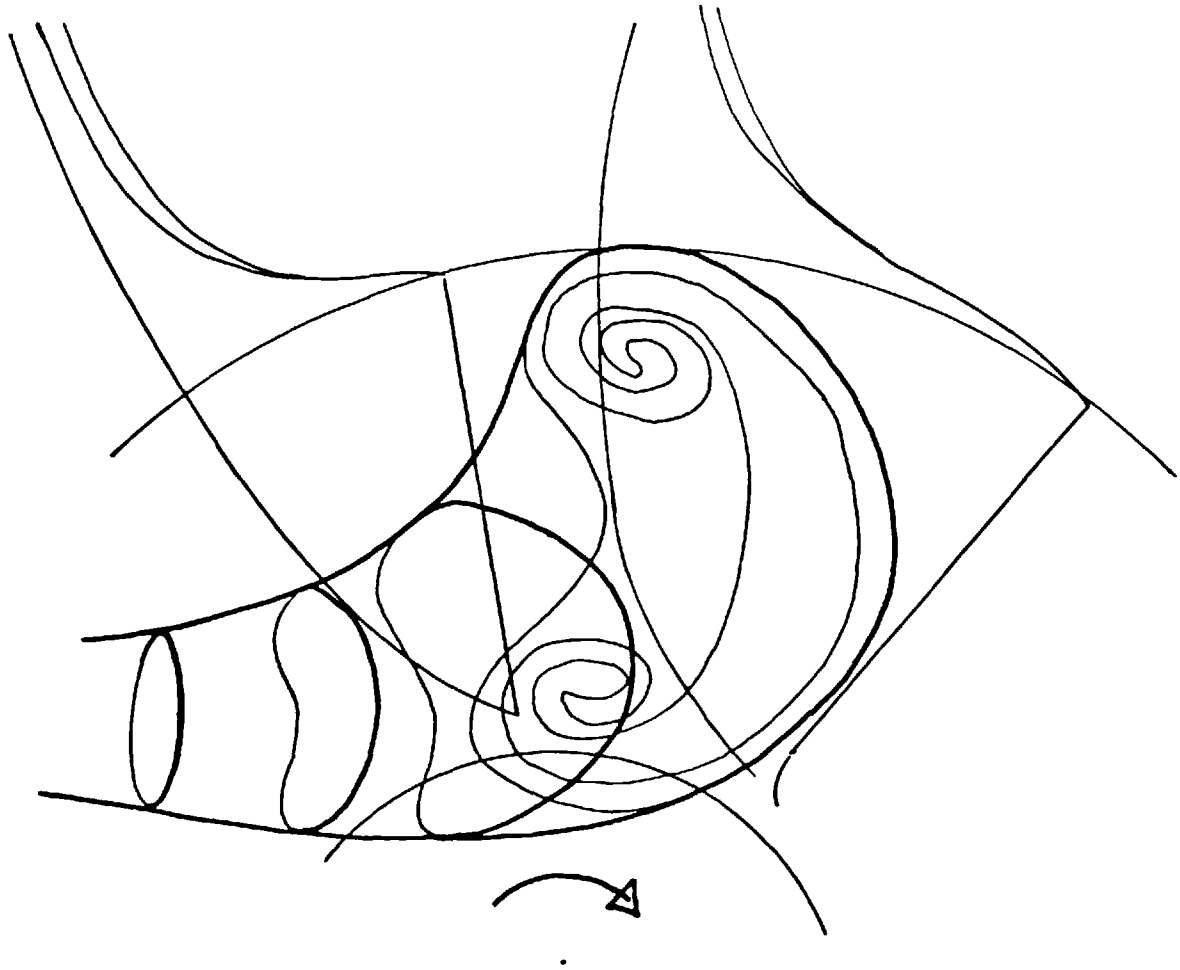


FIG.4.47 Impression of Flow Situation (Jet approaching inducer)

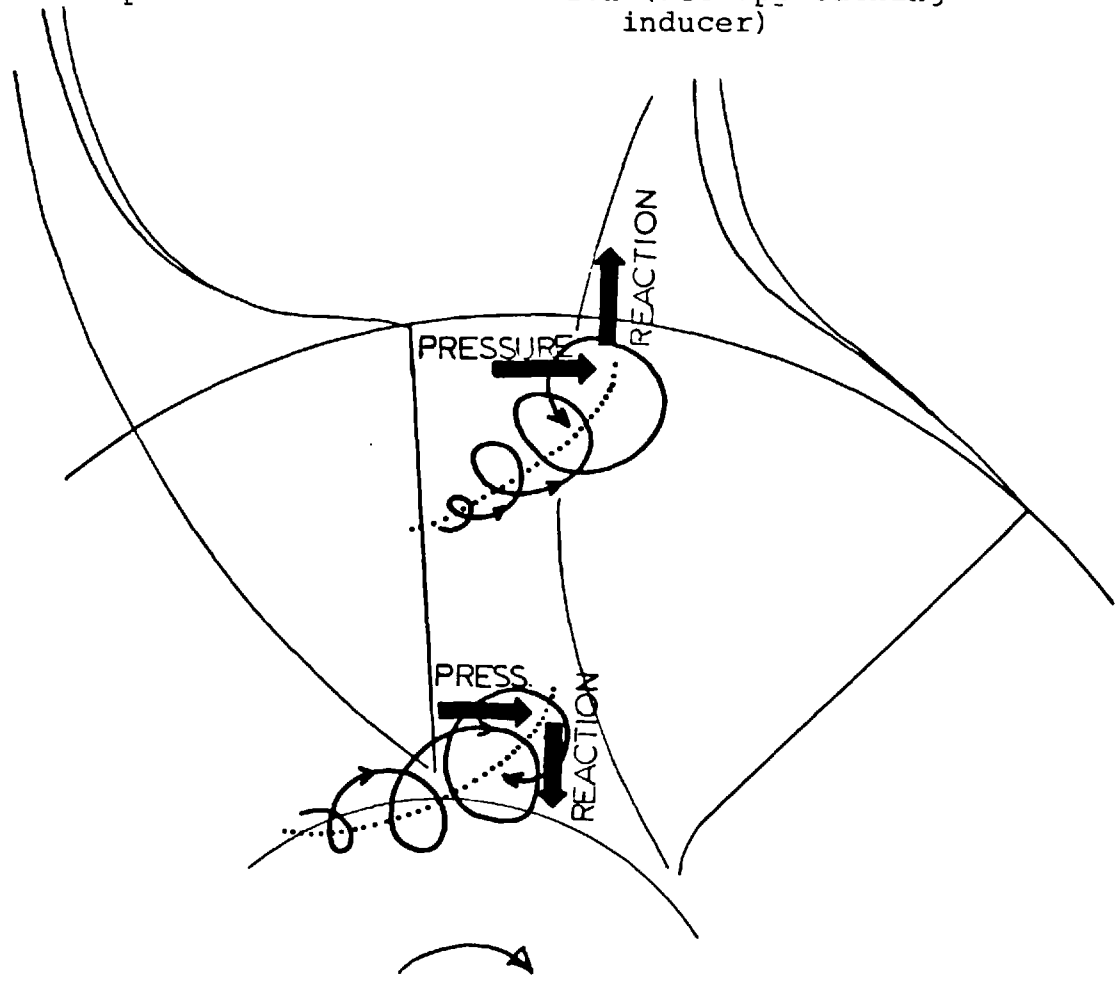


FIG.4.49 Jet Vortices in Impeller Channel

axis. The direction of the reaction is that of the force vector, rotated by 90° in the direction of spin (see Figure 4.48).

If the pressure field inside the impeller passage, is equivalent to the applied force, then the reaction of the two vortices will be towards the hub and shroud respectively, (see Figure 4.49) thus energising the boundary layers through mixing and momentum exchange, with possible beneficial effects.

4.10.2.3 The experiments

A series of experiments to measure the flow profile at the impeller face plane for several velocity ratios (R) was performed. The experimental procedure was as follows:-

A velocity ratio (R) was chosen. The cross flow was adjusted to obtain a certain flow velocity at the jet exit plane cross section. Then the jet flow was adjusted to obtain the jet exit velocity required for the postulated velocity ratio. This was an approximation since the cross flow velocity decreased, because the jets formed a barrier and "throttled" the main flow. Therefore the main flow had to be readjusted.

Then the yawmeter probe was traversed along a radius of the inlet pipe, on the virtual impeller face plane, from the pipe axis to the pipe wall, so that the measured deflection angles would correspond to the inducer inlet angles.

Both the 7-jet and 6-jet arrangements were examined.

4.10.2.4 Results from the experiments

Figures 4.50 - 4.55 show the profile variation along

the inlet pipe radius for different values of velocity ratio (R), for the 7-jet arrangement. Figure 4.58 shows selected smoothed profile variations with radius for different velocity ratios (R), as well as the percentage of flow required for each velocity ratio. It must be noted that these percentages were found to be independent of the absolute mass flow values.

The change in slope of the curves near the wall and near the pipe axis is attributed to the presence of the jet vortices. With high velocity ratios (see Figure 4.55) the jets probably hit the wall, with the nearside vortex collapsing, hence there is no change in the slope of the curve. In all cases the profile resembles a forced vortex profile.

Based on the theoretical model and for the 7-jet design configuration, a deflection angle of 40° was expected at a radial distance of 5.5 mm from the wall, for the design velocity ratio R = 4. However this was only realised with R = 4.4. Figures 4.56 and 4.57 show some results with the 6-jet arrangement. Since the distance between the jets is greater than in the 7-jet arrangement there are larger variations in the flow angle for the same radial distance, but different peripheral positions. In Figure 4.56 large deflection angles are evident near the wall but the deflection soon diminishes moving towards the centre.

The incomplete flow mixing and the low jet interaction is revealed by the negative value of the deflection angle, attributed to the presence of a strong eddy behind the jet.

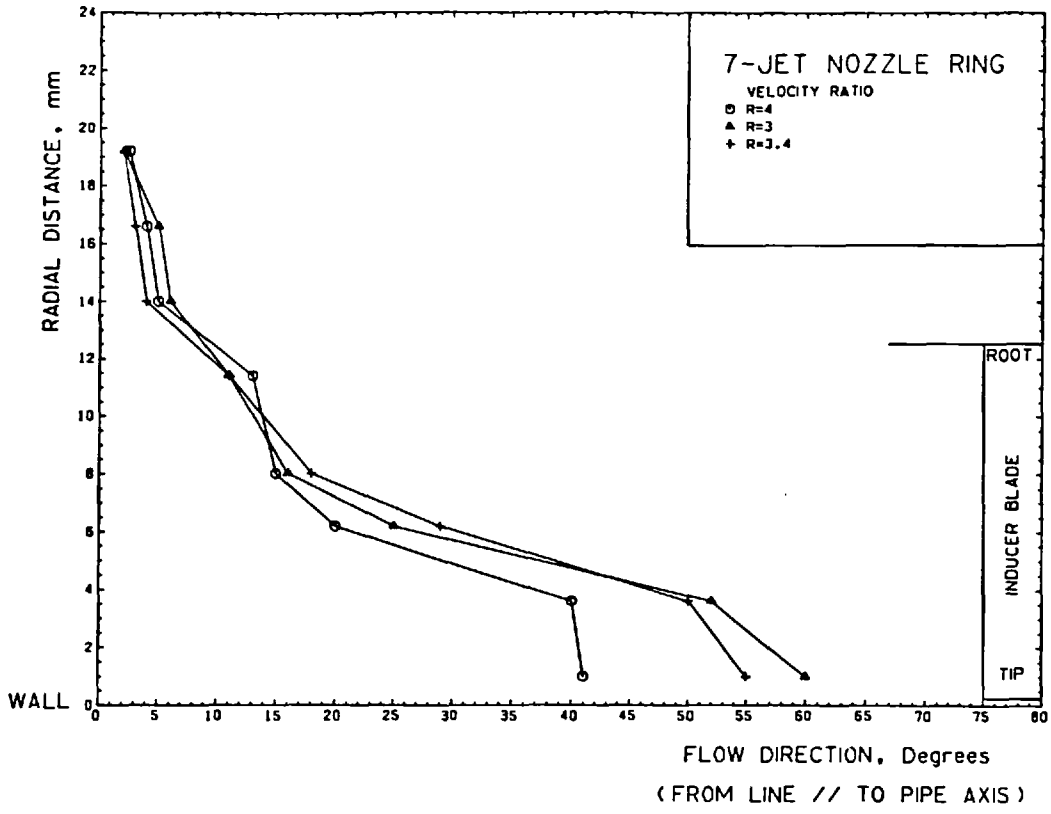


FIG.4.50 Radial Flow Deflection Variation

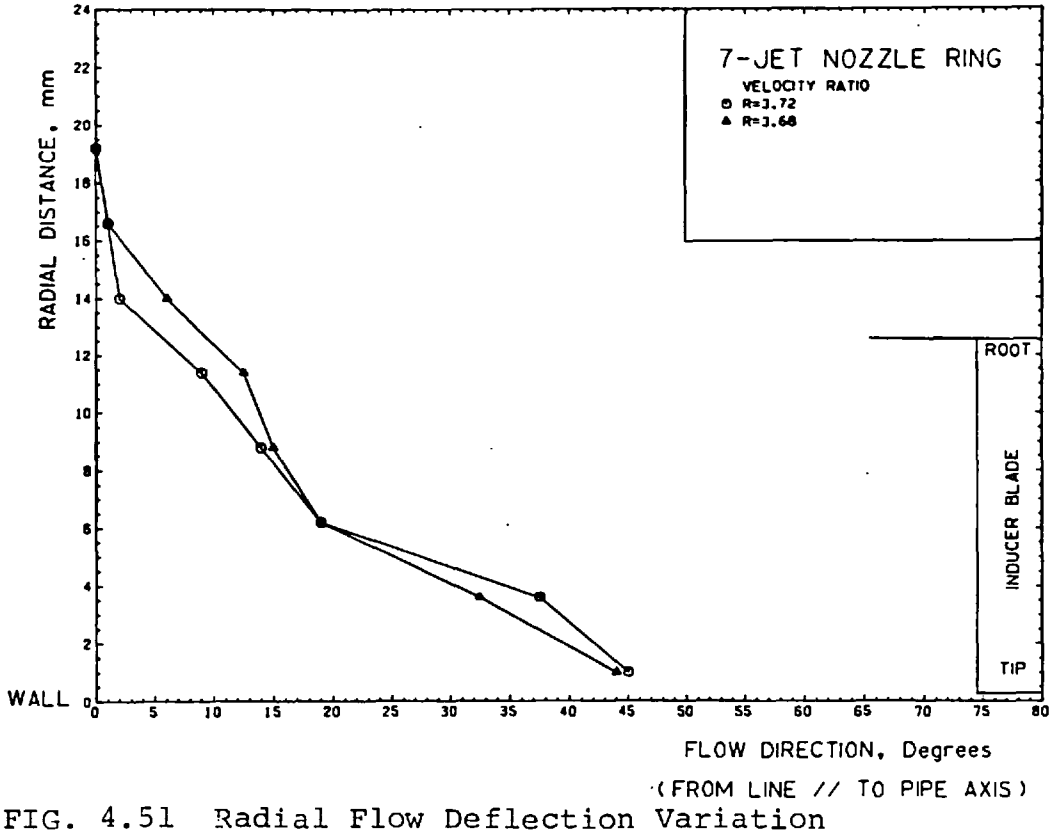


FIG. 4.51 Radial Flow Deflection Variation

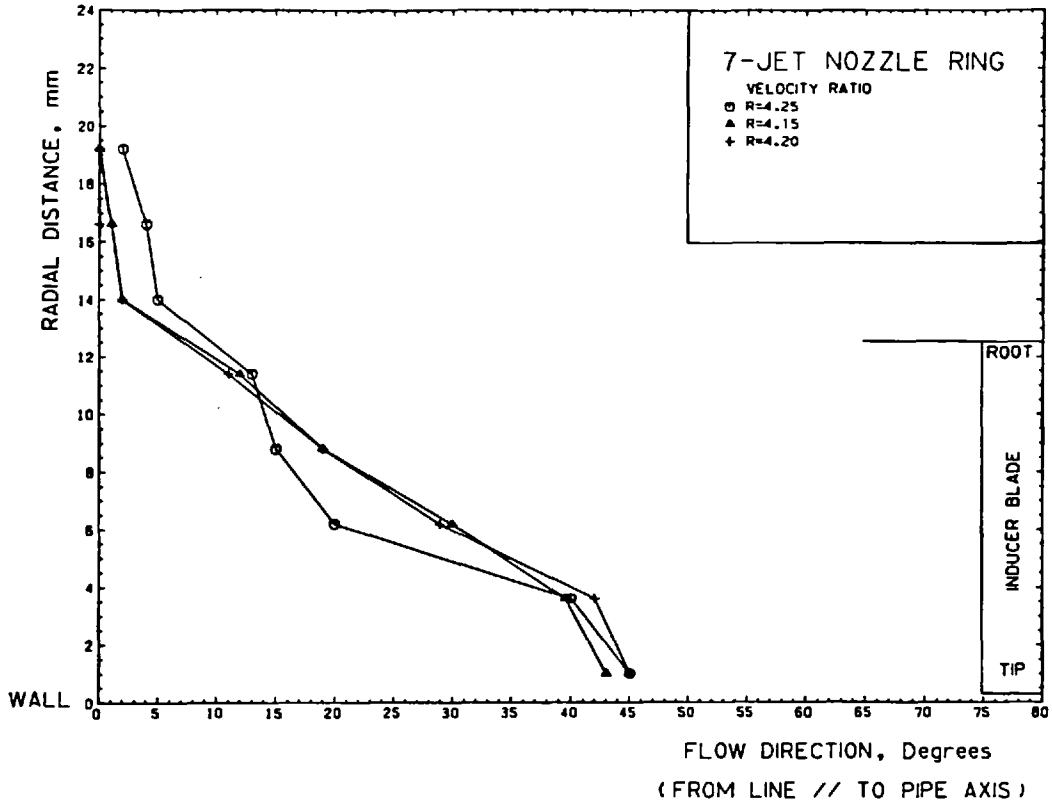


FIG.4.52 Radial Rlow Deflection Variation

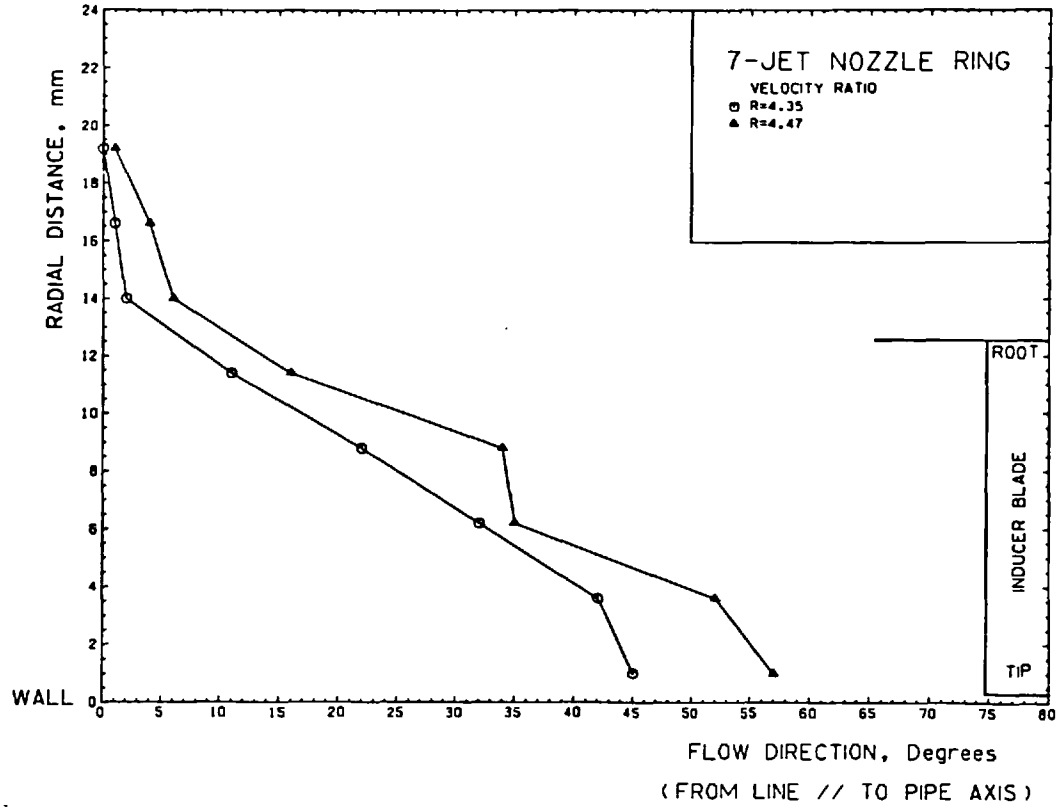


FIG.4.53 Radial Flow Deflection Variation

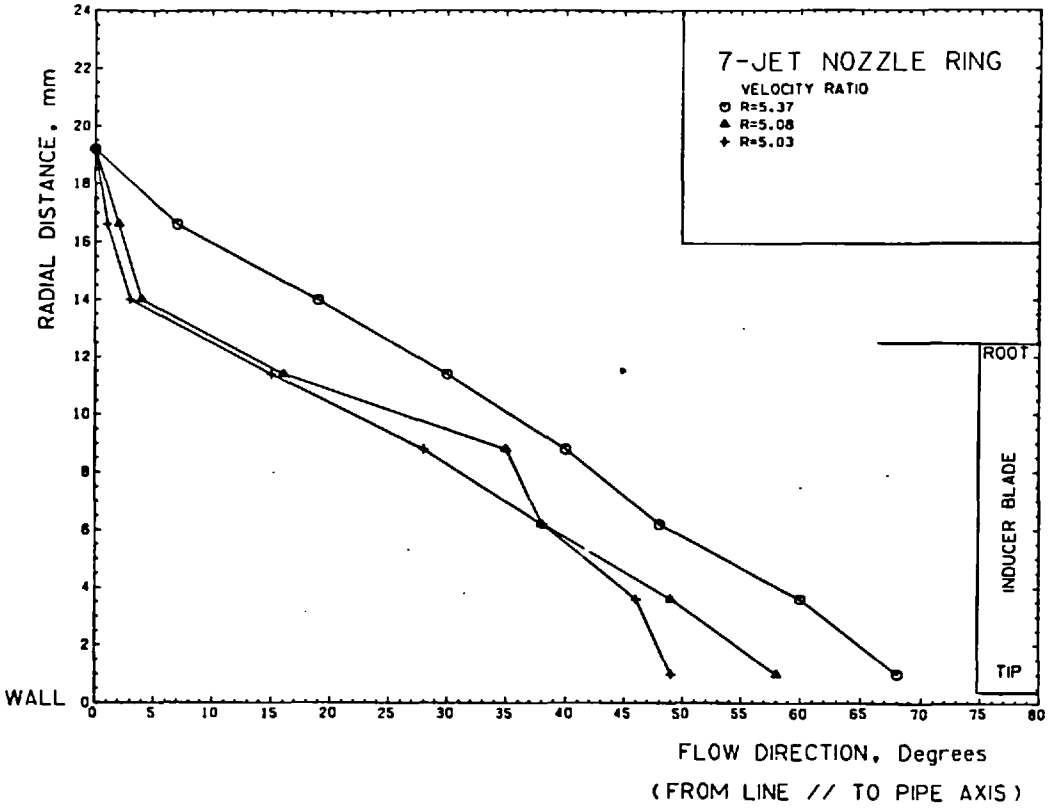


FIG.4.54 Radial Flow Deflection Variation

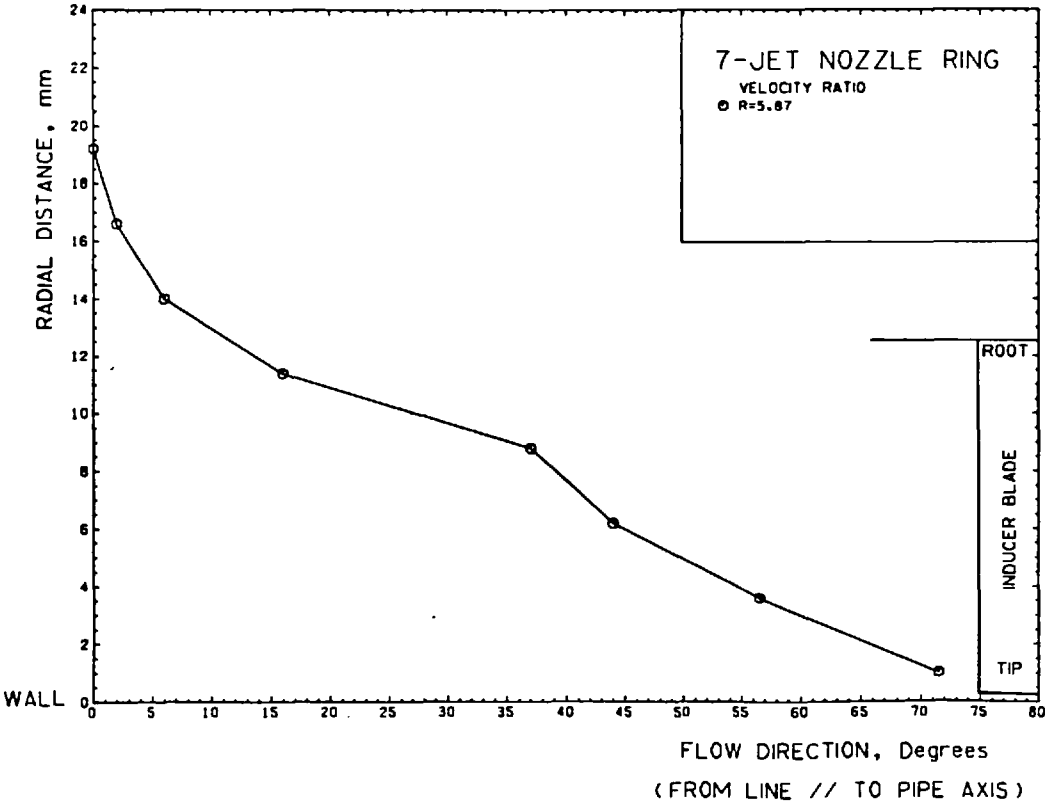


FIG.4.55 Radial Flow Deflection Variation

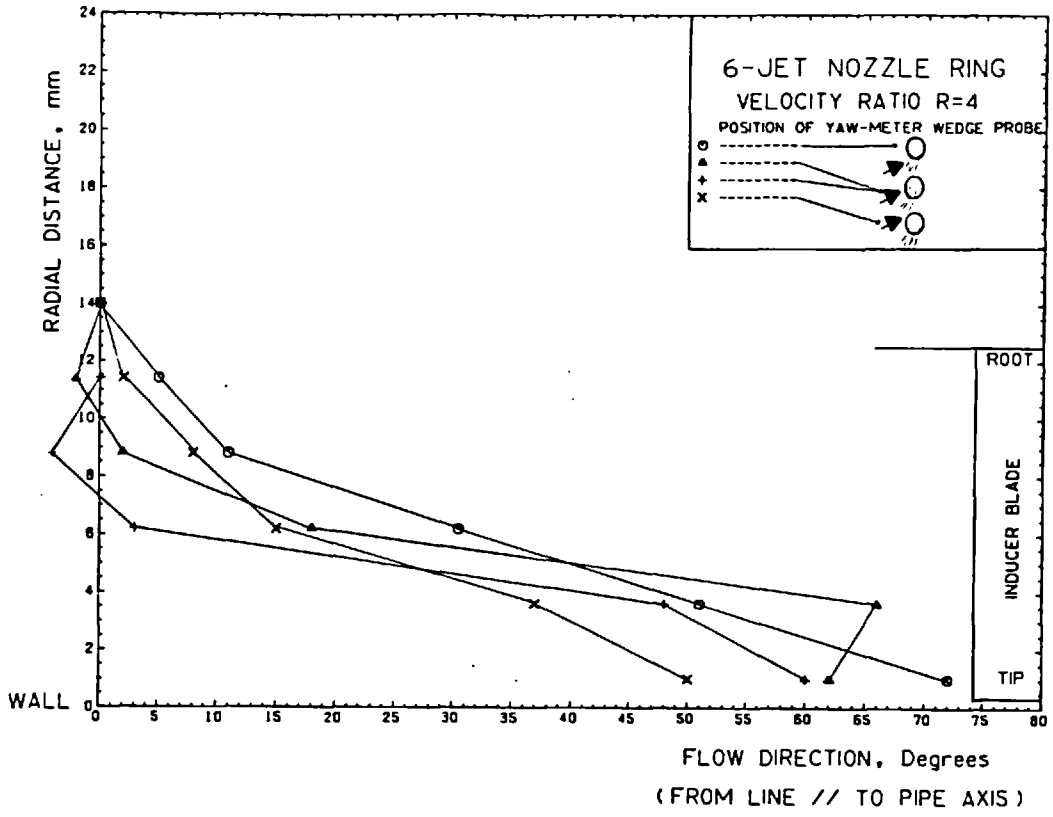


FIG.4.56 Radial Flow Deflection Variation

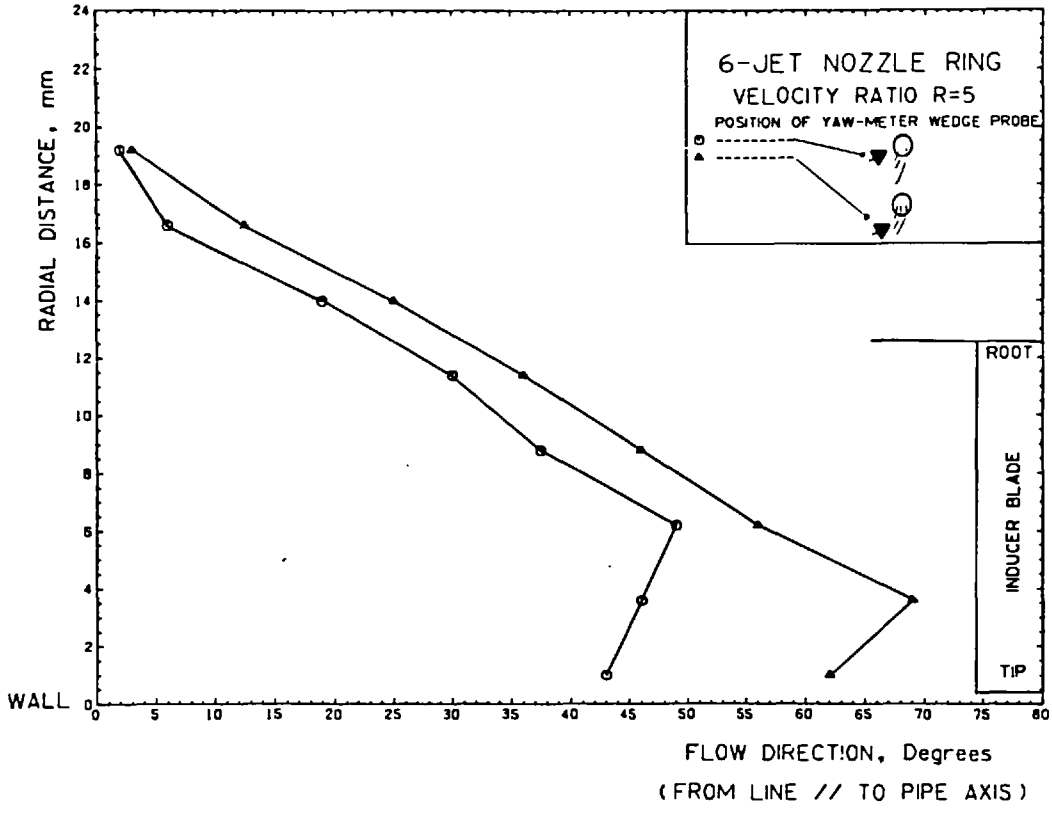


FIG.4.57 Radial Flow Deflection Variation

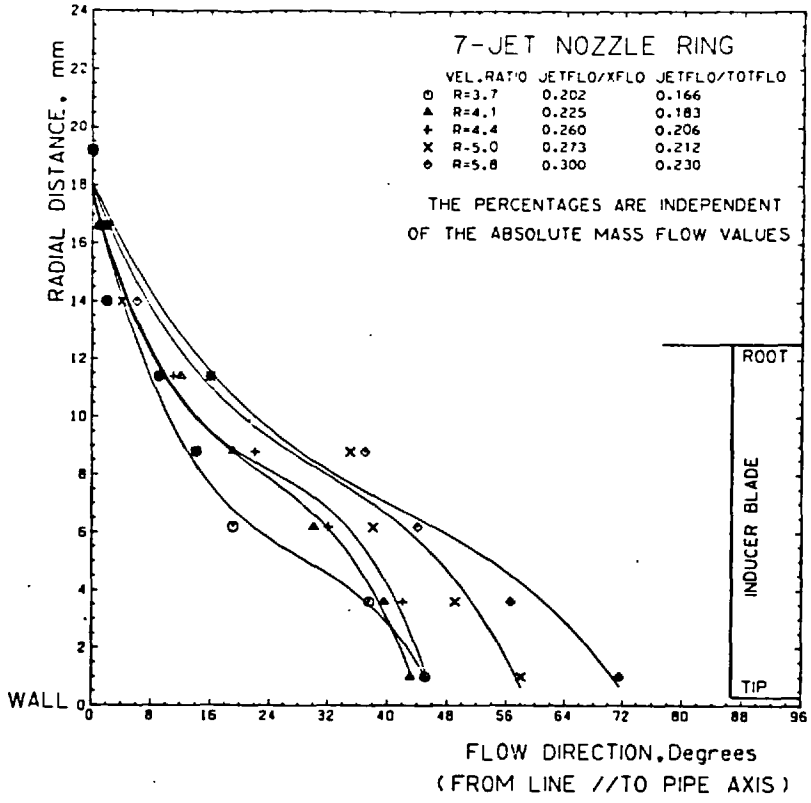


FIG.4.58 Selected Smoothed Radial Profile Variation

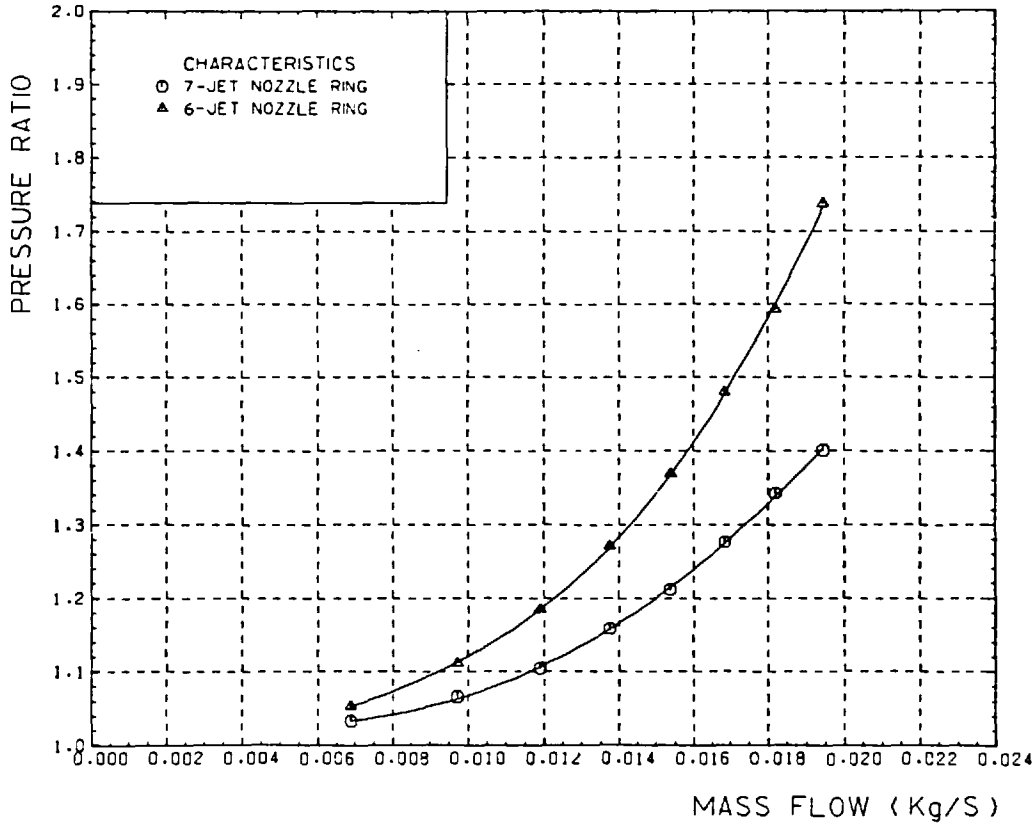


FIG.4.59 Mass-Flow Pressure-Ratio Characteristics of the Nozzle Rings

In Figure 4.57 it is obvious that with the 6-jet arrangement there are large differences in the profile depending on the peripheral position. This confirms that there is little jet interaction. The variation of the profile with radius, as well as the values of the flow angles, probably means that the jets do not attach to the wall with that configuration. The mass flow-pressure ratio characteristic curves for the 6 and 7-jet nozzle rings are shown in Figure 4.59.

4.10.2.5 Comparison of the two jet arrangements

In the 6-jet arrangement each jet has the opportunity to expand further and entrain more fluid before being influenced by a nearby jet, because the distance between the jets is greater. However the limited jet inter-mixing results in large differences in flow angle round the periphery.

The 7-jet arrangement, on the other hand, provides a much smoother overall profile, because of the interaction between the jets, but this results in some momentum loss, hence lower deflections were observed. The 7-jet arrangement was therefore preferable, but it could possibly benefit from slight repositioning of the ejection axis further away from the wall, and lower cross section at ejection, to avoid premature wall attachment.

4.10.2.6 Interaction of compressor and jet-device (prediction)

It was thought that it would be instructive to superimpose some of the experimental points from the 7-jet arrangement, which gave better overall performance, on the AIRESEARCH TO4B-Y3 compressor performance map as provided by

the manufacturers. (This type of compressor was used for that series of experiments.) It would then be possible to find out whether the compressor would be able to provide the necessary (recirculating) flow and pressure ratio, required for the design velocity ratio (R = 4) of the device.

As can be seen in Figure 4.60, curves of constant velocity ratio can be superimposed on the compressor map. In view of the relatively limited information available these were assumed to be straight lines. Above a certain velocity ratio line, higher velocity ratios are available, below the line lower ratios are available.

To predict the change in incidence angle and relative velocity to the inducer, that would be achieved by pre-whirl, as imparted by the 7-jet arrangement at the design point (R = 4), the velocity triangles for two points P1, P2 on the compressor map (see Figure 4.60) were evaluated. The prewhirl deflection angles for R = 4 were taken from Figure 4.58 for 3 positions along the blade (see Figure 4.62). The nomenclature of the velocity trianges is shown in Figure 4.61. The results are shown in Table 4.I.

If it is assumed that inducer incidence is critical for compressor stability, then it was essential to examine the capability of the jet-device to change the incidence angle in the region near the surge line. Five points, PS1 to PS5 were defined on the surge line of the AIRESEARCH TO4B-Y3 compressor performance map, for pressure ratios 1.2 to 1.8 (see Figure 4.60). All these points lie above the R = 4 line, therefore the compressor would be able to

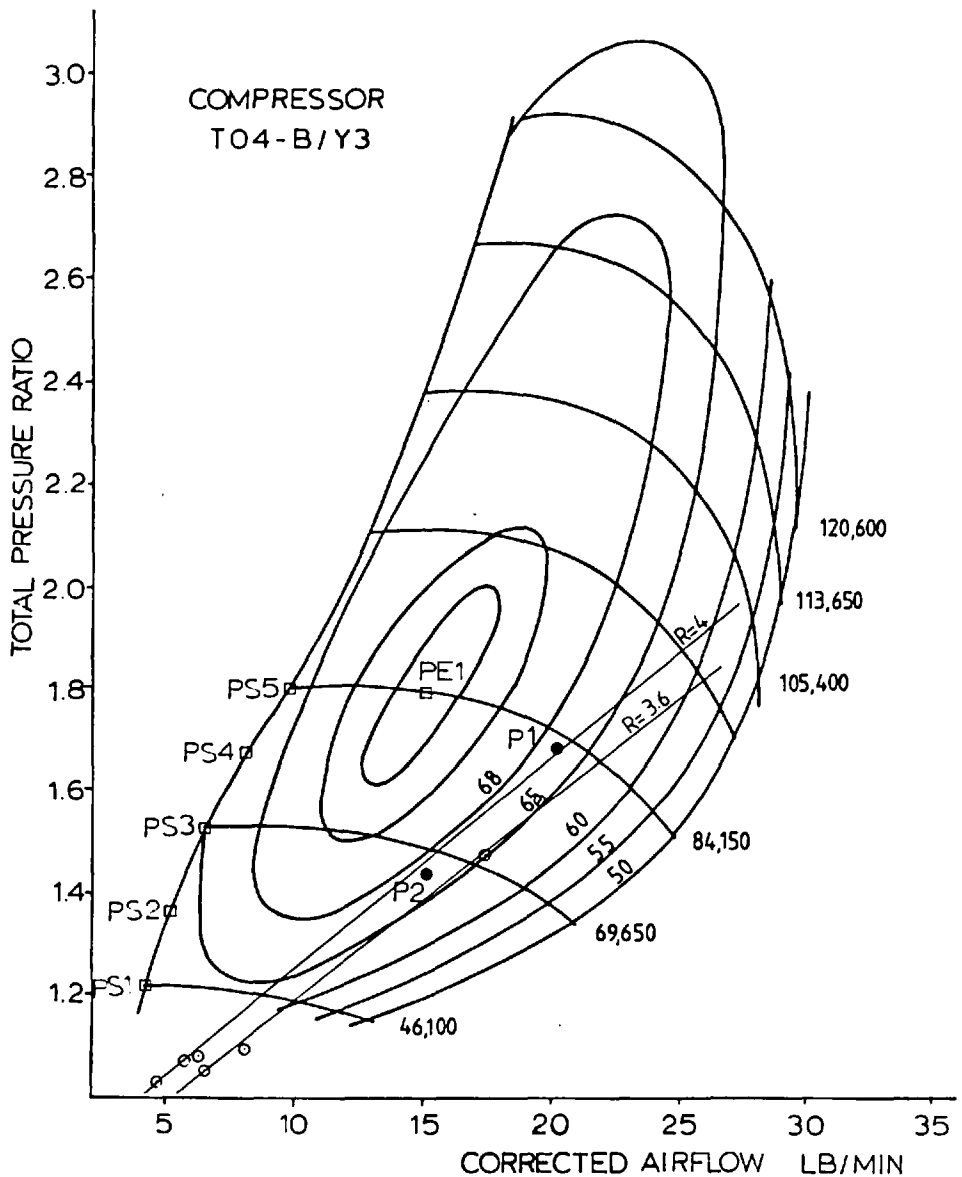


FIG.4.60 Constant Velocity Ratio Curves on T04B-Y3 Compressor Map

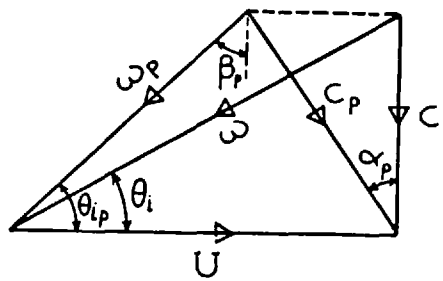


FIG.4.61 Velocity Triangles Notation

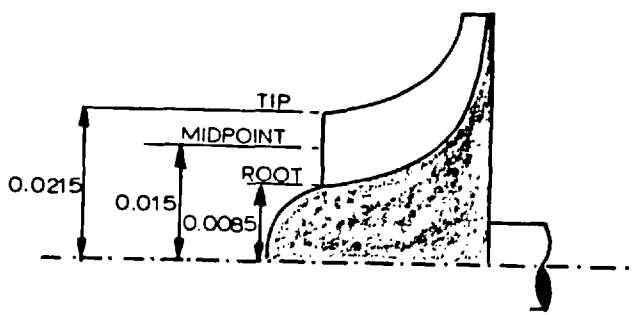


FIG.4.62 Y3 Compressor Inducer Blade Position

TABLE 4.I

	POINT P1 INLET MASS FLOW: 0.152 kg/s ROT. SPEED: 81000 rpm $\Omega = \frac{2\pi N}{60} = 8482.3$ EYE ANNULUS AREA: 0.00123 m^3 AXIAL VEL.$=\frac{\dot{m}_x}{\rho A} = 108.3$ m/s			POINT P2 $\dot{m}_x = 0.114$ kg/s N = 68000 rpm $\Omega = 7120$ $C_x = 80.59$ m/s		
	TIP	MID PT	ROOT	TIP	MID PT	ROOT
C	108.00	108.00	108.00	80.59	80.59	80.59
U	182.00	127.23	72.09	153.10	106.80	60.53
ω	211.63	166.89	129.85	173.02	133.79	100.79
θ_i	30.69	40.32	56.30	27.76	37.04	53.09
α_{PT}	45.00	23.00	5.00	49.00	25.00	5.00
C_p	152.70	117.32	108.41	122.84	88.92	80.90
ω_p	130.00	135.23	124.81	100.71	106.34	96.83
θ_{iP}	55.58	52.99	59.92	53.15	49.39	56.33
$\Delta\theta_i$	25.1	12.67	3.62	25.4	12.35	3.24
$\%\Delta\omega$	38.40	18.97	3.88	42.20	20.52	3.93

provide this velocity ratio.

The mean flow deflection angles for the 7-jet arrangement, for R = 4, were used (see Figure 4.58), to construct the velocity triangles for three positions along the blade (see Figure 4.62). The results are shown in Table 4.II and Table 4.III, the nomenclature corresponding to Figure 4.61. It can be seen that substantial decreases in inlet relative velocity are possible near the inducer tip with this velocity ratio (R = 4) but the incidence angle can only be changed a few degrees. Table 4.III also includes the values for the velocity triangles at the best efficiency point PE1 (see Figure 4.60).

Using the information obtained from the velocity triangles Table 4.IV was constructed.

TABLE 4.II

	POINT PS1 m_x = 0.0317 kg/s N = 46100 rpm Ω = 4827.58 C_x = 22.41 m/s			POINT PS2 m_x = 0.0393 kg/s N = 57000 rpm Ω = 5969 C_x = 27.78 m/s			POINT PS3 m_x = 0.04914 kg/s N = 69650 rpm Ω = 7293.7 C_x = 34.74 m/s		
	TIP	MID PT	ROOT	TIP	MID PT	ROOT	TIP	MID PT	ROOT
C	22.41	22.41	22.41	27.78	27.78	27.78	34.74	34.74	34.74
U	103.79	72.41	41.03	128.33	89.53	50.73	156.82	109.41	62.00
ω	106.18	75.80	46.75	131.3	93.74	57.83	160.62	114.79	71.07
θ_i	12.18	17.20	28.64	12.21	17.23	28.70	12.49	17.62	29.26
α_{PT}	45.00	23.00	5.00	45.00	23.00	5.00	45.00	23.00	5.00
C_p	31.70	24.34	22.50	39.28	30.17	27.88	49.13	34.74	34.87
ω_p	84.41	66.77	45.04	104.31	82.55	55.70	126.92	100.83	68.43
θ_{ip}	15.40	19.61	29.84	15.44	19.66	29.90	15.89	20.15	30.51
$\Delta\theta$	3.22	2.41	1.20	3.23	2.73	1.20	3.40	2.53	1.25
$\%\Delta\omega$	20.50	11.91	3.66	21.03	11.94	3.68	20.98	12.16	3.71

TABLE 4.III

	POINT PS4 m_x = 0.0604 kg/s N = 76000 rpm Ω = 7958 C_x = 42.7 m/s			POINT PS5 m_x = 0.07409 kg/s N = 84150 rpm Ω = 8812 C_x = 52.37 m/s			POINT PE1 m_x = 0.1134 kg/s N = 84150 rpm Ω = 8812 C_x = 80.16 m/s		
	TIP	MID PT	ROOT	TIP	MID PT	ROOT	TIP	MID PT	ROOT
C	42.70	42.70	42.70	52.37	52.37	52.37	80.16	80.16	80.16
U	171.11	119.38	67.64	189.46	132.18	74.90	189.00	132.00	74.90
ω	176.35	126.78	79.99	196.56	142.17	91.96	105.23	170.00	109.71
θ_i	14.01	19.68	32.36	15.45	21.61	35.77	22.90	39.25	46.94
α_{PT}	45.00	23.00	5.00	45.00	23.00	5.00			
C_p	60.38	46.38	42.86	74.06	56.89	53.57			
ω_p	135.32	109.89	76.85	146.75	121.78	88.20			
θ_{ip}	18.39	22.86	33.75	20.90	25.46	37.23			
$\Delta\theta$	4.38	3.18	1.49	5.45	3.85	1.76			
$\%\Delta\omega$	23.27	13.32	3.93	25.34	14.34	4.09			

TABLE 4.IV

		POINT	POSITION ALONG BLADE TIP	MID PT	ROOT
BLOCK 1	FLOW INCIDENCE ANGLE TO A PLANE NORMAL TO AXIS θ_i degrees	PS1	12.18	17.20	28.64
		PS2	12.21	17.23	28.70
		PS3	12.99	17.62	29.26
		PS4	14.01	19.28	32.36
		PS5	15.45	21.61	35.77
		PE1	22.90	39.25	46.94
BLOCK 2	INDUCER BLADE ANGLE θ_b		40.00	50.26	62.00
BLOCK 3	INDICENCE MISMATCH @ POINT PE1 $\Delta\theta_{PE1} = \theta_i - \theta_b$		17.00	11.00	15.00
BLOCK 4	INCIDENCE MISMATCH AT SURGE $\Delta\theta_{PS}$	PS1 ↓ PS5	27.82 ↓ 24.55	33.00 ↓ 28.65	33.36 ↓ 26.23
BLOCK 5	$\Delta\theta_{PS} - \Delta\theta_{PE}$	PS1 ↓ PS5	10.82 ↓ 7.55	22.00 ↓ 17.65	18.36 ↓ 11.23
BLOCK 6	INCIDENCE IMPROVMENT WITH JETS $\theta_{ip} - \theta_i$	PS1 ↓ PS5	3.20 ↓ 5.45	2.40 ↓ 3.85	1.20 ↓ 1.76

Comments:

BLOCK 2. Blade angle was measured at tip and root. Midpoint value was found assuming the following relationship of blade angle as a function of radius ratio

$$\tan\beta_x = \frac{r_x}{r_{TIP}} \tan\beta_{TIP}$$

BLOCK 3. The inducer may possibly be slightly separated. It is noted however (42) that maximum efficiency of aerodynamic blading normally occurs with a slight degree of separation.

BLOCK 4. Surge at point PS1 occurs with incidence mismatch of approximately 30° (6° variation along the blade). Surge at PS5, with incidence mismatch approximately 26° (4° variation). As speed increases surge occurs at smaller incidence mismatch.

BLOCK 5. At the blade tip there is small difference in incidence for the best efficiency point PE1 and the surge points, becoming smaller at higher speeds. It is possible that tip incidence is critical for surge.

BLOCK 6. Comparison of the values with those in Block 5, shows that improvement in blade incidence, especially at large flows and near the blade tip, is possible using the jet-prewhirl device. Improvement in compressor stability or efficiency is only possible to the extent that these are affected by the

inducer incidence. A more balanced profile with additional incidence bias towards the hub might be obtained with appropriate design of the jet arrangement.

With the collected information it was possible to predict the approximate available velocity ratios at any point on the TO4B-Y3 compressor performance map for the 7-jet arrangement. Using the mass flow-pressure ratio characteristic for the 7-jet nozzle-ring (see Figure 4.59) it was possible to obtain a jet exit velocity-pressure ratio characteristic.

In Figure 4.63 the horizontal lines superimposed on the manufacturers compressor performance map, are the jet velocities that can be obtained with the corresponding compressor pressure ratio. The vertical lines, in the same figure, are the compressor inlet flow velocities (or cross-flow velocities) at the jet exit plane cross section, corresponding to the appropriate inlet mass flows. The velocity ratios were calculated at the nodes of this grid of velocities. Curves of constant velocity ratio were then fitted relative to the node values. For the range considered the curves were assumed to be straight lines.

The arrangement of the constant velocity ratio lines on the compressor map indicates that near the surge line, velocity ratios substantially higher than the design ratio (R = 4) were potentially available. Therefore with appropriate design of the jet arrangement it would be possible to obtain larger deflection angles at the compressor inlet.

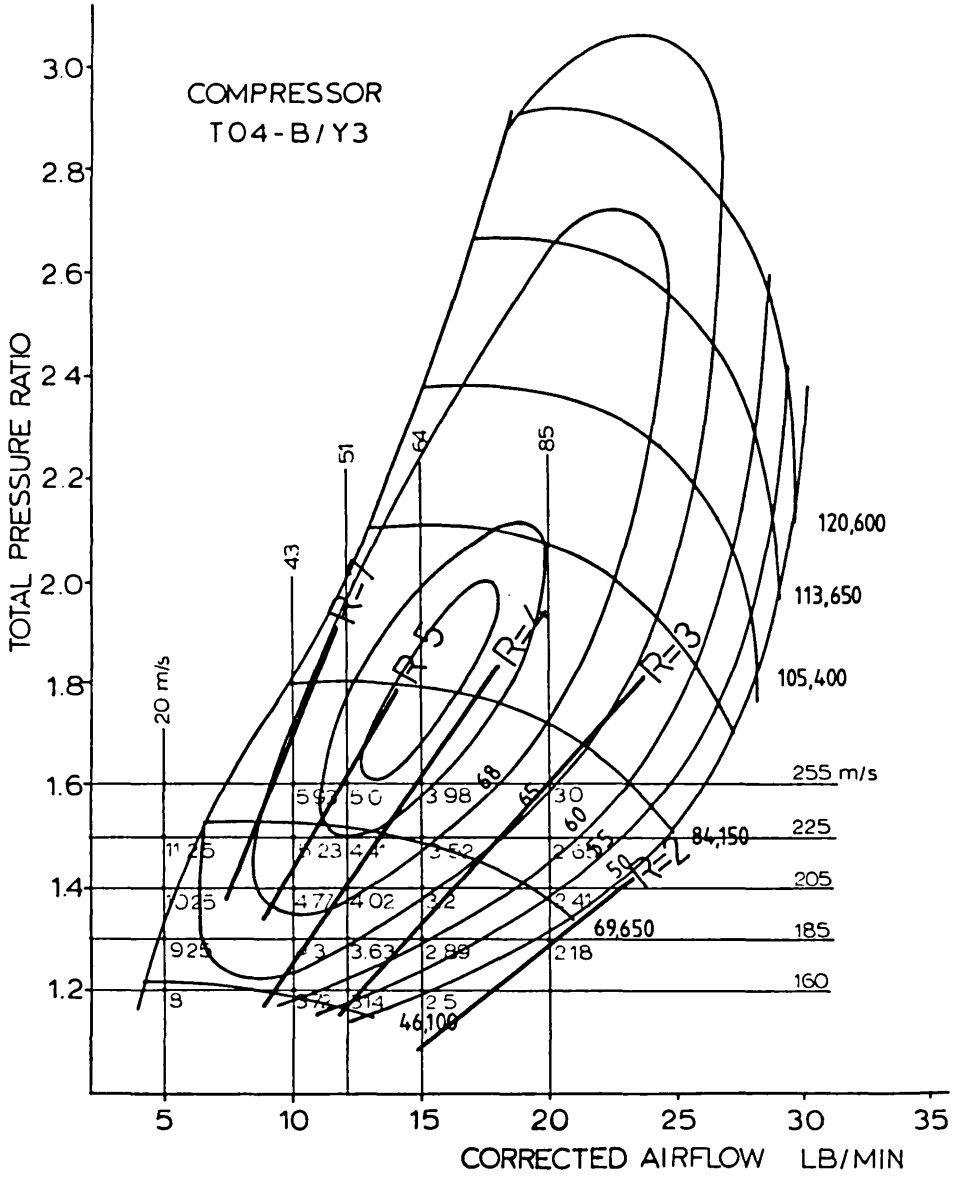


FIG.4.63 Predicted Available Velocity Ratios on T04B-Y3 Compressor Map

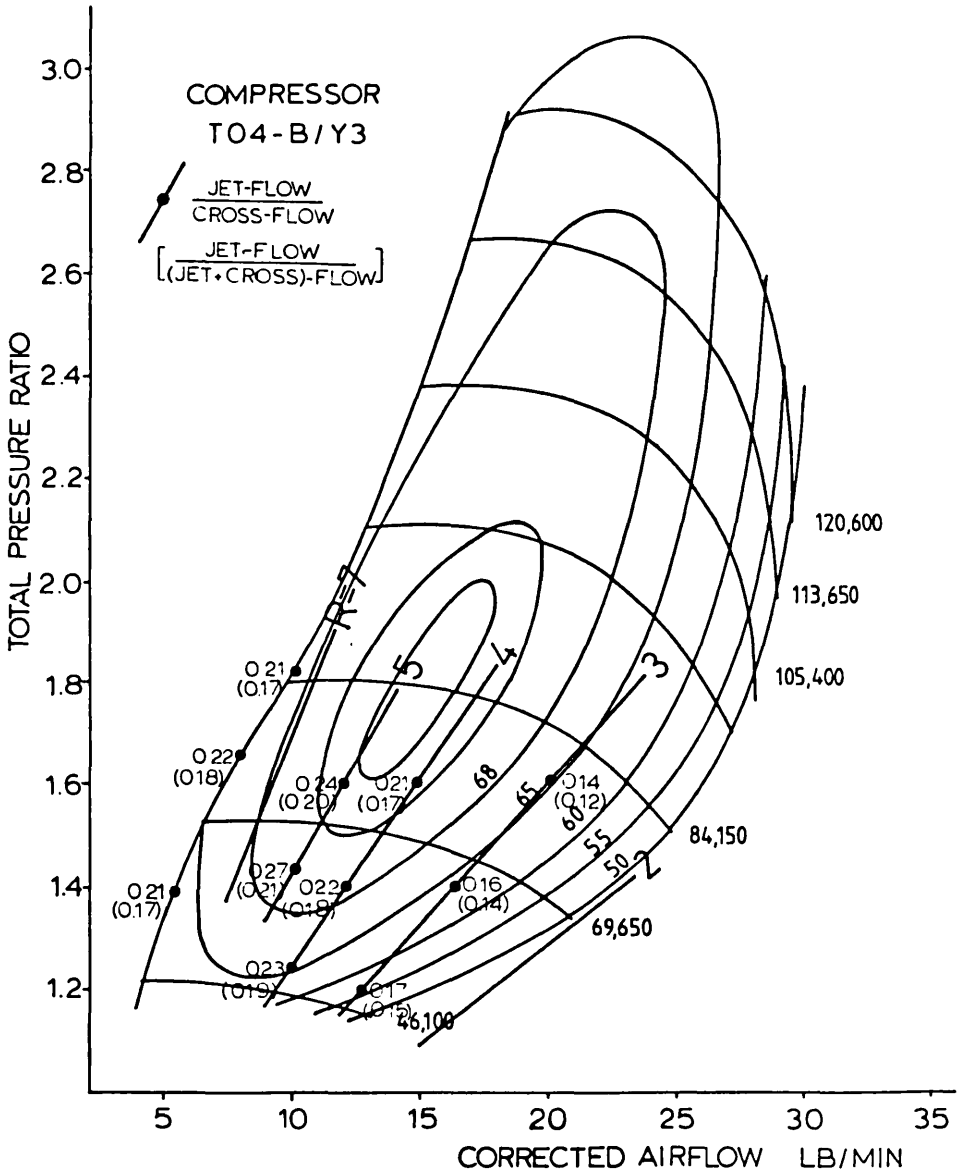


FIG.4.64 Predicted Required Mass Flow Ratios on T04B-Y3 Compressor Map

To predict the approximate jet air flows required to obtain certain velocity ratios in different operating regions on the compressor map, the ratio of jet air mass flow rate to cross flow rate was obtained for various points on the constant velocity ratio lines, based on information in Figures 4.59, 4.63. The result is shown in Figure 4.64, the values of the points on the surge line being for the design velocity ratio R = 4. It can be observed that the mass flow ratios are fairly constant along a constant velocity ratio line, decreasing slightly with increasing pressure ratio.

4.10.2.7 Conclusions

These series of experiments were performed mainly to evaluate the applicability of the theoretical analysis to the design process. It was concluded that the jet in cross-flow model can be successfully used for the design of the device. It was found that the imparted flow deflection was close to the value originally designed for at the design point.

Other influencing factors introduced by the complication of the multiple, confined, oblique, interacting jet arrangement were identified and qualitatively examined. Provided the effect of such factors can be accounted for separately, then the theoretical model may retain its simplicity and flexibility - a desirable feature in the design process.

The resulting flow deflection profile at, and near the design point was measured, and two different jet arrangements were compared, with the 7-jet arrangement found to perform better overall.

Using these results, predictions were made on the ability of the design to change the compressor inlet incidence angle, as well as on the potential ability of the compressor to provide the flow and pressure ratio to meet the design requirements.

Finally any shortcomings of the design were highlighted and design improvements were suggested.

4.10.3 Compressor performance experiments using the jet-device

4.10.3.1 Introduction

The original theme of the research project was concerned with the particular matching problems of turbochargers and small high speed diesel engines. The application scope of the new method of prewhirl was, however, potentially much wider with respect to compressor stability and control. Nevertheless, it had been decided to retain the original frame of reference in order to minimise the number of variables, and so that the results could be tested in a real specific application.

A certain amount of experience with the new method and hardware had been accumulated. It was found, that velocity ratios much higher than the velocity ratio at the design point of the device, could be obtained near the surge line. Hence large prewhirl angles were potentially available near this region of the compressor performance map.

One option would have been to redesign the device to take advantage of the higher velocity ratios. However the AIRESEARCH TO4B-Y3 compressor was not suitable for turbocharging very small engines. It was therefore decided

to design the next "generation" of jet arrangement to be compatible with a particular turbocharger compressor, suitable for a small high speed diesel engine.

It was further decided, that it would be efficient timewise to use the existing experimental arrangement, and test the TO4B-Y3 compressor with the 7-jet nozzle ring (which had given better performance in the previous experiments, but was non-optimum).

Thus additional information and experience would be gained about the design, the interaction with the compressor and its influence on the compressor performance, the hardware, and the experimental method, with the minimum amount of additional effort. Then the cumulative experience would be used to design the next generation of jet arrangement .

4.10.3.2 The (3-D) compressor map

The prewhirl-inducing jet arrangement introduces a new variable in the representation of the compressor performance: the jet mass flow.

The most convenient way to account for the effect of the jet flow in the compressor performance map is to introduce a third axis, the jet flow axis, while the compressor mass flow axis should preferably represent the net compressor throughflow (see Figure 4.65).

Since the jet flow can be continuously variable the performance of the compressor will also be continuously variable and "lines" on the two dimensional compressor performance map will become surfaces on the three dimensional

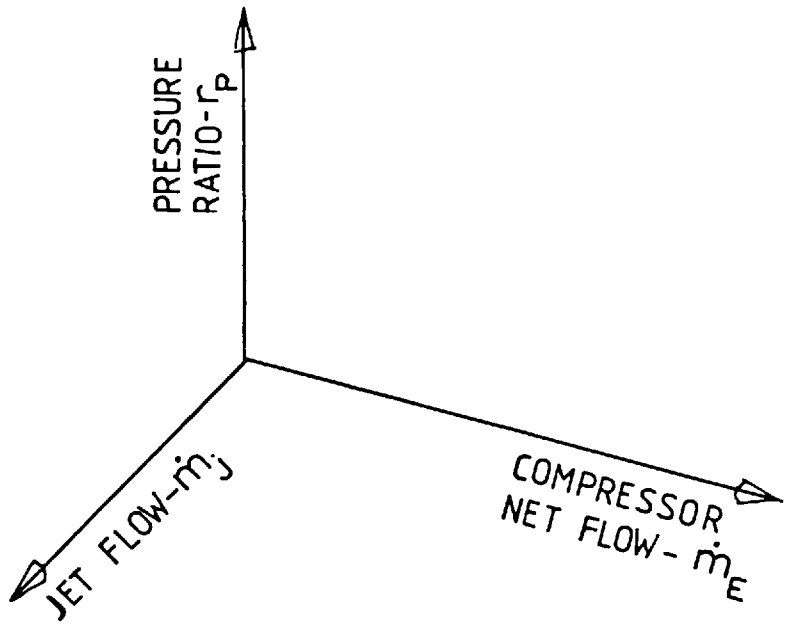


FIG.4.65 (3-D) Cartesian Coordinates for Compressor Performance Map

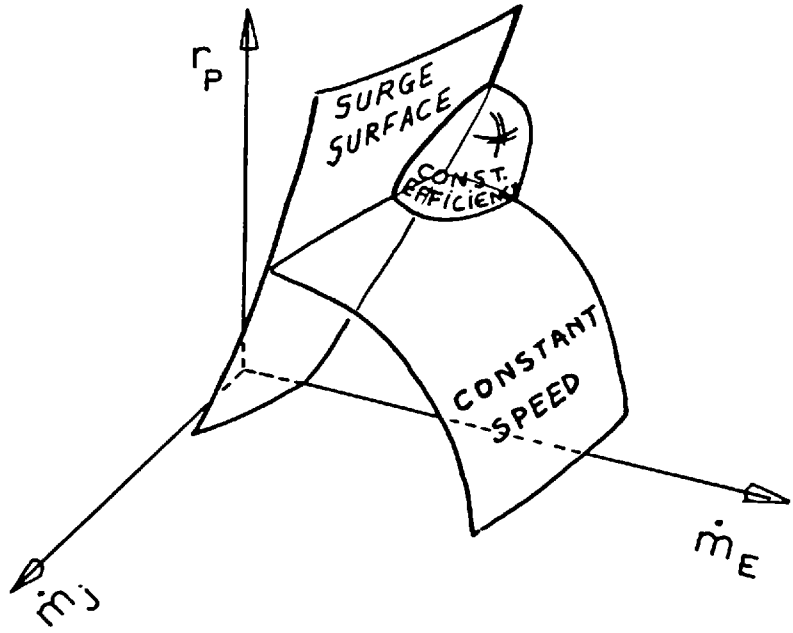


FIG.4.66 (3-D) Compressor Map

map, as shown schematically in Figure 4.66.

4.10.3.3 The experiments

For the series of tests with the TO4B-Y3 compressor and the 7-jet arrangement, it was decided to concentrate on experiments with high-pressure recirculated compressor discharge air feeding the jets. This would be more directly related to the program of future work and also to any practical application of the new method.

However an initial series of experiments was performed using compressed air from an external supply to feed the jets, in order to examine the behaviour of the compressor with the jet device near surge. In that way the jet flow would be an independent variable.

The experimental setup is schematically shown in Figure 4.67 This was essentially the same as in Figure 4.1 except the jet device arrangement and instrumentation.

4.10.3.4 External jet flow supply experiments

These were basically qualitative experiments of the near surge behaviour of the compressor. The surge point was to be determined audibly. The general remarks were:

At all turbocharger speeds a marked increase in noise level was detected on increasing the back pressure on the compressor.

At some medium speeds (≈60000 rpm) further closing of the back pressure valve was thought to result in a slight reduction in the noise level.

With the mass flow further decreased there was a

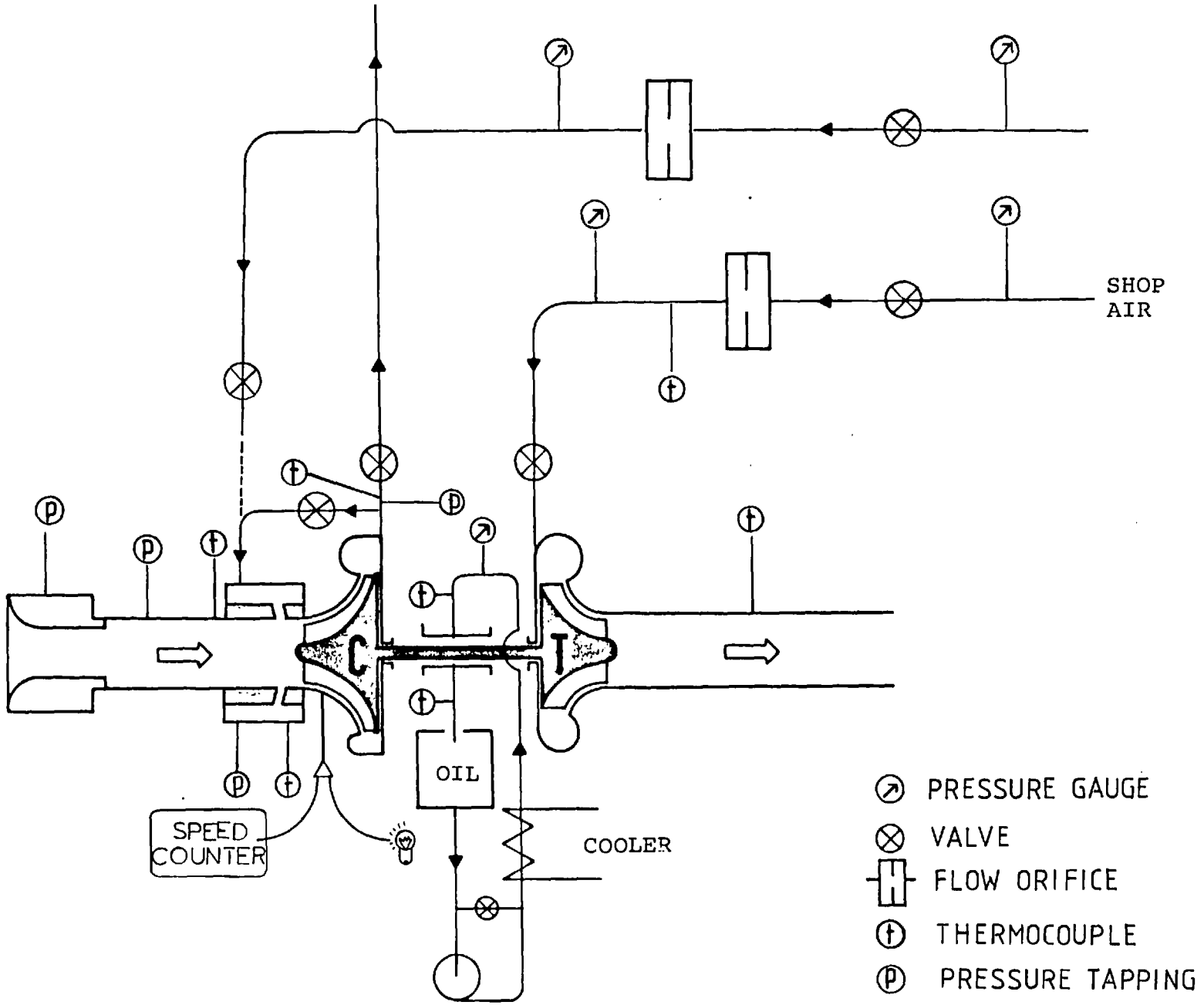


FIG.4.67 TO4B-Y3 Experimental Setup

staccato noise emanating from the compressor on top of the overall noise level. This was taken as the beginning of flow breakdown.

With the jets operational the initial sudden increase in noise level appeared to be subdued. However with the jets, a high pitched noise emerged, the frequency related to the jet flow. This was thought to be due to the jets' expanding and interacting with the compressor blades. The difficulty of establishing the point where the instability was initiated by aurally monitoring the noise level was apparent.

To decide whether there was any improvement in the compressor flow range when the jets were activated, a noise level needed to be defined at the starting point of instability and then used as the basis for comparison.

It was not possible however to compare consistently the two modes of operation (with and without jets) since the noise level judgements were subjective and the events were not coincident.

If the flow was each time reduced so much as to get complete flow breakdown and reverse flow through the compressor, perturbations in the pressure signals would give a positive surge indication. This method was not advisable, from structural considerations. Clearly an alternative, consistent method of defining the instability initiation point was required.

The externally fed jets were also used to examine the effect of the new method in dropping the compressor pressure ratio, at the same rotational speed.

A typical set of results is shown in Figure 4.70. The pairs of points correspond to the two modes of operation, without and with prewhirl. The velocity ratio was obtained by measuring the mass flows of the jets and inlet flow. The turbine power was adjusted to keep the rotational speed constant. As expected, the use of positive prewhirl brought a reduction in the power required. At low pressure ratios and high mass flows there was a large drop in mass flow, with the introduction of the jets. At high pressure ratios, the drop in pressure ratio is more pronounced.

4.10.3.5 Notes on noise from centrifugal rotors

It was thought possible to achieve consistency in determining the level of noise emanating from the compressor, by using a noise level meter placed in front of the inlet duct. A particular noise level could then be associated with the initiation of instability at a certain speed, thus ensuring repeatability of the measurement.

The exceptional characteristic of the spectra emitted by ducted centrifugal rotors, regardless of the shape or other details, is the very large frequency content.

Stalled areas of rotor blades are the basic contributors to a broadband component of the noise spectrum of a centrifugal rotor, covering about eight octaves. It is believed that flow separation over large areas of the rotor blades give rise to the observed low frequency sound (94). Therefore high levels of broad band noise are probably a sign of poor aerodynamics (93). Suction noise is also prominent at high mass flow rates.

Noise power increases roughly as the fifth power of

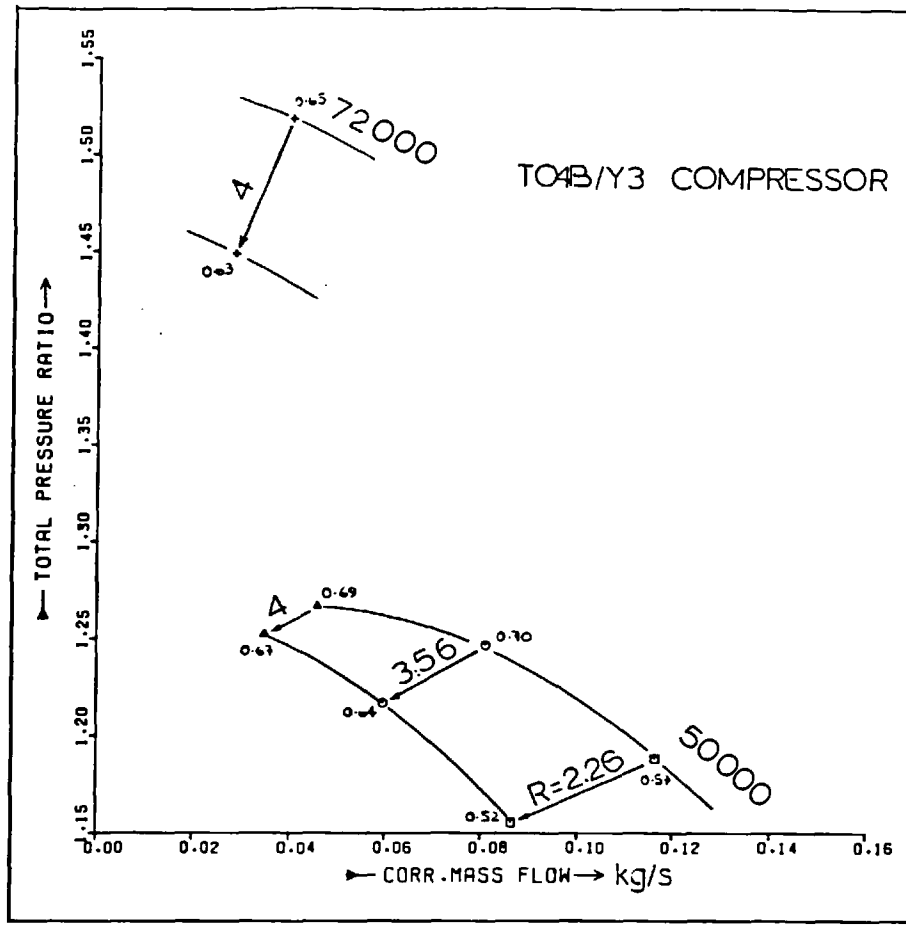


FIG.4.70 Externally Fed Jets. Influence on T04B-Y3 Compressor Performance

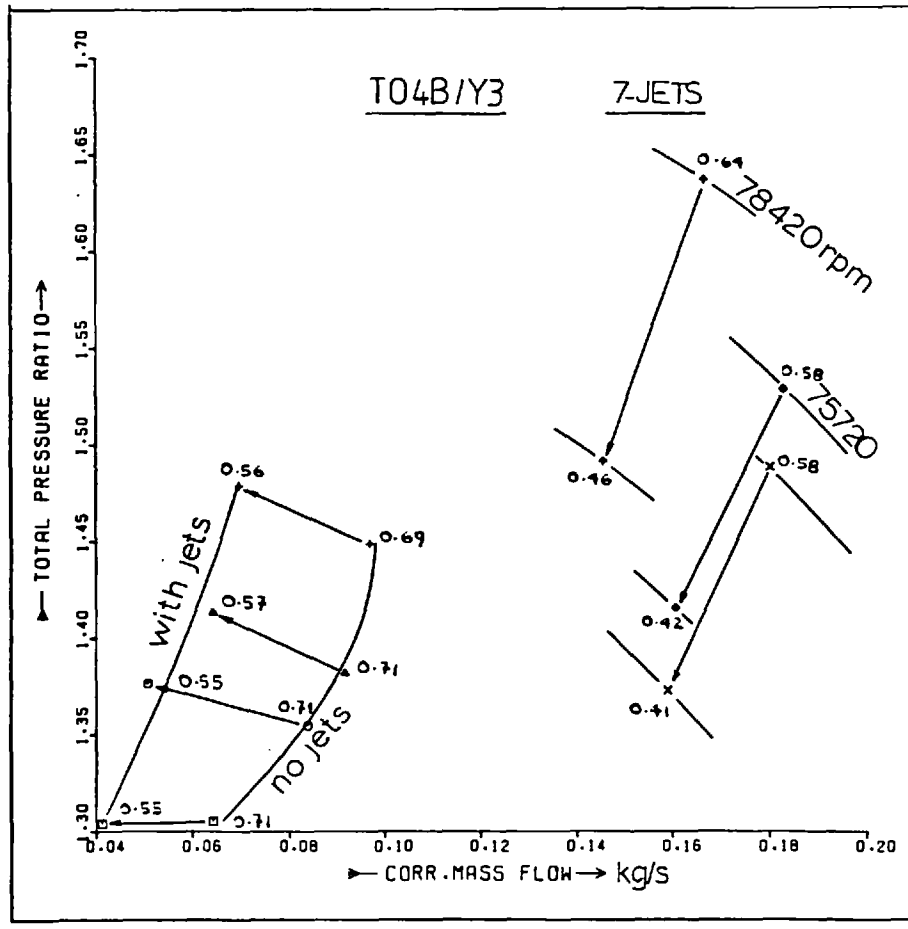


FIG.4.71 Recirculation Fed Jets. Influence on T04B-Y3 Compressor Performance

the speed (96). If the speed remains constant then the increased noise may be from the increased flow separation at low flows.

The ratio of noise power escaping down the outlet duct to that radiating out of the intake was found to be a function of frequency only, being largely independent of aerodynamic variables (94). This implies that any increase in the sound level will be proportional at outlet and inlet.

Intake terminal impedance has a very powerful effect on the acoustics of the machine hence on the sound power delivered. The introduction of the jets in the intake duct would therefore affect the noise pattern, in addition to the jets' contribution to the overall noise level.

High tone levels emanate from stationary obstructions near moving parts. This is the case with vaned diffusers, with the interaction of impeller blades and diffuser vanes. Generally there is no such problem in vaneless diffusers.

The interaction of the jets with the impeller blades will produce pressure disturbances. These will have frequencies of the product of the number of blades, the number of jets and the frequency of rotation and therefore they were not expected to interfere with the low frequency noise due to surge or rotating stall.

4.10.3.6 Recirculation jet flow supply experiments

The experimental set up is shown in Figure 4.67. The jet air was supplied through a bleed in the compressor discharge, upstream of the back pressure valve, the jet flow adjusted through a valve in the line. To minimise pipe friction losses the recirculation loop was made as

small as possible.

4.10.3.6.1 Noise level measurement apparatus

The instrument used for the noise level measurement was a Bruel and Kjaer Typ. 2203 + 1613 Precision Sound Level Meter with Octave Filter Set, which is portable and battery operated. The microphone used was of the condenser type. The amplifier in the Sound Level meter is supplied with the standardised A, B and C weighting networks.

Provision for external filters is made and a separate Octave Filter Set was mechanically connected directly on to the Meter. Hence a 1/1 octave band analyser was obtained.

The build-in read-out consists of an R.M.S. rectifier and a meter circuit the dynamic characteristics of which are specified in the relevant international standard.

Two different meter damping characteristics termed "fast" and "slow" respectively are thus available, the slow characteristic being used when the reading obtained with the fast characteristic fluctuates too much (more than approximately 4 dB), to give a reasonably well defined value of the sound level.

A set of output terminals allows the noise signal to be recorded or monitored on an external recording device if desired. As the instrument was positioned near the entry section of the compressor inlet pipe, a wind screen was used round the microphone to eliminate suction interference.

4.10.3.6.2 Definition of instability initiation point

The method to determine the point of initiation of flow instability was as follows:

The noise meter was switched to scale A. This frequency network has a characteristic which shows a very pronounced frequency dependency for frequencies below 1000 Hz. (Even though the human perception of sound is much too complicated to be even approximated by a simple frequency weighting, a certain guidance with regard to noise problems may, in many cases, be obtained from measurements with the A-characteristic) (97).

Then, after choosing a certain compressor rotational speed the back pressure on the compressor was increased, keeping the speed constant, until a sharp increase in the sound level was detected. For the T04B-Y3 compressor this sudden increase occurred after passing a sound level of 102-109 dB(A) for the range of speeds examined. Until then the sound level remained fairly constant or increased slowly on reducing the mass flow rate.

The value of the threshold noise level as well as the value of the compressor mass throughflow at that point, were defined as the primary values corresponding to the initiation of instability. Then the back pressure was reduced to re-establish stable flow conditions.

The recirculation valve was then opened and the Octave Filter Set was used, to filter certain frequency bands in succession, in order to find a frequency band not affected by the jet noise.

Then the recirculation valve was closed, and using the meter with the chosen frequency band, the mass flow was again reduced till a sharp increase in the noise level was obtained. If the main flow at that point was the same as

the primary value of mass flow, the value of the noise level threshold was defined as the secondary value corresponding to the starting of instability. Otherwise the procedure was repeated with another frequency band till a suitable one was found.

The recirculation was then opened and adjusted to keep the secondary noise level value constant while the back pressure was increased, with the compressor speed kept constant. This was repeated until it was no longer possible to suppress the noise increase by adjusting the jet flow. The mass flow rate at that point was noted. The difference between the two values of mass flow was taken as the increase in flow range.

4.10.3.6.3 Results

A set of general results is shown in Figure 4.71. These are plotted in the usual compressor map fashion of mass flow against pressure ratio. The horizontal axis represents the compressor inlet flow (m_E) which is the total compressor flow (m_C) minus the jet flow (m_j).

There are four couples of points on the LHS of the graph. The correspondence is shown by arrows. The points on the LHS of the arrow are for recirculation while the ones on the RHS of the arrow are without recirculation.

The two lines joining the points of similar operating mode represent the movement of the instability initiation locus. This was obtained using the noise meter and the method described, at constant turbine power, for each couple of points.

The efficiency at each point is shown. This is the system efficiency, obtained by measuring the temperatures at the inlet and outlet plenum. If there is no recirculation this coincides with the compressor efficiency.

During these tests it was verified that the compressor can provide very high velocity ratios. Therefore, unless the recirculation is controlled to keep the velocity ratio within reasonable limits excessive prerotation may result. This depends also on the jet arrangement design.

In such a case, because of the centrifugal force, the flow is driven towards the inlet pipe wall, and low pressure areas are created near the pipe axis. It was observed that eventually some of the flow cannot enter the inducer but "folds" inwards and tries to travel upstream, totally disrupting the uniformity of the flow field. This is accompanied by increased noise level. Under certain conditions a flow oscillation occurs across the inlet pipe as pressure differences are generated by the interaction of the excessive prewhirl and the impeller suction, with the cycle of events resembling surging. This is detrimental to the compressor performance since the inlet flow continuity is severely disrupted. This critical phenomenon is important for the jet arrangement performance as it represents another limiting factor in the operating envelope of the jets, and must be accounted for in the design.

The pairs of points in the RHS of Figure 4.71 show the change in performance of the compressor with the activation of the jets at high mass flows-pressure ratios. The

correspondence is shown by arrows. The same turbine power was used for each pair of points, and maximum possible jet flow with fully open recirculation valve was used for the second points.

The points with recirculation are in fact the projection of the operating points on the r_p - m_E plane (see Figure 4.65).

A further set of results is presented in Figure 4.72. On the RHS of the figure there are two sets of points illustrating the change in compressor performance. The arrows show the movement of the operating point with recirculation and prewhirl at constant speed. The system efficiency at every point is shown. The pairs of points on the LHS of Figure 4.72 are the points of instability initiation without and with the jets, at constant turbine power.

The two nearby pairs of points on the lower LHS of Figure 4.72 are at very similar operating conditions but were obtained with different definition of noise level thresholds. They illustrate the difference between instability initiation associated with a sudden increase in noise level and a more advanced condition of flow deterioration, characterised by a higher and fluctuating noise level.

4.11 COMMENTS ON EXPERIMENTS - APPLICATION POTENTIAL OF THE DEVICE

Encouraging results were obtained from the experiments with the prewhirl inducing jet arrangement fitted on the compressor. The more thorough understanding of the flow situation, would enable further optimisation of the design process.

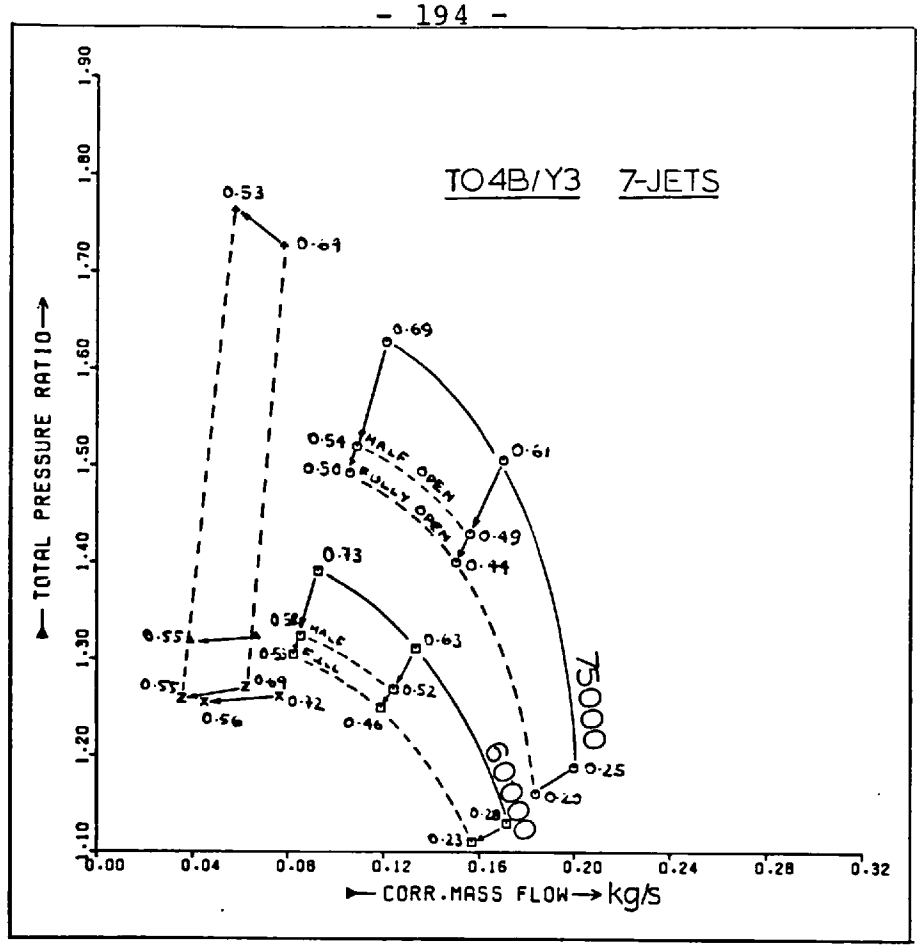


FIG.4.72 Recirculation Fed Jets. Influence on TO4B-Y3 Compressor Performance

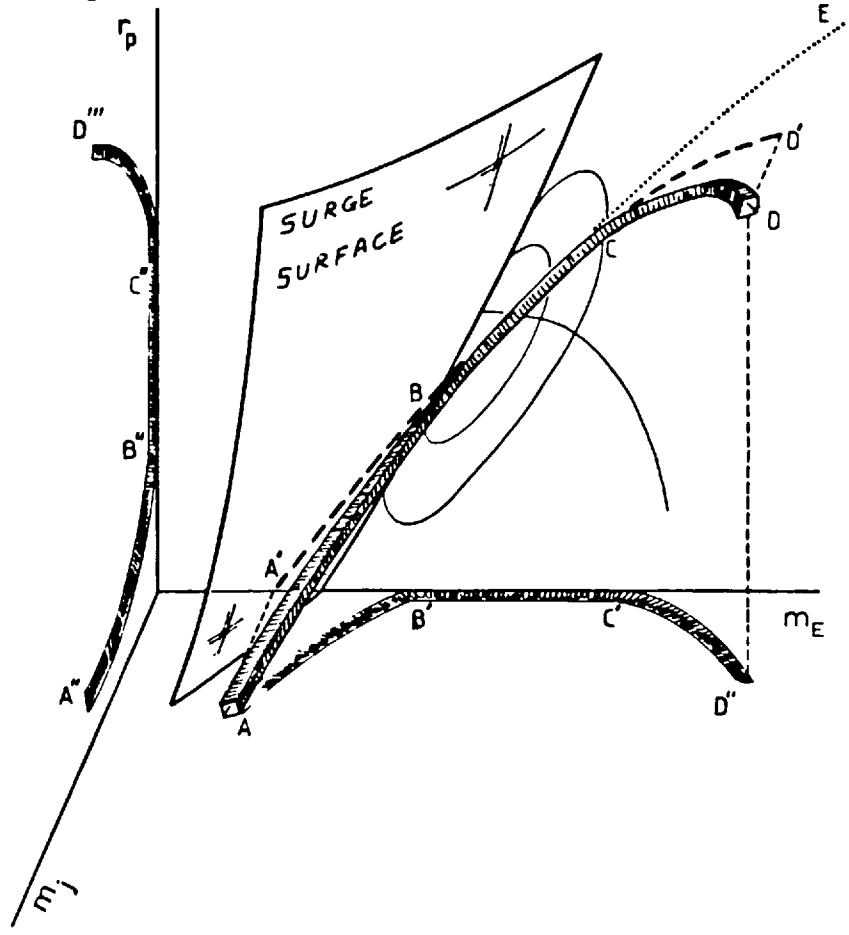


FIG.4.73 Impression of Engine Operating Line in (3-D) Compressor Map

It was shown that the mew method of prewhirl, was able to perform the control function and also to influence the stability and hence flow range of a compressor, in a manner similar to variable inlet guide vanes, and with proper design it can be used in applications where prewhirl is beneficial (Section 3.6.2.4.2).

Additionally the flow range was influenced by the recirculation. The adverse effects of the latter, namely the higher inlet temperature, should be partly compensated by the improvement in aerodynamic efficiency brought about by the improvement in inlet flow angles through prewhirl.

The new method would be effective in improving compressor overall stability to the extent which this is influenced by the inducer stability. Hence the best performance would be realised by using such an arrangement on a compressor which would benefit from prewhirl.

The arrangement must be designed specifically for each particular compressor on which it will be operating. Hence additional information on the design and performance of that compressor would be needed.

It was found that the available velocity ratios and hence the potential flow deflections increase with increasing pressure ratio and decreasing main flow. This would allow greater design flexibility near the surge line, which would be useful for devices to improve the flow range of very high pressure ratio centrifugal compressors.

The compressor performance control function of the novel prewhirl method could be advantageously used in turbo-charger engine matching applications.

The improvement in the compressor stable flow range as well as the ability to control the compressor discharge pressure at constant turbocharger speed would enhance the flexibility of the matching process.

Shown schematically in Figure 4.73 is an engine operating line in a (3-D) compressor performance map, as could conceivably be achieved by using the recirculation fed jets to induce prewhirl.

ABCD is the engine operating line

A'BCD' is the projection of the operating line on the $m_E - r_p$ plane

AB'C'D" is the projection of the operating line on the $m_E - m_j$ plane

A"B"C"D"' is the projection of the operating line on the $m_j - r_p$ plane

Recirculation is used to keep the operating line (AB) within the stable operating space of the compressor bounded by the surge surface. As can be seen the projection A'B is beyond the surge line. The device remains inactive during (BC), where the operating line is in the best efficiency region of the compressor.

However, it is possible that with increasing energy availability at the turbine at higher mass flows, the operating point will move to high pressure ratios (CE) and the resulting high engine boost may be undesirable. Then again recirculation inducing prewhirl would be used to drop the attainable compressor pressure ratio (CD).

In general, prewhirl will tend to decrease the power demand from the turbine, while recirculation will tend to

increase it. The most practical and consistent method to predict the complex interactions of the various systems involved would be to use a numerical cycle simulation. Such a simulation for turbocharging applications was being developed in parallel with these investigations.

CHAPTER 5

THE ENGINE AND TURBOCHARGER SIMULATION

5.1 THE ENGINE SIMULATION - INTRODUCTION

In internal combustion engine development, testing the many combinations required for optimisation of each particular application makes the introduction of a new engine, or major modification of an existing engine, expensive - both in time and money. Consequently mathematical analyses of engine cycles have been used, from the early stages of i.c. engine conception and have since evolved from simple air standard cycle analyses to the present day sophisticated mathematical codes. These model the processes involved and follow the succession of the many interrelated events and the interplay between the system and outside parameters, with the help of digital computers.

The simulation models can be generally classified as "thermodynamic" (or "control volume") and "spatial" models. The former are well established and the relevant literature is very extensive, illustrating the plethora of approaches and degrees of complexity offered for modelling the different sub-processes or component parts of the system (Refs.98,99, 100,101 all include extensive literature surveys). The latter are fairly recent models, still largely in the development stage which include one or more spatial co-ordinates in addition to time as independent variables in the mathematical formulation (102,103).

The choice of approach depends on the particular problem and the stage of development and consequently, from the cost benefit standpoint, there may be an optimum engine simulation program for each application.

5.2 THE COMPUTER CODE

For the present work, it was required to simulate a small high speed indirect injection diesel engine coupled to a turbocharger, for the purpose of matching and system performance predictions. This general framework of requirements, together with the particular needs evolved during the course of the work, dictated the choice and subsequent line of development of the simulation program.

An in-house code had been developed to predict the steady state performance of naturally aspirated and turbocharged direct injection diesel engines using the "filling and emptying" method. The method is well known, since the most widely used performance prediction programs are "filling and emptying" models.

(Ref.104) contains a detailed description of the program in its initial form, and (100) describes one subsequent more advanced form.

The program is based on a full thermodynamic analysis of gas flow between various volumes, and heat and work transfer between each volume and the surroundings. Each cylinder, the inlet manifold and each branch of the exhaust manifold, are considered as separate volumes. The quasi-steady filling and emptying approach is used to describe gas flow and changes in thermodynamic conditions. The turbocharger is also treated on a quasisteady basis using steady state performance characteristics.

In developing the code further to suit the needs of the present work, it was endeavoured to retain the original structure of the base program wherever possible.

5.3 INDIRECT INJECTION DIESEL ENGINE SIMULATION

5.3.1 Divided Chamber Model

To model the indirect injection engine, the swirl- or pre-chamber was treated as a separate thermodynamic control volume.

No account was taken of any spatial effects such as pressure wave propagation, jet flow, swirl, etc.

The prechamber is connected to the main chamber via an orifice.

To use steady compressible flow equations to determine the mass flow through the orifice, a coefficient of discharge needs to be defined. The main influencing parameters in the determination of the value of this discharge coefficient, are the pressure ratio across the orifice and the direction of flow, and therefore the discharge coefficient could conceivably be expressed as a function of these.

However, it is difficult to correlate the pressure ratio resulting from the global quasi-steady control volume pressures in the simulation, with experimentally obtained pressure ratios across the orifice, since the flow within the swirl chamber is exceedingly complex (105).

Large spatial and temporal gradients of temperature, pressure, fluid velocity and species concentrations exist, and, at least partly, such variations may be coupled to the piston motion.

Some form of spatial modelling should be used if the requirements dictate a more comprehensive solution.

For the present work it was found adequate to use discharge coefficients for short sharp edged restrictions with turbulent adiabatic flow (106) and adapted experimental values from (105).

5.3.2 Combustion - Heat Release

5.3.2.1 Introduction

The combustion in a swirl chamber type engine can be thought of as follows:

Injection is directed toward the wall and downstream of the throat. The shape of the chamber has set the air in a swirling motion. The core of the spray is not deflected much, but the sides are torn away (see also jet in a cross flow analysis (Section 4.3). The core is deposited on the wall and follows its curvature. The heavier droplets jump the throat. Some fuel enters the main chamber. Meanwhile ignition occurs in the fine mist near the throat where higher temperatures prevail (premixed flame), and spreads (diffusion flame) in the prechamber with an incurling spiral towards the centre while the heavier air is forced outward by the centrifugal field. Flame also spreads through the throat into the main chamber.

At less than half load combustion can be essentially completed in the prechamber. With increase in load, incomplete combustion is evident with large soot clouds appearing in the swirl chamber. However, throughout the flame development, pressure has been rising rapidly in the swirl chamber and gases flow at high speeds through the throat into the recesses of the piston. A very high secondary swirl is thus created. It is this high secondary swirl that enables divided chamber engines to operate with low amounts of excess air, related to open chamber designs since there is a strong mixing of any combustible element with air into the main chamber (17, 107, 108).

5.3.2.2 Heat Release Model

All the inhomogeneous localised character of combustion is not accounted for in the simulation. The total fuel delivered to each cylinder every cycle, is divided into two portions in proportion to the total heat released in the cylinder and in the swirl-chamber.

The mode of transformation from unburned to burned species was computed using a formulation for combustion by Vibe (109).

This takes the form of apparent heat release curves, which are defined by the beginning of combustion, its duration, and the parameters describing the shape of heat release.

The dependence of the relative dimensionless transformed quantity x to the relative burn (crank) angle y is

$$x = 1 - \exp\ (-\ \alpha\ y^{(m+1)}) \qquad (5.1)$$

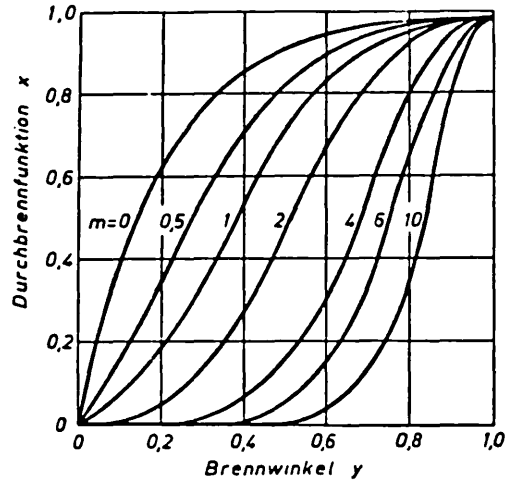
or its derivative w.r.t. y

$$\frac{dx}{dy} = \alpha\ (1 + m) y^{m} \exp\ (-\ \alpha\ y^{(1+m)}) \qquad (5.2)$$

where α can be thought of as a transformation coefficient depending on the combustion efficiency. If the combustion efficiency varies between 99-100% α should vary between 5-10.

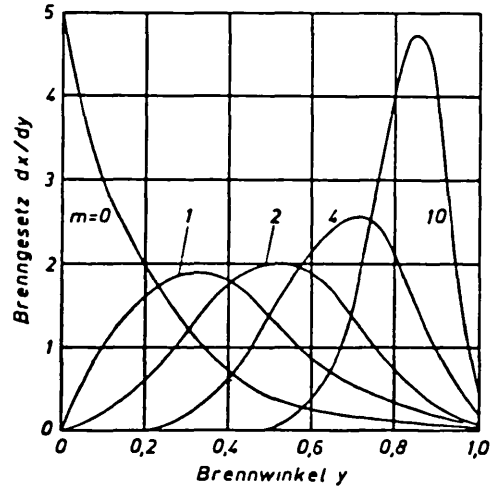
The influence of the shape parameter m can be seen in (Fig.5.1), showing the fraction of the fuel burned against the dimensionless burn angle (combustion duration) using the eq.5.1 for $\alpha = 5$ and different values of m.

It can be seen that increasing the value of m the combustion of the major part of the fuel moves towards the



Durchbrennfunktion x in Abhängigkeit vom Brennwinkel y für verschiedene Parameter m nach [3]

FIG.5.1 Influence of Shape Parameter m



Brenngesetze dx/dy für die in Bild 1 dargestellte Durchbrennfunktion in Abhängigkeit vom Brennwinkel y.

FIG.5.2 Influence of Shape Parameter m

late part of the combustion phase. This can be also observed in (Fig.5.2) showing the rate of heat release against the dimensionless burn angle for different m-values (eq.5.2).

In order to limit the number of variables and on the other hand, to avoid changing those whose relationship to various cycle parameters was not sufficiently well known, the shape of the heat release curve was assumed to be defined by m = 1 or 2, and a value of $\alpha = 6.9$ was normally used.

5.3.3 Heat Transfer

The coefficient of convective heat transfer between the gas and the engine walls used, was based on the formula derived by Sitkei (Ref.110,111) using a Nusselt-Reynolds relationship, and has the form:

$$h = 0.04\ (1 + b)\ \frac{P^{0.7}\ w^{0.7}}{Tg^{0.2}\ de^{0.3}} \qquad (5.3)$$

where

b is a constant depending on the combustion chamber configuration. For a swirl-chamber type engine b = 0.15 - 0.25

P is the instantaneous pressure

Tg is the gas temperature

de is an equivalent diameter

w is a representative fluid velocity

For the main chamber (cylinder)

$$de = \frac{2D\ell}{D + 2\ell} \qquad (5.4)$$

where

D is the cylinder diameter

ℓ is the height of the cylinder space above the piston

w is the mean piston speed

For the pre-chamber

$$de = \frac{2}{3} d \tag{5.5}$$

where

d is the prechamber diameter

w was taken as a function of the instantaneous throat velocity u_t

$w = k.u_t$ where k = 0.75 was used.

5.3.4 Valve Discharge Coefficients

The inlet and exhaust valve discharge coefficients used in the simulation were in the form of algebraic equations as functions of the valve lift over diameter ratio. These were obtained by curve-fitting data given in (Ref.113) for inlet and exhaust valves for the appropriate seat angle.

5.3.5 Numerical Stability

The most critical part of the cycle simulations as far as numerical stability is concerned is the gas exchange period.

Both inlet and exhaust valves are then partly open, the pressures in all interconnected volumes are nearly the same and the piston changes its direction of motion.

In the indirect injection engine simulation, this situation is further complicated since an additional control volume, the pre-chamber, communicates with the cylinder, together with the inlet and exhaust manifolds.

During this period, the cylinder control volume is very small compared with the other intercommunicating control volumes, hence small mass movements in or out of the main chamber will tend to produce large pressure differentials and this initial instability may result in the numerical procedure diverging.

The problem becomes more acute at low engine speeds and with large valve overlaps. This instability can normally be prevented by using a decreased iteration step-size during the gas exchange period. However this method proved unsuccessful for the prechamber engine simulation at low speeds, although a moderate valve overlap was used.

To counteract the inception of instability a relaxation factor was introduced in the computation. This operated by assigning different weighting to the values of parameters obtained in two successive iteration steps, thus "damping" the calculation.

Since such measures are generally required only when the pressure ratio between two control volumes is near unity, the relaxation factor was expressed as a function of pressure ratio:

$$RF = (\alpha_2 - \alpha_1)\left[1 - \exp\left(-7\left(\frac{PR - 1}{PRCR - 1}\right)^3\right)\right] \qquad (5.8)$$

where $\alpha_2 \geq RF \geq \alpha_1$ are the limits of the range of RF.

PR is the pressure ratio between two control volumes.

PRCR is the critical pressure ratio for choked flow.

The above function gives a near sinusoidal variation of the relaxation factor between the limits α_1, α_2 as the pressure ratio changes from PRCR to PR = 1.

5.3.6 Program Outline

The computer program in the form used consisted of 12 subroutines:

1. MAIN Master routine, initialises variables, controls steps, calls all subroutines and prints output.
2. INPUT Routine to read in data. Called by MAIN.
3. ETHERM Routine for thermodynamic calculations in all control volumes. Called by MAIN.
4. PERFOR Routine to calculate overall cycle performance. Called by MAIN.
5. FBR Routine to calculate instantaneous fuel burning rate during combustion. Called by MAIN.
6. PROP Routine to calculate thermodynamic properties of mixtures. Called by MAIN and ETHERM.
7. GEOMET Routine to calculate instantaneous engine geometry. Called by MAIN.
8. HT Routine to calculate heat transfer. Called by ETHERM.
9. RFLOW Routine to calculate instantaneous values of mass flow rate through orifices. Called by ETHERM.
10. TURB Routine to find operating point on steady-state turbine characteristic and calculate turbine available power. Called by ETHERM.
11. VCOMP Routine to find operating point in (3-D) compressor characteristic and calculate compressor required power. Called by ETHERM.
12. CONTROL Routine to determine if the working point is within the compressor operating limits and accordingly to activate appropriate control functions. Called by MAIN.

5.4 THE "VARIABLE PERFORMANCE" COMPRESSOR MODEL

5.4.1 Introduction

The compressor experiments with recirculated flow inducing prewhirl at the intake would give a (3-D) compressor map (see Section 4.10.3.2), over which the performance of the compressor would vary continuously. It was therefore decided to name the unit a "variable performance compressor" (v.p. compressor).

To examine the interaction of the v.p. compressor, as part of a turbocharger coupled to an engine, with the various parameters of this system, it was required to build a mathematical model for the v.p. compressor.

The model should be able to simulate the performance of the v.p. compressor throughout its operating space, so that it could be appended to the engine simulation program for cycle calculations.

It was therefore required to develop a computer code, able to handle the processed experimental information obtained from "steady state" v.p. compressor experiments.

Since the amount of experimental information which can be practically collected is limited, the data points will only define the operating space. Some form of numerical interpolation among the data points would then be required to determine the values of the parameters associated with any other point inside the operating space.

5.4.2 Expected Shape of (3-D) V.P. Compressor Map

The expected shape of the (3-D) map was constructed based on the results obtained from the TO4B-Y3 compressor experiments (see Section 4.10.3.3). This was done to help define the limits to be included in the simulation. (Fig.5.3) shows the 3-axes of the (3-D) compressor map, namely the net compressor flow $\dot{m}_E$-, the jet flow $\dot{m}_j$-, and the pressure ratio r_p - axis.

An assumed surge line as well as the constant velocity ratio lines (see Section 4.10.2.6) are shown on the $\dot{m}_E - r_p$ plane. Two lines are shown on the $\dot{m}_E - \dot{m}_j$ plane. The critical line is the locus of the points where the mass flow ratio ($\dot{m}_j/\dot{m}_E$) is such that incipient backflow occurs at the inlet pipe (see Section 4.10.3.6.3) (assumed straight line).

The R = 4 line is the locus of the points where the mass flow ratio ($\dot{m}_j/\dot{m}_E$) corresponds to a velocity ratio of four (assumed straight line). Considering an operating point A on the surge line with $\dot{m}_E = \bar{OB}$, if $\dot{m}_j = \bar{BC}$ is introduced, the flow can be throttled further back till C", where $\dot{m}_E = \bar{OB}$" and C" touches the "critical line". Then the operating point is D", and its projection on the $\dot{m}_E - r_p$ plane is A".

The line $\bar{AD}$" can be considered as a first approximation to lie on the "surge surface". Similar constructions (Fig.5.4) will give the shape of the surge surface. (Fig. 5.5) shows the expected shape of a constant speed line NN' in (3-D).

For the operating point B' on NN', $\dot{m}_E = \bar{OB}$ and since it lies on R = 2, the available jet flow is $\dot{m}_j = \bar{BC}$ and the

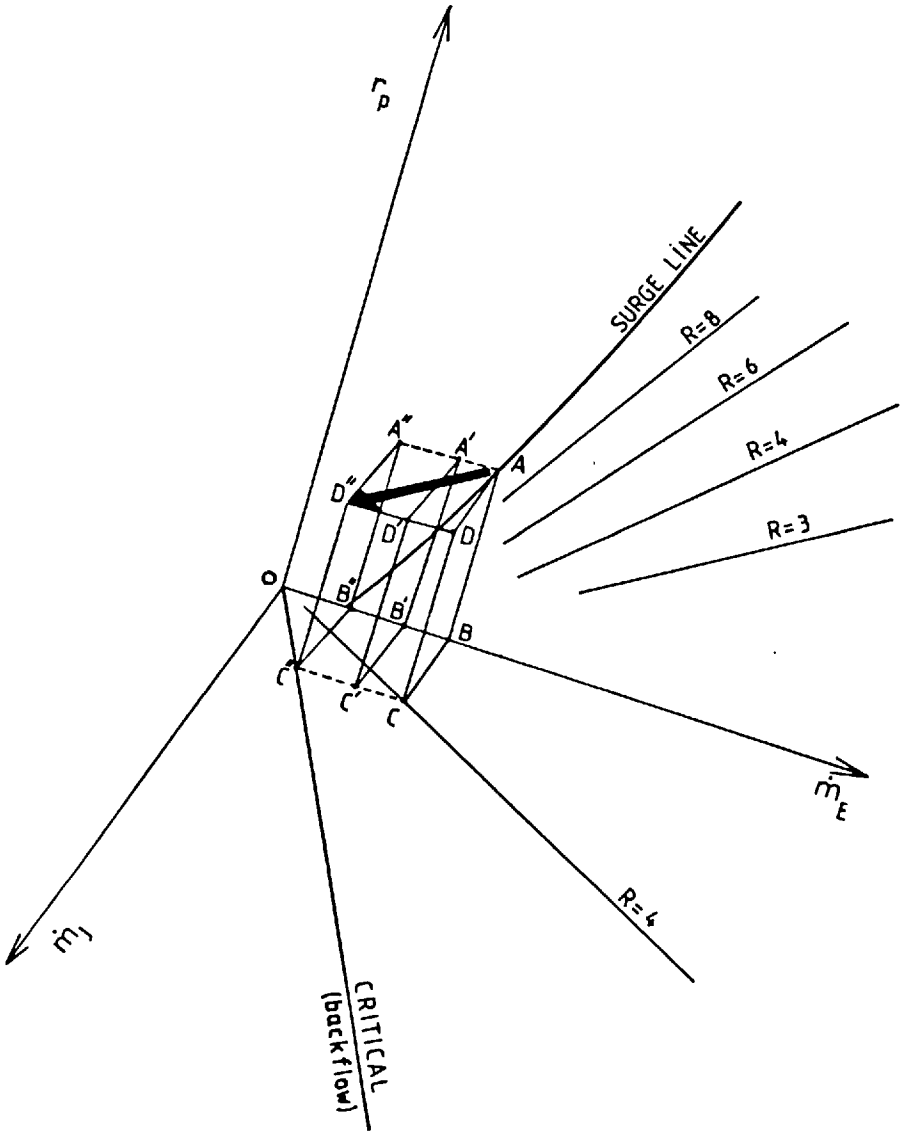


FIG.5.3 Construction of (3-D) Compressor map (I)

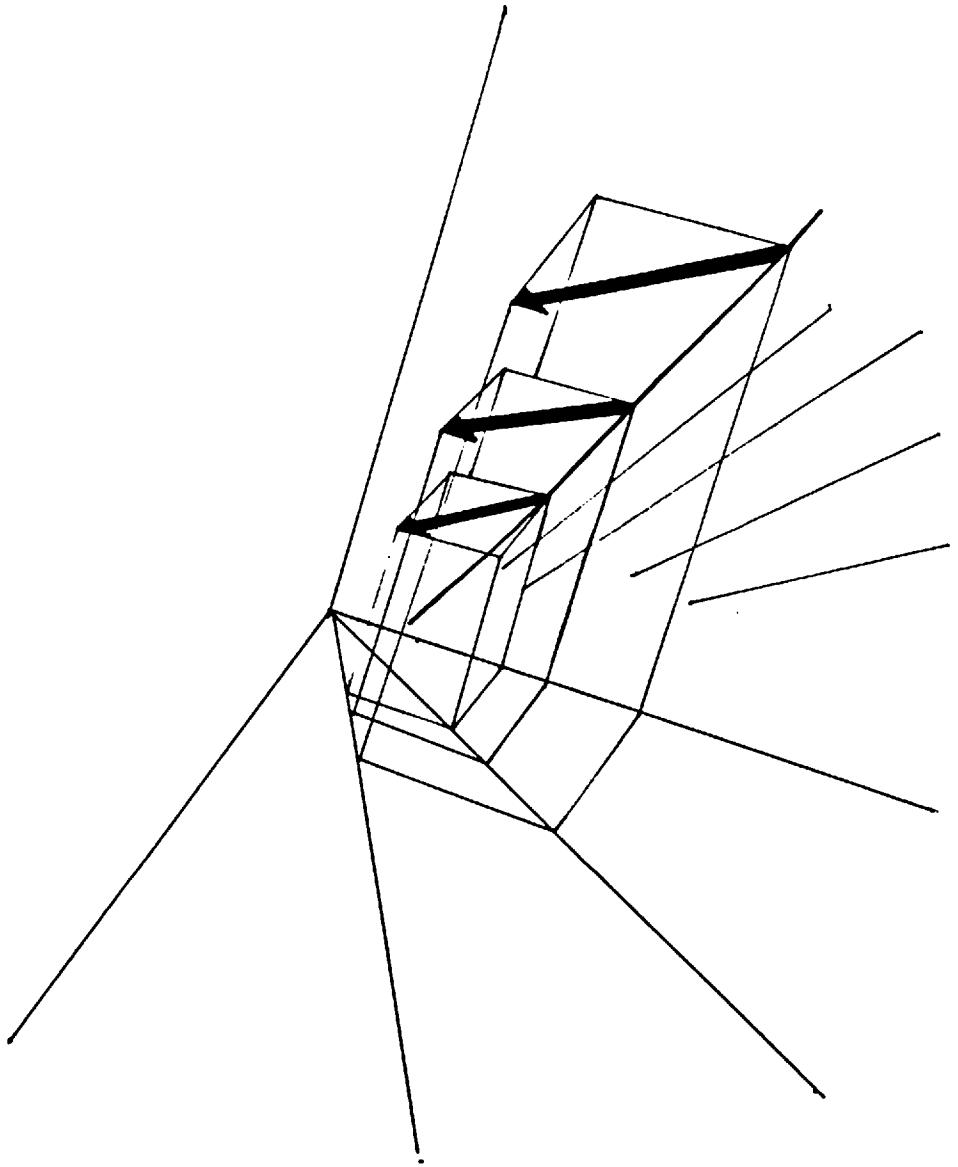


FIG.5.4 Construction of (3-D) Compressor Map (II)

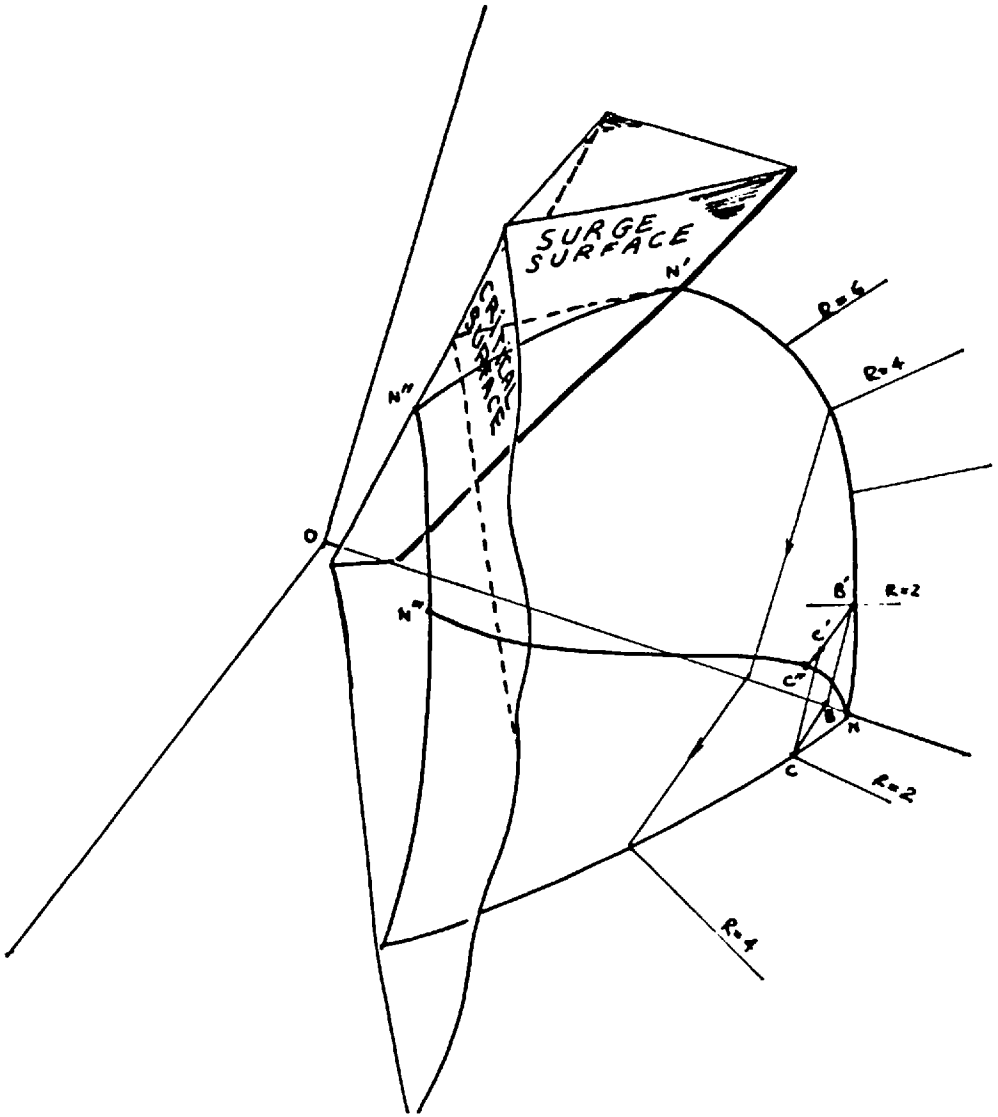


FIG.5.5 Construction of (3-D) Compressor Map (III)

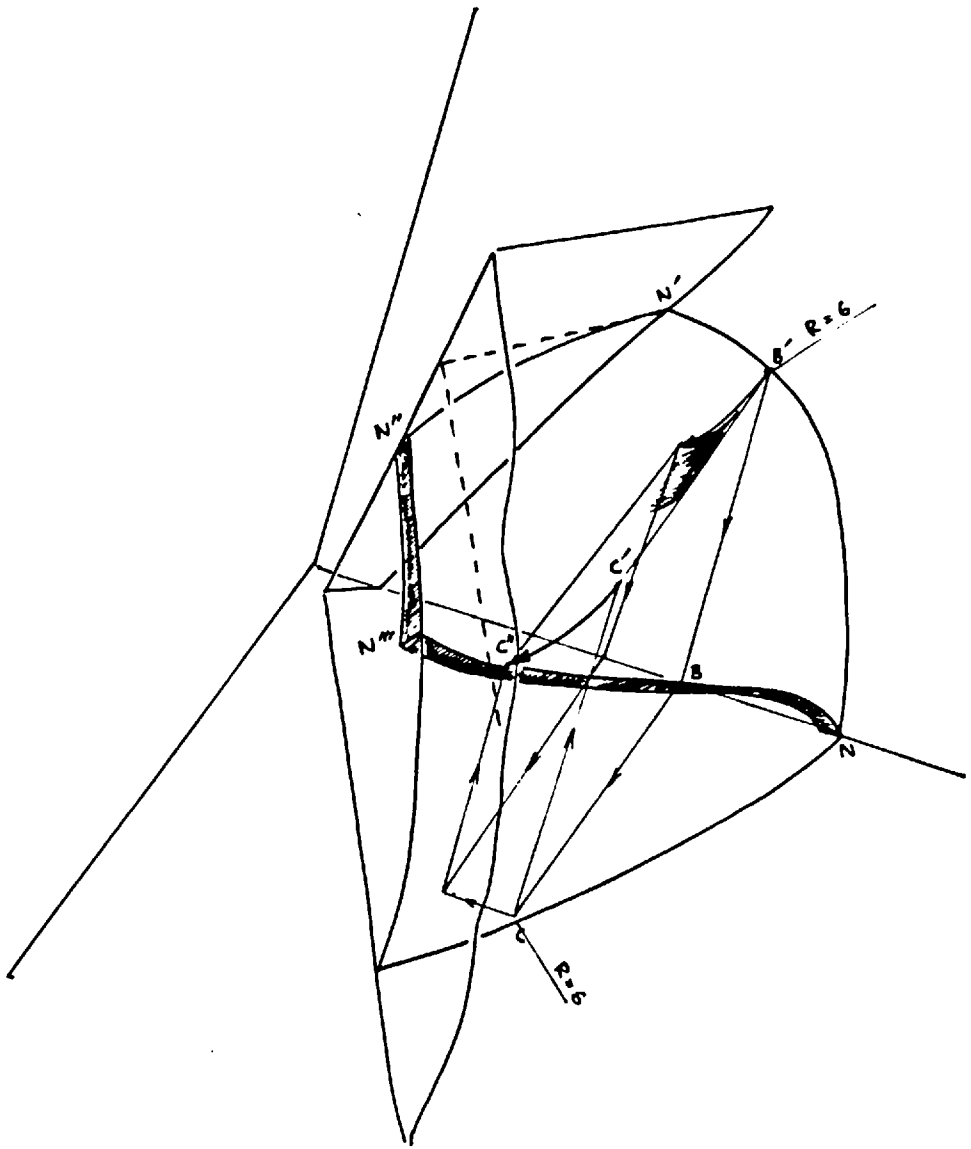


FIG.5.6 Construction of (3-D) Compressor Map (IV)

operating point is C'. There is also a movement $\overline{C'C''}$ due to the recirculation and drop in pressure ratio, and the final operating point is C".

A similar construction gives NN"', until the "critical surface" is reached, where there is available jet flow, but it cannot be used. Therefore the speed surface is NN'N"N'" (Fig.5.6). An overall view of the different surfaces is given in (Fig.5.7).

The nozzle ring jet flow-pressure ratio characteristic on the $\dot{m}_j - r_p$ plane is extended as a surface in (3-D) and introduces a further constraint (Fig.5.8). The final bounded shape of a constant speed surface in (3-D) can be seen in (Fig.5.9).

As it was shown, the expected operating space of the v.p. compressor will be bounded by the following constraints:

1. Compressor surge.
2. Critical velocity ratio for flow breakdown and backflow in the inlet.
3. Nozzle ring mass flow-pressure ratio characteristic.
4. Recirculated air jet velocity availability for flow deflection.

A further constraint may be imposed depending on the application.

5. Maximum pressure ratio level.

Thus the operating space will be fully defined and bounded.

The processed experimental information will be presented as groups of points lying on certain speed surfaces. For any operating point defined by $\left[(\dot{m}_E, r_p, \dot{m}_j)\right]_p$ the simulation code must investigate at first whether the point lies inside the boundaries of the v.p. compressor

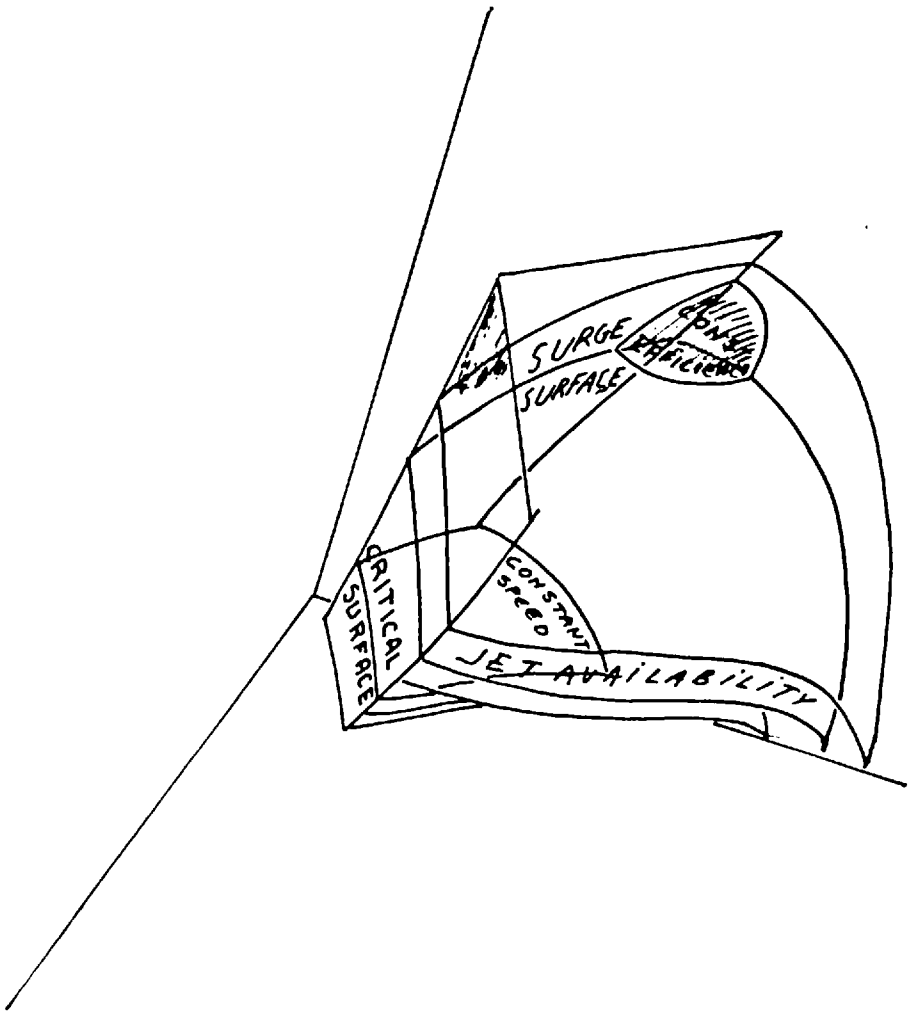


FIG.5.7 Construction of (3-D) Compressor Map (V)

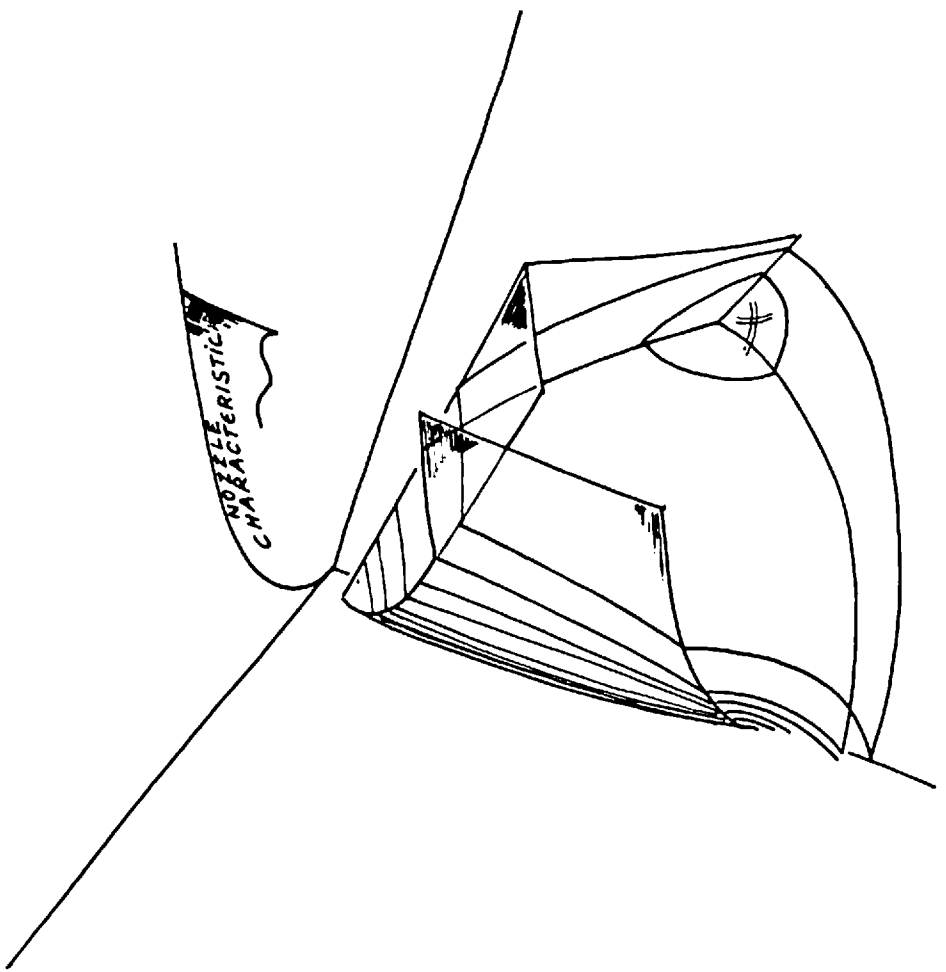


FIG.5.8 Construction of (3-D) Compressor Map (VI)

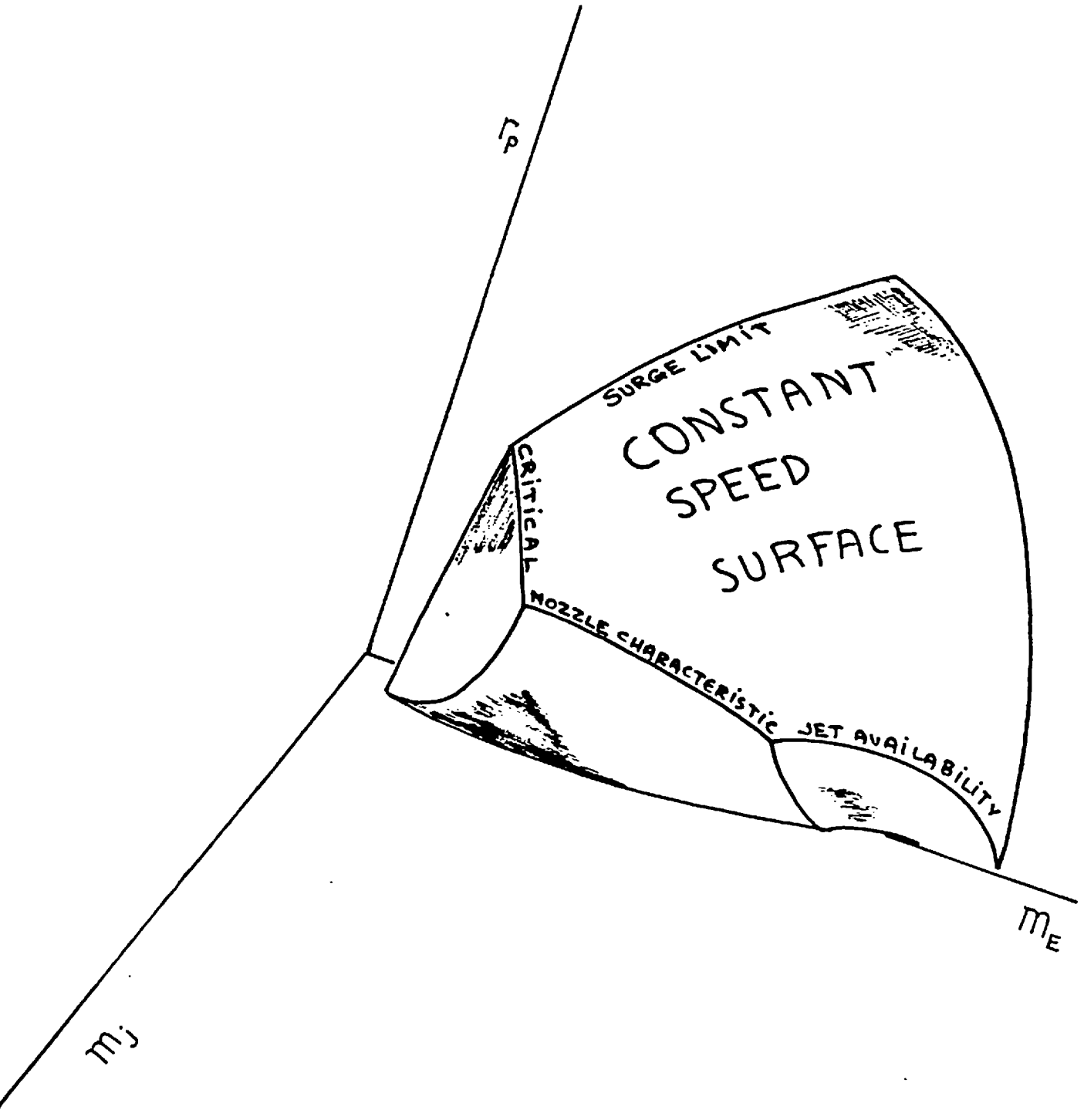


FIG.5.9 Expected Shape of (3-D) Compressor Map

operating space. If not, the appropriate warning and correcting control functions must be triggered.

If the point lies inside the operating space, the code must proceed to determine the rest of the associated parameters (namely compressor speed, efficiency) to be used in the simulation.

5.4.3 Presentation of Limiting Surfaces

The surfaces bounding the v.p. compressor operating space will be the ones containing the edge data points. In the simulation it was decided to represent the limiting surfaces with plane surfaces. Although this simplification introduces "low data density" spaces, the interpolation procedure finally used was able to overcome this problem.

The plane surfaces were defined by choosing suitable triads of edge points from the data.

5.4.4 Space Orientation of Working Point

To decide whether the working point lies within the operating space, the intersection point of a line parallel to the $\dot{m}_j$-axis and passing through the working point, and each of the limiting planes is found.

Then the coordinates of the two points can be compared to determine the position of the working point relative to each plane. Provided the arrangement of the limiting planes is known, the position of the point relative to the operating space can be found.

5.4.5 The CONTROL Subroutine

The procedure for determining the working point orientation w.r.t. the boundaries, as well as the control of the recirculation $\dot{m}_j$ was formulated into a separate subroutine.

This is normally called by the main program on completion of each engine cycle and determines the position of the cycle averaged operating point, adjusts the recirculation accordingly in predetermined steps for the next engine cycle and gives appropriate warnings if the operating point is outside the v.p. compressor operating limits.

The recirculation control statements depend on the relative orientation of the limiting planes. In the case where the operating point is beyond the boundaries and cannot be recovered by suitable changes in the recirculation, the routine stops the program.

This subroutine may also be called by the v.p. compressor subroutine, during the cycle, to check the instantaneous position of the operating point. In this case, the recirculation control is bypassed to avoid inducing instabilities which will hamper convergence.

5.4.6 The VCOMP Subroutine - Interpolation Method

The experimental data points for the v.p. compressor map would normally be in groups of one independent variable (rotational speed).

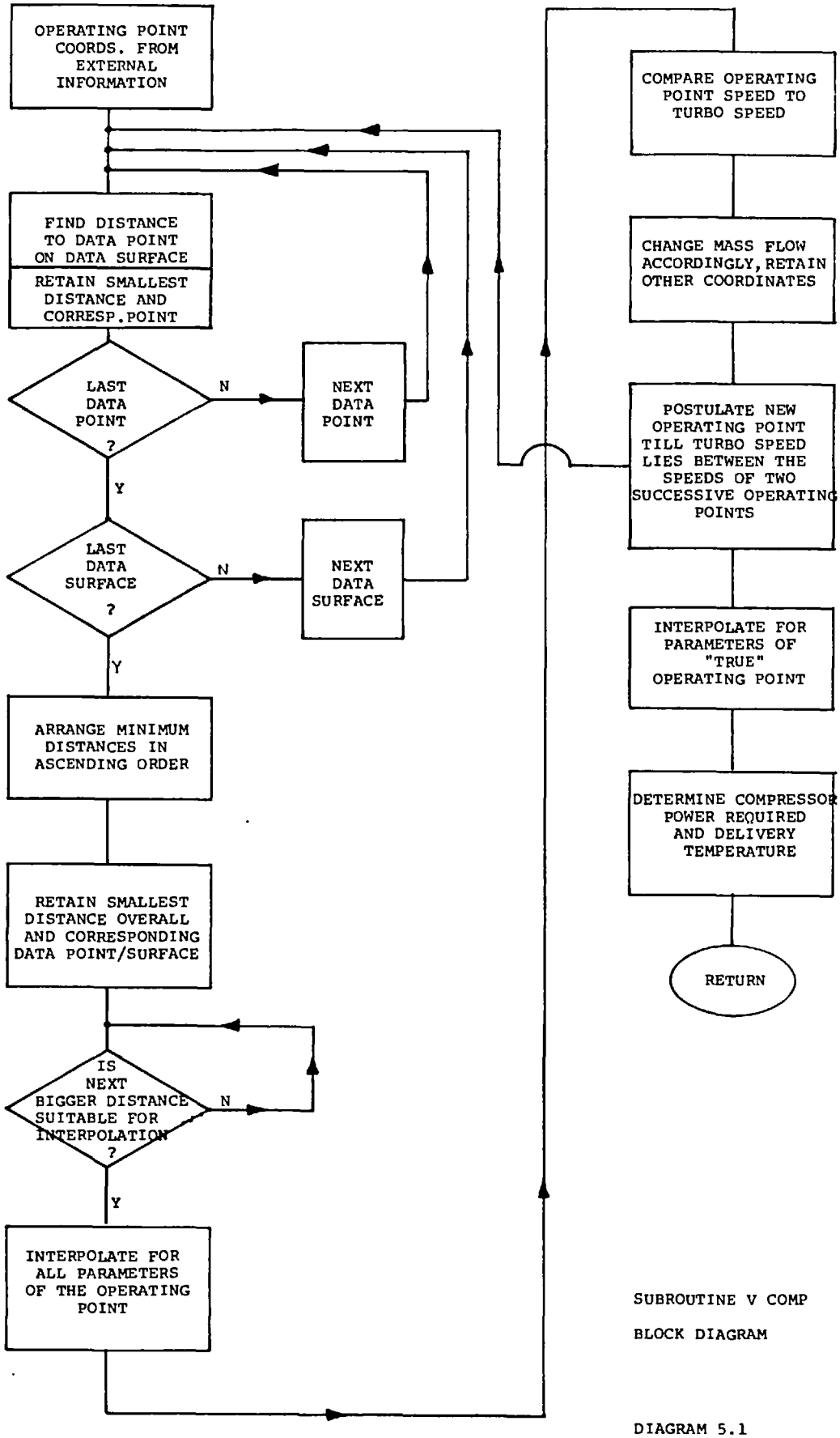
Surface fitting the irregular experimental data either by a family of smooth level surfaces or by cubic linear patches (114) was considered. It would then be possible to manipulate mathematical expressions only, to determine the required parameters. This technique, although elegant, was

found impractical, because of the relative scarcity of data and its irregularity for the first option, and the large storage requirements of the second option.

The method finally used was the following:
The groups of experimental data points are stored separately. By comparing distances, the position of the working point relative to the speed groups in space is determined.
The most appropriate nearby data points are selected for interpolation for the values of the parameters of the operating point.
Linear interpolation between two data points is finally used. The suitability of the points is determined by comparing the vectors from the working point to the data points and the vector between the data points.

The block diagram of the subroutine is shown in Diagram 5.1.

To improve the accuracy of the interpolation and speed up the convergence of the program to an operating point, the following composite interpolation procedure was used:
The position of a working point was fixed externally.
The speed (N_1) of the working point $P_1(\dot{m}_{E_1}, r_{p_1}, \dot{m}_{j_1})$ was obtained by interpolation and was compared with the turbocharger speed (NT), obtained externally from torque demand-supply considerations. Then the compressor net flow was changed by a pre-specified amount ($\pm \Delta\dot{m}_E$) at constant pressure ratio and jet flow, and the speed (N_2) of a second working point $P_2(\dot{m}_{E_1} + \Delta\dot{m}_{E_1}, r_{p_1}, \dot{m}_{j_1})$ was obtained by interpolation.
The same procedure was repeated till the (NT) value lied between (N_1) and (N_2). The parameters of the final operating point P were evaluated by interpolation between the points P_1 and P_2 (Diagram 5.1).



SUBROUTINE V COMP

BLOCK DIAGRAM

DIAGRAM 5.1

To prevent uneven dispersion of the data points from differences in scale magnitude of the three axes, the values were non-dimensionalised.

5.4.7 The Efficiencies Associated with the V.P. Compressor

There are two efficiencies associated with each data point on the v.p. compressor map. One is the compressor efficiency (η_c), and the other the overall system efficiency (η_T).

The compressor efficiency is required in the simulation to calculate the compressor power. The overall system efficiency is required for the calculation of the compressor delivery temperature. To determine the compressor efficiency η_c, the inlet temperature in front of the compressor must be known. It is undesirable to have a temperature measuring probe at close proximity to the compressor inducer leading edge, as would be required to measure the mean temperature of the mixed inlet and recirculating flow.

This temperature (T_2) was found by considering the inlet and recirculation temperatures, (T_1), (T_4), the corresponding mass flows ($\dot{m}_E$), ($\dot{m}_j$), and adiabatic flow mixing.

If suffixes

1 ≡ inlet to system

2 ≡ inlet to compressor

3 ≡ compressor discharge

4 ≡ recirculation

then

$$\eta_T = \frac{To_1(r_p^{\frac{\gamma-1}{\gamma}} - 1)}{To_3 - To_1} \qquad (5.9)$$

$$\eta_c = \frac{To_2(r_p^{\frac{\gamma-1}{\gamma}} - 1)}{To_3 - To_2} \tag{5.10}$$

From eq.5.9

$$To_3 - To_1 = \frac{To_1 . r_p^{\frac{\gamma-1}{\gamma}} - To_1}{\eta_T}$$

$$\therefore To_3 = To_1 + \frac{To_1(r_p^{\frac{\gamma-1}{\gamma}} - 1)}{\eta_T} = To_1\left[1 + \frac{(r_p^{\frac{\gamma-1}{\gamma}} - 1)}{\eta_T}\right] \tag{5.11}$$

Substituting eq. 5.11 into eq. 5.10

$$To_3 - To_2 = \frac{To_2(r_p^{\frac{\gamma-1}{\gamma}} - 1)}{\eta_c}$$

$$\therefore To_3 = To_2\left[1 + \frac{(r_p^{\frac{\gamma-1}{\gamma}} - 1)}{\eta_c}\right]$$

$$\therefore To_2 = \frac{To_1\left[1 + \frac{(r_p^{\frac{\gamma-1}{\gamma}} - 1)}{\eta_T}\right]}{\left[1 + \frac{(r_p^{\frac{\gamma-1}{\gamma}} - 1)}{\eta_c}\right]} \tag{5.12}$$

Hence

$$POWER = \frac{\dot{m}_{total} \cdot C_p \cdot To_2}{\eta_c}(r_p^{\frac{\gamma-1}{\gamma}} - 1)$$

$$= \frac{\dot{m}_{total} . C_p . To_1\left[1 + \frac{(r_p^{\frac{\gamma-1}{\gamma}} - 1)}{\eta_T}\right](r_p^{\frac{\gamma-1}{\gamma}} - 1)}{\eta_c + r_p^{\frac{\gamma-1}{\gamma}} - 1} \tag{5.13}$$

But $\dot{m}_{total} = \dot{m}_E + \dot{m}_j$ (5.14)

Using eq.5.13 and eq.5.14

$$POWER = (\dot{m}_E + \dot{m}_j) . C_p . To_1 \frac{\left[1 + \frac{(r_p^{\frac{\gamma-1}{\gamma}} - 1)}{\eta_T}\right](r_p^{\frac{\gamma-1}{\gamma}} - 1)}{(\eta_c + r_p^{\frac{\gamma-1}{\gamma}} - 1)} \tag{5.15}$$

CHAPTER 6

AN AERODYNAMIC METHOD FOR CONTROL AND RANGE IMPROVEMENT OF ROTARY COMPRESSORS (PART II)

6.1 INTRODUCTION

It was decided to base the next series of investigations on a FORD-YORK 2.4 lt. IDI injection diesel engine (see Section 4.10.3.1). This engine had already been installed on a test bed. Additionally, the engine parameters formed the inputs for the simulation program runs.

The turbocharger, suitable for this engine, which was used in the investigation was a HOLSET-H1A with a compressor wheel Type-6521F and a turbine Type-NO3B6. Particular design features of this compressor include seven blades and seven splitter blades in the radial part, a relatively long inducer and a backward leaning impeller. These series of investigations would involve:

- Designing a new more advanced jet arrangement to suit the H1A-6521F compressor.
- Fitting the device on the compressor and conducting experiments to obtain the (3-D) compressor performance map, and other relevant information.

6.2 THE DESIGN PROCEDURE FOR THE JET ARRANGEMENT

The design procedure involves two basic assumptions:

The first assumption concerns how the stability and efficiency of the compressor are related to the inducer inlet flow angles. It is assumed that the inlet flow angle distribution at the best efficiency point - which may, or may not, coincide with the design point of the compressor - represents a set of optimum angle values.

Hence the best efficiency point is taken as the reference point in the design process, and the corresponding angles as the "reference angles". However, it is not certain that the angle distribution at the best efficiency point, is the optimum incidence distribution for the inducer. The jet-arrangement design point is chosen on the surge line, because this region of incipient flow instability is more critically dependent on the design, than the stable high flow - high pressure ratio region, where prewhirl may also be used (e.g. to limit the boost in vehicle engine turbocharger applications).

The single, unbounded, round jet in a cross-flow theoretical model is used to define the jet needed to provide such a deflection to the inflow (prewhirl) so that the resulting relative flow angles at the jet-arrangement design point, match the compressor best efficiency point (b.e.p.) "reference" flow angles.

As has been explained, when a multitude of jets interact in a confined space (as is the case with the jet arrangement), additional parameters are introduced, complicating the situation (see Section 4.10.2). Most of them are only dealt with qualitatively in the design process, based on experience with former designs of the jet arrangement. It may be possible to quantitatively examine selected parameters or use information from related cases (e.g. multi-jet impingement cooling of turbine blades). Some other influencing factors may still be unidentified, in this extremely complicated flow situation.

The design procedure in its present form is flexible,

consistent, and relatively easy to use, and it is desirable to retain these qualities.

The second assumption is therefore, that the result of the design procedure i.e. the parameters which define the jet arrangement, is a reasonable approximation to the ideal solution, which would be achieved if all influencing factors could be accounted for.

6.4 DESIGN DEFINING PARAMETERS

The following parameters completely define the jet arrangement (see Figure 6.1).

1) Ejection orifice diameter - (D).
2) Distance of ejection point from compressor face - (x).
3) Distance of ejection point from compressor centreline - (R).
4) Jet inclination in (x-z) plane - (θ) (Positive anti-clockwise).
5) Jet inclination in x = const. plane - (ϕ) (Positive anti-clockwise).
6) Number of jets - (N).

The block diagram of the design procedure is shown in Diagram 6.1.

6.4 SHAPE OF JET EJECTION ORIFICES

There are three basic possibilities for the cross sectional shape of the jet orifices: circular, elliptical, and parallelogram.

Jets from square and elliptical orifices (74) were found to penetrate further into a cross flow than circular jets for the same velocity ratio and cross sectional area (see Section 4.3.3). Square and elliptical orifices (with major axis parallel to the cross flow) will give jets present-

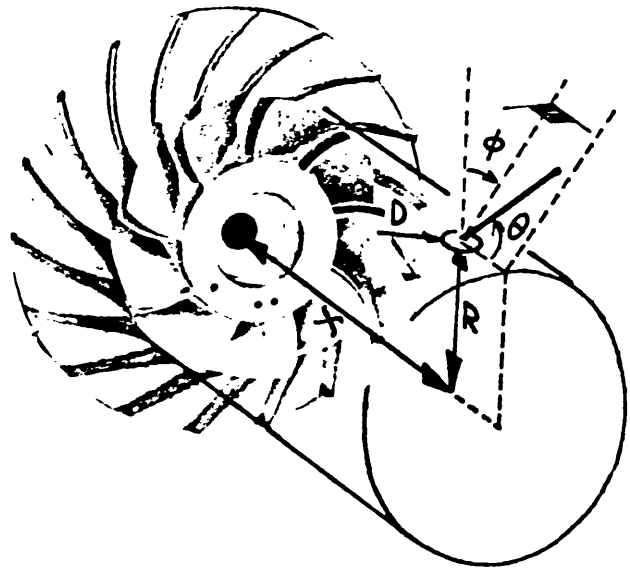


FIG.6.1 Parameters Defining the Design Arrangement

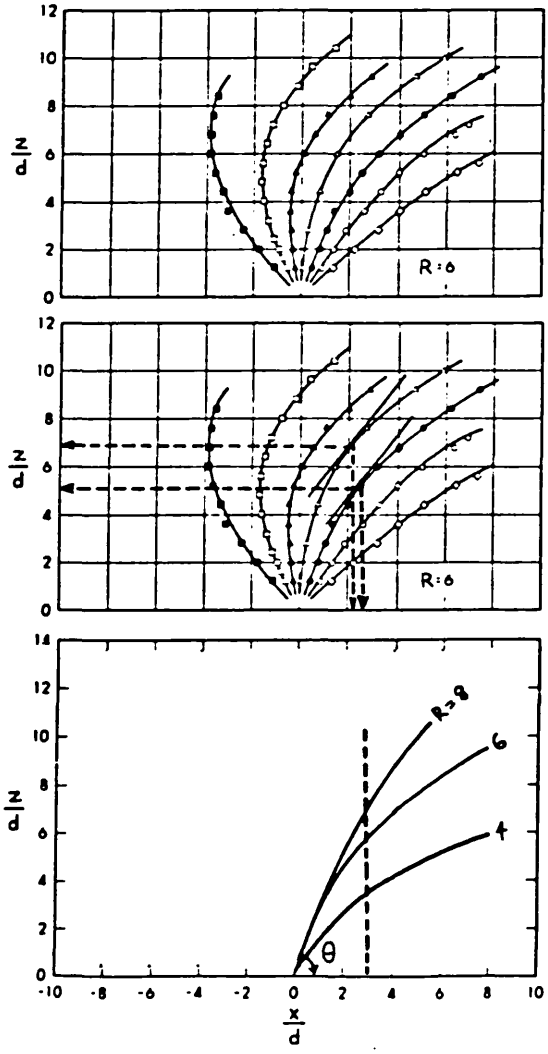


FIG.6.2 Design Procedure. Jets in Cross Flow with Different Ejection Angles

FIG.6.3 Design Procedure. Jets in Cross Flow with Different Ejection Angles

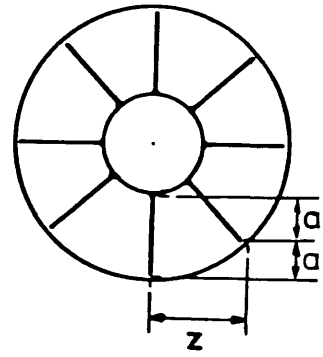


FIG.6.4 Impeller face

FIG.6.5 Design Procedure. Jets in Cross Flow with Different Velocity Ratios

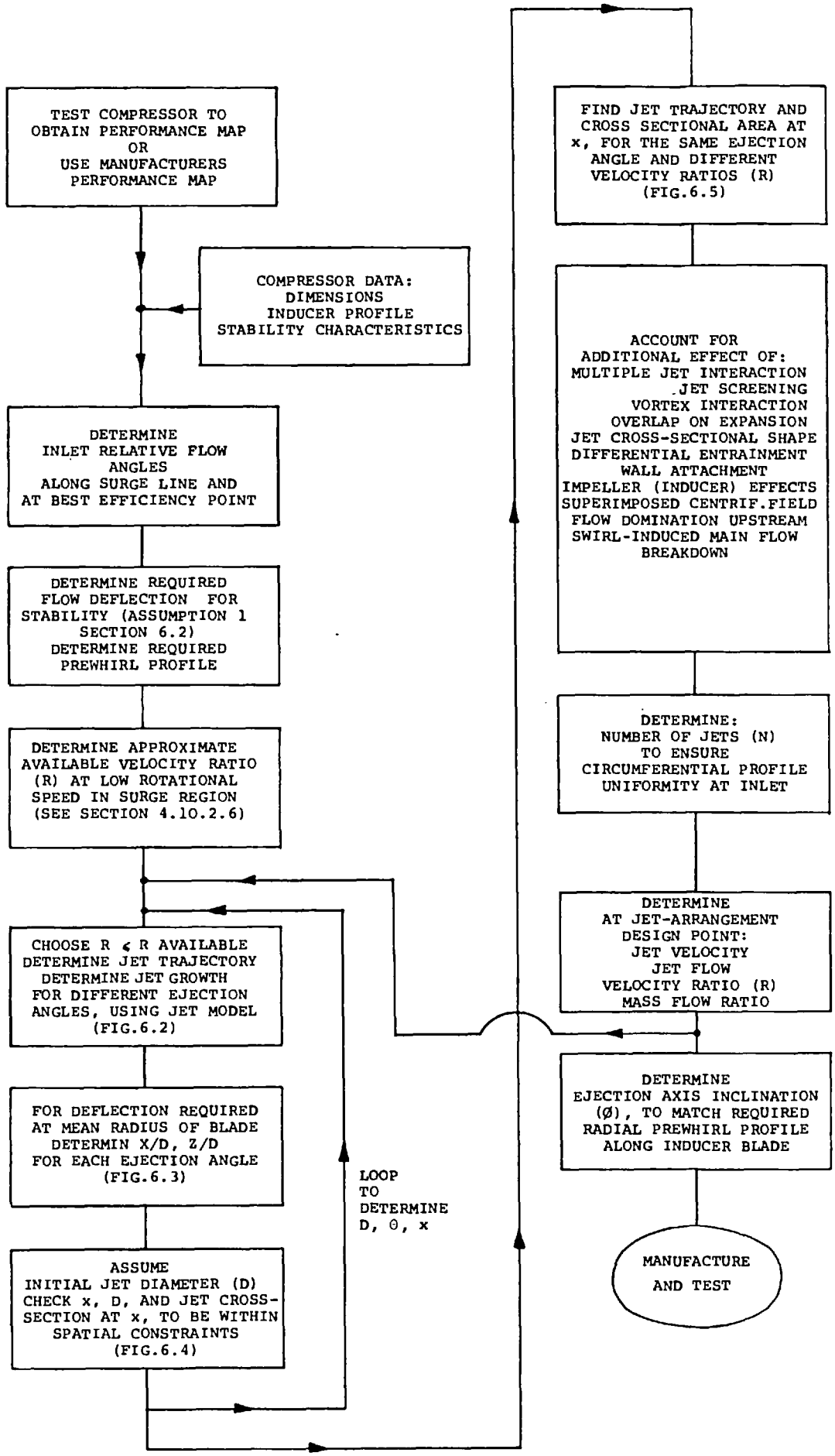

TEST COMPRESSOR TO OBTAIN PERFORMANCE MAP OR USE MANUFACTURERS PERFORMANCE MAP
COMPRESSOR DATA: DIMENSIONS INDUCER PROFILE STABILITY CHARACTERISTICS
DETERMINE INLET RELATIVE FLOW ANGLES ALONG SURGE LINE AND AT BEST EFFICIENCY POINT
DETERMINE REQUIRED FLOW DEFLECTION FOR STABILITY (ASSUMPTION 1 SECTION 6.2) DETERMINE REQUIRED PREWHIRL PROFILE
DETERMINE APPROXIMATE AVAILABLE VELOCITY RATIO (R) AT LOW ROTATIONAL SPEED IN SURGE REGION (SEE SECTION 4.10.2.6)
CHOOSE R ≤ R AVAILABLE DETERMINE JET TRAJECTORY DETERMINE JET GROWTH FOR DIFFERENT EJECTION ANGLES, USING JET MODEL (FIG.6.2)
FOR DEFLECTION REQUIRED AT MEAN RADIUS OF BLADE DETERMIN X/D, Z/D FOR EACH EJECTION ANGLE (FIG.6.3)
ASSUME INITIAL JET DIAMETER (D) CHECK x, D, AND JET CROSS-SECTION AT x, TO BE WITHIN SPATIAL CONSTRAINTS (FIG.6.4)
LOOP TO DETERMINE D, θ, x
FIND JET TRAJECTORY AND CROSS SECTIONAL AREA AT x, FOR THE SAME EJECTION ANGLE AND DIFFERENT VELOCITY RATIOS (R) (FIG.6.5)
ACCOUNT FOR ADDITIONAL EFFECT OF: MULTIPLE JET INTERACTION JET SCREENING VORTEX INTERACTION OVERLAP ON EXPANSION JET CROSS-SECTIONAL SHAPE DIFFERENTIAL ENTRAINMENT WALL ATTACHMENT IMPELLER (INDUCER) EFFECTS SUPERIMPOSED CENTRIF.FIELD FLOW DOMINATION UPSTREAM SWIRL-INDUCED MAIN FLOW BREAKDOWN
DETERMINE: NUMBER OF JETS (N) TO ENSURE CIRCUMFERENTIAL PROFILE UNIFORMITY AT INLET
DETERMINE AT JET-ARRANGEMENT DESIGN POINT: JET VELOCITY JET FLOW VELOCITY RATIO (R) MASS FLOW RATIO
DETERMINE EJECTION AXIS INCLINATION (Ø), TO MATCH REQUIRED RADIAL PREWHIRL PROFILE ALONG INDUCER BLADE
MANUFACTURE AND TEST

DIAGRAM 6.1

ing a smaller frontal area to the cross flow, than circular orifices, and consequently will be less deflected. On expansion a different cross sectional shape is expected, but retaining in some form counterrotating vortices at the sides. An elliptical orifice with the major axis perpendicular to the cross flow would approach a (2-D) slot ejection which would be undesirable (see Section 4.7).

However the gain in penetration with the alternative orifices does not appear to justify the additional manufacturing complexity, at least at this stage of development. The circular orifice is clearly preferable from manufacturing considerations and also has the lowest wall friction losses. In addition, all the previous experimental work, as well as the theoretical jet in a cross flow model, was based on jets issuing from circular orifices. The circular shape was therefore retained for the design.

6.5 MEASUREMENT OF INDUCER INLET ANGLES

One of the prerequisites in the design of the jet arrangement was the radial distribution of blade angles of the H1A-6521F compressor. The contours of the inducer were mapped using a 3-axis universal measuring apparatus (125). With this machine it is possible to define the coordinates of a point in space, related to a fixed origin.

A grid was inscribed on the suction and pressure surfaces of the inducer, and the coordinates of the nodes of the grid were determined, relative to a Cartesian system of axes, one of which coincided with the compressor wheel centreline. Using the coordinates of the points, the angle (θ) of sectors of the blade w.r.t. a radial plane

passing through the compressor axis was calculated. The radial angle distribution is shown in Figure 6.6.

6.6 PRELIMINARY SIMULATION RESULTS

It was required to know the position of the engine operating line on the compressor map, in order to define the operating areas where the use of prewhirl could be beneficial.

The manufacturers' compressor performance map, for the H1A-6521F compressor, was arbitrarily extended into (3-D) to conform with the v.p. compressor simulation model working format (see Section 5.4.6). To achieve the correct order of magnitude, results from past experiments were used (see Section 4.10.3.6.3). The subroutine was modified so that warning was given if the engine operating point on the compressor map did not have adequate surge margin, but recirculation was suppressed since the results would be unrealistic. The "dummy" (3-D) compressor subroutine was used in conjunction with the engine simulation program for preliminary predictions, to be used in the design of the jet arrangement.

Typical results are shown in Figure 6.7 with the engine operating line on the manufacturers compressor performance map. Because of the instantaneous air demand of the four cylinder engine, resulting in large flow oscillations at the inlet manifold (see Section 3.2.1) the instantaneous operating point crossed momentarily the surge line at engine speeds below 1700 rpm. In addition, the boost above 2700 rpm gave rise to pressures that may be unacceptable for the engine.

There are therefore two problem regions as denoted

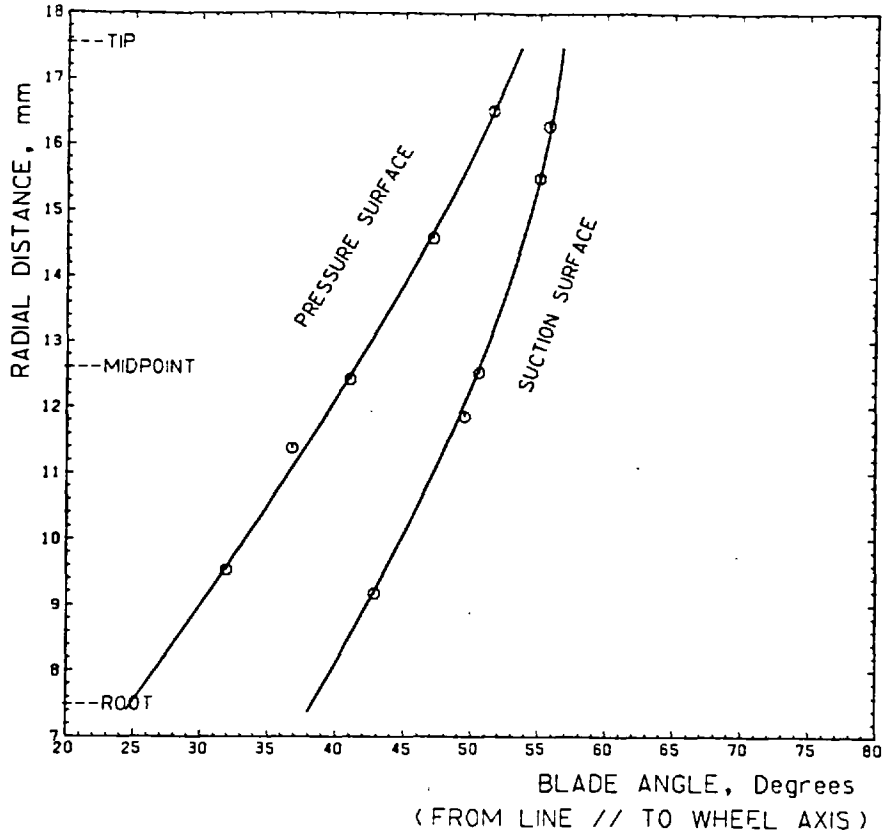


FIG.6.6 Inducer Blade Angle Radial Distribution

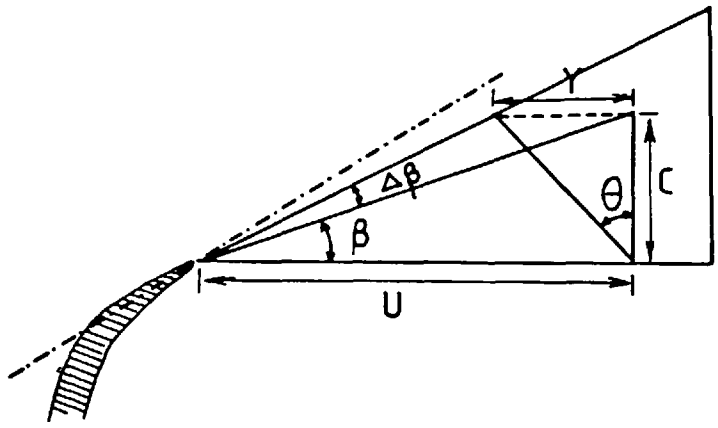


FIG.6.9 Velocity Triangles - Notation

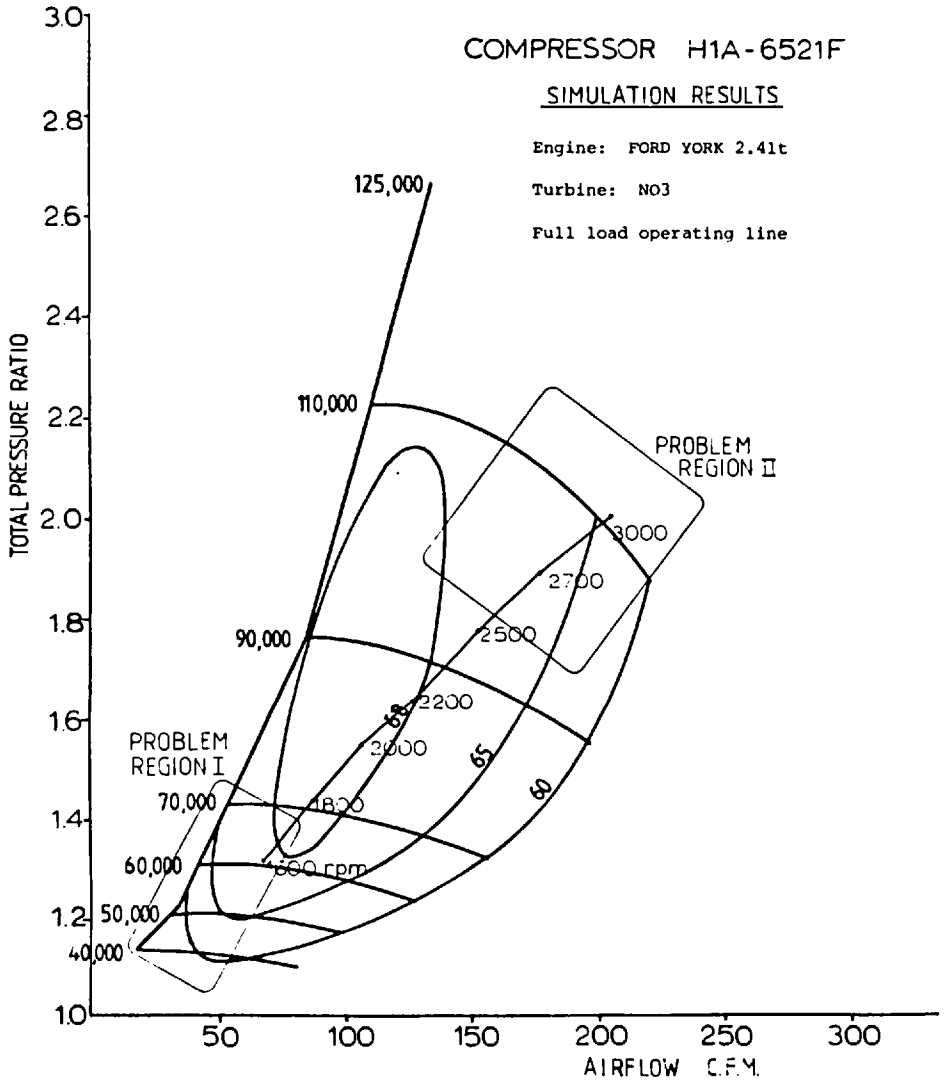


FIG.6.7 Engine Operating Line on H1A Compressor Map

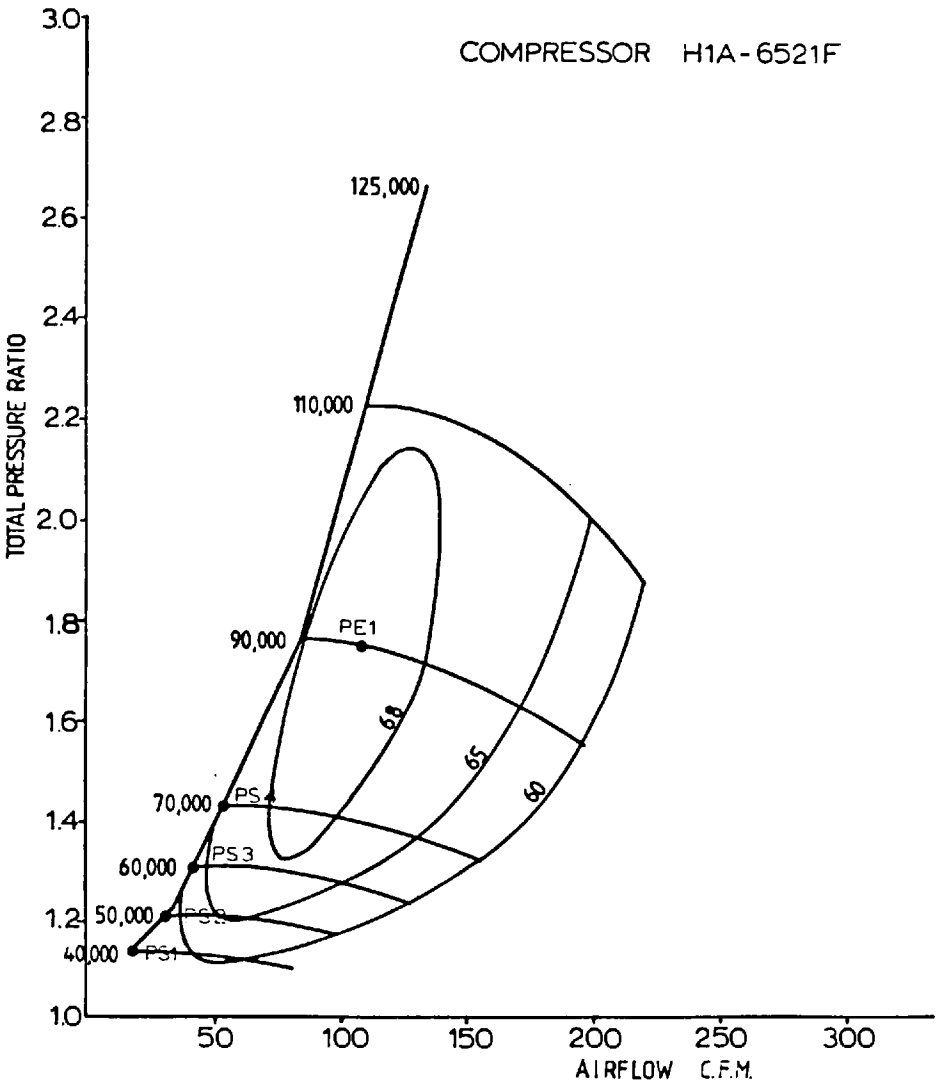


FIG.6.8 H1A-6521F Compressor Performance Map

in Figure 6.7. In the lower region (I), it would be desirable to have an increase in the available surge margin, while in the upper region (II), controlling the boost pressure may be essential.

6.7 THE DESIGN

6.7.1 Compressor Inlet Velocity Triangles

The manufacturers' compressor performance map for the H1A-6521F compressor is shown in Figure 6.8. The velocity triangles at the compressor inlet were evaluated based on velocities calculated from mass flows from the compressor map. Velocity triangles for the points PS1, PS2, PS3, PS4 on the surge line, as well as at the point of best efficiency PE1 (reference point), were constructed using one-dimensional theory, for three positions along the inducer blade (see Figure 6.8). The results are shown in Tables 6.1 and 6.2.

6.7.2 Relation Between Prewhirl Angle and Relative Flow Angle

Referring to Figure 6.9, the relation between the prewhirl angle θ required for a change $\Delta\beta$ in the relative flow angle β is as follows:

$$\frac{C}{U - Y} = \tan(\Delta\beta + \beta) \qquad (6.1)$$

$$\frac{Y}{C} = \tan\theta \qquad (6.2)$$

$$\therefore \quad c \tan\theta = Y$$

TABLE 6.1

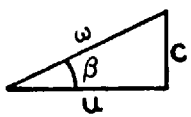
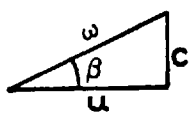
	Point PS1			Point PS2			Point PS3		
$\dot{m}$ (KG. s^{-1})	0.00983			0.01769			0.02303		
N (RPM)	40,000			50,000			60,000		
Ω (s^{-1})	4188.79			5235.98			6283.18		
A (M^2)	8.411×10^{-4}			8.411×10^{-4}			8.411×10^{-4}		
	Tip	Midpoint	Root	Tip	Midpoint	Root	Tip	Midpoint	Root
c	10.16	10.16	10.16	18.29	18.29	18.29	23.80	23.80	23.80
u	73.30	52.35	31.41	91.62	65.45	32.27	109.95	78.54	47.12
ω	74.00	53.33	33.02	93.43	67.95	43.32	112.50	82.06	52.79
β	7.89	10.98	17.92	11.28	15.61	24.97	12.21	16.86	26.80

TABLE 6.2

	Point PS4			Point PE1 (Reference)		
$\dot{m}$ (KG.s^{-1})	0.02949			0.05827		
N (RPM)	70,000			90,000		
Ω (s^{-1})	7330.38			9424.77		
A (M^2)	8.411×10^{-4}			8.411×10^{-4}		
	Tip	Midpoint	Root	Tip	Midpoint	Root
c	30.48	30.48	30.48	60.25	60.25	60.25
u	128.28	91.63	54.97	164.93	117.80	70.68
ω	131.85	96.56	62.86	175.59	132.32	92.88
β	13.36	18.40	29.0	20.06	27.08	40.44

Hence

$$\frac{c}{U - c\tan\theta} = \tan(\Delta\beta + \beta)$$

$$\therefore \frac{u}{c} - \tan\theta = \frac{1}{\tan(\Delta\beta + \beta)}$$

$$\therefore \tan\theta = \left(\frac{1}{\tan\beta} - \frac{1}{\tan(\Delta\beta + \beta)}\right)$$

$$\therefore \theta = \tan^{-1}\left(\frac{1}{\tan\beta} - \frac{1}{\tan(\Delta\beta + \beta)}\right) \qquad (6.3)$$

6.7.3 Required Prewhirl Profile

The steps to determine the required prewhirl profile which would change the inlet flow incidence angles at surge to the reference angles are shown in Table 6.3.

The subscripts used:

$\beta \equiv$ relative flow angle

s ≡ surge point

$\eta \equiv$ best efficiency point

B ≡ blade

FL ≡ flow

Notes

Block 1. It can be seen that at points PS2, PS3, PS4 there is only a small difference in incidence especially at the blade tip.

Block 3. For the suction side there is only a small variation in the value of $\Delta\beta_\eta$.

TABLE 6.3

		HIA-6521F	Inducer Blade Position		
		Point	Root	Midpoint	Tip
Block 1	Relative Flow Angle β_{FL} Degrees	PS1	17.92	10.98	7.89
		PS2	24.97	15.61	11.29
		PS3	26.80	16.86	12.21
		PS4	29.00	18.40	13.37
		PE1	40.44	27.08	20.06
Block 2	Inducer Angle β_B	Suction Side (SS)	52.0	39.5	33.5
		Pressure Side (PS)	66.0	49.0	36.0
Block 3	Incidence Mismatch $\Delta\beta_\eta=\beta_B-\beta_{FL}$ @ PE1	SS	11.56	12.42	13.44
		PS	25.56	21.92	15.94
Block 4	Incidence Mismatch $\Delta\beta_s = \beta_B - \beta_{FL}$ (Degrees) @ Surge Line	Suction Side PS1	34.08	28.52	25.61
		Suction Side PS2	27.03	23.89	22.21
		Suction Side PS3	25.20	22.64	21.29
		Suction Side PS4	23.00	21.10	20.13
		Pressure Side PS1	48.08	38.02	28.11
		Pressure Side PS2	41.03	33.39	24.71
		Pressure Side PS3	39.20	32.14	23.79
		Pressure Side PS4	37.00	30.60	22.63
Block 5	Incidence Difference $\Delta\theta=\Delta\beta_s-\Delta\beta_\eta$ $=\beta_{B_s}-\beta_{FL_s}-\beta_{B_\eta}+\beta_{FL_\eta}$ (Degrees)	PS1	22.52	16.10	12.17
		PS2	15.47	11.47	8.77
		PS3	13.67	10.22	7.85
		PS4	11.44	8.68	6.69
Block 6	Required Prewhirl Angle, θ (from eq.6.3) (Degrees)	PS1	62.48	72.64	77.41
		PS2	44.25	58.37	66.23 ← Design Point
		PS3	38.88	53.35	62.03
		PS4	32.24	46.40	55.75

Block 4. The values for PS1 are quite different from those at higher speeds. A possible explanation is that at low rotational speeds the inertia forces predominate over the rotational forces and the flow pattern may change, with the boundary layer moving from the shroud suction side towards the middle of the channel, and hence the change in behaviour of the impeller. At higher speeds the values vary between 2° - 4°. On the suction side, which is more critical for flow separation, surge coincides with an incidence mismatch of approximately 22.5^{o}. At this indidence the inducer may be stalled. Although it is not necessary that surging is a result of inducer stall, a destabilised inducer may affect the stage stability (see Sections 2.5.2, 2.5.3 and 2.5.4). This particular compressor design incorporates a vaneless diffuser and a backward leaning impeller, both regarded as stabilising elements. On the other hand the long inducer - the splitter blade is situated far back, in the radial part of the impeller - , results in a wide channel giving little directional support to the flow. These may imply that the inducer incidence is critical for stability. The high incidence mismatch at the blade root at low speed, may not be very important as the flow is quickly stabilised by the passage curvature to radial (23).

Block 6. This is the required prewhirl profile to change the relative inlet flow angle from the surge angle to that of maximum efficiency. In this case Equation 6.3 becomes

$$\theta = \tan^{-1}\left(\frac{1}{\tan\beta_{FLs}} - \frac{1}{\tan(\Delta\theta + \beta_{FLs})}\right) \qquad (6.4)$$

$$\text{where } \Delta\theta + \beta_{FLs} = \beta_{FL\eta} \qquad (6.5)$$

The design "target" profile was chosen at point PS2, N = 50000, r_p = 1.22. Point PS2 lies approximately in the middle of "Problem Region I" in Figure 6.7.

In the above calculations it was assumed that the inlet mass flow rate remains constant. This implies that any throttling effect due to the jets, tending to reduce the cross flow (main flow), is balanced by the total jet flow and the impeller does not suffer a change in flow throughput. If there is a change in mass flow rate, and hence a change to the axial velocity component c_x by (δ) per cent, this can be taken into account by modifying Equation 6.4 as:

$$\theta = \tan^{-1}\left(\frac{1}{\lambda.\tan\beta_{FLs}} - \frac{1}{\tan\beta_{FL\eta}}\right) \qquad (6.6)$$

$$\text{where } \lambda = 1 + \delta/100 \qquad (6.7)$$

6.7.4 Choice of Design Velocity Ratio

In past investigations it was found that high velocity ratios were available near the surge line (see Section 4.10.2.6), and consequently in region I (see Figure 6.7). These velocity ratios were in excess of 10. For the new design it was predicted that a ratio R = 7 would be available over region I, hence a conservative R = 6 was chosen as the design preliminary velocity ratio.

Using the jet in cross-flow theoretical model (see Section 4.4) a computational scanning of the region round the design point was made.

The variation of the principal parameters was:

- Velocity Ratio (R). From R = 4 to R = 8.
- Initial jet ejection angle (θ_j). From $\theta_j = 30^o$ to $\theta_j = 150^o$.
- Initial jet diameter (D_j). From D_j = 0.003 m, to D_j = 0.004 m.

For every point on the jet trajectory the model gives the following information:

- Cartesian coordinates of the point.
- Angle of trajectory to the x-axis.
- Rate of change of angle of trajectory.
- Mean jet velocity.
- Mean jet density.
- Equivalent circular cross section radius.

6.7.5 Equivalent Jet Cross-Section

Originally the mathematical model for the jet assumed a circular jet cross section throughout the jet development, with uniform properties across the section. However in

reality the circular jet develops a kidney shaped cross section on expansion (see Section 4.3.2).

Since the jet cross sectional shape at the impeller eye is used to determine the number of jets needed, it was thought desirable for the model to give a better approximation of the actual jet shape on expansion. The circular cross section was therefore transformed into an equivalent semi-circle, which was found to be a good representation of the kidney-shaped section developed, and was used in the design process.

A shape parameter may be defined as $C/\sqrt{a}$ where

C ≡ circumference of the cross section

a ≡ area of the cross section normal to trajectory

For a circular cross section

$$\left[\frac{C}{\sqrt{a}}\right]_{circ} = \frac{\pi D}{\sqrt{\pi D^2/4}} = \frac{2\pi}{\sqrt{\pi}} = 3.54 \qquad (6.8)$$

This is the initial value of the parameter immediately after ejection. For a semi-circular cross section:

$$\left[\frac{C}{\sqrt{a}}\right]_{semi} = \frac{\pi D/2 + D}{\sqrt{\pi D^2/8}} = \frac{(\pi + 2)\sqrt{2}}{\sqrt{\pi}} = 4.102 \qquad (6.9)$$

Since the semi circle is assumed to have an area equivalent to the circular cross section predicted by the theoretical model, then the diameter of the semi-circle:

$$D_{semi} = 1.414\ D_{circle} \qquad (6.10)$$

Figure 6.10 compares an equivalent semi-circle obtained using the jet model, with a measured jet cross section with the same initial parameters and at the same point on the trajectory (72). It can be seen that the semi-circle is a good representation of the frontal area and the main part of the jet section, but excludes the two sides.

From results of other investigators (87) $c/\sqrt{a}$ was found to change from 3.5 to 6 along the trajectory of a jet from (circular) ejection point to full development (see Figure 6.11). If the jet cross section normal to the trajectory is semi-circular, the cross section that the inducer face plane (x = const. plane) makes with the jet is semi-elliptical with minor axis D and major axis $D/\cos\theta$, where D ≡ diameter of the semi-circle, θ ≡ gradient of the trajectory at the compressor face.

6.7.6 The Two Alternative Designs

From the results of the theoretical investigation two alternative design initial ejection angles were chosen, $\theta_j = 90^o$ and $\theta_j = 70^o$. Table 6.4 is from the loop to determine D_j, θ_j, x in the design procedure (Diagram 6.1), and shows the values of parameters for a set of initial conditions D_j = 0.003 m and z/D = 4.33, with z determined from the impeller dimensions (see Figure 6.4). It can be seen that at the required $z/D, \theta_j = 80^o$ gives a gradient θ = 58.33 which is exactly the blade midpoint prewhirl angle required (θ = 58.37), at the design point (see Table 6.3). Tables

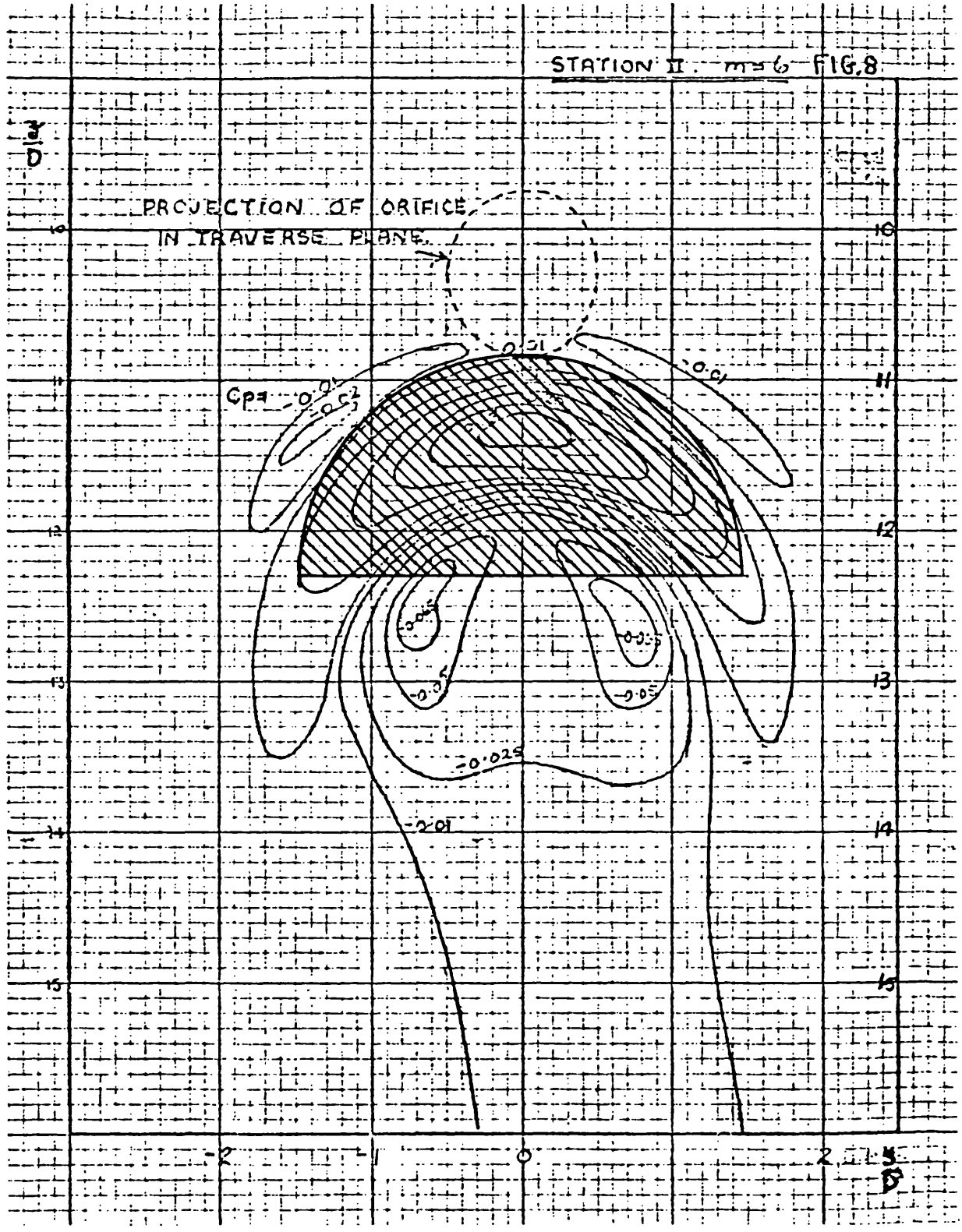


FIG.6.10 Comparison of Jet Cross-Section from (72) and Equivalent Semi-Circle from Theoretical Model (R = 6, x/D = 1.26, y/D = 5.2)

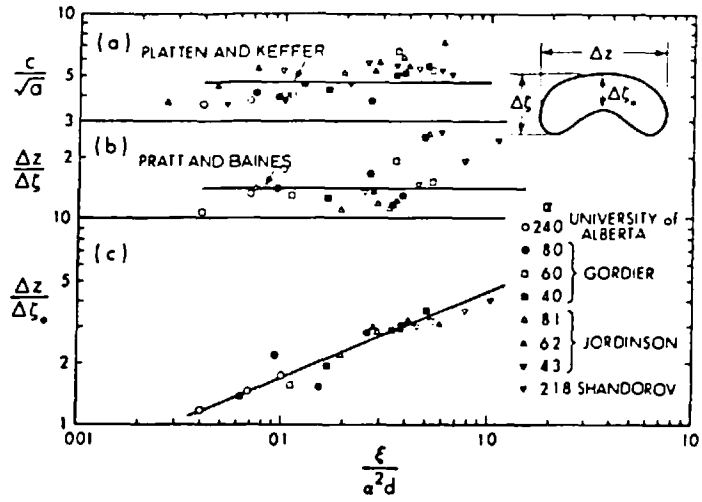


FIG.6.11 Geometry of the Kidney Shape of the Circular Jet in a Cross Flow

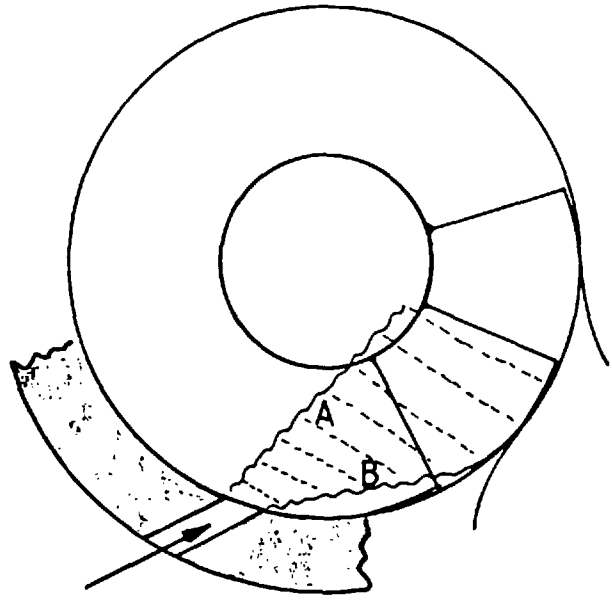


FIG.6.12 Oblique Jet Ejection Effects

TABLE 6.4

Velocity Ratio R = 6		Initial Diameter D_j = 0.003 m		Z/D = 4.33	
Ejection Angle θ_j	Trajectory Slope θ	x/D	x mm	Velocity u $m.s^{-1}$	Equiv. Diameter $D_{eq.}$ mm
70	49.5	2.499	7.50	55.69	8.65
80	58.33	1.627	4.88	54.13	8.65
90	66.58	0.847	2.54	52.52	8.65

TABLE 6.5

$\theta_j = 70^o$		x/D = 2.4999			
Velocity Ratio R	z/D	z mm	Trajectory Slope θ	Velocity u $m.s^{-1}$	Equiv. Diameter $D_{eq.}$ mm
4	3.63	10.89	42.41	43.2	7.95
5	4.03	12.09	46.58	49.3	8.29
7	4.60	13.80	52.42	61.8	8.94
8	4.8	14.40	54.40	68.1	9.14

TABLE 6.6

$\theta_j = 90^o$		x/D = 0.847			
Velocity Ratio R	z/D	z mm	Trajectory Slope θ	Velocity u $m.s^{-1}$	Equiv. Diameter $D_{eq.}$ mm
4	3.26	9.78	60.09	41.5	6.12
5	3.80	11.40	64.10	47.34	8.12
7	4.83	14.49	68.45	57.30	9.16
8	5.26	15.78	70.28	62.01	9.62

6.5, 6.6 show the off-design parameters for a specific θ_j and D_j at the appropriate x/D shown in Table 6.4.

With the 90° ejection angle the jets will be ejected very close to the compressor face. The region downstream of the jet, especially near the ejection point, is a region of low pressure and this may affect the inducer performance. The ejection angle (ϕ) of the following jet must be chosen so that on expansion, the latter jet fills as much as possible of this low pressure region of the former jet.

Again because of the close proximity to the inducer, the jets cannot be accommodated so that at the design point, on expansion, each jet goes below the next one, which in turn will act as a screen to the cross flow, thus enabling the former jet to suffer less deflection. Therefore some degree of jet to jet interaction, tending to push the jets towards the wall, is expected with this design. This is aggravated further because of the presence of the centrifugal field due to the inducer and may lead to the jet's attaching to the wall because of differential entrainment. This would be undesirable as the increased friction would consume jet energy and must be avoided by suitable choice of ϕ angle.

With $\theta_j = 90^o$ the shift of the trajectory in the z-direction for different velocity ratios R is large which means that the off-design conditions may differ considerably from the design point. However the 90° ejection gives the maximum jet expansion at the compressor inducer face (except than the backward ejecting jets, which may lead to

flow breakdown and were not adopted). Thus the inducer annulus can be provided with a fairly uniform circumferential velocity profile, with a minimum number of jets. In this way the recirculation is minimised. Very large flow deflections are potentially available and the velocity ratio must be carefully controlled to avoid adverse flow conditions which will deteriorate the aerodynamic performance of the blades.

The jets with initial ejection angle $\theta_j = 70^o$ have the advantage that the trajectory shift in the z-direction at off-design velocity ratios, is relatively smaller hence the deviation from the design point smaller. Also, at higher ratios the jets are aimed towards the shroud-suction side of the impeller. Since this is the most delicate position for flow breakdown (see Section 2.3), the mixing action of the jet may stabilise the flow. Further, with the $\theta_j = 70^o$ jet there is less danger of flow breakdown and backflow in the inlet pipe,because of the jet action towards the impeller.

However the lower angles that are potentially available may mean that the $\theta_j = 70^o$ jet will perform less satisfactorily at the "problem region II" on the compressor map (see Figure 6.7) where low velocity ratios would be available. The $\theta_j = 70^o$ jet will have less opportunity to expand before reaching the inducer, so more jets are needed to avoid "patches" i.e. non-uniform circumferential velocity profile round the inducer face. On the other hand if the jet spacing is very close there may be problems with jet to jet vortex interaction, tending to deflect the jets further. However

the jets can be better accommodated, since with $\theta_j = 70^o$ each one would tend to go below the next. More jets also mean more recirculation, which is undesirable, but the higher flow will help the arrangement performance in "problem region II".

Unlike the assumption in the theoretical model, the velocity profile across the section of the jet is not uniform, but would resemble a Gaussian distribution. This must also be accounted for when choosing the ϕ angle. Another factor to be considered is that the jet ejection is oblique to the cross flow. This results in one side of the jet being subjected earlier to the cross flow, Side A (see Figure 6.12). Side A will be deflected earlier than Side B and this will result in an asymmetric profile relative to the ejection axis. This slightly distorted profile will tend to align the jet cross section at the impeller face with the blades, on higher-than-design velocity ratios, as the jet will move further along the z-axis and the blades move in a circular path.

The two final designs for the jet arrangement were:

DESIGN 1		DESIGN 2	
N	= 7 (Angular dispersion = 51.43°)	N	= 8 (angular dispersion = 45°)
θ_j	= 90°	θ_j	= 70
D_j	= 0.003 m	D_j	= 0.003
ϕ	= 35°	ϕ	= 40°
x	= 0.00254 m	x	= 0.0075 m

Design point 1	Design point 2
z/D = 4.33	z/D = 4.33
z = 13 mm	z = 13 mm
R = 6	R = 6
x/D = 0.847	x/D = 2.5
θ = 66.58	θ = 50.17
r = 3.06	r = 3.06
Deq = 8.65	Deq = 8.65
u = 52 m/s	u = 55.69
ρ = 1.16 kg/m^3	ρ = 1.16

Experiments using both designs were to be made. In addition a 50 mm extension piece was provided so that the ejection plane could be moved away from the compressor face. This was an arbitrary distance, to test the effect of full expansion of the jets before reaching the inducer. Thus the resulting profile presented to the inducer will be more uniform, but all the losses from the full jet expansion would have been incurred. Comparison experiments using the extension piece were to be made.

6.7.7 Adaptor Design

In designing the adaptor-jet nozzle assembly to be fitted to the H1A-6521F compressor for the new series of experiments, the concept of the independent jet nozzle ring was retained.

In addition several design requirements were dictated by the particular experimental arrangement.

- To minimise the loading on the compressor casing for structural integrity and also to preserve the blade shroud clearances, the adaptor should be as light as possible. This

was most important as the assembly would be subjected to severe vibration when used on the diesel engine.

- The jet scroll volume should be large, for low flow velocities, to minimise friction losses. However, dimensional and shape constraints were imposed, by considerations of the compressor casing strength which should not be impaired by the necessary machining.
- The adaptor should be removable to facilitate interchange of different individual nozzle rings.
- The jet nozzle ring should be thick enough to ensure flow reattachment inside the jet passage, so that the jet diameter at the ejection point is defined.

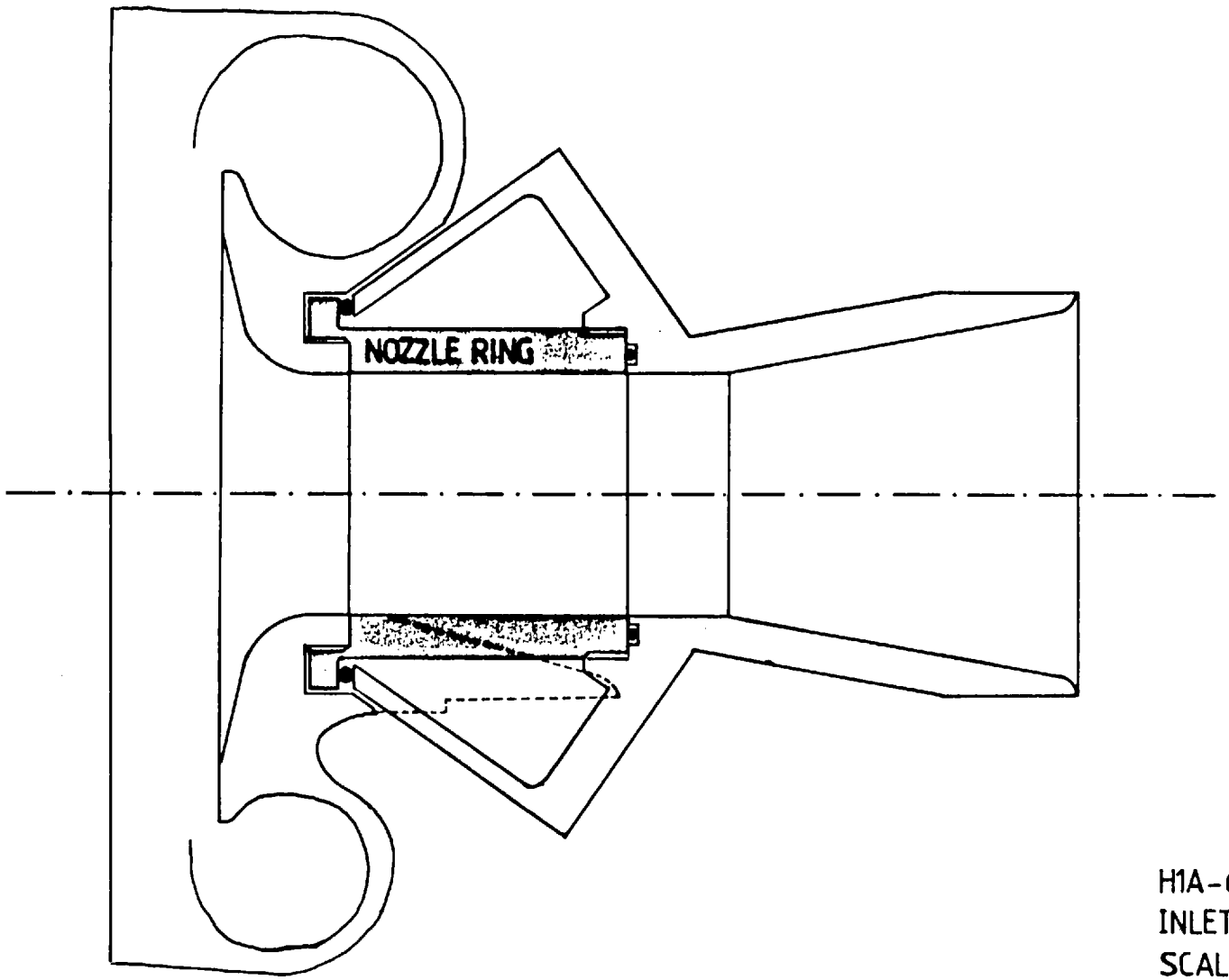
The scroll around the jet nozzle ring was fed with air through an oblique inlet and was designed so that a vortex chamber effect was produced. This would prevent unequal jet flow among the different jet nozzles. In addition the centrifugal effect would minimise the possibility of any large impurities blocking the jet passages during operation. The overall assembly is shown in Figure 6.13 (see Figures 6.14, 6.15, 6.16).

6.8 THE V.P. COMPRESSOR EXPERIMENTS

6.8.1 The Experimental Rig

In these series of experiments the FORD YORK diesel engine was used naturally aspirated, as a gas generator, to drive the turbocharger for the v.p. compressor experiments.

The turbocharger was mounted with its axis at right angles to the engine axis to improve access to the unit and enhance the accuracy of the noise measurements. Because



H1A-6521F
INLET ADAPTOR ASSEMBLY
SCALE 1:1

FIG.6.13 Adaptor and Nozzle Ring Assembly for H1A-6521F Compressor

Fig. 6.14 Compressor H1A/6521F, Housing, and Inlet Adaptor Components

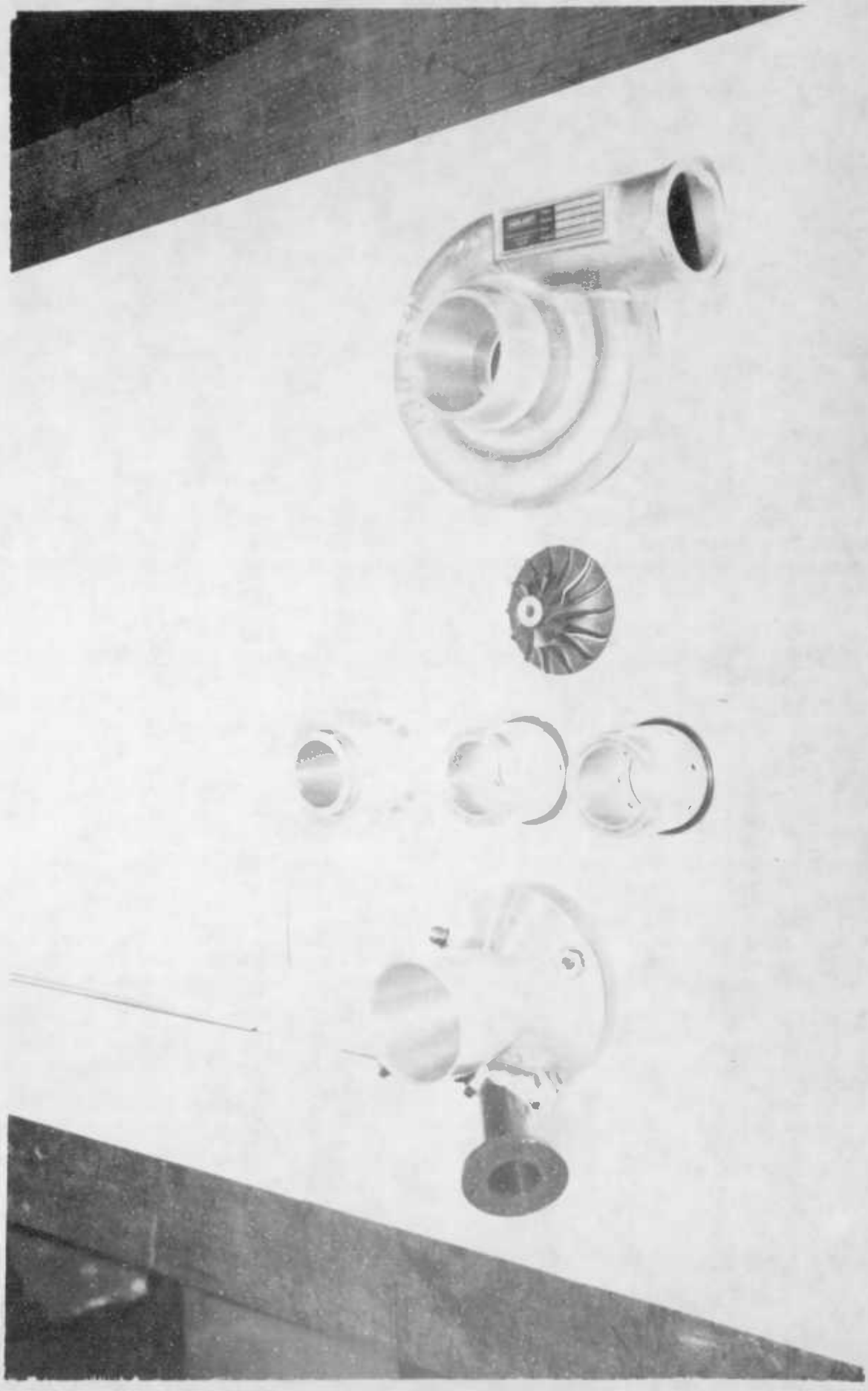




Fig. 6.15 Impeller 6521F, 70° Nozzle Ring and Inlet Adaptor

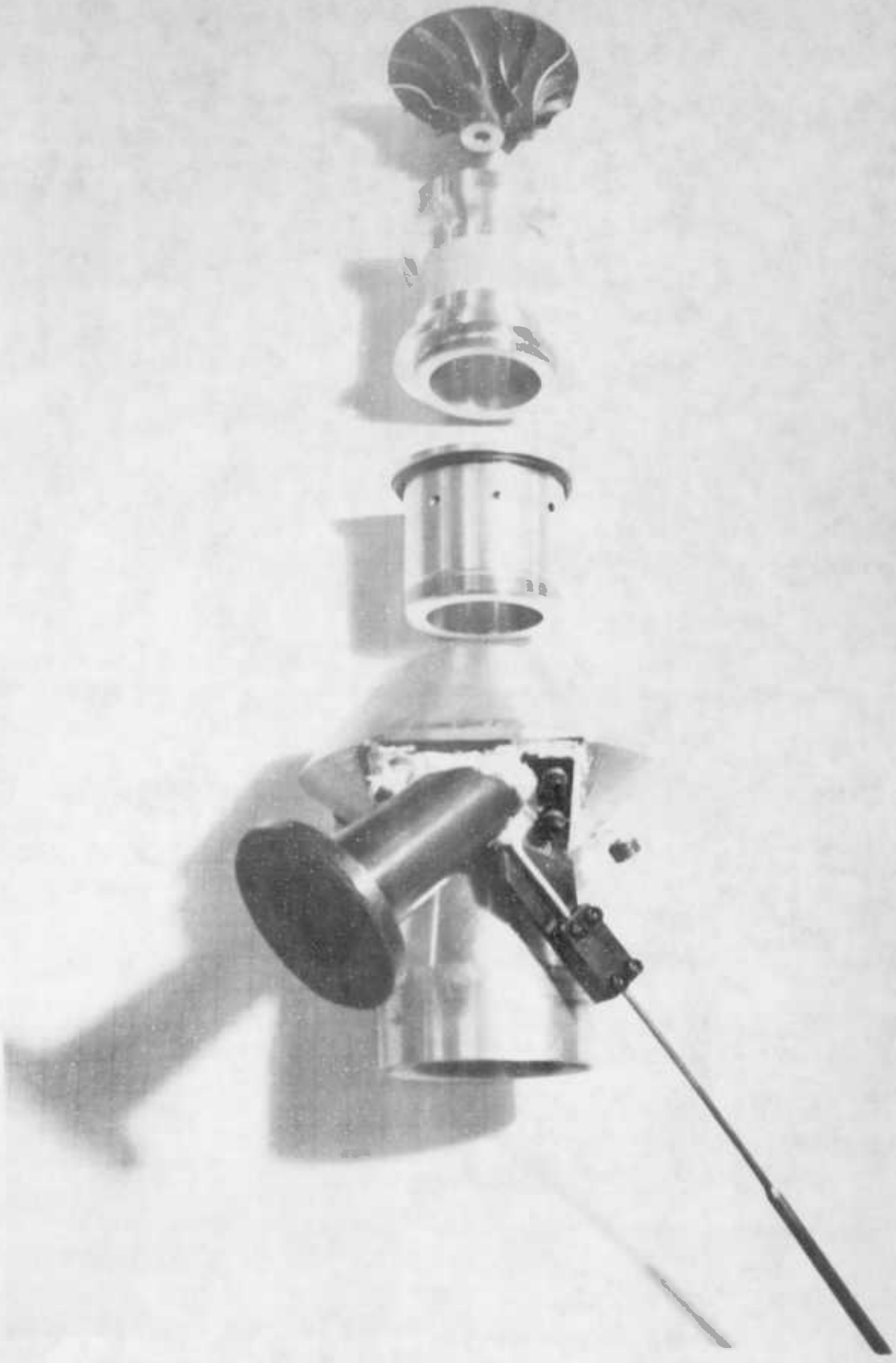


Fig. 6.16 Impeller 6521F, 50 mm Extension Piece, 70° Nozzle Ring and Inlet Adaptor

of its considerable overhang weight the turbocharger-adaptor assembly was mounted directly to the engine block via a bracket.

The experimental arrangement is shown schematically in Figure 6.17 and also in Figure 6.18, 6.19 6.19a. All the control valves were manually operated. The compressor discharge plenum volume was approximately equal to the FORD YORK engine inlet manifold volume, to cancel any influence on compressor surge characteristics in subsequent tests. The compressor mass flow was measured using two different size BS1042 nozzles to cover the whole flow range. The recirculation mass flow was measured using a calibrated pitot static tube and a micromanometer. This was done to minimise the pressure losses in the recirculation line. As a safety measure, the turbocharger was enclosed in protective steel plates.

Two methods were considered for turbocharger speed measurement:

1) A magnetic pick up. In this system the (rotating) magnetic field produced by transversely magnetising the compressor wheel retaining nut, is sensed by the voltage induced in a search coil. Structural constraints dictated that the search coil had to be placed outside the duralumin inlet adaptor. The adaptor walls would tend to screen all the high frequencies, hence this method was not adopted.

2) An optical tachometer. In this method (115), light is directed through flexible glass fibre bundles to the compressor impeller and is reflected off the compressor blade

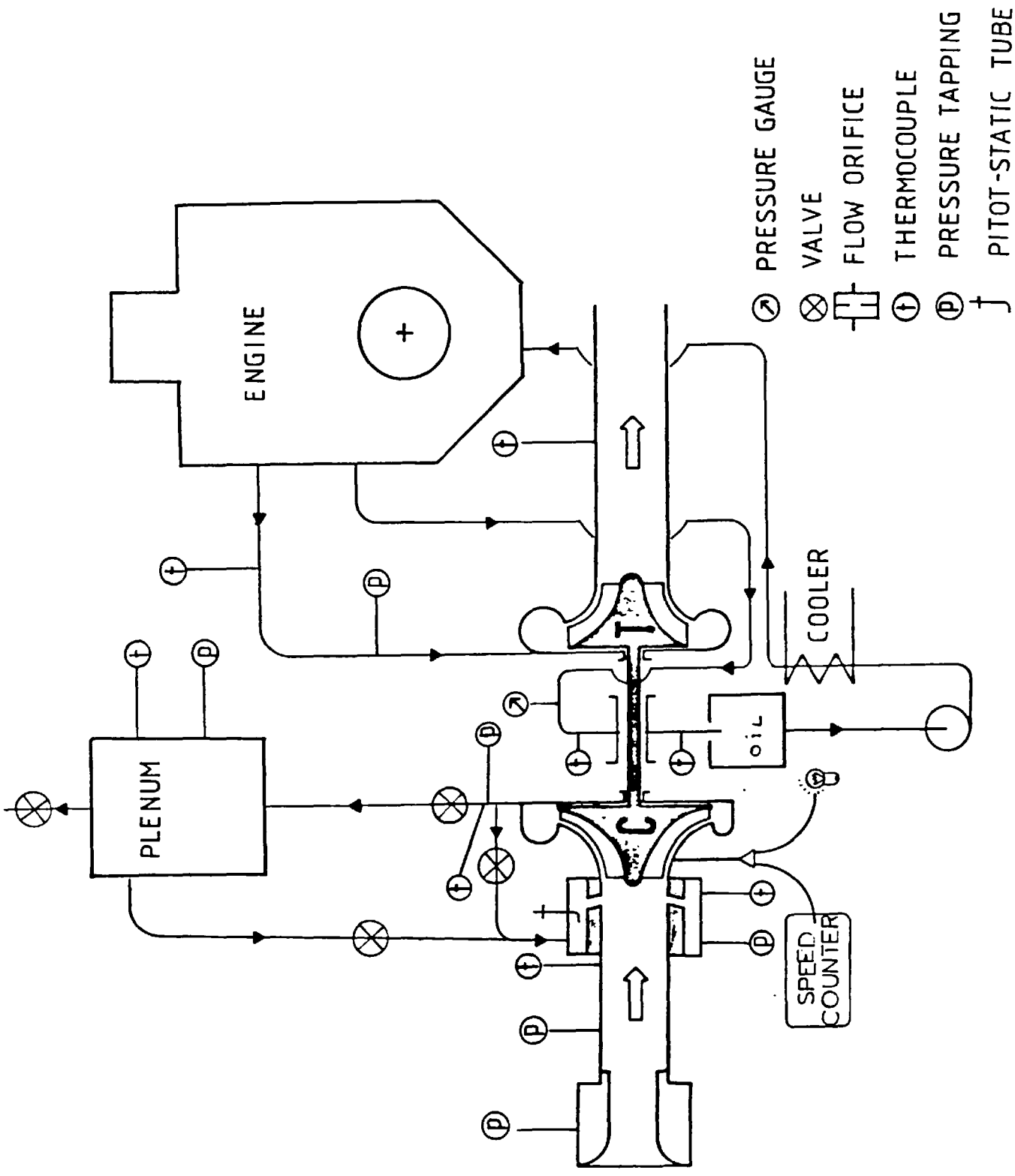


FIG.6.17 H1A Compressor Experimental Rig with FORD YORK Engine Driving the Turbine

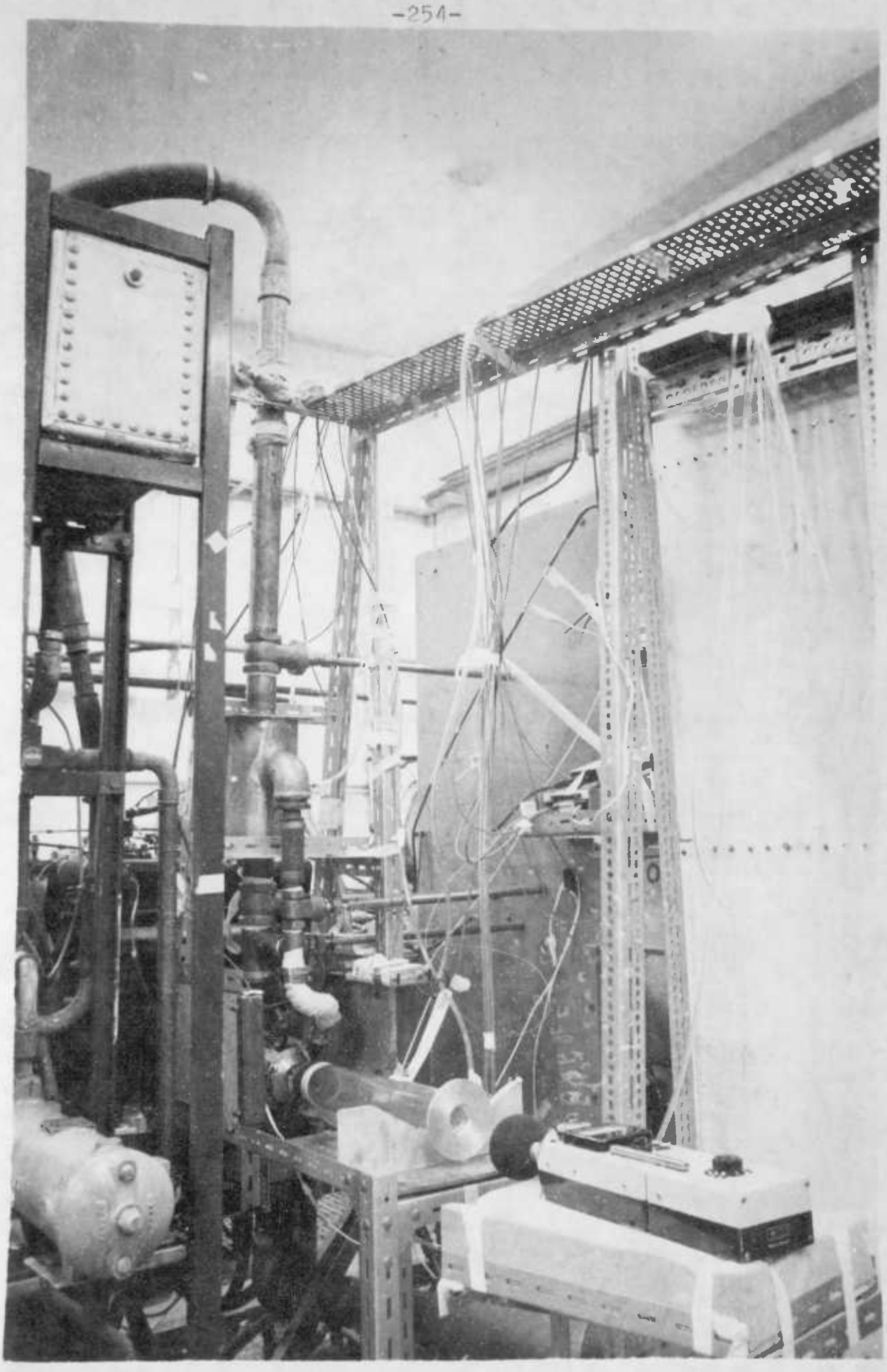


Fig. 6.18 Overall View of the H1A Compressor Test Rig.
The Noise Meter is in Front of the Inlet Pipe.

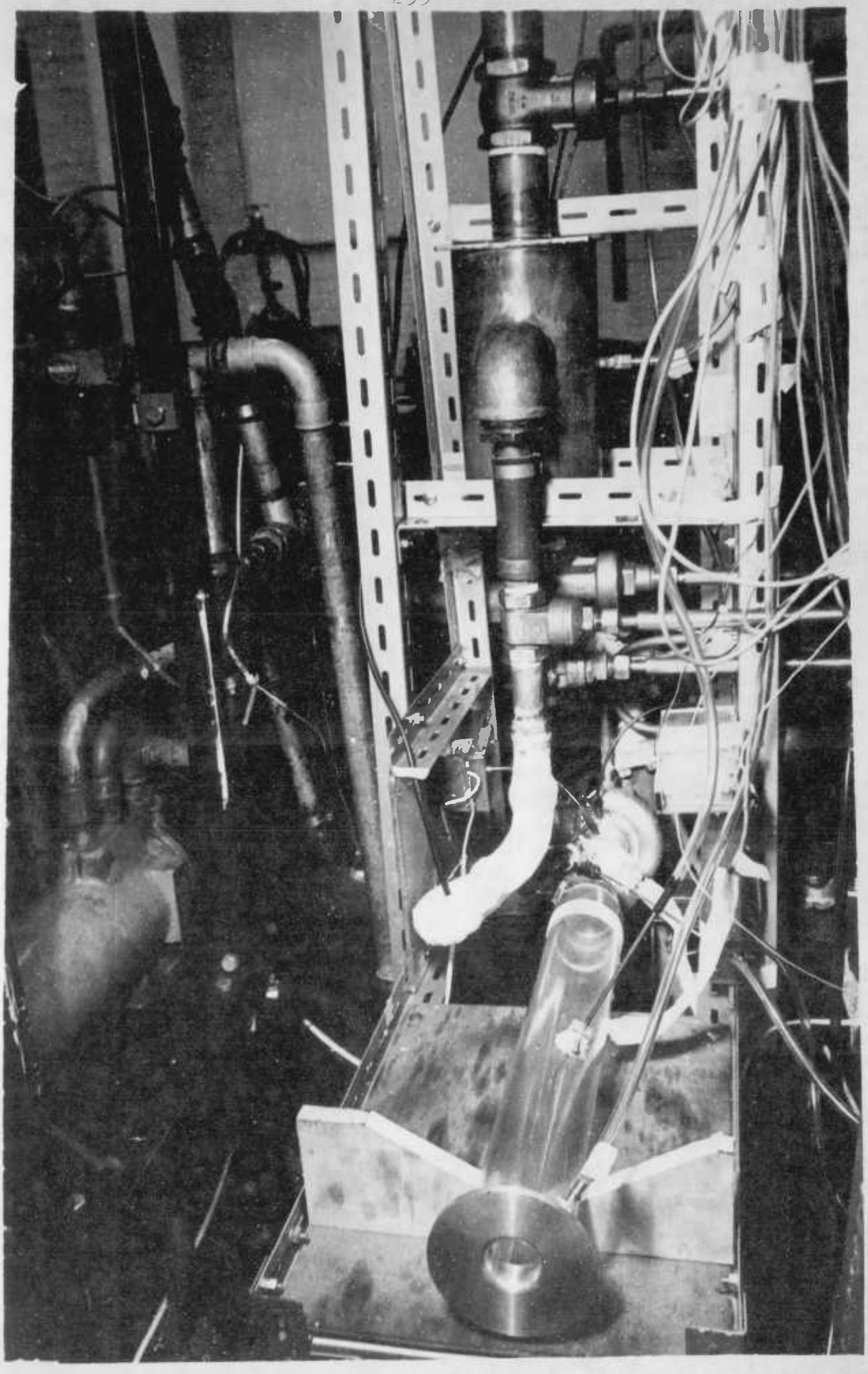


Fig. 6.19 Front View of the H1A Compressor Rig

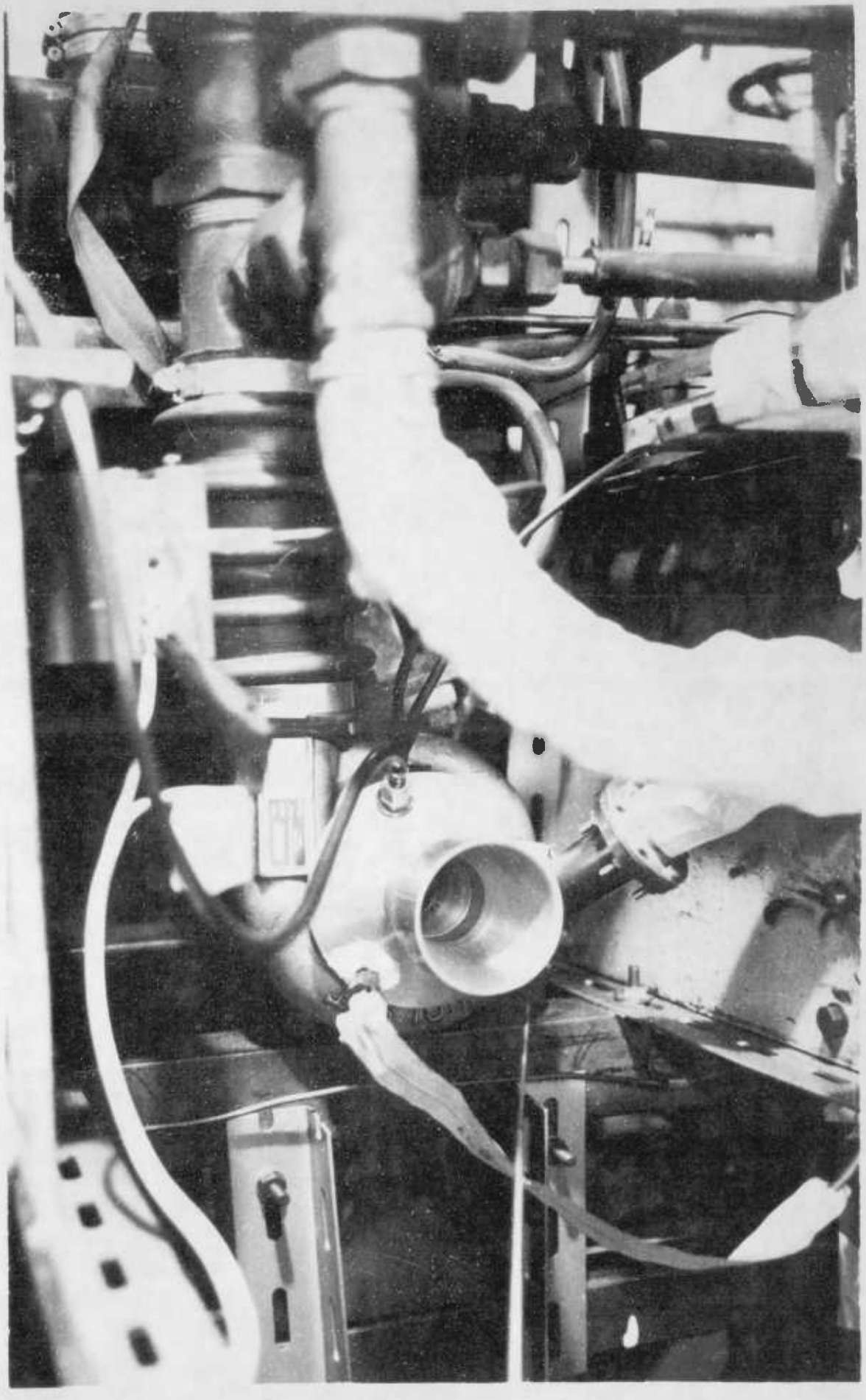


Fig. 6.19a Close-up of H1A Compressor Showing Nozzle Ring Adaptor

edges, triggering a light activated switch (LAS). Since the turbocharger speeds envisaged were high, to conform with the switching characteristics of the LAS, it was endeavoured to get the signal off one blade only.

In past experiments when this system had been used, matt black paint was applied to all but one blade, and the latter was polished to enhance reflection. However this technique was not very successful, since the paint was abraded at extreme operating conditions.

To avoid this, the aluminium alloy compressor wheel was anodised and then dyed using a black cotton dye. In this way the dye is locked inside the porous aluminium oxide layer formed by anodising and is very resistant to wear. One of the blade tips was masked during anodising and then polished.

The compressor stability limits were to be defined using a noise meter in front of the compressor inlet duct (See Section 4.10.3.6.1/2). With the experimental arrangement used however, the engine broad band noise was superimposed on the turbocharger noise. This would make the definition of the stability limit at high speeds more difficult by narrowing the choice of suitable filters.

6.8.2 The Experiments

Four sets of experiments on the compressor performance were conducted.

1) With the 70° jet arrangement.
2) With the 90° jet arrangement.
3) With the 70° jet plus extension piece.
4) With the 90° jet plus extension piece.

The testing schedule was as follows:

For a chosen compressor speed and a given back pressure valve setting, the recirculation valve was opened in predetermined steps. The speed was regulated, and after a settling time of 5 minutes the readings were taken. This was repeated until a "critical condition" (see Sections 5.4.2 and 4.10.3.6.3) was reached, or the recirculation valve was fully open. The back pressure was then increased in steps and the whole procedure was repeated until the unstable range was entered.

The compressor stability limit without recirculation at that speed, was defined using the noise meter. Then the procedure was repeated but both the back pressure and recirculation were changed in smaller steps.

A 10 minute settling time was allowed between different speeds. The operating envelope of the diesel gas generator allowed turbocharger speeds up to N = 80000 to be obtained. The experimental information was processed and the following parameters were obtained for each experimental point.

- Compressor speed
- Net mass flow (cross flow or engine flow)
- Total pressure ratio
- Recirculation mass flow (jet flow)
- Compressor efficiency
- System efficiency (see Section 5.4.7)
- Ratio of jet to cross flow velocities
- Ratio of jet to cross flow mass
- Ratio of jet to total flow mass
- Power required by compressor

6.8.3 Observations

(These comments apply mainly to the experiments with the 70° jet design, since this was subsequently found to give the best performance).

At compressor speeds N = 30,000; 40,000; 50,000 rpm the 500 Hz filter was used in the noise meter. The stability limit could be defined very sharply. At N = 30,000 on reducing the mass flow further, after an initial noise increase, a relatively quiet region was encountered. It was thought that the first indication of instability may be due to rotating stall and the quiet region to precede full surge. At the same speed, by suitable regulation of the recirculation, zero net flow was achieved.

An oscillation of the noise level near the N = 40,000 rpm defined stability limit was possibly caused by rotating stall (see Section 2.5.4).

At N = 50,000 rpm a "critical" condition (see Sections 5.4.2 and 4.10.3.6.3) was reached. While still inside the stable operating range, excessive recirculation caused local backflow in the inlet duct. As the recirculation increased, the compressor could not process all the flow at the prevailing inlet flow angles and some of the flow turned upstream. This initial excitation was apparently amplified by a possible resonance in the inlet duct, and a "surge" at the inlet phenomenon occurred. The ensuing oscillation of the flow was clearly observed with the noise meter. This phenomenon was also observed at other instances beyond the nominal stability limit.

No violent surging was observed at these low speeds, but rather, a gradual degradation of the stable flow, witnessed by increased noise level (see Section 2.5.3.2.1/2). At speeds N = 60,000 rpm and higher the 2,000 Hz or 8,000 Hz filters were used for defining the stability limit. The performance of these was not as good as the 500 Hz filter at lower speeds.

Especially at high speeds, some oil escaping from the turbocharger lubrication system, was carried round with the recirculation as fine mist, and was deposited on the inlet wall by the centrifugal field, condensing and subsequently trickling along the shroud. Although this did not affect the compressor performance, it created problems with the speed sensing device.

On shutdown immediately after surging, oil traces were observed moving helically upstream along the inlet wall with a helix angle of 15°, indicating the direction of the backflow near the wall. Full surge was only reached a few times to prevent any possible structural damage to the unit.

The signal from the speed sensing device can be used to indicate full surge, if suitably processed, and if the compressor power can be kept reasonably constant. Because of the flow reversals and the consequent torque reversals within the compressor, associated with surge, an oscillation of the compressor speed will result. Such oscillations (±360 rpm at N = 60,000) of the instantaneous compressor speed during surge were observed.

6.8.4 Results

6.8.4.1 Introduction

From the four sets of experiments it was concluded that the performance of the compressor was best overall when using the 70° jet arrangement. Hence the following sections refer to that arrangement. A comparison of the different arrangements will then follow.

6.8.4.2 Improvement in surge margin

(N.B. The term "surge" is adopted here as equivalent to the defined stability limit.)

Shown in Figure 6.20 is the projection of the (3-D) v.p. compressor map on the $r_p - \dot{m}_\varepsilon$ plane. The net compressor flow would be the engine flow in a turbocharging application and is denoted as such in Figure 6.20. The movement of the surge line to the left can be seen. The surge line on the left (with jets) corresponds to the locus of the points of minimum compressor flow achieved adjusting the jet flow, for the defined stability limit at each speed. There is an inward kink of the surge lines at N = 50,000. Since this discontinuity appears in the manufacturers' compressor performance map as well (see Figure 6.8), it is possible that instability is precipitated by different mechanisms at low and high speeds.

It is mentioned in the literature that, as a general rule, centrifugal compressors with vaned diffusers surge at low speeds mainly because of impeller (inducer) stall, while at high speeds the diffuser stalls first (see Section 2.5.9). Although the test compressor has a vaneless

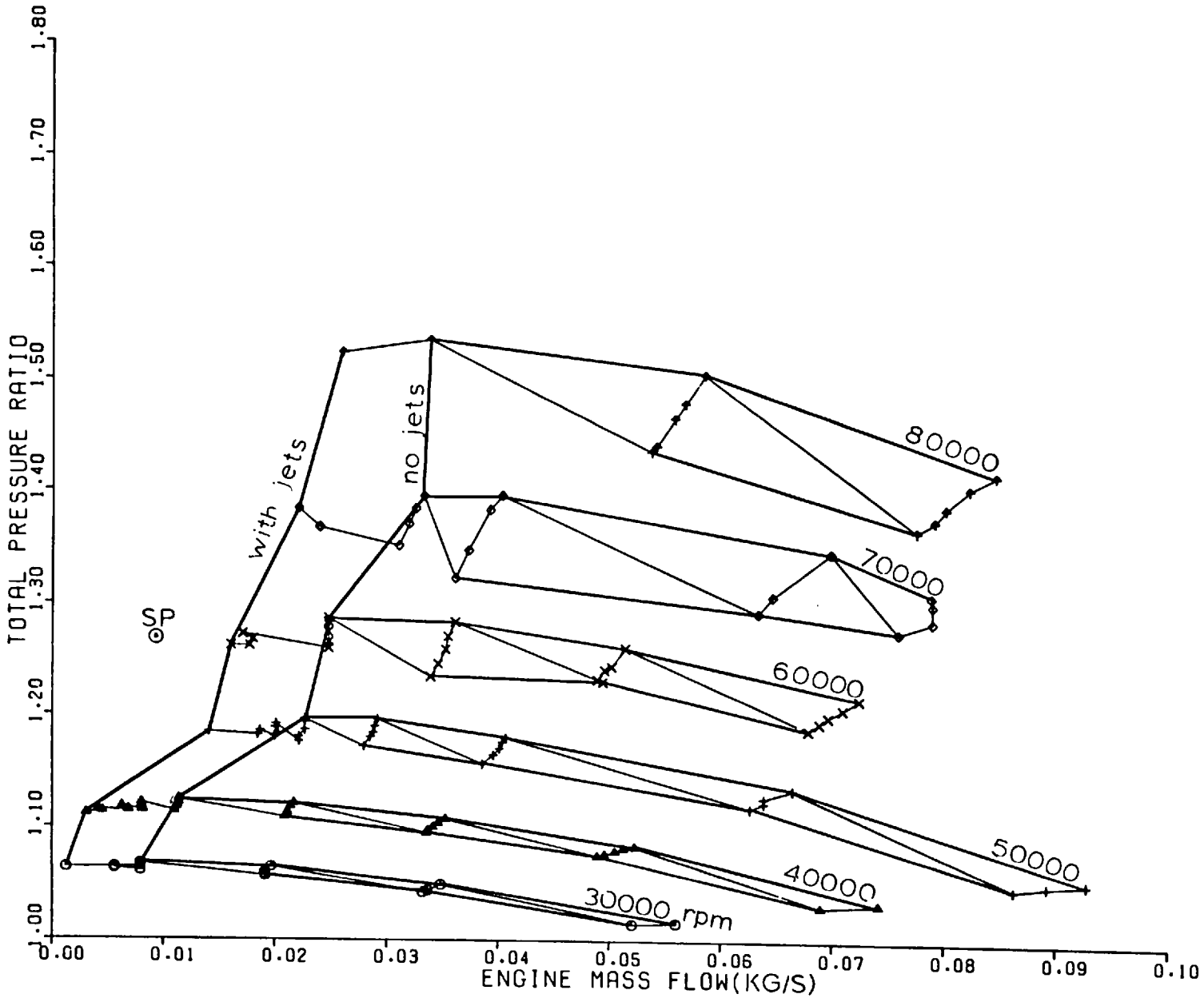


FIG.6.20 H1A-6521F (3-D) v.p. Compressor Map

diffuser it is possible that the above is true in the present case.

A change in the flow pattern inside the impeller channel at low and high speeds is also a possible cause for the observed behaviour (see Table 6.3 and Block 4 notes). The percentage improvement in surge margin at any speed may be defined as:

$$\left(1 - \frac{(\dot{m}_s)_i}{(\dot{m}_s)_N}\right) * 100$$

where

$(m_s)_i \equiv$ minimum mass flow rate with surge inhibiting device

$(m_s)_N \equiv$ minimum mass flow rate for standard compressor

The improvement in surge margin for different speeds is shown in Table 6.7 Col. 4. The percentage contribution of prewhirl to this improvement was found by subtracting the recirculation flow from the surge flow $(m_s)_N$ and is shown in Table 6.7 Col. 8.

In general, fairly conservative stability limits were defined, to prevent mechanical damage. However, the compressor was brought to full surge at N = 60,000, under carefully controlled conditions, since the system was in an unstable balance, which could be destroyed by any sudden changes to the settings. The recirculation was adjusted as the net flow was decreased, to avoid reaching a critical condition.

The operating point SP is shown in Figure 6.20 and

TABLE 6.7

Speed (RPM)	Engine Flow @ Normal Surge $\dot{m}_{s_N}$ (kG/s)	Engine Flow @ Inhibition Surge $\dot{m}_{s_i}$ (kG/s)	% Improvement in Surge Margin $(1-\frac{\dot{m}_{s_i}}{\dot{m}_{s_N}})*100$	Recirculation Flow (Jet Flow) $\dot{m}_j$ (kG/s)	$\dot{m}_{s_N}-\dot{m}_{s_i}$	$\frac{\dot{m}_j}{\dot{m}_{s_N}-\dot{m}_{s_i}}$	% Contribution of Prewhirl
30000	0.00794	0.0126	84	0.00471	0.00668	0.71	29
40000	0.01137	0.00307	73	0.00656	0.00830	0.79	21
50000	0.02263	0.01403	38	0.00745	0.00860	0.87	13
60000	0.02479	0.01602	35	0.00800	0.00877	0.91	9
70000	0.03333	0.02210	34	0.00994	0.01123	0.89	11
80000	0.03391	0.02603	23	0.00494	0.00788	0.63	37
60000 Special Min.Flow Point (r_p=1.27)	0.02479	0.00972	60	0.00757	0.01507	0.50	50

the results in Table 6.7 Row 7. A 60 per cent improvement in surge margin was obtained, with prewhirl contributing 50 per cent to it.

The contribution of prewhirl to the improvement in surge margin can be seen to vary for different speeds. It seems that the prewhirl induced by the jet arrangement becomes more effective in stabilising the compressor as the speed drops below N = 50,000, in which case it is possible that the inducer is stabilised.

The largest contribution (excluding the special point, SP) can be seen at N = 80,000. This does not fit the above explanation and may have resulted from a happy combination of the relevant parameters (such as recirculation, velocity triangles, stability limit definition).

6.8.4.3 Drop in pressure ratio

The projection of each speed surface on the $\dot{m}_\varepsilon$ - r_p plane can be seen in Figure 6.20. As the jet flow is increased at constant speed the pressure ratio decreases. This drop in pressure ratio becomes larger at higher speeds. The net compressor flow decreases as the jet flow is increased. This throttling effect of the jets to the cross flow had also been observed in earlier experiments (see Section 4.10.2.3).

6.8.4.4 Recirculation jet flow

Shown in Figure 6.21 are the projections of the speed surfaces on $\dot{m}_\varepsilon$ - m_j planes, assembled so as to give an impression of the (3-D) compressor map (axonometric). It can be seen that, in terms of compressor total flow, the

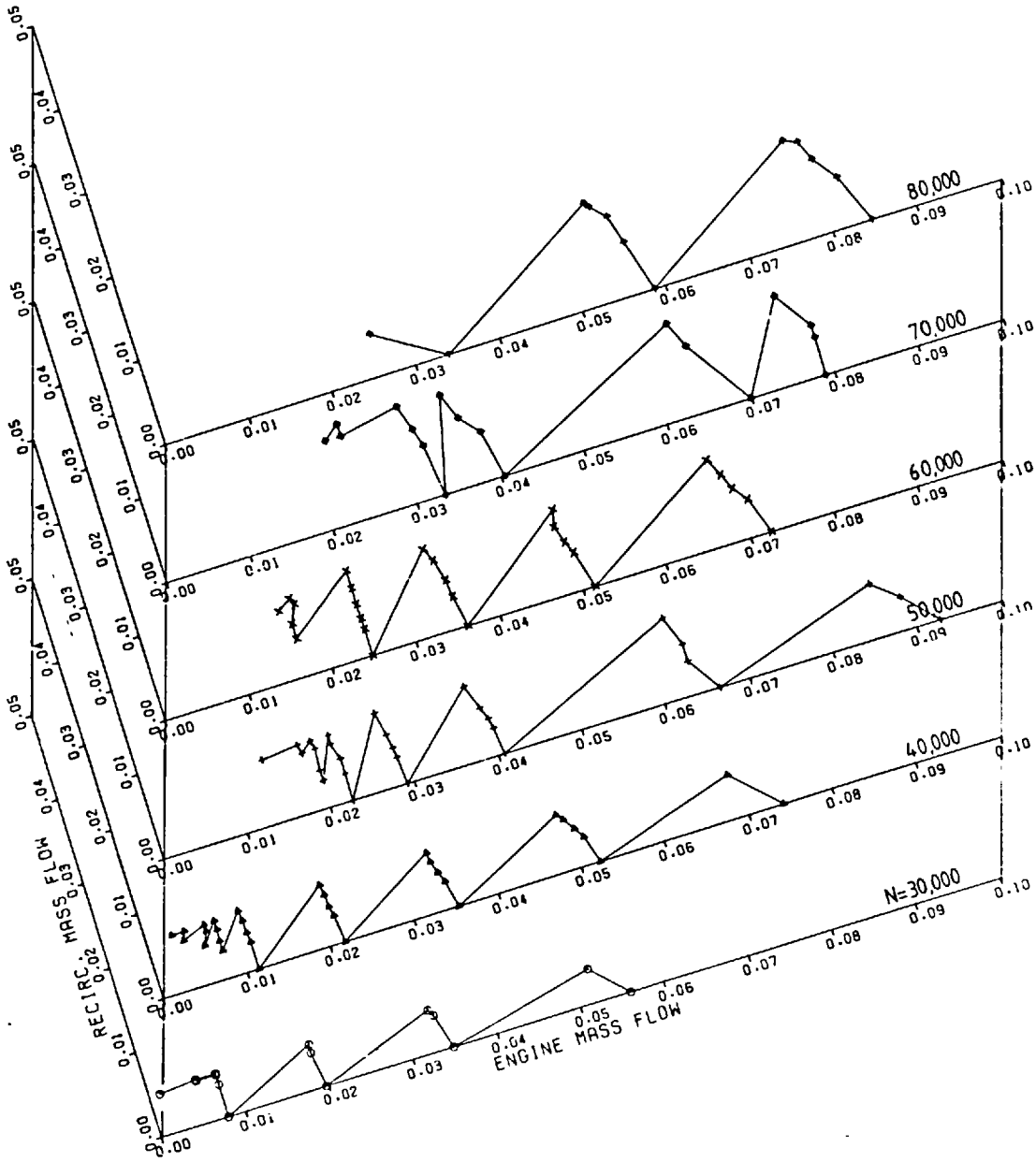


FIG.6.21 H1A-(3-D) v.p. Compressor Map

recirculating jet mass flow more than compensates for the drop in net flow due to the throttling effect of the jets. It would appear then that the action of the jets increases the absolute approach velocity of the flow to the compressor, in addition to presenting "easier" inflow angles for the inducer. The latter however is reflected as a drop in discharge pressure.

6.8.4.5 Efficiencies

The efficiency contours for the standard compressor without recirculation (η_c) are shown in Figure 6.22. The maximum efficiency region lies well inside the stable flow range. The compressor efficiency (η_c) contours for the different constant speed surfaces of the v.p. compressor, projected on $\dot{m}_e$ - $\dot{m}_j$ planes are shown in Figure 6.23, assembled so as to give a (3-D) impression (axonometric). It can be seen that in general the compressor efficiency increases as the jet flow is increased.

The contours exhibit two distinct patterns. At low speeds (N = 30,000; 40,000) the maximum efficiency is where the ratio of jet flow to "engine" flow is at a maximum. A long thin high-efficiency island extends from that point towards the maximum efficiency point of the standard compressor at that speed. As the speed increases a second high efficiency region is created at higher "engine" flow, but still maximum recirculation. Eventually the first region disappears and the maximum efficiency point shifts to the second region. The efficiency islands grow in size as the speed increases.

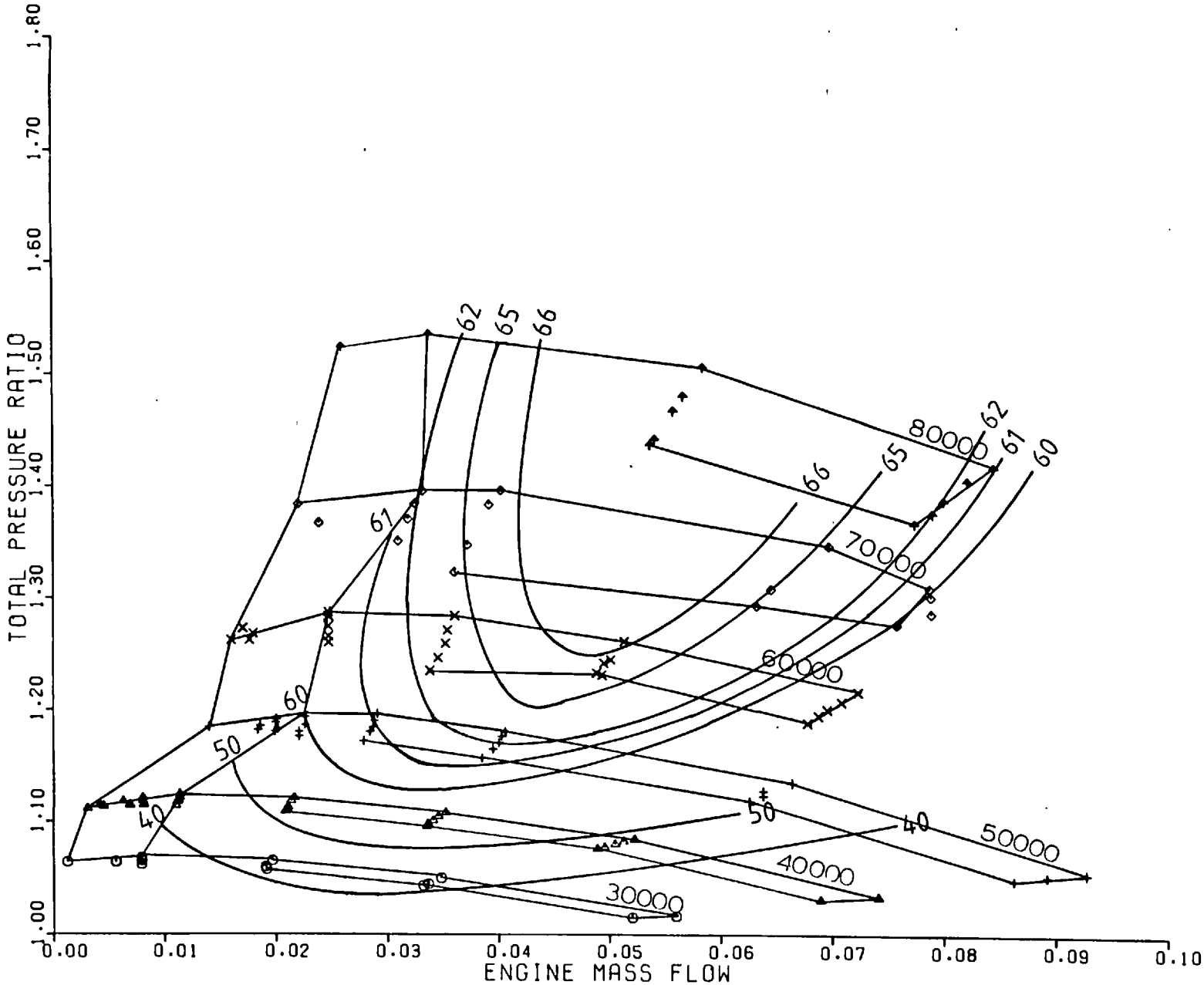


FIG.6.22 H1A-6521F Efficiency Contours

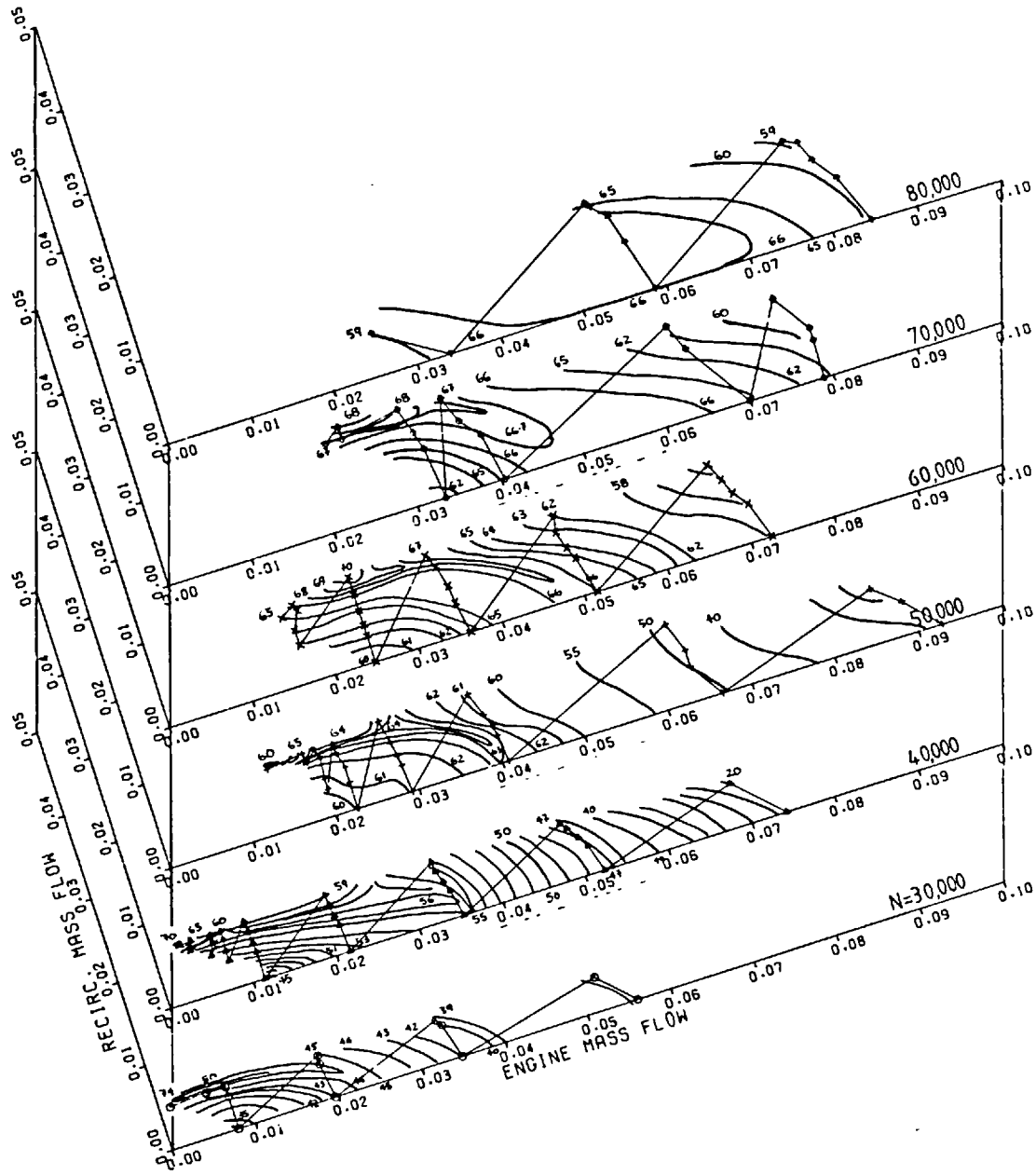


FIG.6.23 (3-D) v.p. Compressor Efficiency Contours

High maximum compressor efficiencies were obtained at all speeds. This must be due to the better inflow angle distribution hence better blading efficiency. Also at very high velocity ratios, the inlet relative flow direction is possibly such that positive work is done on the impeller. The latter may explain the first high efficiency region obtained at low speeds, while the former is likely to be the cause of the second high efficiency region at higher speeds.

It can be seen that there can be an optimum path for an operating point on the (3-D) v.p. compressor map, which will keep it within the high efficiency islands. It must be noted that because of inadequate information the contour arrangement for N = 80,000 was based on the established pattern at lower speeds. Shown in Figure 6.24 are the overall system efficiency (η_T) contours for the different constant speed surfaces of the v.p. compressor, projected on $\dot{m}_\varepsilon$ - m_j planes in axonometric assembly.

As the jet flow is increased η_T is reduced, mainly because of the recirculation of hot discharge air which increases the intake temperature. There is also a possibility of inlet flow-blade mismatch under certain conditions.

6.8.4.6 Velocity ratios

The contours of maximum available velocity ratio (R) of jet flow to cross flow ("engine" flow) are superimposed on the v.p. compressor map in Figure 6.25. It can be seen that the curves are not straight lines as had been assumed in the results of earlier experiments (see Section 4.10.2.6). High velocity ratios are available near the

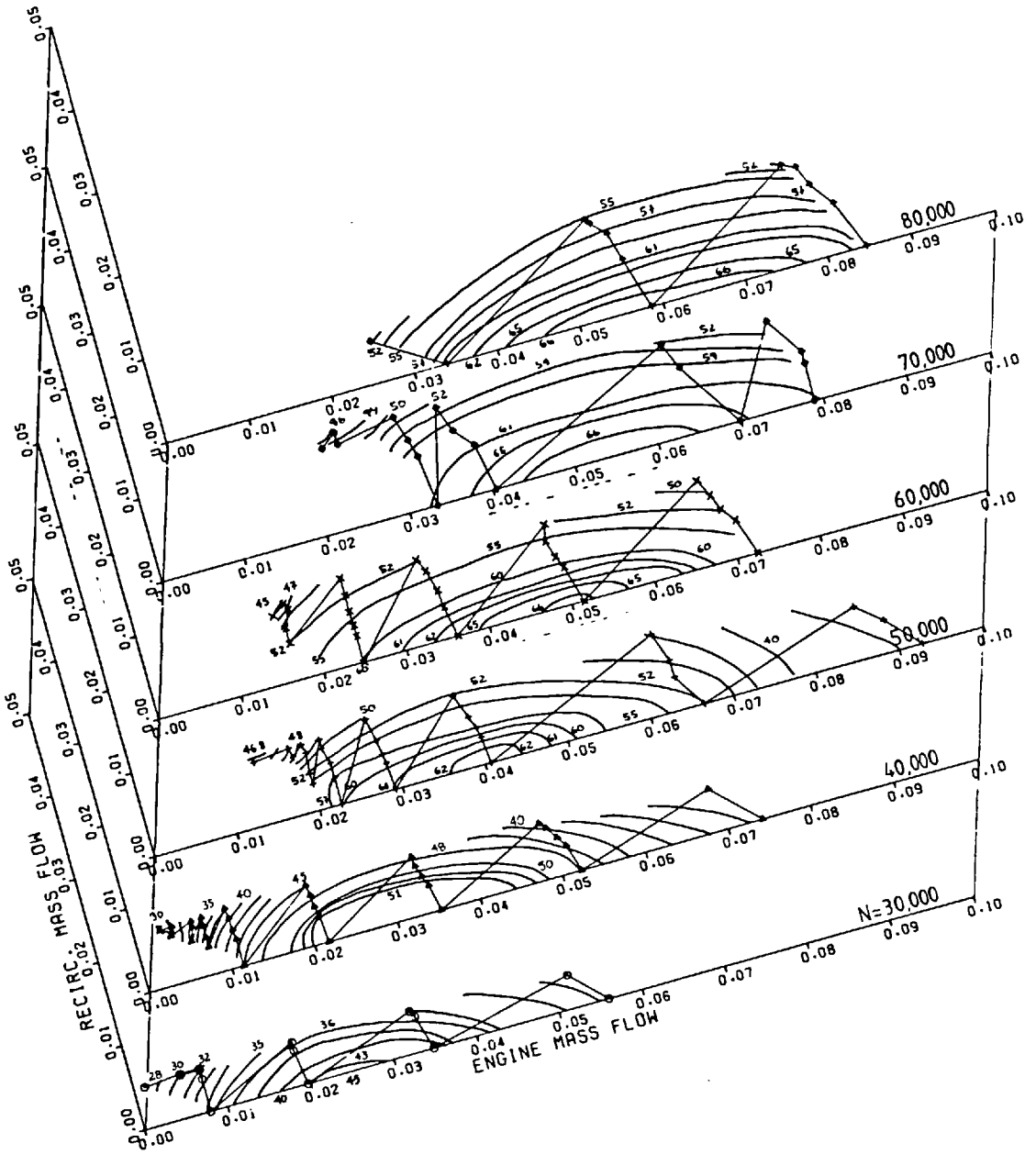


FIG.6.24 (3-D) v.p. Compressor System Efficiency Contours

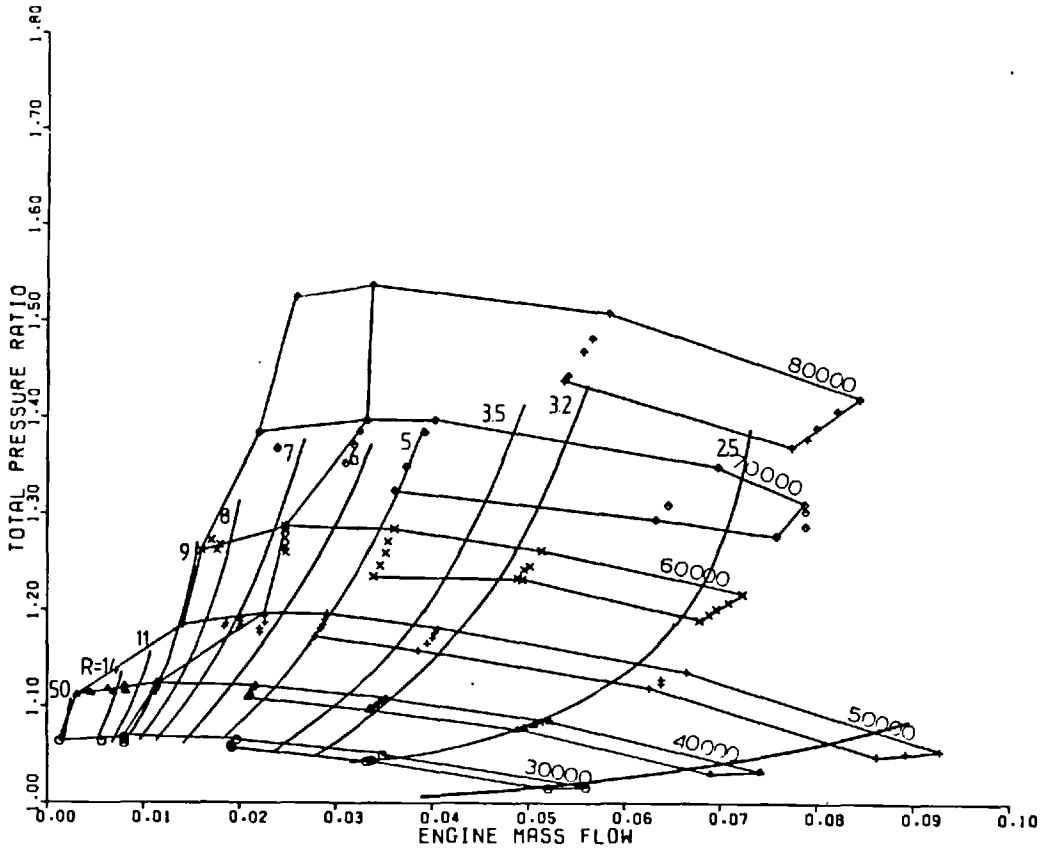


FIG.6.25 Constant Velocity Ratio Lines

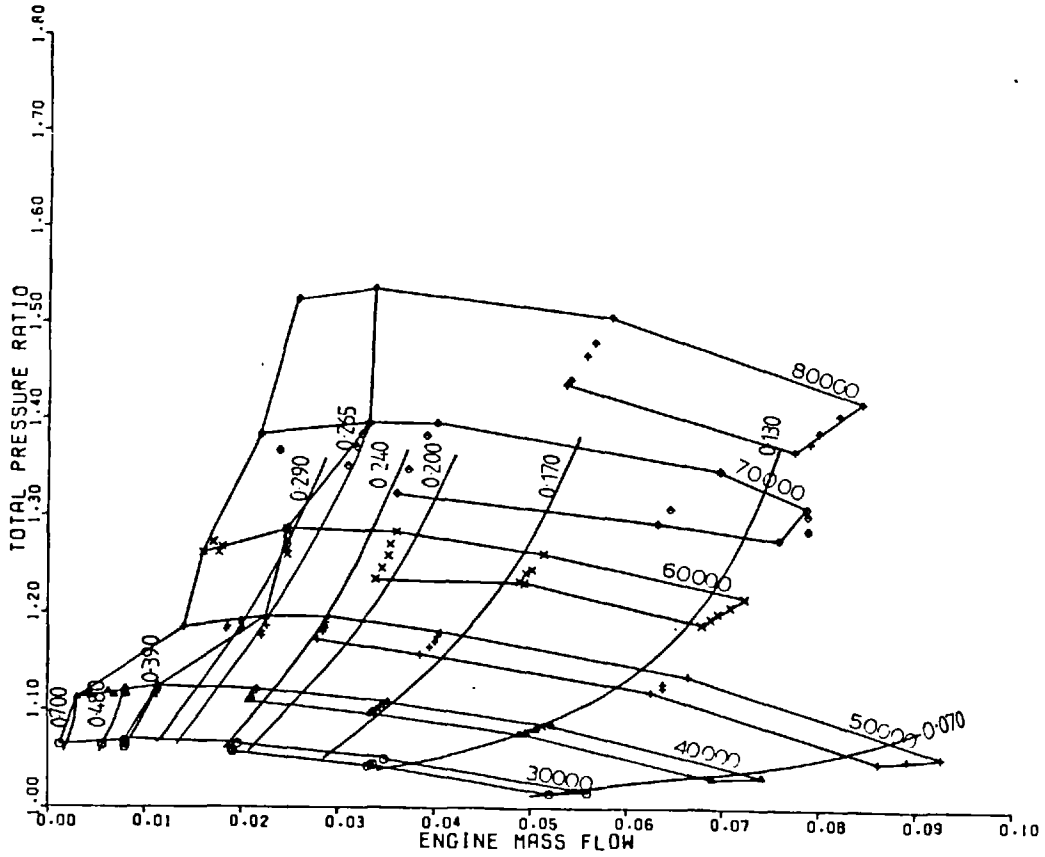


FIG.6.26 Constant Mass Ratio Lines

surge line (R > 7). In problem region II the availability is quite low (2.5 < R < 3.5).

6.8.4.7 Mass ratios

The contours of maximum available mass ratios (recirculation jet flow to total compressor flow) superimposed on the v.p. compressor map is shown in Figure 6.26.

In problem region I, it is possible to recirculate 30 - 50 per cent of the flow with this jet arrangement, while in problem region II only 13 - 20 per cent recirculation is possible. The curves are similar to the velocity ratio curves (see Figure 6.25).

6.8.4.8 Compressor power

The contours of compressor power for the standard compressor without jet flow are shown superimposed on the compressor map in Figure 6.27. The respective contours with full jet flow are shown in Figure 6.28. The latter ones must be viewed in relation to the lower of each pair of constant speed lines, which corresponds to the maximum recirculation-flow edge of a constant speed surface in (3-D).

Higher power is required with recirculation jet flow at the same speed since the total compressor flow is higher, although prewhirl reduces the difference. An impression of the constant power surface in 3-D is shown in Figure 6.29.

6.8.4.9 Comparison of jet arrangements

In Figure 6.30 the performance of the 70° jet arrangement (A70) and the 90° jet arrangement (A90) design is compared at the two problem regions. The background in

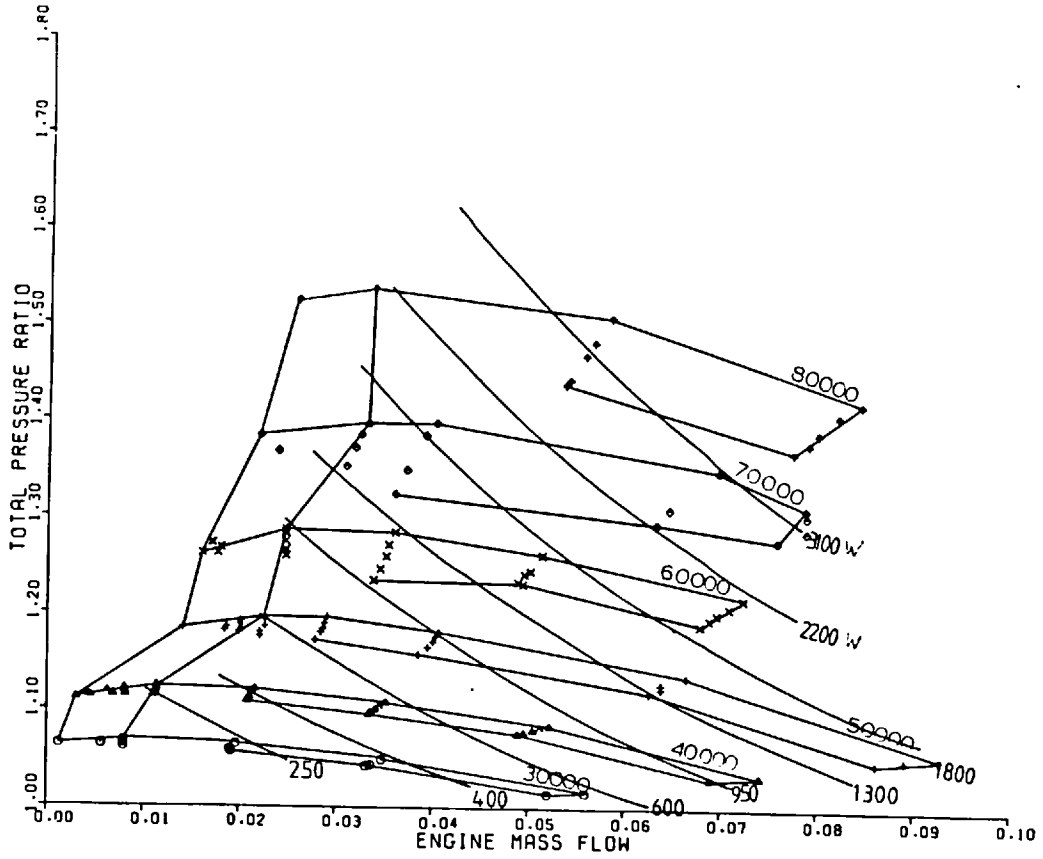


FIG.6.27 Standard Compressor Power Contours (WATTS)

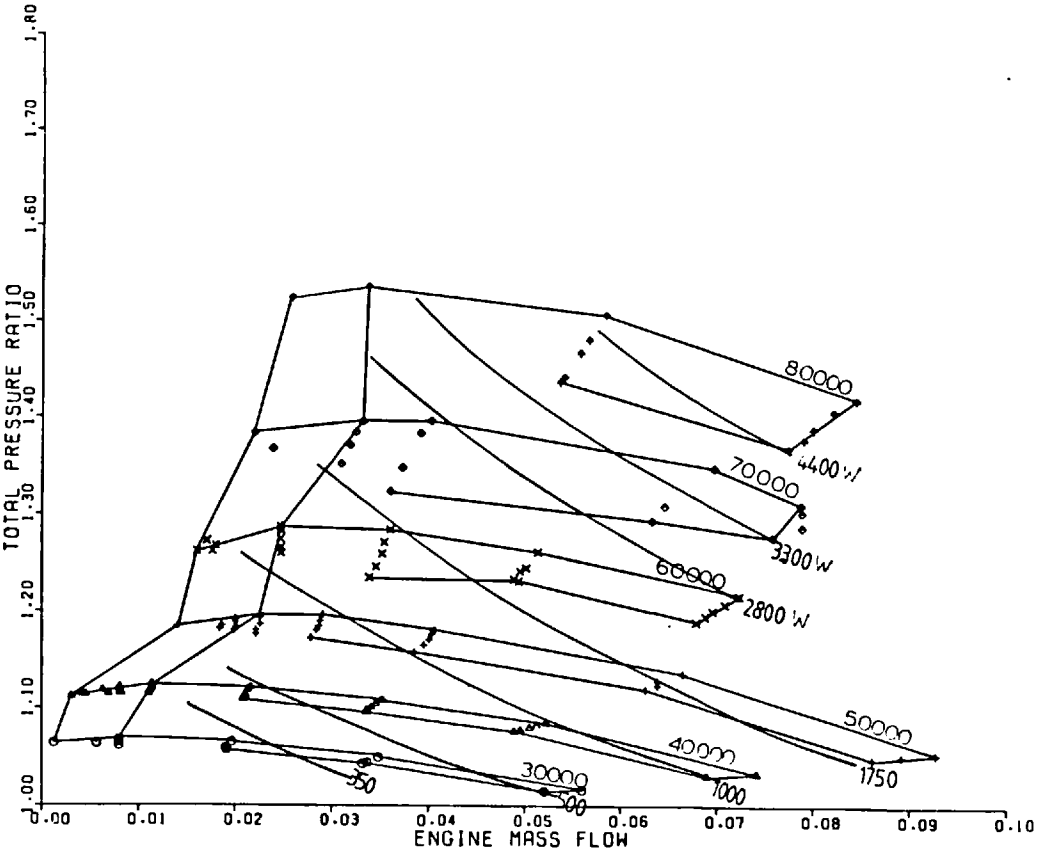


FIG.6.28 Full Jet Flow Power Contours (WATTS)

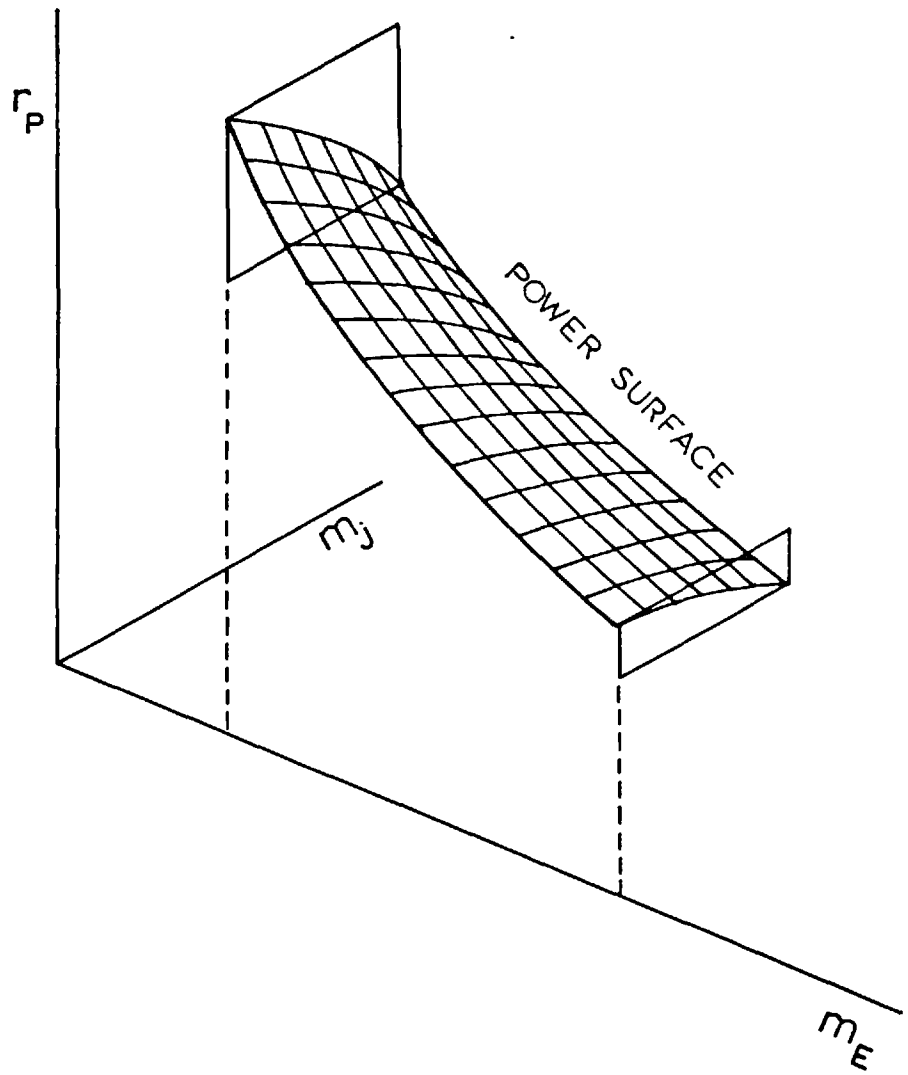


FIG.6.29 Impression of Power Surface

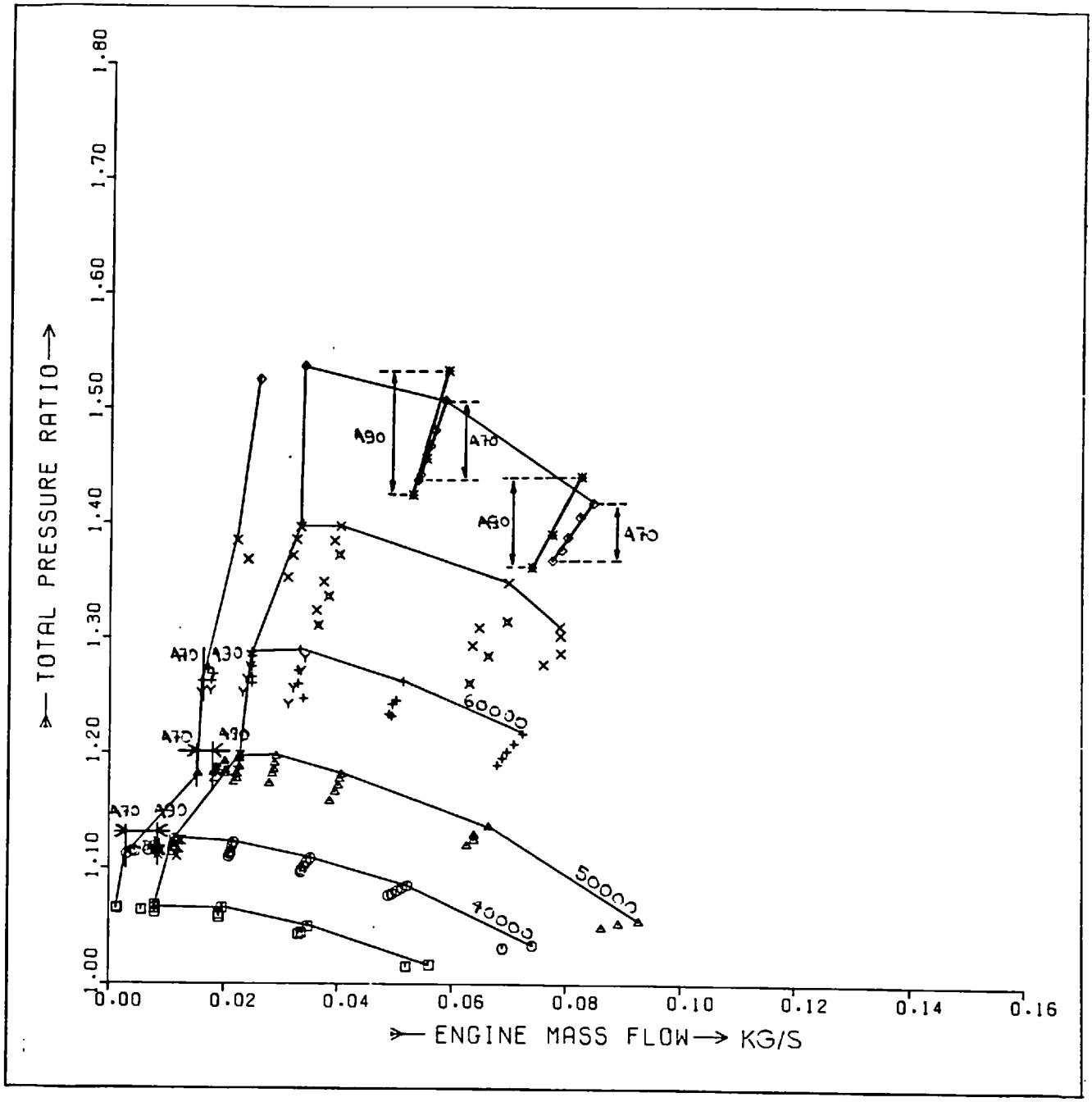


FIG.6.30 Comparison of the Performance of Two Jet Designs with 70° and 90° Initial Ejection Angle

Figure 6.30 is the A70 compressor performance map. In problem region I the minimum values of "engine" mass flow that was achieved with the two designs, i.e. the movement of the surge line, is compared. It can be seen that the deficit of A90 increases as the speed is decreased. As the velocity ratio increases, A90 has backflow problems while A70 can tolerate much higher velocity ratios without becoming "critical". Another possible explanation for the poor performance of A90 in that region, is that the jets are situated very close to the inducer and their wakes may influence adversely the impeller stability (Section 6.7.6).

In problem region II, A90 performs better and the resulting drop in pressure ratio is larger. With this jet arrangement the penetration into the cross flow achieved for a certain velocity ratio is better hence the deflection (or prewhirl) larger.

Figure 6.31 and Figure 6.32 compare the performance of A70 with the 70° jet plus extension piece arrangement (E70) and the 90° jet plus extension piece arrangement (E90) respectively, on the displacement of the surge line, for three intermediate speeds. The extension piece moved the jet ejection plane 50 mm away from the compressor face, therefore the analysis on which the jet designs were based did not hold true. E70 performed better compared to E90 at low speeds and high velocity ratios, where E90 tended to induce "critical" flow. Both however performed worse than A70.

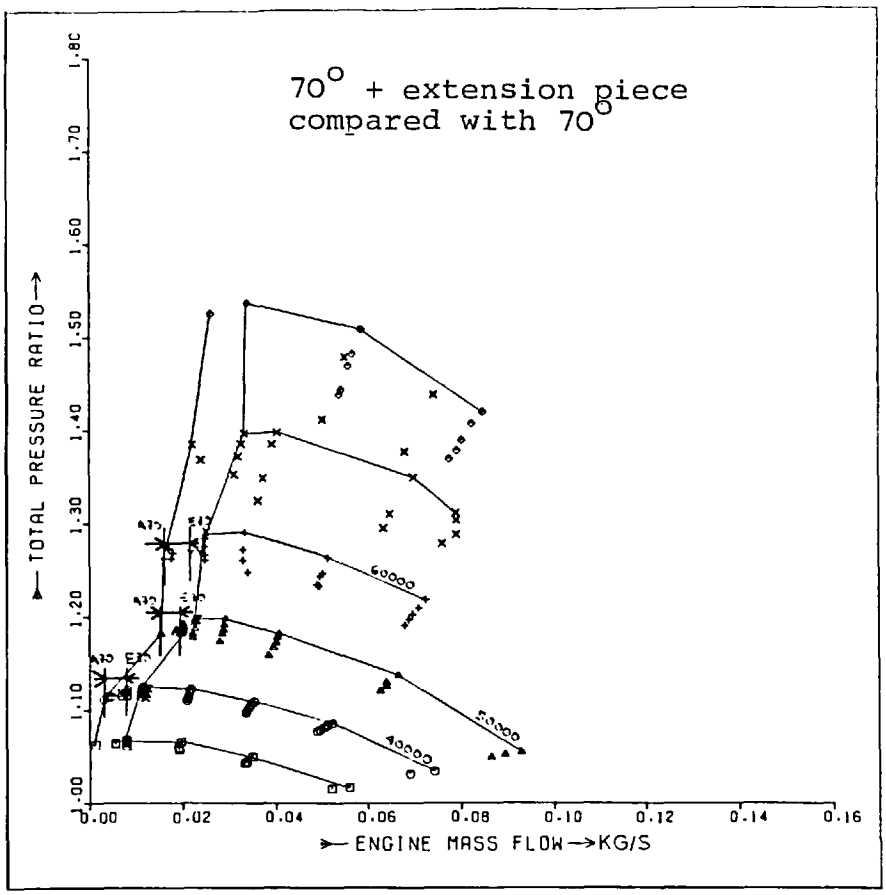


FIG.6.31 Extension Piece Influence-Comparison

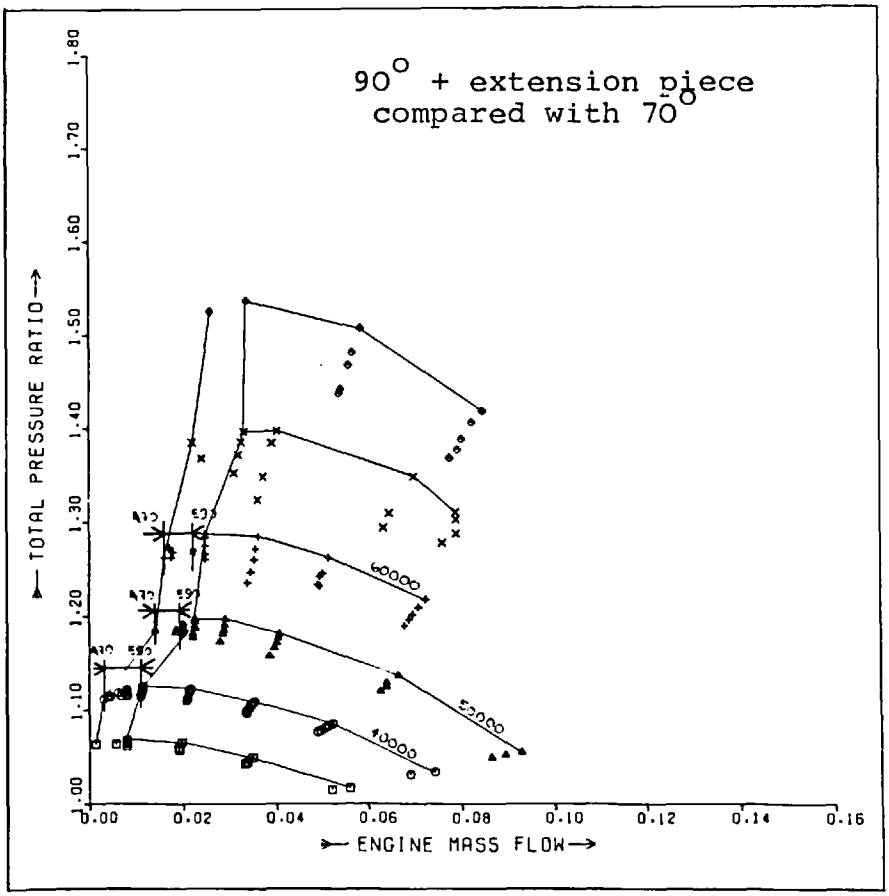


FIG.6.32 Extension Piece Influence-Comparison

With the extension piece fitted, the jets are allowed to expand and mix further, their deflection increasing in the process. After hitting the inlet pipe wall the jets continue in a helical path towards the inducer. If the velocity ratio is high the jets will concentrate near the wall and create a low pressure region along the pipe axis which may result in a "critical" condition.

The final flow profile presented to the inducer will probably be more uniform circumferentially because of the prolonged flow mixing. It appears however that the radial profile distribution was detrimental to the performance of the compressor, since the stability limits of the E70 or E90 compressor with recirculation jet flow, were reached when the total compressor throughflow was greater than the minimum standard-compressor stable flow at the same speed.

6.8.5 Comments on the experiments

The experiments gave a complete (3-D) v.p. compressor map for speeds up to 80,000 rpm. It was established that high velocity ratios hence high deflection (prewhirl) of the inflow are possible near the surge line. Conservative stability limits were chosen and all pairs of minimum stable flow, with and without recirculation, were consistent, in each case, with the definition of the noise level-stability limit relation.

It was assumed that the improvement in surge margin was due to the effects of recirculation and prewhirl only. All other factors possibly introduced by the jet arrangement and influencing the stability limit (e.g. turbulence) were not accounted for.

The contribution of prewhirl to the improvement in surge margin was generally low. The potential for better performance was however demonstrated by the special point at 60,000 rpm. The influence of prewhirl would have possibly been greater, if the compressor was designed accordingly.

The compressor efficiency was improved with recirculation. However, relatively little detail is known about the flow situation to rigorously explain the shape of the efficiency contours obtained.

Despite the low available velocity ratios at high flows, the potential for pressure drop with recirculation was satisfactory in problem region II. Larger or more jet orifices would enable higher recirculation rates at this region and thus improve the potential performance. The flow must then be appropriately regulated at problem region I to keep recirculation within acceptable limits.

Comparing Figures 6.21, 6.23, 6.24 with Figure 5.9, the limiting planes can be discerned, although the scale is different.

CHAPTER 7

THE TURBOCHARGED ENGINE SIMULATION AND EXPERIMENTAL INVESTIGATIONS

7.1 INTRODUCTION

Turbocharged engine simulation runs were performed, using the v.p. compressor map data in a suitable form in conjunction with the engine simulation program for matching predictions.

Based on the predictions from the simulation, a series of experiments was planned and executed, using the v.p. compressor to turbocharge the FORD YORK diesel engine. This was done to verify the applicability of the jet-induced pre-whirl method and the prediction ability of the simulation program.

7.2 SIMULATION RUNS

The simulation runs were planned in order to examine the interaction of the v.p. compressor and the diesel engine, over a range of operating conditions.

The results would be useful as a design tool, to pin-point any shortcomings of the jet arrangement device which were not obvious from the compressor performance tests, and suggest areas for improvement in any future designs.

The experimental data from the v.p. compressor tests was reduced to a form compatible with the engine simulation program, as dictated by the requirements of the (3-D) compressor subroutine.

However the region covered in the compressor performance experiments was limited to a maximum compressor speed $N = 80{,}000$ rpm because of experimental rig constraints. This

region could only accommodate a limited range of engine speeds. To be able to use the simulation program at higher engine speeds, the compressor map was extended to N = 110,000, using the manufacturers' performance map data and extrapolating the available experimental recirculation results.

Two recirculation data points extrapolated from the experimental results, corresponded to each additional no recirculation data point, from the standard manufacturers performance map. The expected displacement of the constant speed line, i.e. the projection of the maximum recirculation edge of a speed surfaces on the $\dot{m}_\varepsilon$ - r_p plane and the amount of recirculation, were determined by extrapolating the mass ratio curves (Fig.6.26) and the velocity ratio curves (Fig.6.25). Thus the full recirculation points for each speed were determined. The other recirculation point was placed in the middle of the line joining the full-recirculation and the no-recirculation points in the (3-D) map.

The contours for compressor efficiency (Fig.6.23) and total system efficiency (Fig.6.24) for the constant speed surfaces, were extended for the additional surfaces, using the manufacturers figures for the standard compressor as boundary conditions.

(Fig.7.1) shows the outline of the v.p. compressor map as used in the simulation. Pairs of constant speed lines are shown. The upper line in each pair is the no-recirculation standard constant speed line. The lower lines are the projections of the full recirculation edge of the constant speed surface on the r_p - $\dot{m}_\varepsilon$ plane. The standard and improved surge lines are shown.

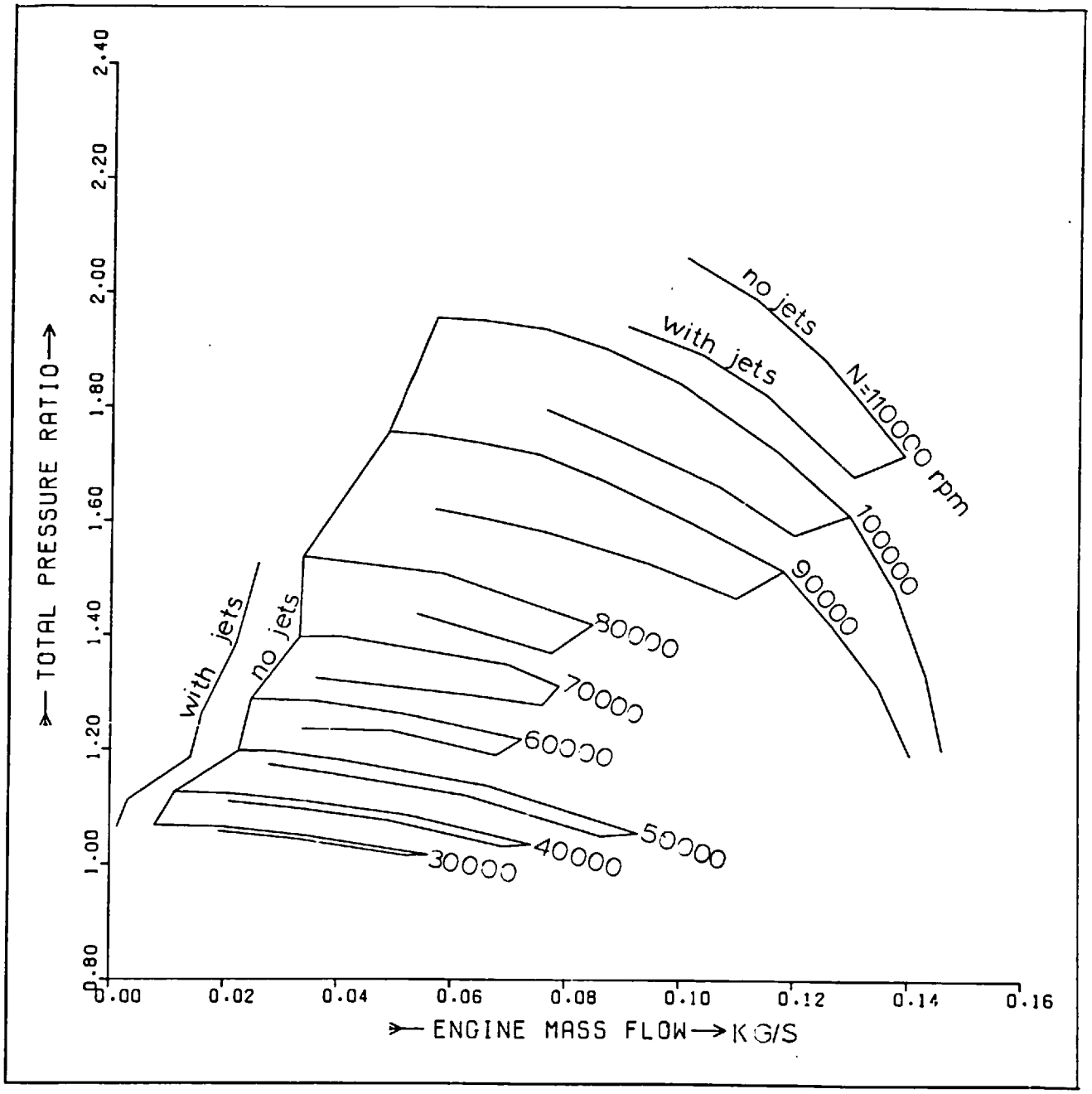


FIG.7.1 H1A-6521F Variable-Performance Compressor Map Outline, as used in the Simulation

No attempt was made to include additional improved surge points for the higher speeds, since only extended data in problem region II was required for the simulation.

The (3-D) compressor map was non-dimensionalised. Appropriate factors for the three axes were used, to preserve the proportions of the map, and prevent segregation or wide dispersion of data points. The limiting surfaces were represented by plane surfaces, defined by suitably chosen end points in the data matrix. (Section 5.4.3.)

The simulation program input data included a full geometrical description of the FORD YORK diesel engine. Heat release and ignition delay data from (105) were used to adapt VIBE type fuel burning rate functions for the cylinder and prechamber. Fuelling was based on the naturally aspirated maximum fuel delivery curve increased by 20 per cent.

Three turbine swallowing capacity curves for different size turbines were successively used to "drive" the v.p. compressor in the series of simulation runs.

The recirculation is adjusted internally from the program in an effort to keep the operating point within the stable operating space. In the control procedure used, once the cycle averaged point is inside the operating space no further action is taken.

As the flow near surge is more sensitive a small step increase in recirculation flow between consecutive cycles was chosen for this region. Comparatively, a larger step increase was used in problem region II, to achieve a rapid drop in boost, if the cycle operating point crossed the boost pressure limit plane.

7.2.1 Simulation Results

The full load engine operating lines on the v.p. compressor map, projected on the $\dot{m}_\varepsilon$ - r_p plane, for the simulation runs with the three sizes of turbocharger turbine are shown in Figs.7.2, 7.3, 7.4.

Each operating line branches into two lines as the speed increases. The upper from these two lines is the standard operating line without recirculation.

A boost limit plane at pressure ratio r_p = 1.4 had been postulated. If the cycle operating point was above this value, the recirculation was increased in steps in subsequent cycles. The lower line is therefore the projection of the full recirculation engine operating line, and must be associated with the projections of the full recirculation constant speed lines on the $\dot{m}_\varepsilon$ - r_p plane.

Figs. 7.5, 7.6, 7.7 show the displacement of the operating points when the jets are activated, for the three engine operating lines. Again the projection on the $\dot{m}_\varepsilon$ - r_p plane is shown. The displacement vectors have similar slopes. The drop in pressure ratio and engine mass flow is also shown.

The operating point did not remain on the same speed surface when prewhirl was used, but dropped to a lower speed. Hence larger drops in boost pressure with prewhirl may be achieved, if the pressure drop within a speed surface with recirculation is increased by appropriate design of the device.

Figs. 7.8, 7.9, 7.10 show the range of cyclic fluctuation of mass flow values for every operating point. In certain cases the instantaneous flow is below the minimum stable flow of the standard compressor.

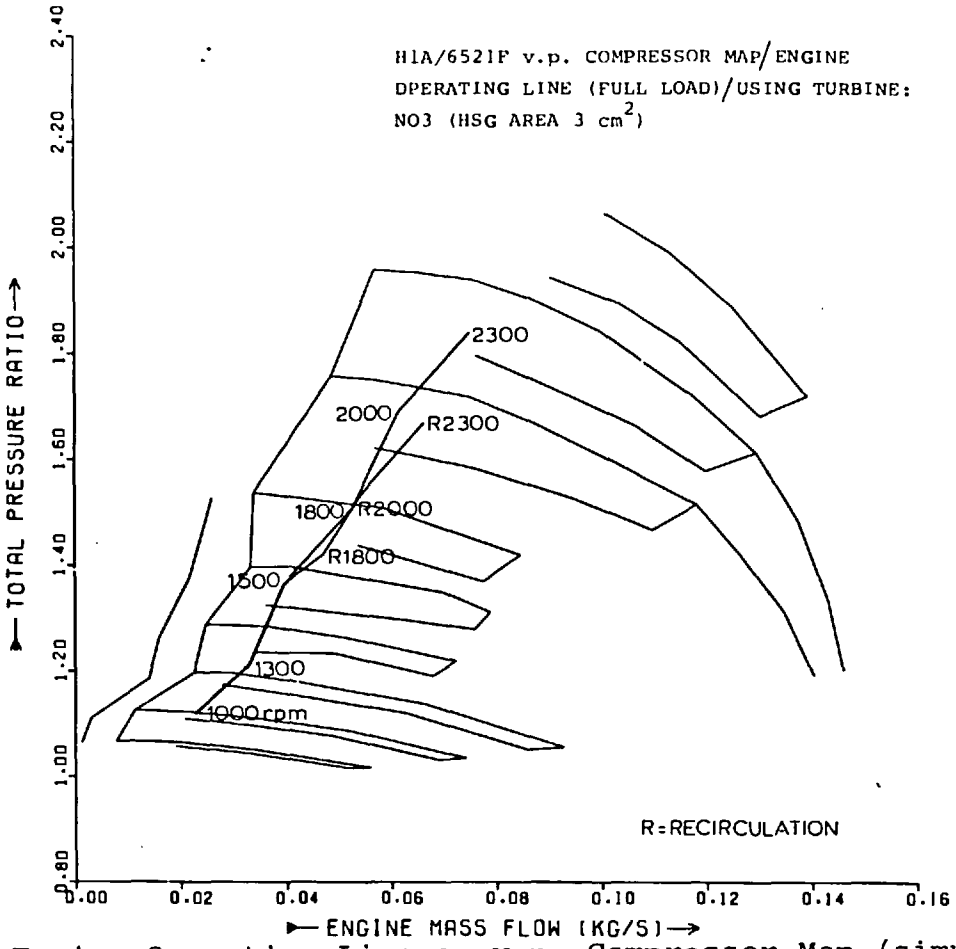


FIG.7.2 Engine Operating Line on v.p. Compressor Map (simulation)

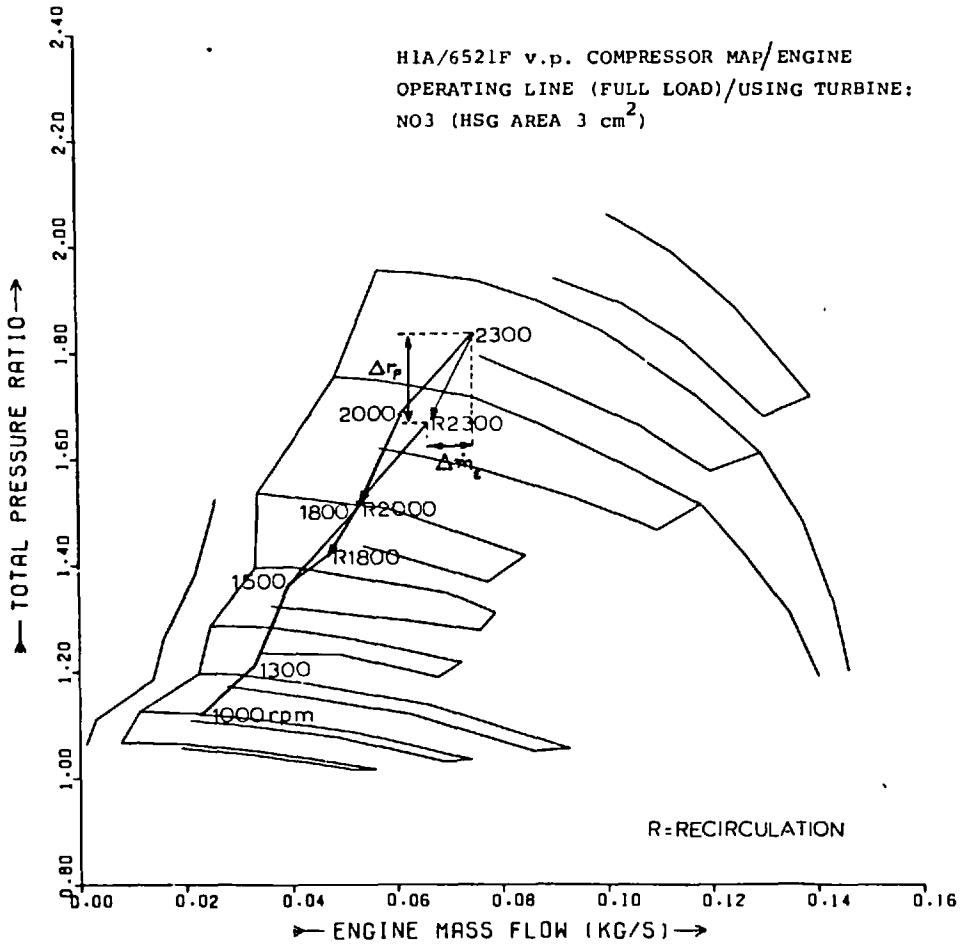


FIG.7.5 Effect of Jets on Operating Points

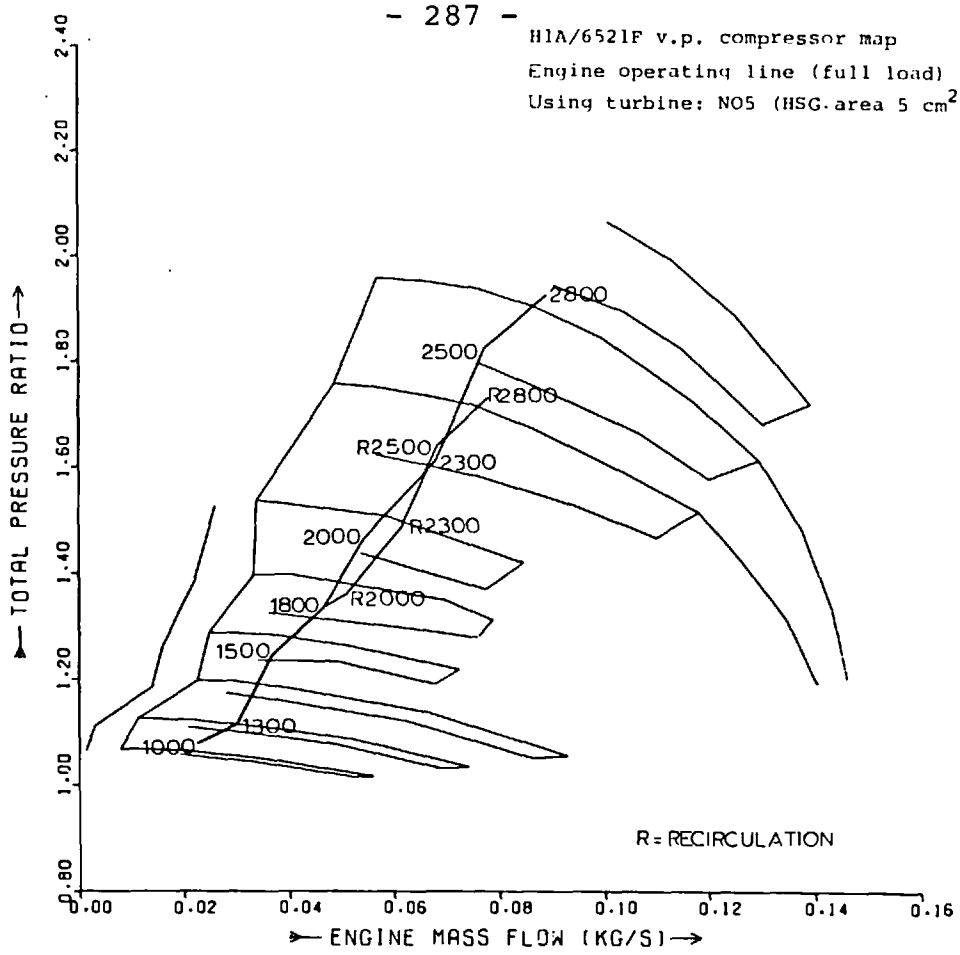


FIG.7.3 Engine Operating Line on v.p. Compressor Map (simulation)

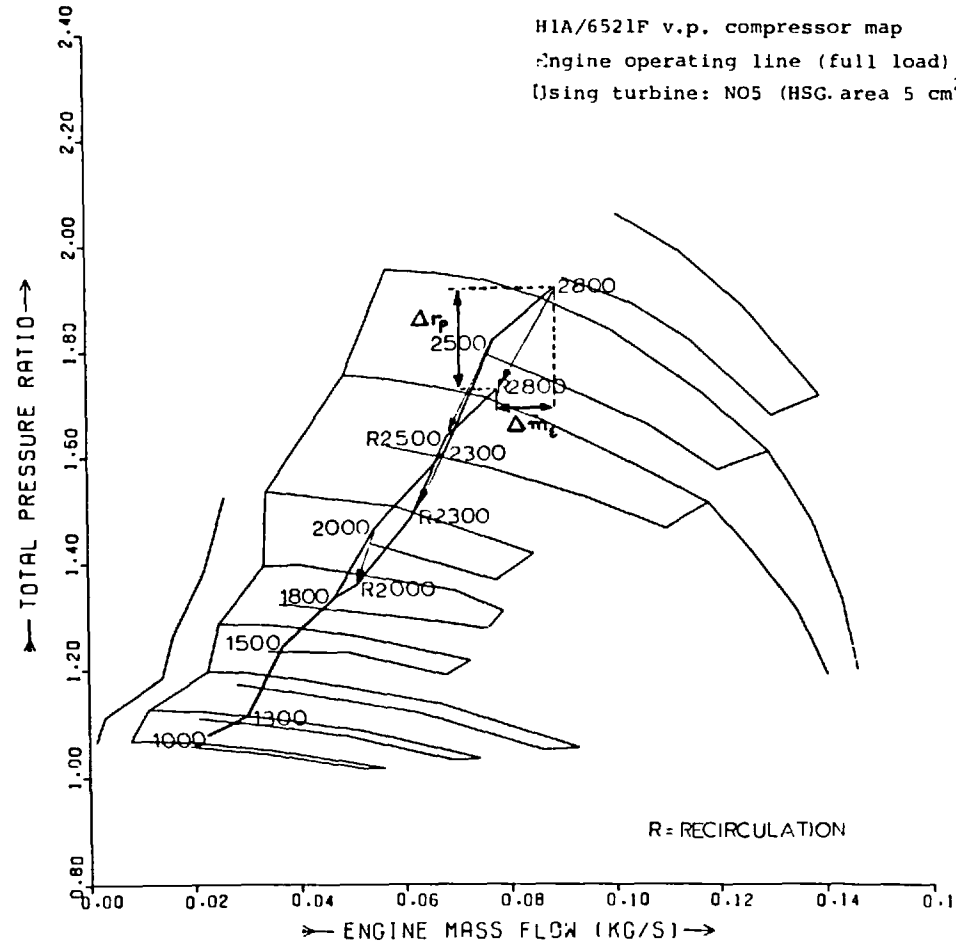


FIG.7.6 Effect of Jets on Operating Points

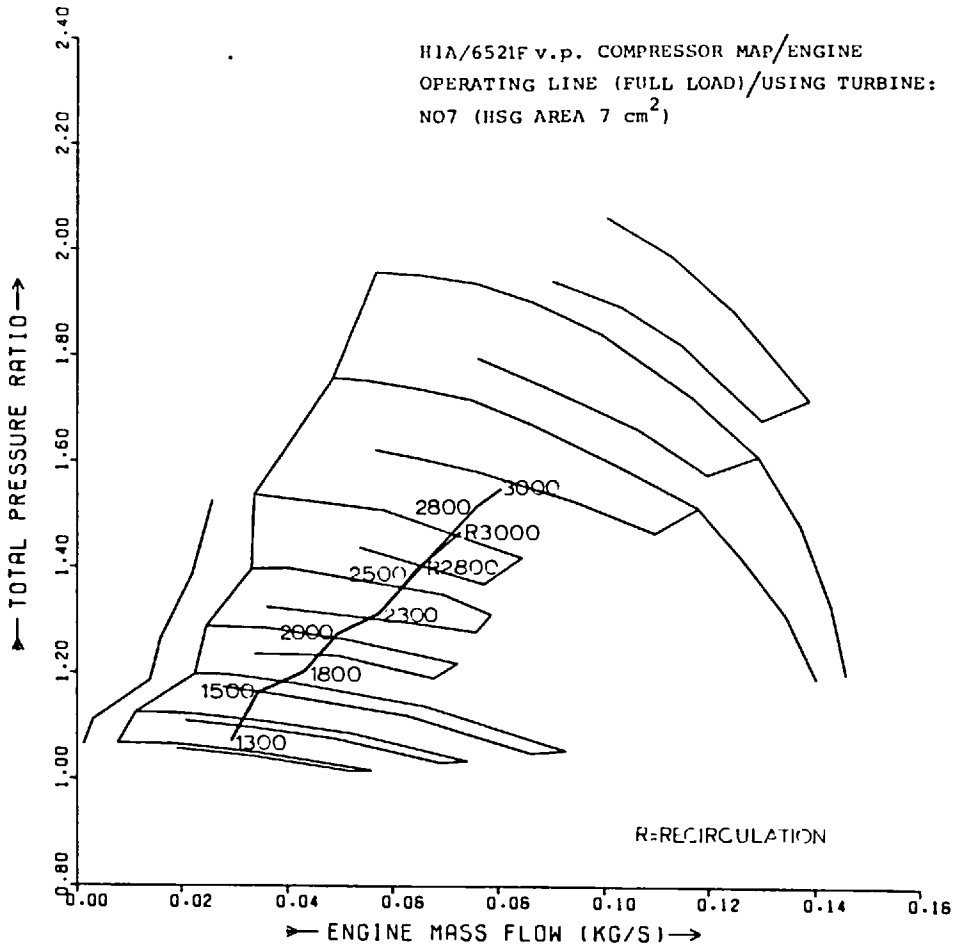


FIG.7.4 Engine Operating Line on v.p. Compressor Map (simulation)

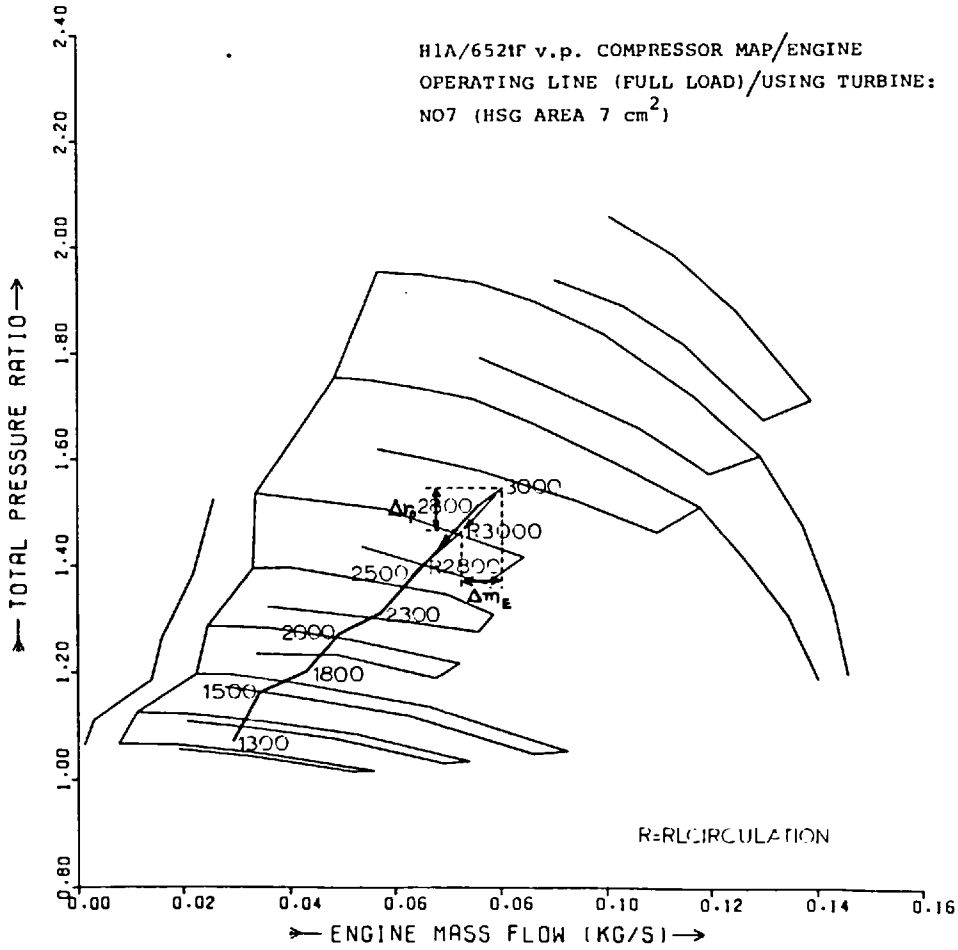


FIG.7.7 Effect of Jets on Operating Points

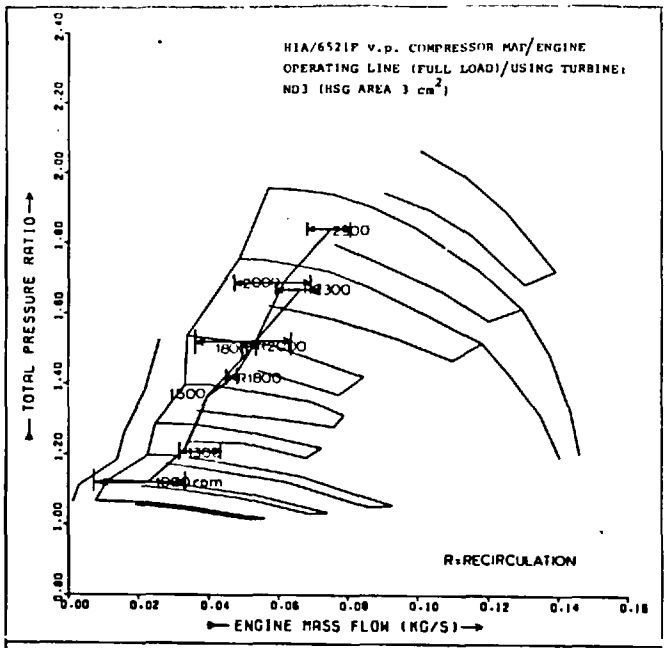


FIG.7.8 Cyclic Fluctuation of Engine Flow Demand

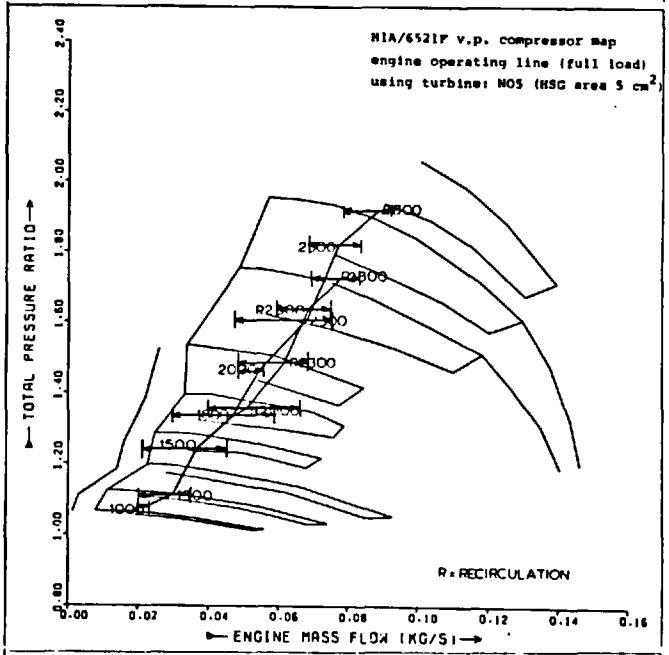


FIG.7.9 Cyclic Fluctuation of Engine Flow Demand

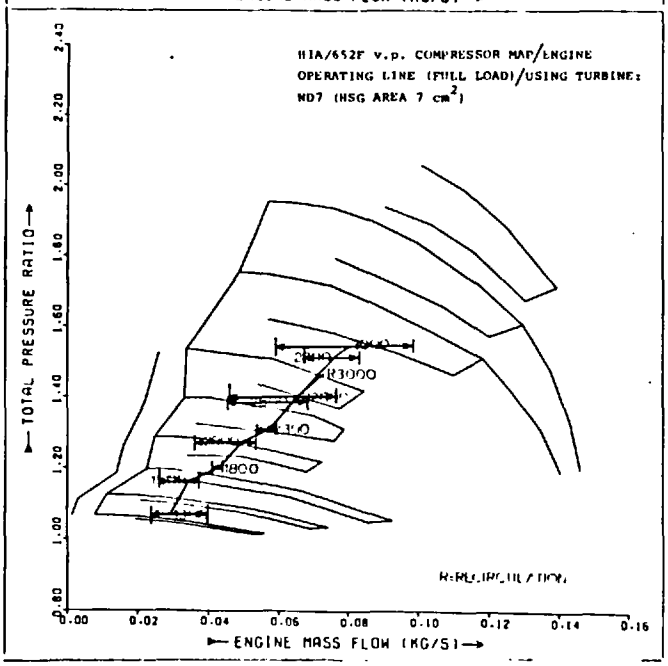


FIG.7.10 Cyclic Fluctuation of Engine Flow Demand

The oscillation in the compressor flow, followed the oscillation in engine flow demand through the cycle with a small phase difference and much smaller amplitude.

It is possible that the different ranges of flow oscillation at different speeds are also affected by the different response of the simulation program, (i.e. numerical method and particular combination of variables) at each engine speed. The amplitude of oscillation may be increased if the operating point lies in a region of relative scarcity of data in the (3-D) compressor operating space.

The (3-D) compressor model interpolation procedure, allows operation beyond the surge surface. While the efficiencies will not be realistic, since they would be based on the values of the nearest stable flow data points, the turbocharger speed will be reasonably accurate, and the compressor mass flow will correspond to the instantaneous demand. The flexibility of the simulation is thus enhanced.

It can be seen in Fig.7.2, that the engine operating line using the smallest turbine has a fairly small surge margin at low speeds. If the fuelling was further increased the margin would probably be inadequate. The "steady state" compressor characteristic may change when placed on the engine, decreasing the surge margin further (Section 3.2.1).

The operating line with the NO5 turbine (Fig.7.3) has a better surge margin at low speeds. In problem region II, although there is a drop in boost using the jets, it is evident that the design of the jet arrangement for this area must be further optimised.

The operating line with the NO7 turbine (Fig.7.4) is far removed from the surge line, towards the low-efficiency region at high speeds, indicating that the turbine is too large for this application.

Table 7.1 shows the change in several parameters with recirculation from the simulation results. The exhaust manifold temperature rises, while the maximum cylinder pressure, the power, and the turbocharger speed, fall.

TABLE 7.1

SIMULATION RESULTS

(Full Load)

Turbine	Engine Speed RPM	Difference (Standard-Recirculation)			
		ΔBHP	ΔP.Max Maximum Cylinder Pressure (Bars)	ΔNTC Turbo Speed (RPM)	ΔTEX Exhaust Manifold Temperature (^{o}k)
NO3	1800	0.3	3.31	1367	- 28
	2000	0.6	3.67	3571	- 48
	2300	0.5	7.09	2870	- 47
NO5	2000	0.73	4.26	2537	- 40
	2300	0.76	5.04	2674	- 43
	2500	0.90	7.53	2899	- 52
	2800	0.75	10.06	5454	- 50
NO7	2800	0.90	5.00	4572	- 44
	3000	0.40	3.00	3343	- 43

7.2.2 Comments

The simulation results gave further insight into the jet arrangement device by testing the v.p. compressor on a particular application.

With the two smaller turbocharger turbines the instantaneous engine operating point crossed the standard compressor surge line. As it has been explained (Section 5.4.4), recirculation is not activated unless the cycle averaged operating point crosses the v.p. compressor operating limits, hence the jets remained inoperative in these regions.

However, it would be possible to postulate a certain amount of recirculation as initial condition, if the surge margin is seen to be very small, although the operating point is inside the stable region of the compressor.

The device was designed for problem region I, with primary objective to change the inducer incidence angles and increase the surge margin at low speeds. The pressure drop at high speeds was effectively the result of the behaviour of the jet arrangement off-design. The simulation showed that the operating point dropped to lower speed as the recirculation was increased, resulting in a larger drop in boost pressure.

There is much potential for performance improvement of the device in the upper end of the compressor map. Excess turbine energy is available in that region, making higher recirculation rates possible. Thus the jet arrangement can be designed so that the boost control ability in problem region II is increased.

7.3 The Experiments

Based on the simulation results a series of experiments was planned. In these experiments the FORD YORK engine was turbocharged using the HOLSET H1A 6521F/NO3B6 turbocharger with the jet prewhirl device. This included the 70° nozzle ring which gave best performance in the v.p. compressor tests, and its data was used in the simulation.

Since very little was known about the actual behaviour of the engine - v.p. turbocharger system, the simulation program was used as a true prediction program.

The predictions (Fig.7.2) showed a small surge margin at low speeds, and due to the wide fluctuation of air demand of the four-cylinder engine through the cycle, the instantaneous operating point sometimes crossed the standard surge line (Fig.7.8). It was therefore probable that surging could be encountered during the experiments.

Although the amount of recirculation required to suppress surging at each operating condition, could be determined from the v.p. compressor experimental results, the only means of recirculation control was a manually operated valve. An automatic control system would monitor any relevant parameters (pressure, speed, flow). If an open loop system was used, the recirculation would be adjusted in a predetermined way, based on the v.p. compressor results. Alternatively a closed loop system could regulate the optimum recirculation flow, if appropriate reference and feedback signals could be provided.

Precise adjustment of the recirculation is essential near the surge line, since the velocity ratio availability

is high, and excessive recirculation may result in "critical" flow. The adverse flow conditions and the torque reversals inside the impeller, associated with surge or backflow at the inlet, would present problems, especially at high speeds. Further, the influence of the engine on the compressor map was not known and could not be predicted.

Usually, hard surge, which would be quite unacceptable, is preceded by some milder flow instability, but it would be quite difficult to pinpoint this, on the turbocharged engine. In the v.p. compressor experiments, the instability initiation point was defined as a particular noise level at a certain frequency range, using a sound level meter (Section 4.10.3.6.2).

It would not be possible to use the same definitions, as the background noise from the turbocharged engine would be quite different. Since the turbocharger and engine were not anymore independent, and the definition of the stability noise assumes a constant background noise, the noise meter could not be calibrated. These uncertainties about the position of the surge point, prevented operating near the surge line at high speeds. Hence for the runs to high speeds, the naturally aspirated maximum fuel delivery curve was retained.

Additionally the inlet plenum volume was increased, to decrease the pressure fluctuations at the compressor discharge. To reduce the maximum cylinder pressures, the engine timing was retarded 5° crank angle and a limiting boost pressure ceiling of $r_p = 1.7$ was imposed.

7.3.1 Experimental Results

The experimental engine operating lines for full and half load without prewhirl are shown in Fig.7.11 plotted on the v.p. compressor map. The two shorter lines are the projections of the operating lines with prewhirl on the $\dot{m}_{\dot{\epsilon}}$ - r_p plane. The arrows indicate the movement of the end points with increasing jet flow. Since the two shorter lines were obtained with full recirculation, they should be viewed in conjunction with the lower compressor constant speed lines. It can be seen that the drop in boost increased as the pressure ratio level was increased.

The engine mass flow dropped with recirculation. Some rough running of the compressor was experienced at full load at 1300 rpm engine speed.

Fig.7.12 compares the engine operating lines obtained from the simulation, on which the planning of the experiments was based, with the experimentally obtained lines. (The experimental runs were done with 20 per cent less full-load fuelling compared with the simulation runs.)

Both the magnitude and the direction of movement of the operating point are similar for both cases.

As shown in Table 7.2 the variation of parameters with recirculation verifies the trends shown in the simulation results.

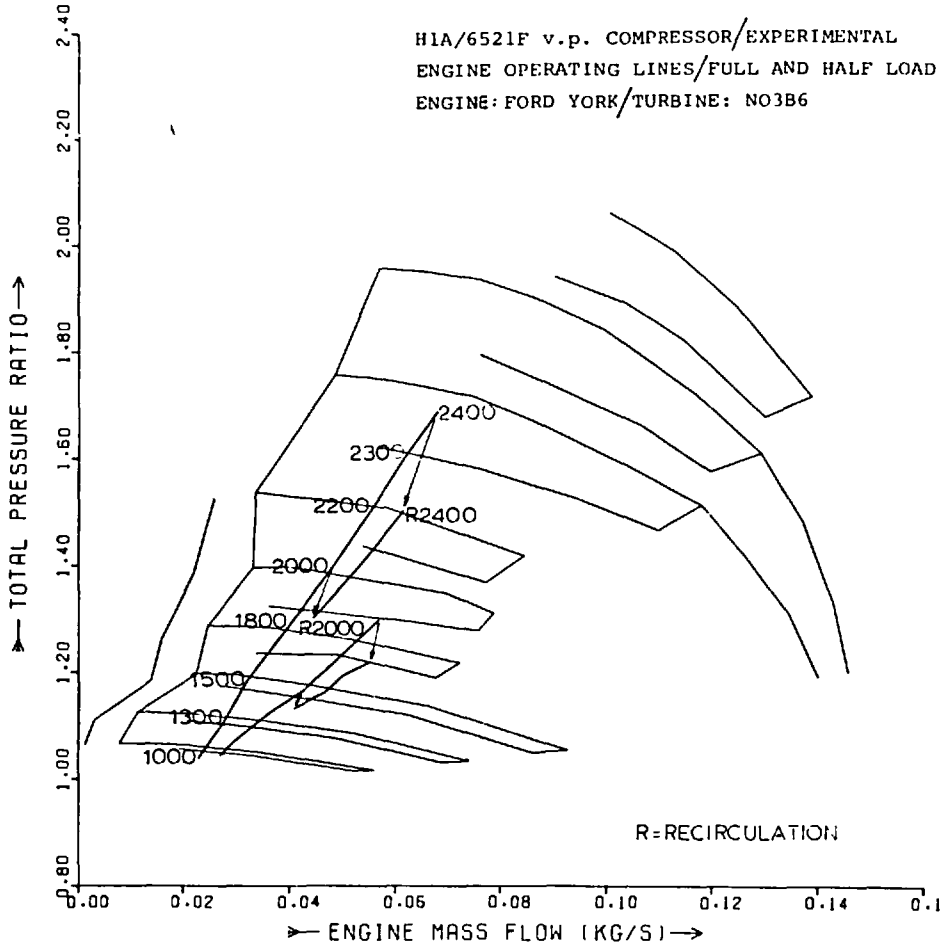


FIG.7.11 Engine Operating Lines on Compressor Map (experimental)

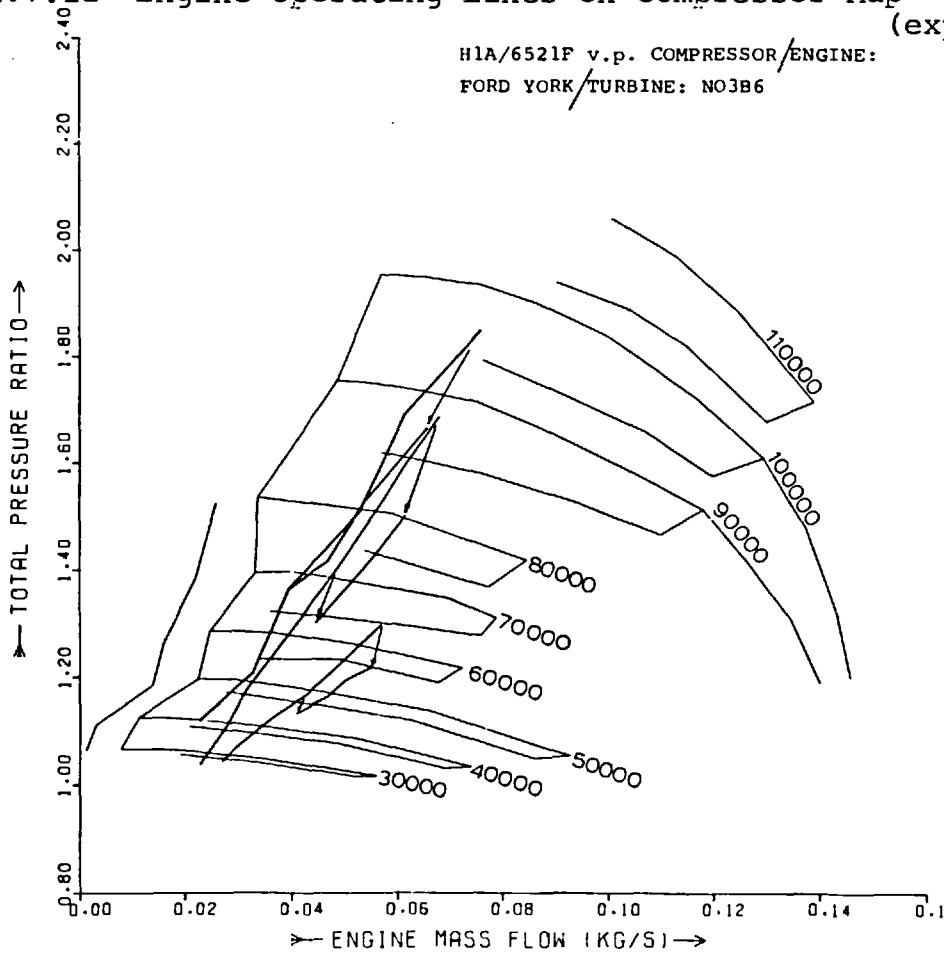


FIG.7.12 Comparison of Simulation Line used for Experimental Planning and Experimental Operating Line (expt.line at 20% less full load fuelling)

TABLE 7.2

EXPERIMENTAL RESULTS

(Full Load)

Turb.NO3	Difference (Standard-Recirculation)				
Engine Speed RPM	BHP	ΔNTC Turbo. Speed RPM	ΔTPL Compres. Discharge Temp. °K	ΔTEX Exhaust Manifold Temp. °K	ΔPC Compres. Power W
2000	0.76	3450	0.4	- 40	175
2200	1.33	6060	5.9	- 35	478
2300	1.22	4920	4.8	- 37	521
2400	1.81	6420	6.6	- 34	731

The engine power falls because of the drop in pressure ratio.

The turbocharger speed falls with the operating point moving into the (3-D) compressor map, crossing the constant speed lines. The compressor discharge temperature falls since the drop in pressure ratio counteracts the effect of the drop in system efficiency.

The engine exhaust temperature increases, since the engine airflow drops. The power required by the compressor falls, since although the compressor throughflow increases and the compressor efficiency in this region falls slightly, the drop in pressure ratio due to prewhirl counteracts these. Comparing Tables 7.1 and 7.2 it can be seen that the simulation predicted smaller changes in engine power and turbocharger speed and larger changes in exhaust manifold temperature, with recirculation. The different full load fuelling would account for part of these differences.

In addition the data used for the turbine efficiency in the simulation did not correspond to the actual turbine used in the experiments (and was probably overestimated). Also the proportion of heat release in the cylinder and prechamber of the engine, used in the simulation,was obtained by scaling data from another engine. Changes in this proportion and also in the shape of the heat release curves would have some influence on the engine operating point.

7.3.2 Experiments Near Surge

To examine the behaviour of the device when the engine operating point approaches the surge line, it would be necessary to increase the fuelling, although for reasons already explained this was only attempted at low speeds. In order to draw valid conclusions, comparative testing with and without recirculation was required for each operating condition. However the difficulty in determining surge on the turbocharged engine, becomes even more pronounced at low turbocharger speeds, where the compressor does not stall abruptly.

A series of pretest runs were made at low engine speeds (1100, 1200 rpm) and the maximum fuelling was increased gradually, by adjusting the fuel pump.

For a particular engine speed the engine was loaded in steps, and for each step the approximate position of the operating point on the compressor map was immediately found.

The amount of recirculation needed to maintain a certain surge margin was found in the v.p. compressor experimental data for the appropriate operating condition. Since the influence of the engine on the compressor surge line was unknown, erring on the safe side, the operating point was

treated as if it was on the surge line, even when it was within the stable flow range. Readings were taken first with the required recirculation, and then gradually closing the recirculation for engine speeds up to 1500 rpm.

Shown in Fig.7.13 are the engine operating lines with and without recirculation, the former being a projection of the line in (3-D), on the $\dot{m}_{\epsilon}$ - r_p plane.

Some rough running of the compressor, coupled with high pitch noise was encountered on closing the recirculation at 1300 rpm but the compressor was not thought to have surged. At both 1400 and 1500 rpm and on closing the recirculation, the speed sensing probe was blocked by turbocharger lubricating oil and the signal was lost.

This was evidence of backflow at the shroud side, and was associated with surge. That was further substantiated on dismantling the unit after the 1500 rpm run, when oil traces directed upstream were found on the inlet duct wall near the compressor face.

It can be seen that these two speeds are near the inward kink of the surge line on the compressor map. It is also possible that the standard surge line has moved to the right because of the engine influence.

At the lowest speeds the change in engine mass flow with recirculation, is relatively large compared to the change in pressure ratio and this results in the two operating line projections on the $\dot{m}_E$ - r_p plane crossing.

The velocity ratio (R) of the jet flow to engine flow in these tests was $3 < R < 4$ and the mass ratio (m) of jet flow to total compressor flow was $0.144 < m < 0.186$.

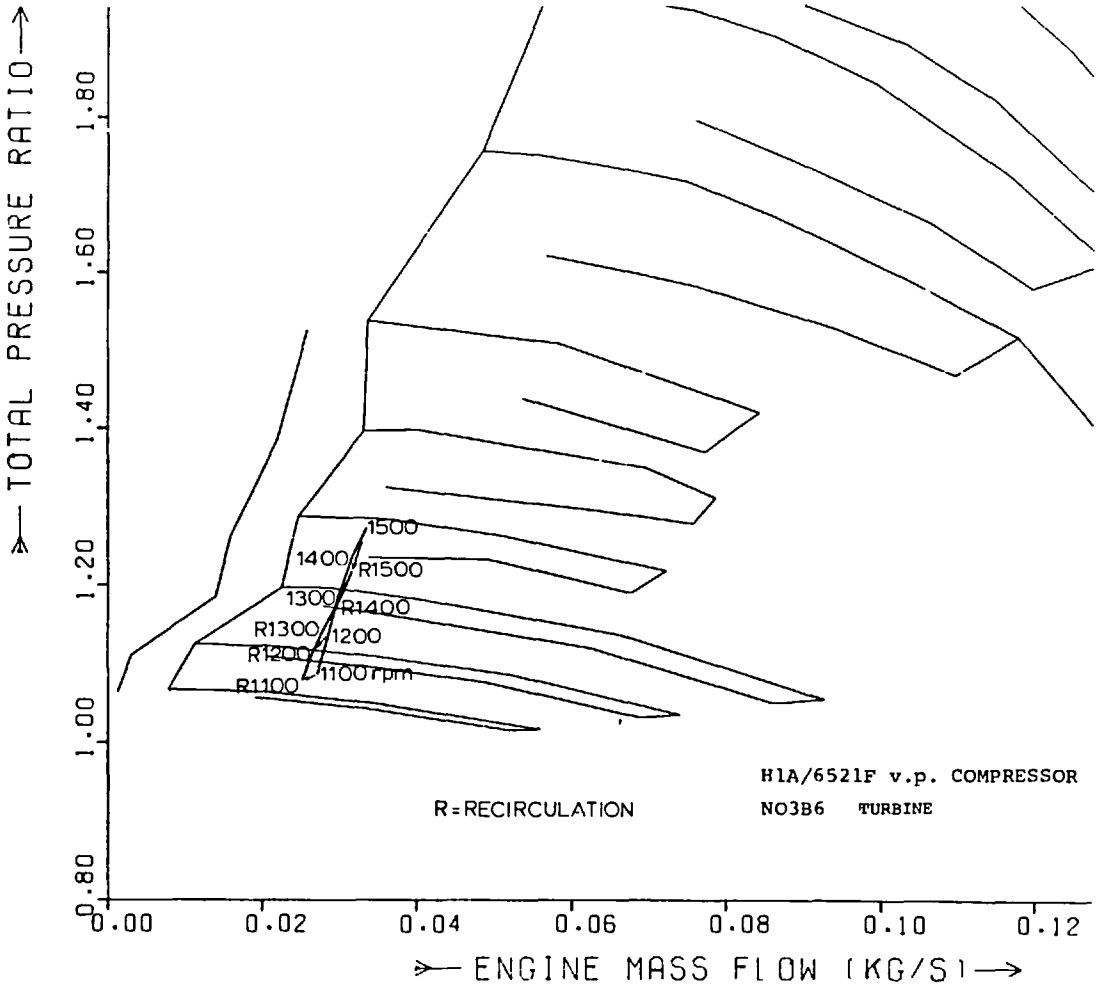


FIG.7.13 Experimental Operating Lines Near Surge

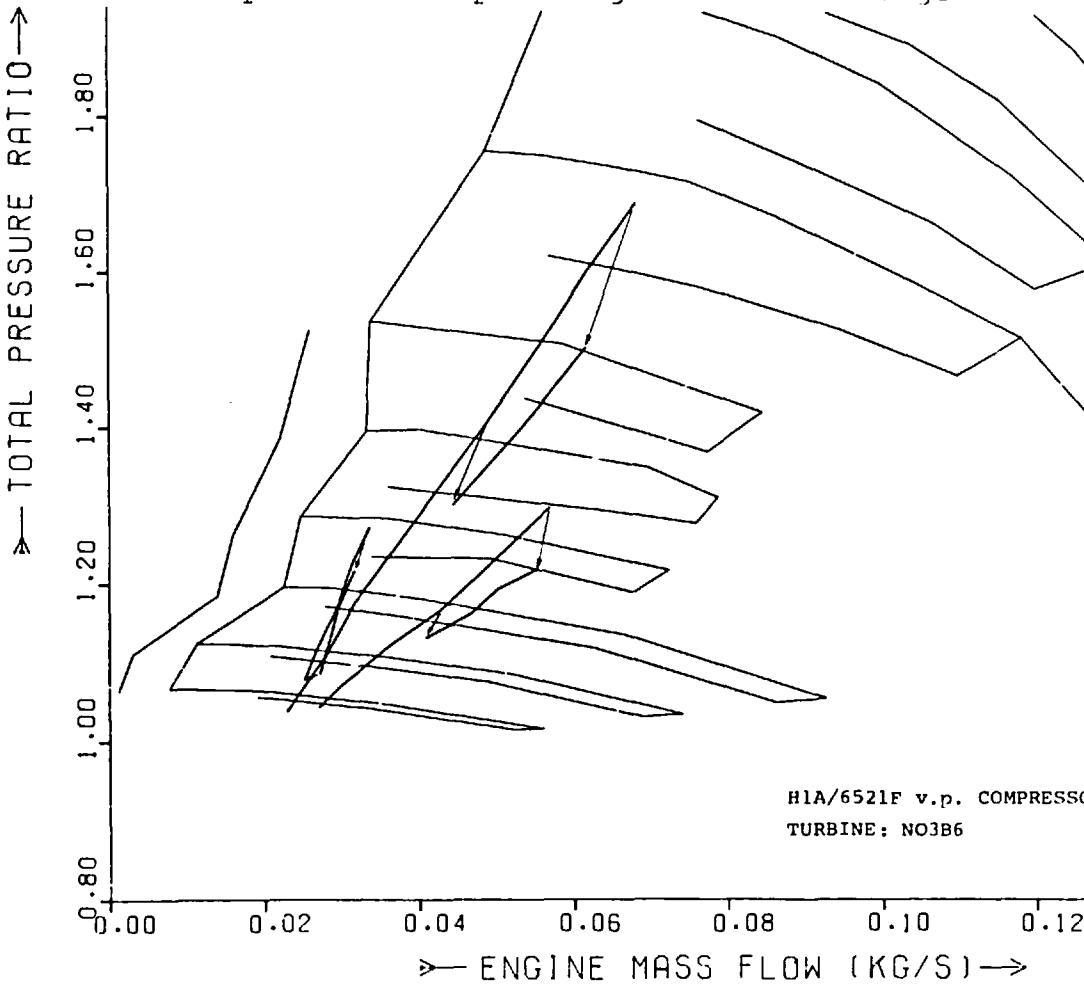


FIG.7.14 Comparison of Experimental Operating Lines (from FIG.7.11, FIG.7.13)

The trends in variation of parameters with recirculation were the same as from the previous experiments and predictions (Table 7.3).

TABLE 7.3

EXPERIMENTAL RESULTS

Turb.NO3	Difference (Standard-Recirculation)				
Engine Speed RPM	ΔBHP	ΔNTC Turbo. Speed RPM	ΔTPL Compres. Discharge Temp. °K	ΔTEX Exhaust Manifold Temp. °K	ΔPC Compres. Power W
1100	0.44	1800	1.9	- 2	67
1200	0.26	3660	1.1	- 5	50
1300	1.16	3900	2.4	- 7	94
1400	1.74	?	3.3	- 17	98
1500	0.57	?	3.5	- 12	124

Fig.7.14 shows the relative position of the experimental operating lines. Due to the flow characteristic of the jet nozzles with increasing pressure, it was found that recirculation was kept within the defined limits with little adjustment of the regulating value. This would be advantageous for a fast acting control system.

7.3.3 Comments

The experiments verified the ability of the jet arrangement to control the pressure ratio of the compressor, hence the engine boost, and showed that there is scope for more development in this area.

In the tests with increased fuelling at low engine speeds, it was found difficult to determine the point of instability initiation in the compressor, so that a consistent reference could be used for comparison.

However the jet arrangement was successful in suppressing flow instability in this region. Fig.7.15 shows an engine running line on the compressor map based on the experiments and prediction results.

Line ABDEG is the standard operating line while line OBCF is the projection of the operating line with recirculation.

A possible schedule for a prewhirl control system could be as follows:

No recirculation is needed for AB since there is adequate surge margin and the compressor is almost "windmilling" at this operating stage. As the operating point moves to B the surge line is approached and recirculation is needed to increase the surge margin. From C to D recirculation is gradually closed as the surge margin increases and the operating point moves into the region of high compressor efficiency. At E the recirculation is again used to prevent overboosting.

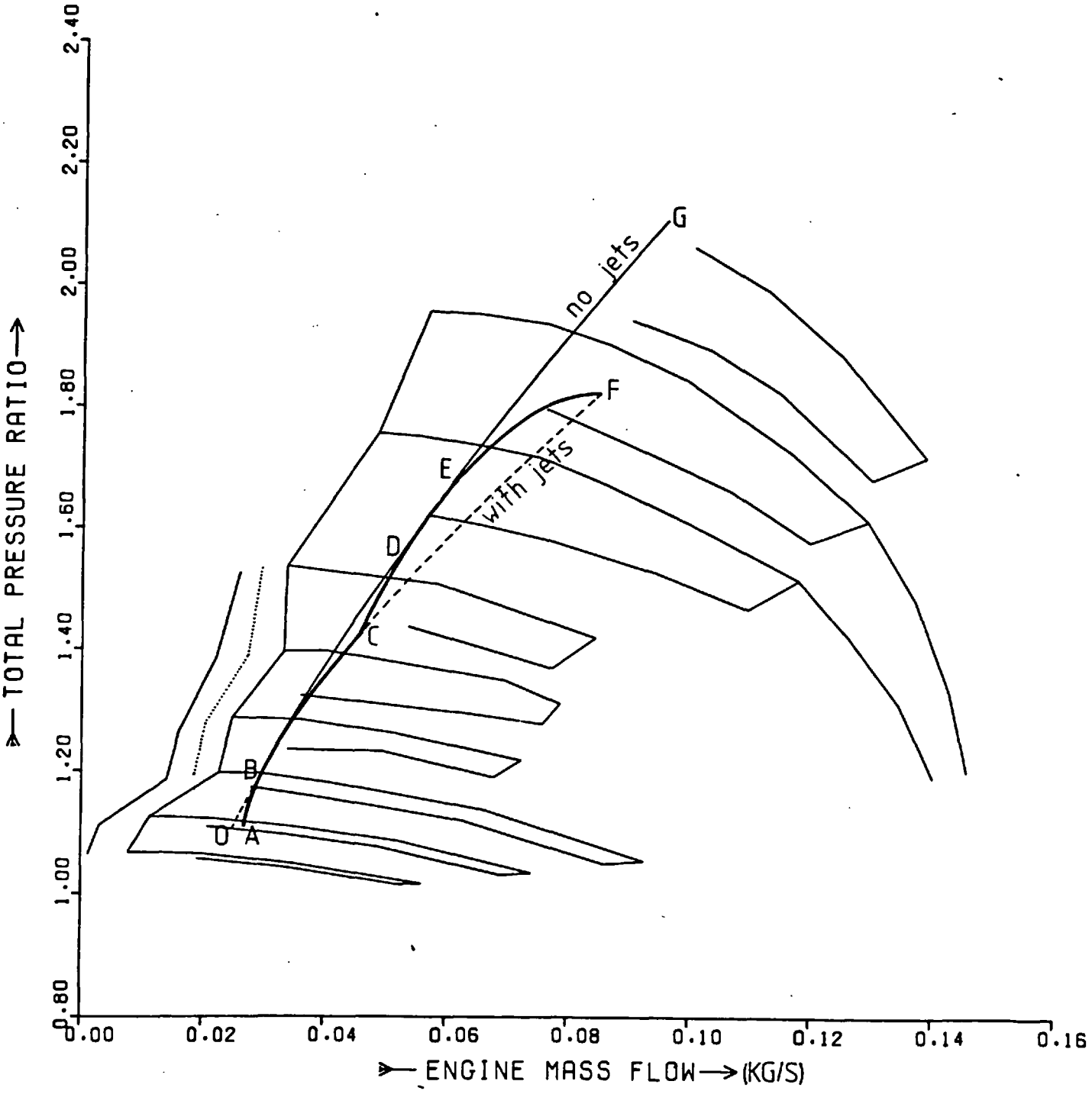


FIG.15 Possible Prewhirl Schedule for Engine Operating Line on v.p. Compressor Map

CHAPTER 8

CONCLUDING REMARKS

8.1 THE AERODYNAMIC PREWHIRL INDUCING DEVICE

The concept of using aerodynamic instead of variable geometry mechanical flow regulators in turbomachinery is attractive because of the simplicity and potential reliability in operation of such a device, provided it can be made to work efficiently. Therefore, it has been endeavoured on several occasions to design systems which use this method.

The present research work describes a novel aerodynamic method for improving the flow range and controlling the pressure ratio of rotary compressors by introducing pre-rotation to the inflow. This investigation originated by considering the particular problems of matching turbo-chargers and diesel engines and was subsequently applied to such a case.

In the method proposed, high pressure fluid is ejected from orifices spaced around the periphery of the inlet pipe, obliquely into the inflow, so as to induce prewhirl. Variable amounts of prewhirl are possible by varying the amount of fluid ejected and positive or negative prewhirl may be obtained depending on the orientation of the orifices. In addition to the influence of prewhirl on compressor performance, if compressor discharge fluid is recirculated and ejected, a further apparent improvement in flow range results. The arrangement of the orifices presents no structural obstruction to the inflow duct and does not interfere with flow or efficiency of the compressor under normal running conditions.

There are no complex mechanisms involved and no moving parts except the high pressure fluid flow regulator (119).

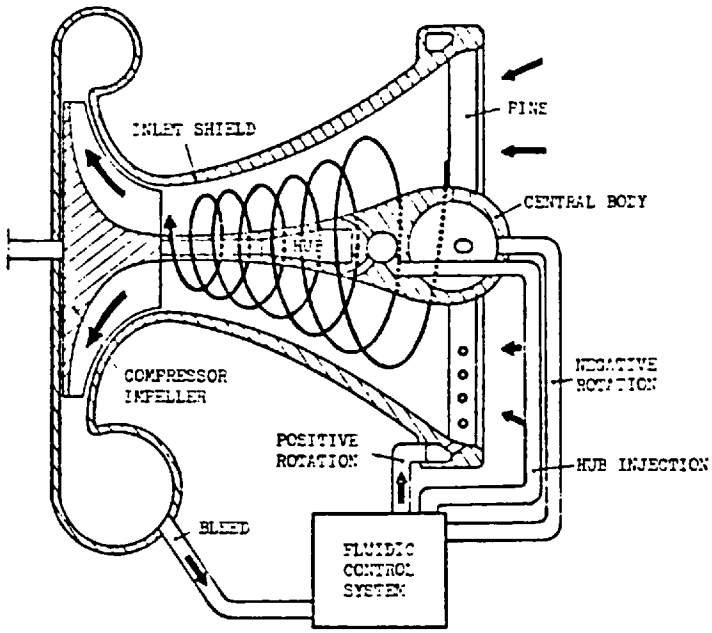
8.2 COMPARISON WITH ALTERNATIVE DESIGNS

It is possible at this stage, with the background of the theoretical analysis presented and the results of the experiments, to critically compare alternative aerodynamic methods, proposed to induce prewhirl to the inflow of compressors.

A device is described (120) to control the velocity profile at the inlet of flow machines by tangentially introducing high pressure fluid into the inlet (Figures 8.1, 8.2). The fluid is introduced as a plurality of radially spaced separate jets, from orifices in a plurality of radially oriented hollow struts, spanning the gap between the inlet duct wall and a central hub.

A fluidic amplifier control system is proposed to give injection in the direction of the rotor rotation or opposite to it. Experiments using this device are reported elsewhere (121). The compressor performance map obtained is shown in Figure 8.3. The results appear impressive, especially since they were obtained with 5.8 per cent recirculation, from 1 mm diameter jet orifices situated quite some distance away from the compressor. Based on the analysis and results of the present work it would seem unlikely that such small orifices would give jets with any appreciable penetration at such low recirculation rates.

Also in addition to the structural complexity of the



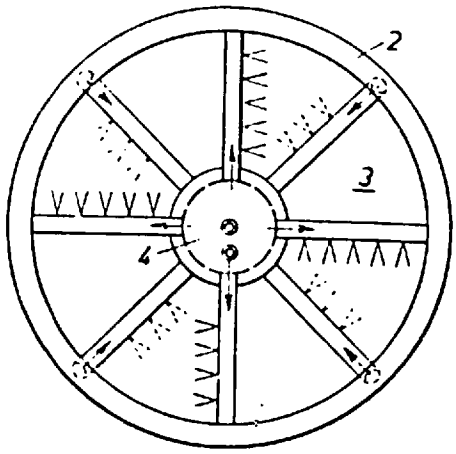
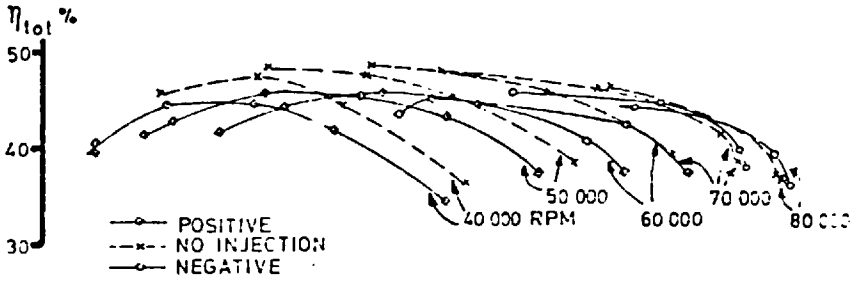


FIG.8.2

FIG.8.1 Alternative Aerodynamic Prewhirl Method (120)



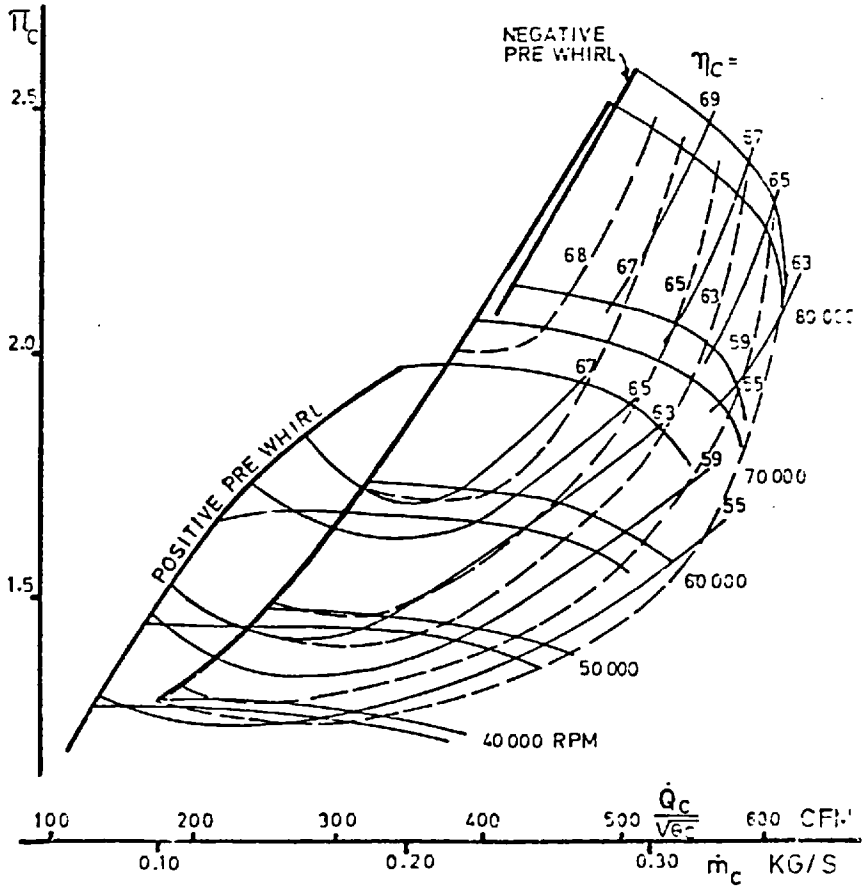


FIG.8.3 COMPRESSOR PERFORMANCE CHART WITH AND WITHOUT INJECTION POSITIVE AND NEGATIVE PRE WHIRL (121)

arrangement, the reliable operation of such small orifices is questionable.

A better arrangement, but suited to axial multistage compressors is presented (122). The air is ejected from radial slots at the trailing edge of hollow stator blades (see Figure 8.4). This gives a (2-D) jet but with appropriate design it may act as a flap to the stationary vane, to change the angle of flow incidence to the rotor. It would seem possible, to vary radially the flow deflection to match the rotor blade radial inlet angle distribution.

Results of tests are presented (123) with a jet re-entry arrangement, using a turbine type scroll with a peripheral slot at the impeller inlet, to eject high pressure discharge air (see Figure 8.5). The arrangement is similar to the one considered in Section 4.7, where the disadvantages of such a system were discussed.

A (2-D) jet is obtained, but the resultant flow differs from that of the arrangement (122). In the latter the main flow reaches the downstream side of the jet as well, and reduces the recirculation eddy which probably affects the compressor performance. The results (123) indicate a considerable increase in flow range with large amounts of recirculation, at the expense of a large reduction in pressure ratio and efficiency (see Figures 8.6, 8.7).

The air injection used (50, 51) for improving turbo-charger transient response by blowing high pressure air on to the impeller, had no appreciable effect on the standard compressor performance. The surge line was found to have

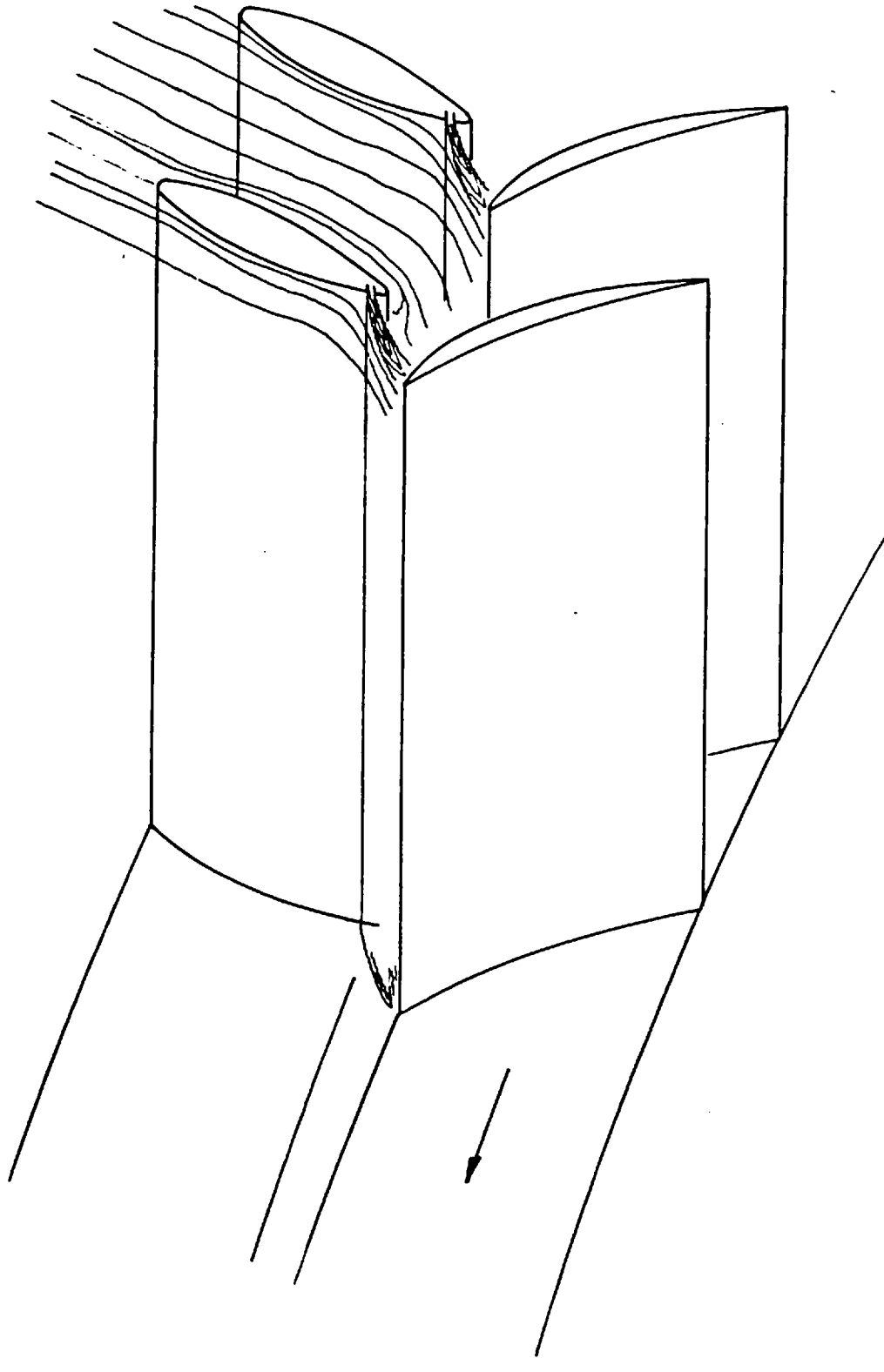


FIG.8.4 Alternative Aerodynamic Prewhirl Method (axial compressor) (122)

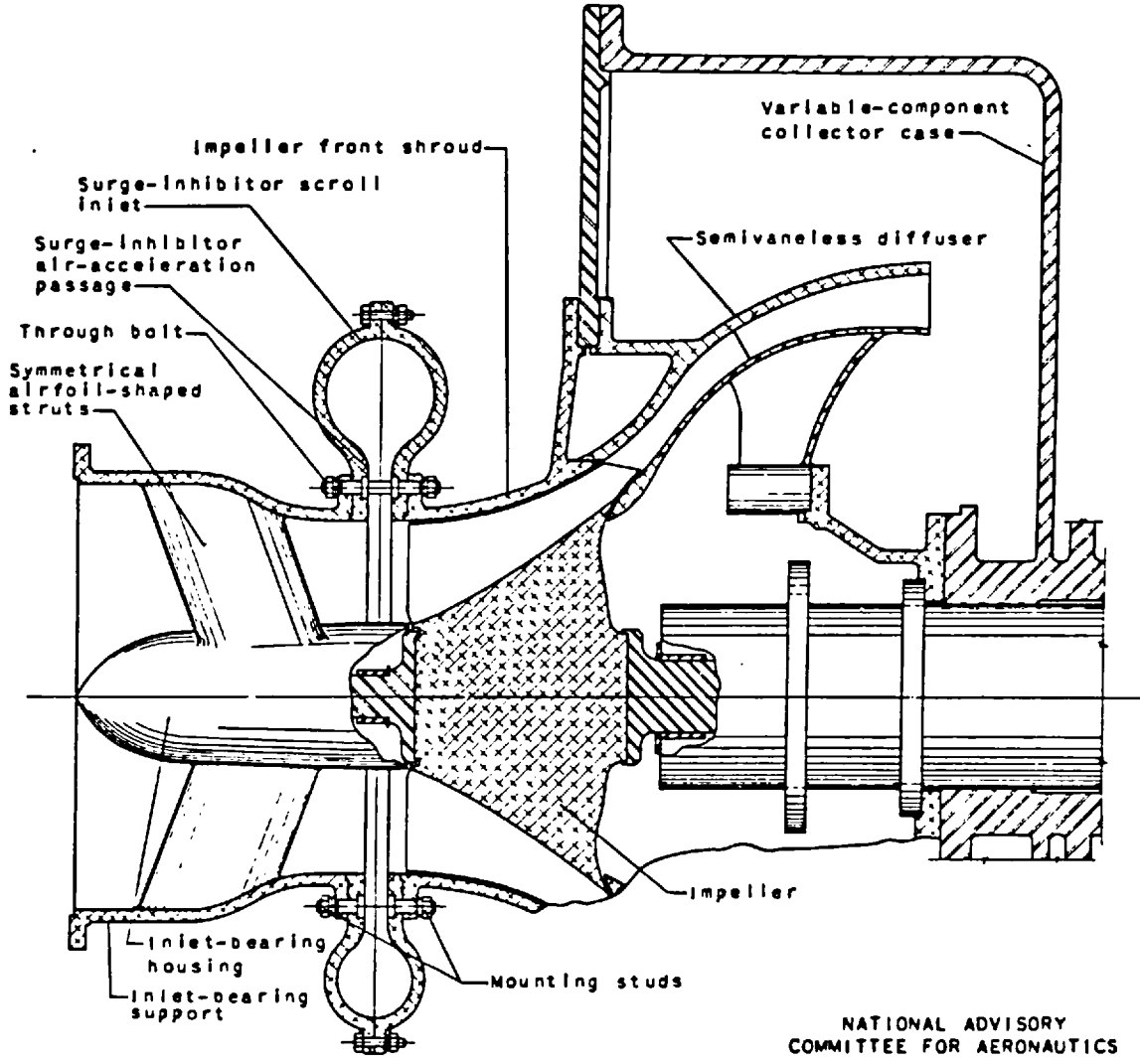
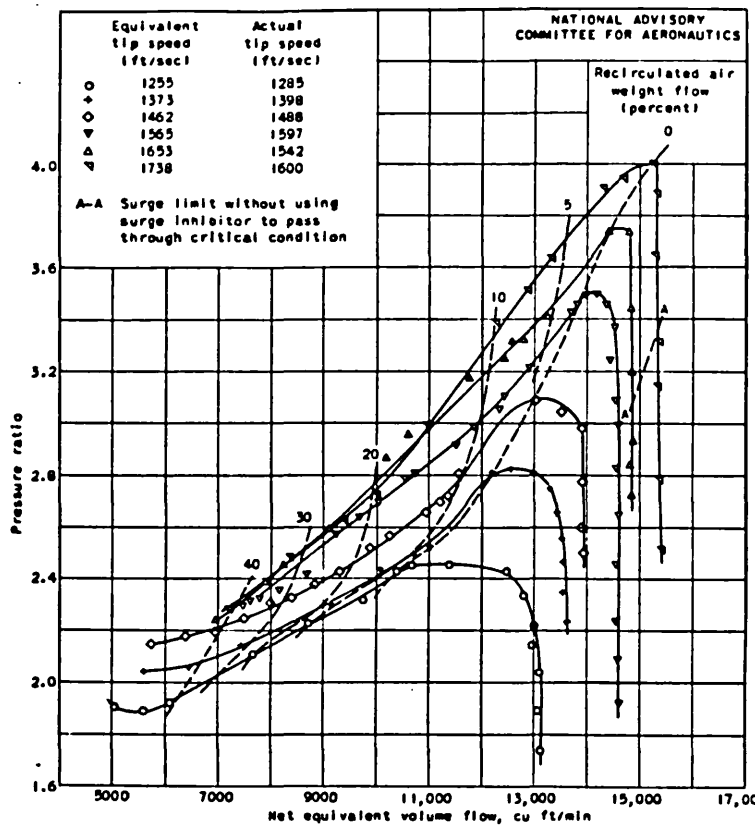


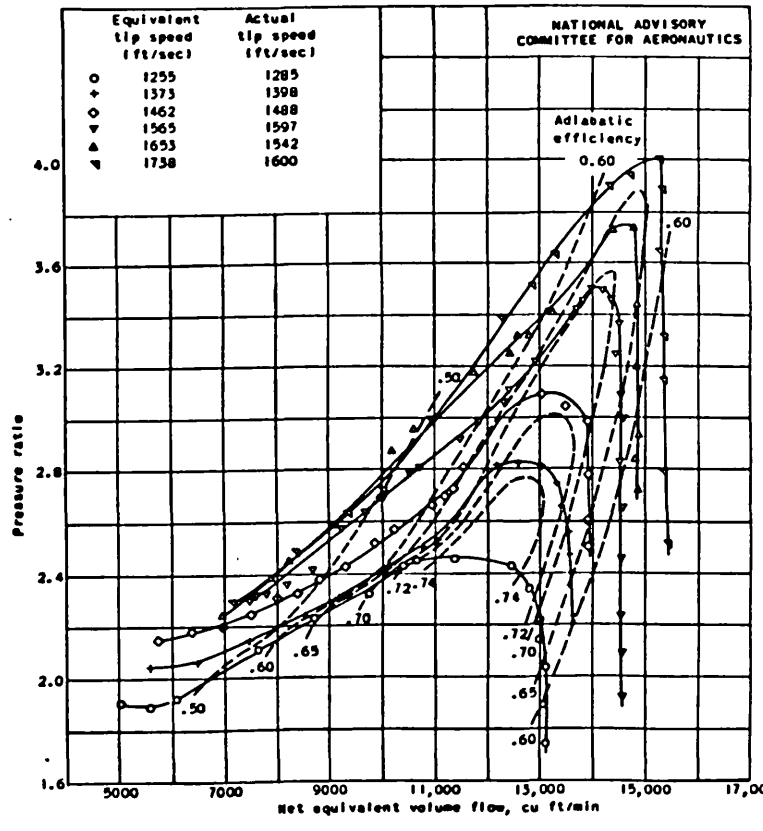
Figure 2. - Cross-sectional drawing of surge inhibitor assembled with compressor unit on variable-component collector case.

FIG.8.5 Alternative Aerodynamic Prewhirl Method (123)



- Percentage of net air weight flow to be recirculated for given increase in net stable-air-flow operating range.

FIG.8.6 Compressor Performance Map with Jet Re-entry (123)



- Performance characteristics of compressor unit with surge inhibitor installed.

FIG.8.7 Compressor Performance Map with Jet Re-entry (123)

moved only slightly to lower flow. It is possible that the mixing action of the jet injection delayed separation of the flow in the impeller.

An investigation (124) was conducted to induce prewhirl to the inflow of a centrifugal compressor using tangential nozzles ejecting air perpendicular to the axis of the inlet duct (similar to the initial experiments described in Section 4.1). Although two and four nozzles were used, it was suggested, correctly, that the injection should be imparted in a less concentrated way to produce a uniform whirling flow. The influence of the jets on the main flow (see Section 4.2 - first method) is found using angular momentum conservation to find the ideal jet flow (no losses) needed to produce a certain prewhirl. This however gives little insight to the actual flow situation.

When the jets are introduced tangentially, the high speed flow is squashed against the wall and suffers high friction losses. Also it influences only a small part of the cross flow and a long mixing length is needed to produce a uniform flow deflection profile (see Section 4.6) which further increases the losses.

8.3 CONTRIBUTION

To enable the design of the aerodyanamic prewhirl-inducing device, the flow situation was analysed and a mathematical flow model was developed. The solution for the trajectory and growth of an axisymmetric round jet, ejected obliquely at various angles to a cross flow, was found to be in good agreement with relevant published experimental data.

Using the analysis, prototype prewhirl-inducing devices were designed manufactured and tested. A design procedure evolved, allowing the development of an aerodynamic jet arrangement to suit a particular compressor. Each design was partly based on knowledge accumulated from previous investigations. For example, it was found that high velocity ratios are available near the surge line, compared to problem region II. To account for this larger or more orifices must be used to enable larger flow deflections and better performance in problem region II, and the recirculation then adjusted near surge. Also it was found that initial ejection angles $\theta_j < 90^o$ are preferable, since they resist backflow at the inlet, and should be used in future designs.

The applicability of the method was verified by simulation and experimental investigations on a turbocharged engine.

All the investigations were based on small turbocharger compressors with relatively wide flow range and low maximum pressure ratio. According to the trends shown in the engine application investigations, there is potential for more effective performance control in problem region II.

High pressure ratio compressors will have larger velocity ratio (R) availability at the upper end of their range, which would allow greater design flexibility. If the compressor range is affected by choking, prewhirl should be beneficial.

As has been mentioned, the device would be more successful on a compressor designed so as to benefit from prewhirl.

Further, the variable prewhirl option, would allow an added degree of freedom to an initial compressor design.

8.4 PROBLEM AREAS

In the design procedure for the jet arrangement there were two basic assumptions (see Section 6.2). The first assumption concerning the compressor inlet flow vectors was inevitable, since little design information about the compressor was available.

To match the (assumed) compressor requirements, analytical and experimental information was used. The mathematical flow model supported with the accumulated experimental information, formed a design tool, so that a jet-arrangement device could be tailored to suit a particular compressor.

However the knowledge about the actual flow situation is still relatively small. Many variables were only qualitatively accounted for, and possibly some have not even been identified. Additionally, little is known about the influence of the jet-arrangement on the internal flow of the compressor, especially at off-design conditions, but the latter is a problem in itself.

In the overall performance evaluation, the problem of the precise and consistent definition of the surge point was overcome by the use of the noise level concept, which however cannot be used in turbocharged engine tests.

The success in emulating the performance of V.I.G.V. could not be accurately evaluated, since this would require some norm for comparison. It would appear that the "ultimate" test would be to substitute an appropriately designed device in the place of a V.I.G.V. arrangement and to compare the

compressor performances using the two systems.

8.5 SUGGESTIONS FOR FUTURE WORK

Further development and optimisation of the jet arrangement is possible using the available information and design methods.

The device should preferably be designed round a compressor chosen primarily because of its "acceptance" of prewhirl. Detailed information about the design and performance of particular compressors would thus be required. If the compressor is suitable, the changes in performance with prewhirl should be more pronounced. Additionally the results will give an indication of the potential performance of a compressor designed with prewhirl as a prerequisite.

If an optimum prewhirl schedule is required for a particular application, such as a turbocharged engine, a control system for jet flow regulation should be designed, to enable correct matching over the operating range.

In the longer term, a more basic analytical and experimental study should be undertaken. A parametric study of different jet arrangements, to measure the flow profile at the compressor face, would promote a more thorough understanding of the flow situation and the influencing parameters. This could be combined with improved theoretical flow modelling.

To the extent that the jets can emulate V.I.G.V. the spectrum of further research possibilities in the application side is quite large. However, small turbocharger or small gas turbine centrifugal compressors would probably be the more likely applications. In the field of

turbocharging some additional possibilities are:

- Performance of the device on a highly rated engine (high pressure ratios available). If charge cooling is employed, cool air can be recirculated. Effect on response by using prewhirl to temporarily unload the compressor.
- Performance of the device on a two-stage turbocharged engine, the H.P. compressor discharge supplying the jet air to keep the L.P. compressor working in a best efficiency region.
- Compressor performance with the jet arrangement inducing negative prewhirl (power augmentation, transient response).
- Use of exhaust gas recirculation to provide the jets.

REFERENCES

1. ZINNER, K. Zur Entwicklung der Hochaufladung von Dieselmotoren-Rückblick und Ausblick. MTZ 38, (1977), 5, p.191-198.

2. A New Diesel Engine Development. The Motorship, Vol.VII, No.83, (February 1927), p.389-393.

3. STODOLA, A. Leistungsversuche mit Buchischer Aufladung, Z.VDI 72 (1928), p.421-428.

4. SYASSEN, O. Zukunftsaussichten der Zweistufigen Aufladung für Zwei-Und Viertact-Grossdieselmotoren, Part 1, MTZ 37 (1976), 11, p.467-473. Part 2, MTZ 37 (1976), 12, p.517-522.

5. A Half Century of Turbocharging. Diesel Engineering, Spring 1977, p.3.

6. JANOTA, M.S. Opening Address, Paper C49/78, "Turbocharging and Turbochargers", Conference I.Mech.E., 1978.

7. Turbocharging Tomorrow. Diesel Engineering, Spring 1977.

8. GOODLET, I.W. Turbocharging of Small Engines. Proc. I.Mech.E., Vol.188, 3/74, p.77-87.

9. MONAGHAN, M.L., FRENCH, C.C.J., FREESE, R.G. A Study of the Diesel as a Light-Duty Power Plant, E.P.A. Report, 460/3-74-011, July 1974.

10. LARKINSON, D.E., JEWSBURY, B.R. A Diesel Engine for Light Duty Applications. S.A.E. Paper 750333.

11. BARNES-MOSS, H.W., SCOTT, W.M. The High Speed Diesel Engine for Passenger Cars. I.Mech.E. Conference Paper, C15/75.

12. BARNES-MOSS, H.W., SCOTT, W.M. The Light Duty Diesel Engine for Private Transportation. S.A.E. Paper 750331.

13. HAYASHI, Y. A Series of Light Duty Indirect Injection Diesel Engines. S.A.E. Paper 760212.

14. MYERS, P.S. The Diesel Engine for Truck Application. S.A.E. Paper 750128.

15. HARTLEY, J. Light Diesel Engines. Automotive Design Engineering, Jul/Aug/Sept. 1975.

16. WEITZEL, H. Development of a High Speed Four-Cylinder Diesel Engine under consideration of the Existing Machine Tools Equipment for the Production of the Gasoline Engines. I.Mech.E. Conference, pub. C347/73, 19-1973.

17. OBERT, E.F. Internal Combustion Engines and Air Pollution. Intext Educational Publishers, N.Y. 1973.

18. MONAGHAN, M.L. Boosting for a Purpose. Paper C55/78, I.Mech.E. Conference, "Turbocharging and Turbochargers".

19. SCHERENBERG, H. Abgasturboaufladung für Personenwagen-Dieselmotoren. ATZ 79, (1977), 11.

20. OBLÄNDER, K., FORTNAGEL, M. Design and Results of the Five-Cylinder Mercedes.Benz Diesel Engine. S.A.E. Paper, 750870.

21. MARTIN, D.Q. Turbocharging of Diesel Engines. J.Automotive Eng., February 1971, p.9-12.

22. DEAN, R.C. The Fluid Dynamic Design of Advanced Centrifugal Compressors. Creare Inc., TN-185, July 1974.

23. ECKARDT, D. Detailed Flow Investigation within a High Speed Centrifugal Compressor Impeller. ASME Paper, 76-FE-13.

24. JANSEN, W. Steady Fluid Flow in a Radial Vaneless Diffuser. Trans.ASME, J.Basic.Eng., Series D, Vol.86, 1964, p.607-619.

25. McCUTCHEON, A.R.S. Aerodynamic Design and Development of a High Pressure Ratio Turbocharger Compressor. Paper C73/78, I.Mech.E., "Turbocharging and Turbochargers", Conference.

26. DEAN, R.C., YOUNG, L.R. The Time Domain of Centrifugal Compressor and Pump Stability and Surge. Trans.ASME, J.Fluids Eng., March 1977, p.53-63.

27. GREITZER, E.M. Surge and Rotating Stall in Axial Flow Compressors. Part I: Theoretical compression system model, ASME Paper 75-GT-9.

28. GREITZER, E.M. Surge and Rotating Stall in Axial Flow Compressors. Part II: Experimental results and comparison with theory, ASME Paper 75-GT-10.

29. TOYAMA, K., RUNSTADLER, P.W., DEAN, R.C. An Experimental Study of Surge in Centrifugal Compressors. Trans.ASME J.Fluids.Eng., March 1977, p.115-131.

30. AMANN, C.A., NORDENSON, G.E. "The Role of the Compressor in Limiting Automotive Gas Turbine Acceleration". Centrifugal Compressors, Technical Progress Series, Vol.3, ASME, New York, 1961, p.74.

31. BULLOCK, R.O., WILCOX, W.W., MOSES, J.J. Experimental and Theoretical Studies of Surging in Continuous Flow Compressors. NACA TN-1213, 1947.

32. EMMONS, H.W. Introduction, Symposium on Compressor Stall, Surge and System Response. ASME, New York 1960, p.1.

33. RODGERS, C. Impeller Stalling as Influenced by Diffusion Limitations. Trans.ASME, J.Fluids.Eng., March 1977, p.84-97.

34. RODGERS, C. A Diffusion Factor Correlation for Centrifugal Impeller Stalling. ASME Paper, 78-GT-61.

35. SENOO, Y., KINOSHITA, Y. Limits of Rotating Stall and Stall in Vaneless Diffuser of Centrifugal Compressors. ASME Paper 78-GT-19.

36. DUSSOURD, J.L., PFANNEBECKER, G.W., SINGHANIA, S.K. An Experimental Investigation of the Control of Surge in Radial Compressors using Close Coupled Resistances. Trans.ASME J.Fluids.Eng., March 1977, p.64-75.

37. JANSEN, W. Rotating Stall in a Radial Vaneless Diffuser. J.Basic.Eng., Trans.ASME, Vol.86, Series D, December 1964, p.750-758.

38. SENOO, Y., KINOSHITA, Y., ISHIDA, M. Asymmetric Flow in Vaneless Diffusers of Centrifugal Blowers. Trans.ASME, J.Fluids Eng., March 1977, p.104-113.

39. SENOO, Y., KINOSHITA, Y. Influence of Inlet Flow Conditions and Geometries of Centrifugal Vaneless Diffusers on Critical Flow Angle for Reverse Flow. Trans.ASME, J.Fluids.Eng., March 1977, p.98-103.

40. DUSSOURD, J.L., PUTMAN, W.G. Instability and Surge in Dual Entry Centrifugal Compressor. Symposium on Compressor Stall, Surge and System Response, ASME, New York, 1960, p.6.

41. MIZUKI, S., HATTORI, T., ARIGA, I., WATANABE, I. Reversed Flow Phenomena within Centrifugal Compressor Channels at Lower Flow Rate. ASME Paper No.76-GT-86.

42. RODGERS, C. Variable Geometry Gas Turbine Radial Compressors. ASME Paper 68-GT-63.

43. FUCHS, E.R.R., PARKER, K.G. Turbocharging the 31t. Ford Essex, I.Mech.E., Proceedings, Vol.188, No.5, (1974), p.483.

44. OATWAY, T.P. et al. Investigation of a Variable Geometry Compressor for a Diesel Engine Turbocharger. Report SR-21, AD-784003, NTIS, August 1973.

45. BENSON, R.S. A Comparative Study of the Cyclic Operating Conditions in the Compressor Delivery in Single and Two Stage Turbochargers under High Boost Conditions. Paper C75/78. "Turbocharging and Turbochargers" Conference, I.Mech.E., 1978.

46. SPÄTI, H. Measurement, Analysis and Assessment of Compressor Characteristics in Turbochargers. Brown Boveri Review, 4-77, Vol.64, April 1977, p.215-220.

47. THOLEN, P., KILLMANN, I. Investigations on Highly Turbocharged Air-Cooled Diesel Engines. ASME Paper 77-DGP-11.

48. CSER, G. Some Results of Combined Charging Application. Paper C64/78, "Turbocharging and Turbochargers", Conference, I.Mech.E., 1978.

49. TIMONEY, S.G. High Pressure Turbocharging of Two Stroke Engines. SAE Paper, 690747.

50. WINTERBONE, D.E., BENSON, R.S., MORTIMER, A.G., KENYON, P., STOTTER, A. Transient Response of Turbocharged Diesel Engines. SAE Paper 770122.

51. LEDGER, J.D., BENSON, R.S., FURUKAWA, H. Improvement in Transient Performance of a Turbodiesel by Air Injection in the Compressor. SAE Paper 730665.

52. ZEHNDER, G., MEIER, E. Exhaust Gas Turbochargers and Systems for High Pressure Charging. Brown Boveri Review, 4-77, Vol.64, April 1977, p.201-214.

53. ANDRE-TALAMON, T. New Aspects of Turbocharger Utilisation with the Hyperbar Parallel Supercharging. Paper C66/78, "Turbocharging and Turbo chargers" Conference, I.Mech.E., 1978.

54. Neue Fahrzeugmotoren Mit Abgasturboadern Auf Der IAA 77. MTZ, 38, 1977, 11.

55. ZINNER, K. Supercharging of Internal Combustion Engines. Springer-Verlag, Heidelberg, 1978.

56. MAIER, S. Mittel der Regelung von Abgasturboladern Fahrzeugmotor-Abgas-Entgiftung. Seminar 1095 (3-4 February 1975), Technische Akademie E.V. Wuppertal Ausseninstitut der Rheinish-Westfälishen Technishen Hochschule Aachen.

57. EMMONS, H.W., PEARSON, C.E., GRANT, H.P. Compressor Surge and Stall Propagation. Trans.ASME, Vol.77, April 1955, p.455-469.

58. TAYLOR, E.S. The Centrifugal Compressor. Aerodynamics of Turbines and Compressors, Vol.X, High Speed Aerodynamics and Jet Propulsion, Princeton Univ. Press. 1960.

59. BODINE, A.G. Sonic Control of Dynamic Compressor Instability. Symp. on Compressor Stall, Surge and System Response. ASME, New York, 1960.

60. RODGERS, C. Design and Test of an Experimental Rotating Diffuser Centrifugal Compressor Test Rig. SAE Paper 760927.

61. STEPANOFF, A.J. Inlet Guide Vane Performance of Centrifugal Blowers. ASME Paper No.60-WA-130, J.Eng. Power, Series A, Vol.83, 1961, p.371-380.

62. SHOUMAN, A.R., ANDERSON, J.R. The Use of Compressor-Inlet Prewhirl for the Control of Small Gas Turbines. ASME Paper No.63-AHGT-55, Trans.ASME J.Eng.Power, Series A, Vol.86, No.2, 1964, p.136-146.

63. WALLACE, F.J., WHITFIELD, A., ATKEY, R.C. Experimental and Theoretical Performance of a Radial Flow Turbo-charger Compressor with Inlet Prewhirl. I.Mech.E.Proc. Vol.189, 43/75.

64. PAMPREEN, R.C. The Use of Variable Inlet Guide Vanes for Automotive Gas Turbine Engine Augmentation and Load Control. SAE Paper 760285.

65. SHOUMAN, A. Prewhirl: An Added Degree of Freedom to the Designer of Small Single Shaft Gas Turbines. ASME Paper No.66-GT-89.

66. SHULHAN, G.M., SARAVANAMUTOO, H.I.H. Variable Geometry Compressors for Improvement of Gas Turbine Part Load Performance. SAE Paper 760283.

67. WHITFIELD, A., WALLACE, F.J., ATKEY, R.C. The Effect of Variable Geometry on the Operating Range and Surge Margin of a Centrifugal Compressor. ASME Paper No.76-GT-98.

68. KEMLIN, S. Turbocharger Line Covers 150-500 HP Engine Range. Diesel and Gas Turbine Progress, Jan/Feb,1969.

69. Small Swedish Turbochargers. Gas and Oil Power, Nov/Dec. 1967.

70. Incompressible Aerodynamics. B. Thwaites (ed.), Chapter 6, Clarendon Press, 1960.

71. KELLET, E., BETTERIDGE, J.F., MISTOVSKI, M. Investigation of Diesel Engine and Turbocharger Inter-action. I.Mech.E., Vol.182, Pt.1, No.15, p.331-360.

72. JORDINSON, R. Flow in a Jet Directed Normal to the Wind. Aeronautical Research Council, London, R and M, No.3074, 1956.

73. MARGASON, R.J. The Path of a Jet Directed at Large Angles to a Subsonic Free Stream. NASA-TN-D-4919, 1968.

74. RUGGERI, R.S., CALLAGHAN, E.E., BOWDEN, D.T. Penetration of Air Jets Issuing from Circular Square and Elliptical Orifices Directed Perpendicular to an Air Stream. NASA-TN-2019, February 1950.

75. KEFFER, J.F., BAINES, W.D. The Round Turbulent Jet in a Cross Wind. J.Fluid Mech., Vol.15, No.4, 1963, p.481-496.

76. CHASSAING, P., GEORGE, J.,CLARIA, A., SANANES, F. Physical Characteristics of Subsonic Jets in a Cross Stream. J.Fluid Mech., Vol.62, Part 1, 1974, p.41-64.

77. RUDINGER, G., MOON, L.F. Laser Doppler Measurements in a Subsonic Jet Injected into a Subsonic Cross Flow. ASME Paper No.76-FE-L.

78. KAMOTANI, Y., GREBER, I. Experiments on Confined Turbulent Jets in Cross Flow. NASA CR-2392, March 1974.

79. STOY, R.L., BEN-HAIM, Y. Turbulent Jets in a Confined Crossflow. Trans.ASME, J.Fluids.Eng., Series 1, Vol.95, No.4, Dec.1973, p.551-556, Paper No.73-FE-15.

80. PLATTEN, J.L., KEFFER, J.F. Entrainment in Deflected Axisymmetric Jets at Various Angles to the Stream. Technical Publication Series, Univ. of Toronto, UTME-TP-6808, June 1968.

81. BRAUN, G.W., McALLISTER, J.D. Cross Wind Effect on Trajectory and Cross Sections of Turbulent Jets. Analysis of a Jet in a Subsonic Cross Wind, NASA-SP-218, 1969.

82. HOULT, D.P., WEIL, W.C. Turbulent Plume in a Laminar Cross Flow. Atmosph.Environment, Vol.6, 1972, p.514-531.

83. HOULT, D.P., FAY, J.A., FORNEY, L.J. A Theory of Plume Rise Compared with Field Observations. J.Air Pollution Control Association, 19, 1969, p.585-590.

84. SUSEC, J., BOWLEY, W.W. Prediction of the Trajectory of a Turbulent Jet Injected into a Cross-Flowing Stream. ASME Paper No.76-FE-8.

85. CHIEN, J.C., SCHETZ, J.A. Numerical Solution of the Three-Dimension Navier-Stokes Equations with Applications to Channel Flows and a Buoyant Jet in a Cross Flow. ASME Paper No.75-APM-21, 1975.

86. PATANKAR, S.V., BASU, D.K., ALPAY, S.A. Prediction of the Three-Dimensional Velocity Field of a Deflected Turbulent Jet. Trans.ASME, J.Fluids Eng., December 1977, p.758-762.

87. RAJARATNAM, N. Jets in Cross-Flow. Turbulent Jets, Chapter 9, p.184-210, Elsevier Scientific Publishing Co., Amsterdam, 1976.

88. SCHLICHTING, H. Boundary Layer Theory. McGraw-Hill, New York, 1968.

89. RICOU, F.P., SPALDING, D.B. Measurements of Entrainment by Axisymmetrical Turbulent Jets. J.Fluid Mech., 11, 1961, p.21-32.

90. MORTON, B.R. Forced Plunes. J.Fluid Mech., 5, 1959, p.151-163.

91. CAMPBELL, J.F., SCHETZ, J.A. Analysis of the Injection of a Heated Turbulent Jet into a Cross Flow. NASA-TR-R-413, December 1973.

92. BHINDER, F.S. Investigation of Flow in a Nozzleless Spiral Casing of a Radial Inward Flow Gas Turbine. I.Mech.E. Proc., Vol.184, Pt.3G(II), 1970.

93. CUMPSTY, N.A. A Critical Review of Turbomachinery Noise. Trans.ASME, J.Fluids Eng., June 1977, p.278-293.

94. YEOW, K.W. Acoustic Modelling of Ducted Centrifugal Rotors. J.Sound and Vibration, 32, (1), 1974, p.143-152.

95. ANDERTON, D., DUGGAL, V.K. Effect of Turbocharging on Diesel Engine Noise, Emissions and Performance. SAE Paper 750797.

96. IKONOMU, J., KARRER, H., WATSON, J. Reduction of Noise Emission in Exhaust Gas Turbochargers. I.Mar.E., Vibration and Noise Conference, 1976.

97. BROCH, J.T. Acoustic Noise Measurements. Brüel and Kjaer Publications, February 1969.

98. STREIT, E.E., BORMAN, G.L. Mathematical Simulation of a Large Turbocharged Two-Stroke Diesel Engine. SAE Paper 710176.

99. BORMAN, G.L., MYERS, P.S., UYEHARA, O.A. Some Problem Areas in Engine Simulation. SAE Paper 710172.

100. MARZOUK, M. Simulation of Turbocharged Diesel Engines under Transient Conditions. Ph.D. Thesis, Imperial College, Univ. of London, 1976.

101. WALLACE, F.J., CAVE, P.R. Matching of High Output Diesel Engines with Associated Turbomachinery. Proc.I.Mech.E., Vol.187, 48/73, 1973.

102. SIRIGNANO, W.A. One Dimensional Analysis of Combustion in a Spark-Ignition Engine. SAE Paper 719010.

103. BONI, A.A., CHAPMAN, M., SCHNEYER, G.P. A One-Dimensional Variable Area Computer Simulation of Combustion in a Divided Chamber, Stratified Charge Engine. ASME Paper No.75-WA/DGP-1.

104. MARZOUK, M., WATSON, N. Program Imcoeng - Mark 1A - Program Manual. Dept. Mech.Eng., Imperial College, Univ. of London, 1975.

105. KAMEL, M.M.M. Thermodynamic Analysis of Indirect Injection Diesel Engine Operation. Ph.D. Thesis, Imperial College, Univ. of London, 1977.

106. ZALMANZON, L.A. Components for Pneumatic Control Instruments. Pergamon Press, 1966.

107. KLOMP, E.D., DeBOY, G.R. The Effects of Fluid Motions on Combusion in a Prechamber Bomb. SAE Paper 760162.

108. BRANSTETTER, W.R., DECKER, G. Fundamental Studies on the Volkswagen Stratified Charge Combustion Process. Combustion and Flame, 25, 15-23, 1975.

109. VIBE, I. Brennverlauf und Kreisprozess von Verbrennungsmotoren. VEB Verlag, Technik, Berlin, 1970.

110. WRONA, R. Rechenmodell zur Elektronischen Berechnung der Kenngrössen Eines Mit Schichtladung Betriebenen Ottomotors, MTZ, 35, 1974, 1, p.8-13.

111. SITKEI, G., RAMANAIAH, G.V. A Rational Approach for Calculation of Heat Transfer in Diesel Engines. SAE Paper 720027.

112. SITKEI, G. Heat Transfer and Thermal Loading in Internal Combustion Engines. Budapest, Aladémiai Kiado, 1973.

113. ANNAND, W.J.D., ROE, G.E. Gas Flow in the Internal Combustion Engine. Power, Performance, Emissions, Control and Silencing. Yeovil, Som., Foulis, 1974.

114. SMITH, D.J.L., MERRYWEATHER, H. The Use of Analytical Surfaces for the Design of Centrifugal Impellers by Computer Graphics. Intern.J.Num.Methods in Eng., Vol.7, 1973.

115. GOULAS, A., BAKER, R.C. An Optical Tachometer for Turbocharger Research. I.J.M.E.E., Vol.5, No.4, p.347-350.

116. MEZGER, H. Turbocharging Engines for Racing and Passenger Cars. SAE Paper 780718.

117. OBLÄNDER, K., FORTNAGEL, M., FEUCHT, H-J., CONRAD, U. The Turbocharged Five-Cylinder Diesel Engine for the Mercedes-Benz 300 SD. SAE Paper 780633.

118. INDRA, F. Entwicklung Eines Aufgeladenen Ottomotors für Personenwagen Mit 73,5 kW Literleistung. ATZ 80, 4, 1978, p.141-146.

119. U.K. Patent Appl.No.37489/78.

120. U.K. Patent No.1283561.

121. WETTERSTAD, L. Fluidic Injection System for Turbochargers and Gas Turbines. 9th Cimac Congress, B2, Stockholm, 1971.

122. U.S. Patent No.3751909.

123. LASKIN, E.G., KOFSKEY, M.G. Increase in Stable-Air-Flow Operating Range of a Mixed-Flow Compressor by means of a Surge Inhibitor. NACA RM No.E7C05, 1947.

124. MILES, L., ROUND, P. Air Induced Pre-Swirl Applied to a Centrifugal Compressor. Project Rep.No.93, School of Engineering, Bath University of Technology, June 1967.

125. S.I.P. 3-Axis Universal Measuring Apparatus.
Type: MU-214B/No.783, Societe Genevoise d'Instruments de Physique, Users Manual.